Anti-oxidised Low Density Lipoprotein Antibodies for the Serology and Imaging of Atherosclerosis

A thesis submitted for the degree of Doctor of Philosophy in

Cardiovascular Medicine

Imperial College London

December 2014

Dr. Ramzi Yousef Jabra Khamis

Supervised by

Professor Dorian O Haskard

Professor Paul M Matthews

Vascular Sciences Section

National Heart and Lung Institute

Imperial College London

Hammersmith Hospital Campus

Du Cane Road

London W12 0HN

To my Parents

'You are the bows from which your children as living arrows are sent forth' - Jibran Khalil Jibran.

DECLARATION

This thesis comprises results produced by myself except for some technical procedures, as indicated in the text. This work has been carried out at in the Vascular Sciences Section of the National Heart and Lung Institute, Faculty of Medicine, Imperial College, London, as well at the CVRC laboratories at Harvard Medical School. Some of the work was undertaken at the GSK laboratories in Stevenage, UK, and at Bristol University, Bristol UK.

Professor Alun Hughes both supervised statistical analyses of the ASCOT-related work and also ensured independent statistical review of the data.

COPYRIGHT DECLARATION

The copyright of this thesis rests with the author and is made available under a Creative Commons Attribution Non-Commercial No Derivatives licence. Researchers are free to copy, distribute or transmit the thesis on the condition that they attribute it, that they do not use it for commercial purposes and that they do not alter, transform or build upon it. For any reuse or redistribution, researchers must make clear to others the licence terms of this work.

ACKNOWLEDGEMENTS

This work would have not been possible without the generous funding provided by my Translational Medicine Fellowship awarded by the Wellcome Trust and GSK, as well as the laboratory funding from the BHF, the NIHR Imperial BRC, and the Binks Travel Award to Harvard from the British Atherosclerosis Society.

There are a plethora of people that have helped me through this PhD to make it possible. I am very grateful to each and every one of them.

First and foremost, I would like to express my sincere gratitude to my supervisor Professor Dorian Haskard who has taught me how to think like a physician, learn like a scholar, conduct my research like a scientist, and teach science and medicine as one entity. Most valuable of all, I learnt to appreciate the gratifying process of conducting exciting research. To him, I shall be eternally grateful.

I would like to also thank Professor Paul Matthews, whose supervision, guidance and support have been invaluable.

I would also like to especially thank Professor Alun Hughes for his co-supervision and constant support of the ASCOT related work.

Professor Martin Wilkins, Professor Jamil Mayet and Professor Michael Schneider for all their guidance d support.

I would also like to thank the team at the NHLI Vascular Sciences Section including Dr. Mike Johns, Dr. Joseph J Boyle, Dr. Gareth Hyde, Miss Rebecca Allen, my hard working

research assistant Mikhail Caga-Anan, the team at FILM, GSK especially Dr. David Granger, my imaging 'brother in arms' Dr. Kevin Woollard, and my collaborator Dr. Jason Johnson at Bristol.

A special thanks to my host laboratory at Harvard including Dr. Farouc Jaffer, Adam Mauskaupf and Tetsuya Hara.

The ups and downs of research would have been intolerable without Dr. Nikki Ambrose and Dr. Bilal Iqbal offering their moral support and the continued interventional cardiology mentorship of Drs Ghada Mikhail and Iqbal Malik.

I am indebted to my BSc and MSc students over the past four years for all their hard work: I am proud of their great achievements: Oliver Gale-Grant, Thomas Batty, Ivy Wong, Tareq Ammari, Kishan Patel and Priyank Shah.

I would also like to thank Danuta Mahiouz, Desmond Chow and Grace Nakate for their amazing managerial and organisational support.

Most importantly, a heart-felt special thanks to my hard working and loving wife Manal, for taking on the hardest job of all, looking after our wonderful children Yousef and Mira, to whom I am also grateful to for being really well behaved and very understanding of their dad either being on call or in the science laboratory.

Finally I would like to thank my parents without their support in every way none of my career would have been possible. I will never be able to pay back what they have given me, but I hope that at least they can get satisfaction and pride that our clinical and research work may help people who are vulnerable to cardiovascular disease and its sequelae.

PRIZES AWARDED IN RELATION TO THIS THESIS

- British Cardiovascular Society (BCS): Winner of the Young Research Worker's Prize, 2014
- American College of Cardiology: Young Investigator of the Year Award Finalist 2014
- British Atherosclerosis Binks Travel Award (For collaborative work at Harvard Medical School), 2013
- British Atherosclerosis Society/ British Cardiovascular Society: Young Investigator of the Year Award Finalist, 2013
- Best Postgraduate Presentation Prize, Imperial College British Heart Foundation Centre of Research, 2013
- Poster travel Prize. World Molecular Imaging Conference, 2012

TABLE OF CONTENTS

Declaration 3
Acknowledgements 4
Table of Contents 7
List of tables and figures 12
Abbreviations 14
1.0 Abstract
2.0 Background
2.1 Pathology of Atherosclerosis, a Chronic Inflammatory Disease 19
2.1.1 An introduction to the structure and function of Low Density Lipoprotein 19
2.1.2 LDL as a pathological entity 22
2.1.3 'Oxidised LDL' is not a single entity and reflects many forms of modified LDLs. 25
2.1.3.1 Malondialdehyde modified LDL (MDA-LDL) 25
2.1.3.2 Phosphocholine (PC) 25
2.1.3.3 Enzymatically modified LDL (E-LDL) 26
2.1.3.4 Minimally modified LDL (mmLDL) 26
2.1.3.5. Electronegative low density lipoprotein (LDL(-)) 26
2.1.4 Macrophage handling of modified LDL 27
2.1.5 The progression of atherosclerosis is partly driven by multiple pro and anti-inflammatory factors. 29
2.1.5.1 Role of flow 29
2.1.5.2 Complement plays both an atheroprotective and atherogenic role in atherosclerosis. 29
2.1.5.3 The role of vascular smooth muscle cells 30
2.2 From Stable Atherosclerotic Plaque to Vulnerable Plaque 31
2.3 The role of anti-oxidised LDL antibodies in atherosclerosis. 33
2.4 Anti-oxidised LDL antibodies as serological biomarkers in atherosclerosis 35
2.4.1 The need for better cardiovascular risk stratification tools 35
2.4.2 Summary of the evidence for the use of anti-oxidised LDL antibodies as serological biomarkers of cardiovascular risk 36
2.5 Measuring Circulating OxLDL 37
2.6 Imaging Beyond the Lumen. Plaque Characterisation Using Morphological Imaging Techniques. 38
2.7 Molecular Imaging of Atherosclerosis- Visualising the Invisible. 41
2.7.1 Requirements for successful molecular imaging of atherosclerosis 41
2.7.2 Non-optical imaging modalities: 41
2.7.3 The development of Near-Infrared Optical imaging into 'state of the art' molecular imaging technology 43
2.8 Agent Development for the Molecular Imaging of Atherosclerosis. 46
2.8.1 Molecular targets and the challenge of translation. 46
2.8.2 Radionuclear and MRI based Molecular targets 48
2.8.3 Optical molecular imaging targets 49
2.9 Antibody-based Imaging of Oxidised LDL Targets 52
2.10 Use of Recombinant Antibodies to Optimise in Vivo Imaging and Allow for Further Translational Use. 53
2.11 Work Leading Up to the Project and Pilot Data 55
2.11.1 Introducing LO1 and LO9 55

2.12 Aims and Hypotheses....56
3.0 Methods
3.1 Study Ethics....58
3.2 LDL Modification....58
3.2.1 Generation of Malondialdehyde-conjugated MDA-LDL....58
3.2.2 Trypsinisation of LDL.....59
3.2.3 Hypochlorite modification....60
3.2.4 Autooxidised LDL....60
3.3 Human Serology Assay Optimisation....60
3.4 the ASCOT Anti-ox Study Methods....62
3.4.1 Study design and subjects....62
3.4.2 IgG and IgM anti-PC-BSA and MDA-LDL antibody levels....63
3.4.3 General measurements....63
3.4.4 Statistical analyses....64
3.5 Methods for the Isolation, Characterisation and Development of Monoclonal Antibodies LO1 and LO9.....65
3.5.1 Culture of LO1 and LO9 hybridomas and generation of antibodies....65
3.5.2 Enzyme-linked immunosorbent assay (ELISA)....66_Toc405050085
3.5.2.1 Correcting for equal loading of LDL....66
3.5.2.2 Variation in concentration of salt....67
3.5.2.3 Variations in Ph....67
3.5.2.4 LDL Capture ELISA....67
3.5.2.5 Native LDL incubation ELISA....67
3.5.2.6 Serum incubation ELISA....68
3.5.2.7 Preservative incubation ELISA....68
3.5.2.8 Bone marrow derived macrophages....68
3.5.2.9 Zymosan opsonisation....69
3.5.2.10 ELISA to test mouse macrophage TNFα production by an an FcγR-mediated mechanism....69
3.5.2.11 conditioned medium ELISA....70
3.5.3 Peptide synthesis....70
3.5.4 Biotinylation of LO1....70
3.5.5 Biotinylation of LO9....71
3.5.6 Production of H3-Biotin (including western blotting to demonstrate biotinylation)....71
3.5.7 Purification of LO1 on H3 biotin column....72
3.5.6 Identification of LO1 and LO9 sequence....73
3.5.6.1 Sequencing of the LO1 VH variable region....73
3.5.6.2 LO1 VL Sequencing and generation of LO1-Fab....73
3.5.6.3 Generation of a chimeric LO1-Fab-Cys construct....74
3.5.6.4 Sequencing of LO9....75
3.5.7 Fluorescence labelling of LO1, LO9 and LO1-Fab-Cys and isotype controls.....77
3.5.8 Animal models of experimental atherosclerosis....78
3.5.8.1 Mouse model of atherosclerosis....78
3.5.8.2 Rabbit model of atherosclerosis....79
3.5.9 Immunohistochemistry and confocal microscopy....79
3.5.9.1 Mouse and Human IHC....79
3.5.9.2 Ex vivo in situ IHC and en face analysis in the mouse model....81
3.5.9.3 IHC in the rabbit model....82
3.5.9.4 Ex vivo fluorescence microscopy on rabbit aortae....82
3.6 IVIS Spectrum Fluorescence Imaging and Computed Tomography (IVIS/CT)....83
3.7 Fluorescence Molecular Tomography-Computed Tomography (FMT/CT)....83

3.7.1 LO1 studies:.....83
3.7.2 LO9 studies.....84
3.8 Two-dimentional NIRF Imaging Device and Catheter.....84
3.8.1 Intravascular NIRF and IVUS imaging.....85
3.9 Fluorescence Reflectance Imaging.....85
3.10 Statistical analyses.....86
4.0 Serological Assay Optimisation and the Anglo-Scandinavian Cardiac Outcomes Anti-oxLDL Substudy
4.1 Chapter Summary.....87
4.2 Assay Optimisation.....89
4.2.1 Estimating total IgG and IgM levels by ELISA.....89
4.2.2 Optimisation of an ELISA based assay to estimate anti-MDA-LDL and an anti-PC-BSA IgG and IgM antibody levels in serum.....91
4.2.3 Estimation of IgG anti-MDA-LDL isotype levels.....93
4.2.4 IgG3 anti-MDA-LDL antibody assay optimisation.....94
4.2.5 IgG1 anti-MDA-LDL antibody assay optimisation.....95
4.3 IgG Antibodies Against Anti-malondialdehyde-LDL Predict Freedom from Cardiovascular Events Independently of Traditional Cardiovascular Risk Factors in ASCOT. (The ASCOT Anti-OxLDL Substudy).....97
4.3.1 Assay variability.....97
4.3.2 IgG anti-MDA-LDL antibodies are a strong predictor of freedom from MACE.....98
4.3.3 IgG anti-MDA-LDL antibodies are unrelated to FRS, CRP or other classical predictors of cardiovascular risk.....100
4.3.4 Anti-oxLDL antibodies are unchanged over one year, and are unaffected by atorvastatin treatment despite reduction in LDL and CRP.....101
4.3.5 IgG1 and IgG3 isotypes are also stable over one year, and are independent entities.....105
4.3.6 Total IgG anti-MDA-LDL antibodies but not individual IgG1 or IgG3 isotype levels are strong predictors of protection from MACE.....107
5.0. The Characterisation of LO1, A Monoclonal Autoantibody Against MDA-LDL And Its Development Into A Molecular Imaging NIRF Agent In Experimental Atherosclerosis.
5.1 Chapter Abstract:.....108
5.2 in Vitro Characterisation on LO1.....109
5.2.1 LO1 ELISA studies.....109
5.2.2 Characterisation of H3.....111
5.2.3 Biotinylation of H3.....115
5.2.4 Isolation of purified LO1.....118
5.2.5 LO1 sequencing.....118
5.2.6 LO1 labelling.....119
5.2.6.1 Biotinylation:.....119
5.2.6.2 Fluorescence labelling of LO1.....121
5.2.7 Binding of LO1 to atherosclerotic lesions in mouse, rabbit and human.....123
5.3 *In vivo* studies.....131
5.3.1 Clearance of LO1-750 after intravenous injection in mice.....131
5.3.2 *In vivo* aortic imaging of LO1-750 in the mouse using hybrid IVIS Spectrum/ CT imaging.....133
5.3.3 Quantitative analysis of LO1-750 imaging of mouse atherosclerosis using FMT/CT.....135
5.3.4 Quantification of LO1-750 localisation distinguishes stages of lesion progression.....139
5.3.5 *En face* validation of LO1-750 localisation in mouse atherosclerosis using *ex vivo* confocal microscopy.....142
5.3.6 2D NIRF intravascular imaging of oxidised LDL with LO1-750.....144
5.4 Generation and Characterisation of LO1-Fab-Cys As a Potential Imaging Agent.....147

6.0 Mab LO9, a Novel Immunoglobulin G Autoantibody, Against an Allosteric Epitope on Low Density Lipoprotein (LDL)
6.1 Chapter Abstract: 150
6.2 Generation and Initial Characterisation of LO9 151
6.2.1 LO9 reacts with native adherent LDL and less with Cu^{++}oxLDL. 152
6.2.2 LO9 only binds to LDL when adherent, and not when captured. The LO9 and adherent LDL interaction is not blocked by abundant LDL in fluid-phase or by serum. 154
6.2.3 The LO9 epitope is not alcohol sensitive and is partially sensitive to 'on plate' light trypsinisation, ... 156
6.2.4 Cloning and sequencing immunoglobulin genes 159
6.3 LO9 Exhibits Pathological Functions in Vitro 161
6.3.1 LO9 bound to adherent LDL causes mouse macrophages to release TNFα by an FcγR-mediated mechanism 161
6.3.2 The LO9 epitope is further revealed by activated macrophage conditioned medium 163
6.4 Biotinylation and Fluorescence Labelling of LO9 164
6.5 Detection of LO9-reactive Material in Atherosclerosis 165
6.5.1 Immunohistochemistry in mouse aortic root and cusp and human carotid and coronary lesions. 165
6.5.2 LO9 injected intravenously localises to atherosclerosis. *The in vivo detection of LO9-750 with FTM-CT* 169
6.5.3 Ex vivo characterisation of the localisation of injected LO9-750 in murine atherosclerosis. 171
7.0 Discussion: From identifying the vulnerable patient to the targeting and identification of the vulnerable plaque- The identification and utilisation of autoantibodies against oxidised LDL
7.1 A Brief Summary of the Findings 174
7.2 the Development and Utility of Anti-oxidised LDL Antibodies As Biomarkers for Cardiovascular Risk 176
7.2.1 Choice and Optimisation of assays detecting antibodies against oxidised LDL 176
7.2.2 Assay development 176
7.2.3 IgG anti-MDA-LDL antibodies are independent markers of protection from incident cardiovascular events in the the Anglo-Scandinavian Cardiac Outcomes anti-oxLDL substudy 178
7.2.4 Anti-oxidised LDL antibodies are stable despite one year treatment with atorvastatin. 180
7.2.5 Proposed mechanisms by which anti-oxidised LDL antibodies maybe protective against cardiovascular events 180
7.2.6 Not all anti-oxidised LDL antibodies correlated with protection from cardiovascular disease, despite a general positive correlation amongst them. 182
7.2.6 Dissecting the IgG response to MDA-LDL 182
7.3 the Generation, Characterisation and Development of LO1 and Its Molecularly Expressed Chimeric Fab Construct for the Targeted Imaging of Oxidised LDL *in Vivo* 184
7.3.1 In vitro characterisation of LO1 184
7.3.2 LO1 identifies atherosclerotic lesions *in vitro* 186
7.4.4 LO1 specifically targets experimental atherosclerosis *in vivo* in the *Ldlr*$^{-/-}$ mouse model 187

7.4.6 LO1 tracks the effects of high fat and aging *in vivo.* 189
7.4.7 Could LO1-750 and MMPSense have a commentary role in the identification of vulnerable atherosclerotic plaque? 190
7.4.8 *Ex vivo* validation of LO1-750 targeting in atherosclerotic plaque. 190
7.4.9 Proof of concept intravascular imaging of LO1 targeting OxLDL in the atherosclerotic, balloon-injured rabbit model 191
7.4.10 The generation and expression of LO1-Fab and LO1-Fab-Cys 191

7.5 LO9, an IgG Monoclonal Autoantibody Reacting with a Cryptic Allosteric Epitope on Low Density Lipoprotein 193
7.5.1 LDL deposition within the sub-endothelial space may represent an initial event in atherosclerosis, presenting adherent LDL an antigen to the innate immune system 193
7.5.1 LO9 is unique as an IgG autoantibody specific to adherent LDL, and not to captured LDL or LDL in solution 193
7.5.2 LO9 sequence suggests that it is an adaptive rather than a germ-line antibody 195
7.5.2 LO9 is likely to have pathological functions when reacting with solid phase antigen, and its epitope is further revealed by macrophage activation. 195
7.5.3 LO9 can be labelled, and utilised to identify atherosclerosis *in vitro* and *in vivo* 197
7.6 Conclusion and Further Work 198

LIST OF FIGURES

Figure 2.1 Structure of Apolipoprotein B-100 (ApoB) of LDL. 21
Figure 2.2. The illustration of OSE as pathogen associated molecular patterns (PAMPs). 24
Figure 2.3. Pathological characteristics of both vulnerable and stable plaques. 32
Figure 2.4 Chemograms derived from NIRS, combined with IVUS. 40
Figure 2.5. Intravascular NIRF molecular imaging. 45
Figure 2.6. Schematic representation of various engineered antibody fragments. 54
Figure 2.7 Peptide sequence of both the heavy and light chains of H3 56
Figure 3.1 Agarose gels of native LDL Vs MDA-LDL and native LDL vs trypsinised LDL. 59
Figure 3.2. LO9- PCR using several combinations of Ig variable domain primers 76
Figure 4.1. ELISA optimisation curves for total IgG and total IgM. 90
Figure 4.2. Optimisation curves for the IgG and IgM anti-PCX-BSA and anti-MDA-LDL antibody assays 92
Figure 4.3 Levels of IgG isotypes 93
Figure 4.4 Optimisation of the IgG3 anti MDA-LDL antibody assay 94
Figure 4.4 ELISA of IgG3 anti-MDA-LDL antibodies in dilution series. 95
Figure 4.5 Optimisation of the IgG1 anti-MDA-LDL antibody assay. 96
Figure 4.6 A representative analysis of total and isotype levels of IgG anti-MDA-LDL antibody levels in one serum from ASCOT. 96
Figure 4.7 Kaplan-Meier survival estimates for population tertiles of IgG anti-MDA-LDL levels 100
Figure 4.8 Distribution of anti-MDA-LDL IgG1 antibody levels 106
Figure 5.1 Initial characterisation of LO1 110
Figure 5.2 LO1 identifies H3 selectively 112
Figure 5.3 LO1 binds H3 and MDA-LDL in similar Ph. and salt conditions 113
Figure 5.4 Linear peptides derived from H3 do not block LO1 binding. 115
Figure 5.5 Production and biotinylation of H3. 117
Figure 5.6. Colloidal blue staining shows both heavy and light chains of both purified and unpurified LO1. 118
Figure 5.7. Amino acid sequences of the LO1 VH and VL 119
Figure 5.8 The retention of activity of LO1 to H3 following biotinylation. 120
Figure 5.9. Fluoresceinated LO1 (SAIVI Alex Fluor 647) vs. MDA and Native LDL 121
Figure 5.10 ELISA demonstrating the relative retention of function of LO1 when it is labelled 122
Figure 5.12. Immunofluorescence staining of en face Ldlr$^{-/-}$ mouse aorta, with LO1-750 and isotype control. 126
Figure 5.13. Immunohistochemical staining of rabbit atherosclerosis with LO1. 127
Figure 5.14. Immunocytochemical staining of human carotid atherosclerotic plaque with LO1. 129
Figure 5.15. Immunofluorescence staining of human carotid atherosclerosis with LO1-750. 130
Figure 5.16. Blood clearance and organ distribution of LO1-750 as determined by ex vivo epifluorescence of heparinised serial bleeds and extracted organs 132
Figure 5.17. In vivo aortic imaging of LO1-750 in Ldlr-/- mouse model using hybrid IVIS Spectrum/CT 135
Figure 5.18. FMT/CT imaging and quantification of LO1-750 in the Ldlr-/- mouse model of atherosclerosis. 139
Figure 5.19. FMT Quantification of LO1-750 and MMPSense FAST targeting of the aorta and carotids region of interest in 3 stages of atherosclerosis progression. 142
Figure 5.20. En face confocal microscopy of in vivo targeted extracted aorta of the Ldlr-/- high fat fed mouse atherosclerosis model. 143

Figure 5.21. NIRF molecular imaging of oxLDL in atherosclerotic balloon-injured rabbit abdominal aortae. 146
Figure 5.22. LO1-Fab-Cys characterisation. 149
Figure 6.1: LO9 reacts with adherent LDL. 153
Figure 6.2. LO9 binds only adherent LDL and is not blocked by LDL or human serum 156
Figure 6.3. The LO9 epitope is not alcohol sensitive and can be modulated with on plate light trypsinisation of adherent native LDL. 159
Figure 6.4. Amino acid sequence of the mAb LO9 VH and VL 160
Figure 6.5: LO9 bound to adherent LDL causes mouse macrophages to release TNFα by an FcγR-mediated mechanism 162
Figure 6.6: Treatment of adherent LDL with CM from activated macrophages leads to enhanced LO9 epitope expression. 163
Figure 6.7 Function of LO9 against native adherent LDL when unlabelled, biotinylated and labelled with VT-MAL 750 155
Figure 6.8. Detection of antigen recognised by LO9 in atherosclerosis 168
Figure 6.9. FMT and FMT/CT imaging with LO9-750 and isotype control antibody in $Ldlr^{-/-}$ and WT animals. 170
Figure 6.10 localisation of in vivo injected LO9-750 in the Ldlr-/- aorta 171
Figure 7.1: Hypothetical model of how LO9 and similar antibodies may accelerate atherosclerosis 182

LIST OF TABLES

Table 2.1 Comparison of imaging technologies 43
Table 2.2. Clinically Targeted Molecular Imaging Agents that may be used in atherosclerosis. 47
Table 2.3. A collated list of commercially available optical molecular probes 51
Table 3.1 ELISA conditions for serology studies 61
Table 4.1 Baseline characteristics 99
Table 4.2 Antibody, lipid and CRP measures at 1 year. 102
Tables 4.3 a-c. Correlation Matrices 104
Table 4.4 Relationships Between isotypes of IgG anti-MDA-LDL antibodies, LDL and HDL at baseline 105
Table 5.1 Peptides designed to cover possible binding sites on H3 114

ABBREVIATIONS

ASCOT	The Anglo-Scandinavian Cardiac Outcomes Trial
BSA	Bovine serum albumin
CAC	Coronary artery calcium
CAD	Coronary artery disease
CCB	Calcium channel blocker
CDR	Complementarity determining regions
CHD	Coronary Heart Disease
CIMT	Carotid intima media thickness
CM	Conditioned medium
CoV	Coefficient of variation
CRP	C-reactive protein
CT	Computed tomography
DICOM	Digital Imaging and Communications in Medicine
DMEM	Dubecco's modified eagle medium
DOL	Degree of labelling
ELISA	Enzyme-linked immunosorbent assay
ESC	European Society of Cardiology
FH	Familial hypercholesterolemia
FILM	Facility for Imaging by Light Microscopy
FM	Fluorescence microscopy
FMT	Fluorescence molecular tomography
FRI	Fluorescence reflectance imaging
FRS	Framingham risk score
GWAS	Genome-wide association study

HDL	High density lipoprotein
HF	High fat
HR	Hazard ratios
HRP	Horse radish peroxidase
IC	Isotype control
ICG	Indocyanine green
IG	Immunoglobulin
IgG	Immunoglobulin G
IgM	Immunoglobulin M
IDI	Integrated discrimination improvement
IDL	Intermediate density lipoprotein
IPCoV	Inter- plate correlation of variation
LDL	Low density lipoprotein
LVH	Left ventricular hypertrophy
MACE	Major adverse cardiovascular events
MDA	Malondialdehyde
MI	Myocardial Infarction
NIRF	Near infra-red fluorescence
NIRS	Near-infrared spectroscopy
NRI	Net reclassification improvement
OCT	Optical Coherence Tomography
OFDI	Optical frequency domain imaging
OSE	Oxidation specific epitopes
oxLDL	Oxidised LDL
PAMP	Pathogen associated molecular patterns

PBS	Phosphate buffered saline
PCSK9	Proprotein convertase subtilisin/kexin type 9
PET	Positron Emission Tomography
PVD	Peripheral vascular disease
ROI	Region of interest
RT	Room temperature
SD	Standard deviation
SEM	Standard error of the mean
SMC	Smooth Muscle Cells
SNR	Signal-to-noise ratio
TBR	Target to background ratio
TCFA	Thin Cap Fibro Atheromas
TF	Tissue factor
TMB	3,3′,5,5′-Tetramethylbenzidine
VH	Variable heavy
VL	Variable light
VLDL	Very low density lipoprotein
WT	Wild type

1.0 Abstract

Atherosclerosis and its related major adverse cardiovascular events represent a major worldwide morbidity and mortality burden. The paradigm of identifying 'vulnerable plaques' leading to 'vulnerable patients' remains challenging despite recent advances in cardiovascular medicine.

The project aimed to develop an antibody-based strategy for the translational development of imaging oxidised low density lipoprotein (LDL), a major constituent of vulnerable atherosclerotic plaque. It also aimed to simultaneously develop anti-oxidised LDL antibody-based serological assays for the stratification of individual cardiovascular risk independently of classical risk factors.

In this thesis, I first discuss the development of a number of assays for the measurement of anti-oxidised LDL antibodies in serum and plasma. I then describe our findings, using a subpopulation of the Anglo-Scandinavian Cardiac Outcomes Trial (ASCOT) to discover that IgG anti-Malondialdehyde (MDA)-LDL antibody levels are stable, independent biomarkers of freedom from adverse cardiovascular events over a 5.5 year follow up.

This is followed by describing LO1 and LO9, both murine monoclonal antibodies, isolated in our laboratory, against MDA-LDL and adherent native LDL respectively. We characterise and sequence both, and take LO1 further into development as an imaging agent. I then progress to discussing the utility of directly labelled LO1 (LO1-750) as a near infra-red fluorescence (NIRF) imaging agent. We use two animal models (*Ldlr*$^{-/-}$ and rabbit atherosclerosis models), utilising three different modalities (IVIS Spectrum/ computed tomography (CT), Fluorescence molecular tomography (FMT)/CT and intravascular 2D

NIRF/intravascular ultrasound (IVUS)). I further discuss the generation of a partially humanised tagged molecular construct (LO1-Fab-Cys), as a first step towards the molecular expression and humanisation of LO1 in an optimised form for targeting of oxidised LDL in humans.

Moreover I detail the characterisation of LO9 by delineating in a series of experiments its allosteric epitope on adherent LDL, and describe a potential pathological role for it. We label LO9 with a NIRF agent, and show LO9 localisation *in vitro* and in vivo in mouse studies.

In conclusion, this thesis demonstrates the utility of autoantibodies to oxidised LDL as both serological and potential molecular imaging agents of atherosclerosis in vivo.

2.0 Background

2.1 Pathology of Atherosclerosis, a Chronic Inflammatory Disease

It is widely recognised that atherosclerosis is a chronic inflammatory condition with oxidative stress and oxidation of lipoproteins at its centre [1]. Central to this paradigm is the involvement of the immune system as a 'double-edged sword' with both regulatory and pathological roles.

2.1.1 An introduction to the structure and function of Low Density Lipoprotein

LDL is large complex particle (18-25 nm in diameter) comprised of a single molecule, Apolipoprotein 100 (apolipoprotein B (ApoB)) (Mr 550 kD)[2, 3], which wraps around a hydrophobic triglyceride and cholesterol ester core (Figure 2.1) [2]. There are five major groups of lipoprotein which include: high density lipoprotein (HDL), LDL, intermediate density lipoprotein (IDL), very low density lipoprotein (VLDL) and chylomicrons. When VLDL delivers its triglyceride content to peripheral muscle and adipose tissue, it is hydrolysed by lipoprotein lipase, forming a smaller, denser LDL particle, which retains the ApoB100 shell but has a lower triglyceride content. LDL is essential for supplying lipid to cells as part of normal lipid trafficking, and cell entry is mediated through binding with the LDL receptor. This receptor recognises the ApoB-100 protein and facilitates the endocytosis of LDL. Thus the value of prevention of LDL receptor degradation via the inhibition of Proprotein convertase subtilisin/kexin type 9 (PCSK9), has recently become a focus in the novel treatment of high LDL[4]. Conversely transgenic animals that either lack the gene coding for the LDL receptor, or have had the gene disrupted, are a valuable research tool to study atherosclerosis in an accelerated animal model[5, 6]. We use the *Ldlr*$^{-/-}$ mouse model as our main experimental model in this thesis.

The structure of LDL has been challenging to characterise due to the variability of the molecule. The variable fat and cholesterol ester content makes the molecule difficult to manipulate and characterise in the laboratory[2]. There has been a suggestion that denser, smaller LDL particles may have more pathological potential than larger less dense LDL molecules. This is partly due to the hypothesis that the smaller particles are more capable of penetrating endothelium than the larger ones[7]. Another hypothesis suggests that small dense LDL particles are more susceptible to oxidation than larger more buoyant LDL particles, but this field is in need of further study[8].

The term 'oxidised LDL' includes structural modifications to this molecule of various types, mainly involving the ApoB component. The term is usually generically used to reflect a group of modified LDLs in which expression of neo-determinants transforms the molecule into an antigen.[9]

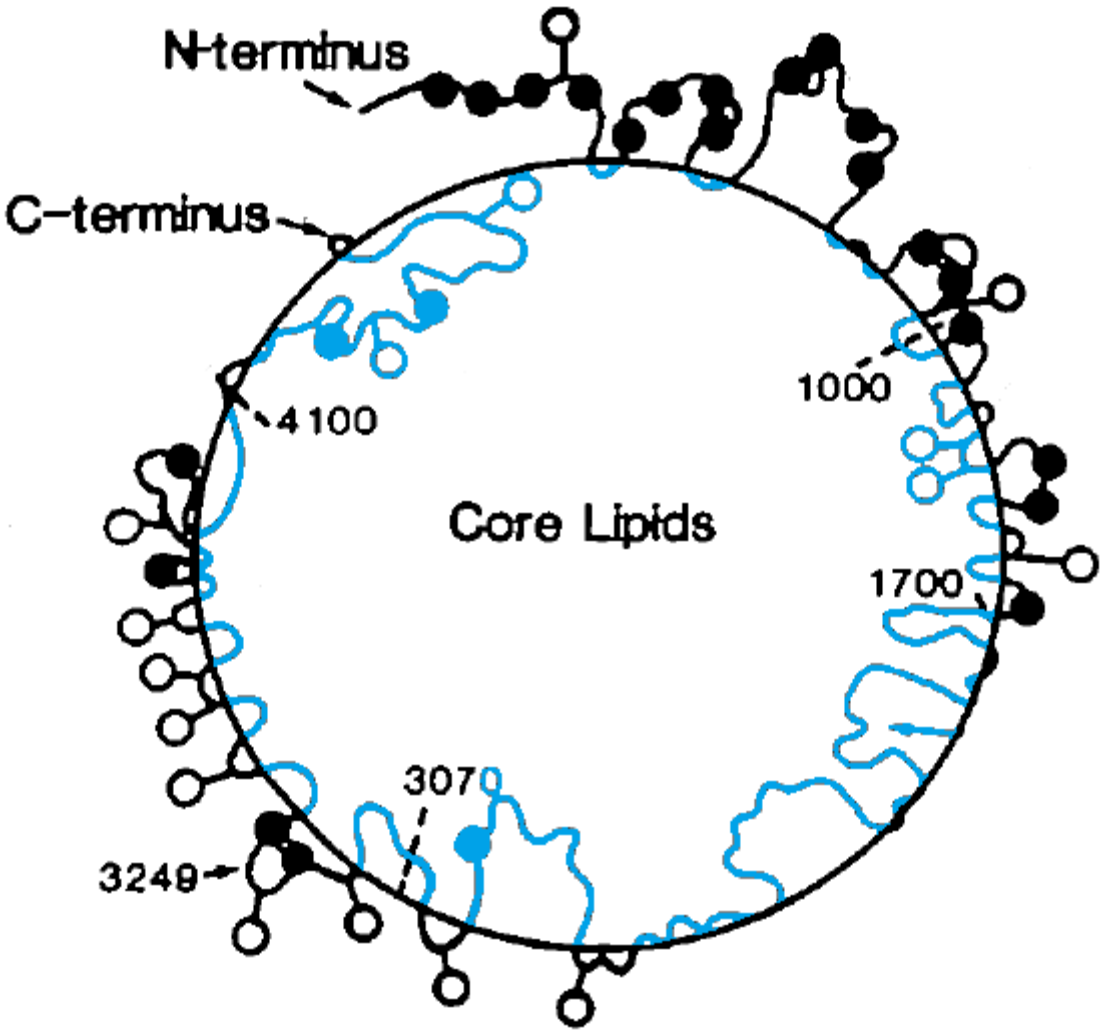


Figure 2.1 Structure of Apolipoprotein B-100 (ApoB) of LDL.

Figure adapted from Figure 5 of Yang et al[10]: Lipid and cholesterol components of ApoB are represented as a circle. The trypsin non-releasable regions are shown in blue on the inside of the circle, and the trypsin releasable regions are on the outside of the circle.

2.1.2 LDL as a pathological entity

Deposition of LDL within arteries can lead to early lesions in young individuals called fatty streaks[11]. These are largely composed of fat-filled macrophages and are reversible and clinically insignificant. However, in hypercholesterolemia, LDL is a major protagonist of atherosclerosis and increased levels directly infer increased risk[12]. When LDL levels are raised, LDL deposits within the arterial intima, partly through interaction of positively charged domains of apoB100 with negatively charged sulphate groups of extracellular proteoglycans [13]. Once within the sub-intimal space, LDL is concealed from antioxidants present in plasma, and may also undergo conformational changes and be more likely to undergo an oxidative insult. Various modifications of LDL have been found within the atherosclerotic plaque[14]. Some of these modifications are due to enzymes such as myeloperoxidase and lipoxygenase, as well as reactive oxygen species, which create endogenous antigenic neo-epitopes[15].

Thus, the modification, or 'oxidation', of LDL to form a pathological entity is central to the process of atherosclorsis[16]. Oxidative stress represents an imbalance between the production and degradation of reactive oxygen species (ROS), e.g., superoxide anion or hydrogen peroxide created by myeloperoxidase, nitric oxide synthase, NADPH oxidase, xanthine oxidase, and other oxidases. These, as well as tissue enzymes (e.g., secretory phospholipase A2), can modify fatty acids, lipoproteins and amino acids, generating different antigenic entities, mostly known as oxidation specific epitopes (OSE)[17]. The release of reactive aldehydes (e.g., MDA) leads to formation of carbonyl adducts with apolipoproteins and phospholipids[9, 18]. This process disrupts physiological processing of LDL, and results in LDL being an important immunological driver of atherosclerosis[9]. Modification of LDL is particularly important in the arterial intima, where uptake into macrophages via scavenger

receptors leads to foam cell formation, cell death, atherosclerotic lesion development and progression [1].

As well as an antigenic entity taken up by macrophages, oxLDL is a thought to be a potent inducer of inflammation, partaking in the activation of monocytes, smooth muscle cells and endothelial cells (EC)[19, 20]. Once the inflammatory cascade initiates, adhesion molecules, chemokines and growth factors attract other cells of the immune system in a self-perpetuating manner[21]. Figure 2.2 demonstrates the interaction of OSE as pathogen associated molecular patterns (PAMPs), involving both the innate and adaptive immune system in their clearance. It is when these clearance mechanisms are insufficient, due to increased supply of OSE, such as in hypercholesterolaemia, or when there is a lack of ability to process the antigenic material, that pathological processes such as atherosclerosis ensue[22].

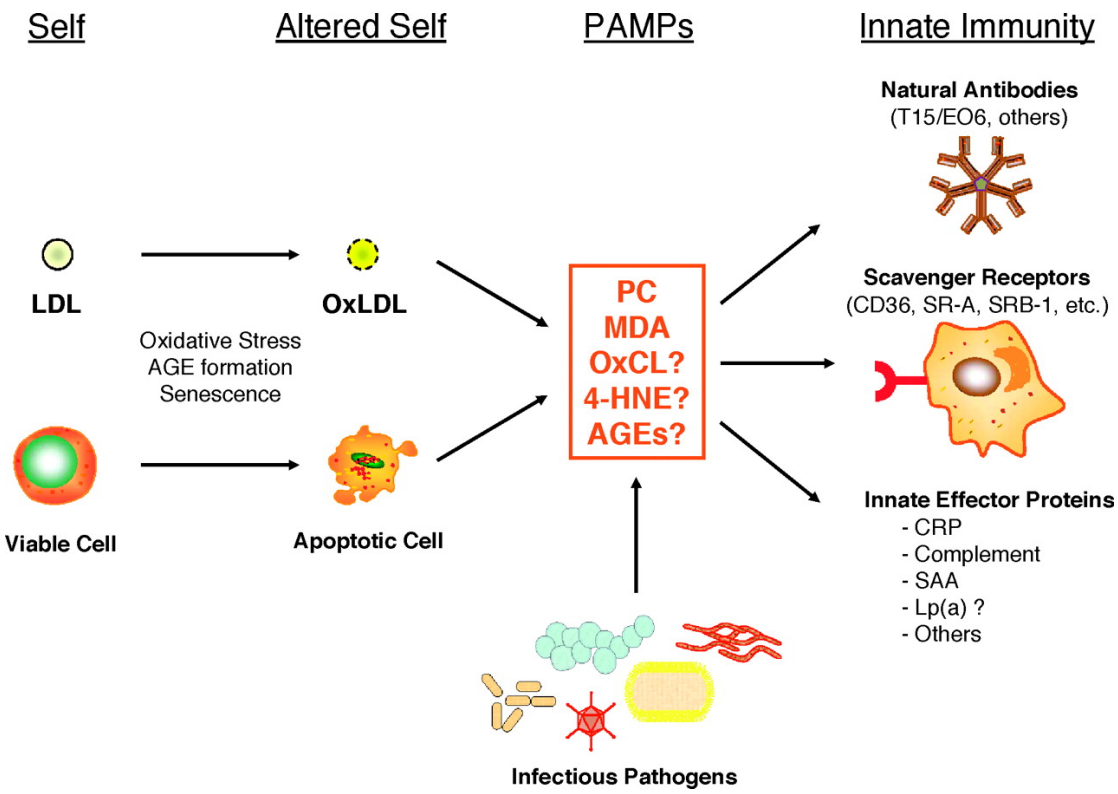


Figure 2.2. The illustration of OSE as pathogen associated molecular patterns (PAMPs).

Figure from Binder et al[23]. Antigens generated by oxidative stress can mimic epitopes expressed by pathogens. Both the innate and adaptive immune system are involved in the processing of OSE. AGE (advanced glycation end product); CRP, C-reactive protein; 4-HNE, 4-hydroxynonenal; Lp(a), lipoprotein [a]; MDA, malondialdehyde; OxCL, oxidised cardiolipin; oxLDL, oxidised LDL; PC, phosphoholine; SAA, serum amyloid A.

2.1.3 'Oxidised LDL' is not a single entity and reflects many forms of modified LDLs.

There is no single 'oxidised LDL' molecule that is the main player in atherosclerosis. Many modifications of the LDL molecule render it antigenic. I discuss here the main known entities, in particular the forms that are relevant to the thesis[16].

2.1.3.1 Malondialdehyde modified LDL (MDA-LDL)

During the process of lipid peroxidation, highly reactive aldehyde products such as malondialdehyde (MDA) are generated, these in turn forms covalent bonds with lysine residues on the ApoB molecule, creating an epitope on the now modified LDL that renders it pathogenic. Rather than being processed by the physiological LDL receptor pathway[24 16], MDA-LDL, like other 'heavily' modified LDLs, internalises into macrophages, eventually leading to lipid laden foam cell formation[20, 25]. Various studies in animal models have demonstrated that MDA-LDL is present in atherosclerotic plaques, such as in the intimal layer of the aorta in the myocardial infarction-prone Watanabe Rabbits[14, 18].

2.1.3.2 Phosphocholine (PC)

Phosphocholine (PC) of oxidised phosphatidylcholine, is a well characterised oxidation specific epitope which has been demonstrated in atherosclerotic lesions. Phospholipid oxidation causes a conformational change involving reorientation of the phosphorylcholine head group relative to the glycerol backbone and protrusion of the sn-2 fatty acid chain into the hydrophilic compartment creating a so called 'Lipid Whisker Model'. These previously cryptic neo-epitopes, which are usually inaccessible, become more accessible for direct interaction with scavenger receptors, such as the class B scavenger receptor, CD36 and autoantibodies for PC (anti-PC). Thus, the change in protein conformation, either by

modification or by cell death and apoptosis, reveals the antigenic cryptic epitope[23]. Moreover, the PC head group has also been shown to be exposed on cell membranes that have been damaged by complement and some phospholipases[26]. Because PC is also present as component of the capsular polysaccharide of encapsulated bacteria, such as *Strep. pneumoniae*, as well as in other gram-positive and gram-negative bacteria, protozoa and worms[26], it provides an example of molecular mimicry between oxidised phospholipids and microbial antigens[27].

2.1.3.3 Enzymatically modified LDL (E-LDL)

Proteolytic cleavage of ApoB in conjunction with hydrolysis of cholesterol esters generates lipoprotein particles that are similar to lesion-derived LDL in structure, biological properties, and composition. This process is thought to be mainly mediated by plasmin and matrix metalloproteinases[28]. E-LDL has been shown to activate complement via the alternative pathway and to deposit in the arterial intima.[29, 30]

2.1.3.4 Minimally modified LDL (mmLDL)

One group has characterised mmLDL, and studied its potential role in atherosclerosis[31]. The entity is mimicked in vitro by incubating LDL in serum-free Dulbecco's modified Eagle's medium for 18 h with 15-LO fibroblasts. This type of modification is recognised by monoclonal antibody EO6 and by lipid hydro peroxides as measured by high pressure liquid chromatography. When compared to oxidised LDL (oxLDL), mmLDL is less readily get taken up by macrophages, but it is thought to prime the macrophage for foam cell uptake by up- regulating scavenger receptor expression [32]

2.1.3.5. Electronegative low density lipoprotein (LDL(-))

LDL(-) is a minor modified fraction of LDL. It comprises a heterogeneous population of LDL particles modified by various mechanisms which share as a common feature increased electronegativity[33]. Modification by oxidation is one of these mechanisms. LDL(-) has inflammatory properties similar to those of oxLDL, such as inducing inflammatory cytokine release in leukocytes and endothelial cells[34]. The role of LDL(-) in atherosclerosis is not yet well described, although there is some evidence that it increases levels of CRP expression in vascular endothelial cells[35]. Furthermore, passive transfer of an IgG2b monoclonal antibody, which is reactive against LDL(-) and present in circulating serum in increased concentration in atherosclerotic mice, reduced development of disease[36]. Another study in children and adolescents showed that offspring of patients with familial hypercholesterolemia (FH), with or without early coronary artery disease in first-degree relatives, have lower titres of anti-LDL(-) (autoantibodies) than children from normal families, independent of serum LDL cholesterol or serum LDL(-). These findings are suggestive of a pathological role for LDL(-), and a protective role for anti-LDL(-) antibodies.

2.1.4 Macrophage handling of modified LDL

Macrophages express scavenger receptors, which contribute largely towards the development of atherosclerotic plaques. Scavenger receptors such as CD36, SR-A I/II, SR-B I and LOX-1 can take up oxLDL[37]. This results in the accumulation of cholesterol esters in the cytoplasm of macrophages, therefore giving rise to foam cells [38]. The aggregation and death of foam cells results in the formation of the atherosclerotic core, which characteristically contains: foam cells, destroyed foam cells, free lipids and cellular debris[39]. The development of the plaque continues with increasing number of foam cells. The vicious cycle of atherosclerosis

is partially driven by cytokines, such as Interleukin 1 (IL-1) and Tumour necrosis factor α (TNFα), which are released by activated macrophages. In addition, the Th1 subpopulation of CD4+ T cells has been shown to be present within the atherosclerotic plaque, with IL-2 and IFN-γ as the major T cell specific cytokines[40]. The accumulative release of cytokines recruits more immune cells including monocytes, causing gradual layering of foam cells around the atheromatous core, which then becomes necrotic, and also in localised regions which form plaque shoulders[39, 41]. There is now extensive literature dealing with the recognition of modified LDL by macrophage scavenger receptors, leading to the above detrimental processes of phagocytosis, foam cell formation, cell stress and apoptosis[42].

Although the receptor-mediated internalisation of modified lipoproteins by macrophages seemingly leads towards a pathological route, it can also facilitate the eventual elimination of these particles from plaques through high density-lipoprotein-dependent mechanisms[22]. Thus the role of the innate immune system in atherosclerosis is that of a double-edge sword where there may be a homeostatic role hidden within the pathological event cycle.

There are other ways in which tissue-bound LDL can be processed by macrophages. Studies using hypercholesterolaemic *ApoE*$^{-/-}$ mice have shown that foam cell formation does not require macrophage scavenger receptors CD36 and SR-A[43, 44]. Importantly, scavenger receptor-mediated phagocytosis may not be possible if LDL is adherent to matrix. Instead, activated macrophages are thought to promote extracellular degradation and aggregation of LDL particles by release of proteolytic (e.g. cathepsin D) and lipolytic (e.g. lysosomal acid lipase) enzymes, resulting in the extracellular accumulation of denatured LDL aggregates, which may then be internalised into macrophages and contribute to foam cell formation[45]. Furthermore, oxidised phospholipids, formed in response to macrophage-derived free radicals, are likely to contribute to macrophage inflammatory activation[46]. This model

therefore places macrophage-mediated extracellular degradation and aggregation of trapped LDL as primary events in the handling of LDL in the arterial wall, with LDL oxidation and phagocytosis of oxidised LDL playing a parallel or even secondary role. How macrophages sense extracellular LDL prior to degrading and aggregating it is largely unknown.

2.1.5 The progression of atherosclerosis is partly driven by multiple pro and anti-inflammatory factors.

2.1.5.1 Role of flow

Atherosclerotic lesions selectively occur at curvatures and bifurcations, probably in relation to vascular endothelium rendered dysfunctional by exposure to complex blood flow and by regional variations in mass-transport[47, 48]. Usually, uniform blood flow within arteries confers protection by the up-regulation of anti-atherogenic, anti-thrombotic, and anti-inflammatory gene signatures[49]. Disturbed flow however, up regulates pro-inflammatory gene signatures and down regulates protective ones, chiefly involving the MAPK, the nuclear factor-kappaB, and the endothelial nitric oxide synthase-NO pathways[49, 50]. This anatomical imperfection has given us the opportunity to study which genes are up regulated in protected areas vs unprotected areas[49]. One example of studies conducted in our group was the activation of sirtuin 1, which suppressed endothelial cell senescence at atheroprone sites[49].

2.1.5.2 Complement plays both an atheroprotective and atherogenic role in atherosclerosis.

In a similar way to other immune mediators, complement has a complex and double-edged role in atherosclerosis. Briefly, activation up to C3 exhibits atheroprotective effects, whereas complement activation beyond C3 has pro-atherogenic effects[51]. The main role of complement is usually homeostatic in removing undesired material. Thus opsonisation by

C3b (amongst other components of the cascade) of apoptotic material promotes homeostatic clearance. If this system is defective, there may be a defective "waste-disposal" effect, and accumulation of debris within the atherosclerotic plaque. Our group has demonstrated that complement C1q reduces early atherosclerosis in *Ldlr*$^{-/-}$ mice [5]. Another group has shown that C3 is also protective as C3 deficiency in a double LDL/C3 knockout mouse leads to greater atherosclerosis and lesions displaying more vulnerable plaque type characteristics, with greater macrophage content and less smooth muscle cells within lesions[52]. On the other hand, a pathogenic role of the alternative complement pathway was shown by Malik et al.[53] who demonstrated that atherosclerosis fails to progress in *Ldlr*$^{-/-}$ animals that also lack Factor B, when compared to animals with an intact alternative pathway. Thus complement has a dual role depending on level of activation.

2.1.5.3 The role of vascular smooth muscle cells

Involvement of vascular smooth muscle cells (vSMC) can be observed in advanced atherosclerotic lesions. These cells secrete extracellular matrix (ECM) proteins, that not only aid in the development of the atherosclerotic plaque, but also result in the formation of the fibrous cap[54]. The fibrous cap is mostly made up of vSMC and collagen, creating a barrier between the vessel lumen and the necrotic core [55]. A thick fibrous cap is considered to be a measure of plaque stability. The proliferation, migration and apoptosis of vSMC are key in determining plaque stability. Thus plaque rupture is associated with apoptosis of vSMC, which are the only cells capable of producing important collagen isoforms that maintain plaque cap stability[56].

2.2 From Stable Atherosclerotic Plaque to Vulnerable Plaque

Progression of the atherosclerotic plaque into a flow limiting obstructive lesion can lead to chronic stable angina. Conversely, death and major morbidity from atherosclerosis is mainly caused by atherothrombotic vascular occlusion, rather than stable atherosclerotic disease[57]. Therefore it is crucial to try and identify the factors that lead to plaque rupture, thrombosis and vessel occlusion. The term 'vulnerable plaque' describes such lesions that are more likely to rupture and in some cases lead to clinical sequelae[58]. The main characteristics of vulnerable plaque are a large necrotic core and a thin fibrous cap[59]. The other important features are summarised in Figure 2.3. In plaque rupture, the constituents of the necrotic core, together with inflammatory macrophages and apoptosis of collagen-producing smooth muscle cells, lead to the thinning and breach in the cap. This in turn exposes lesional thrombogenic material to the lumen, which stimulates thrombosis, leading to ischemia or infarction of distal myocardial or brain tissue. Some of the factors that may contribute to this process are matrix metalloproteinases (MMPs), which are produced by macrophages and cause breakdown of collagen within the fibrous cap, increasing the chances of plaque rupture [60]. There is an array of MMPs that are active in atherosclerosis[60]. The most recent studies in ApoE$^{-/-}$ mice have suggested that MMP13 is more important than MMP8 in degrading atheroma in mice[61]. There are other factors that act on the plaque to make it unstable; for example, Tissue factor (TF) has been identified in human atherosclerotic lesions, and shown to be an important determinant of thrombosis [62-64].

There is now growing evidence that levels of MDA-LDL in blood correspond with both plaque vulnerability, as assessed by interventional imaging[65, 66], as well as on carotid

atherosclerosis ex vivo studies[67]. Exploring the role of oxidised LDL and anti-oxidised LDL antibodies in plaque vulnerability is in need of further study.

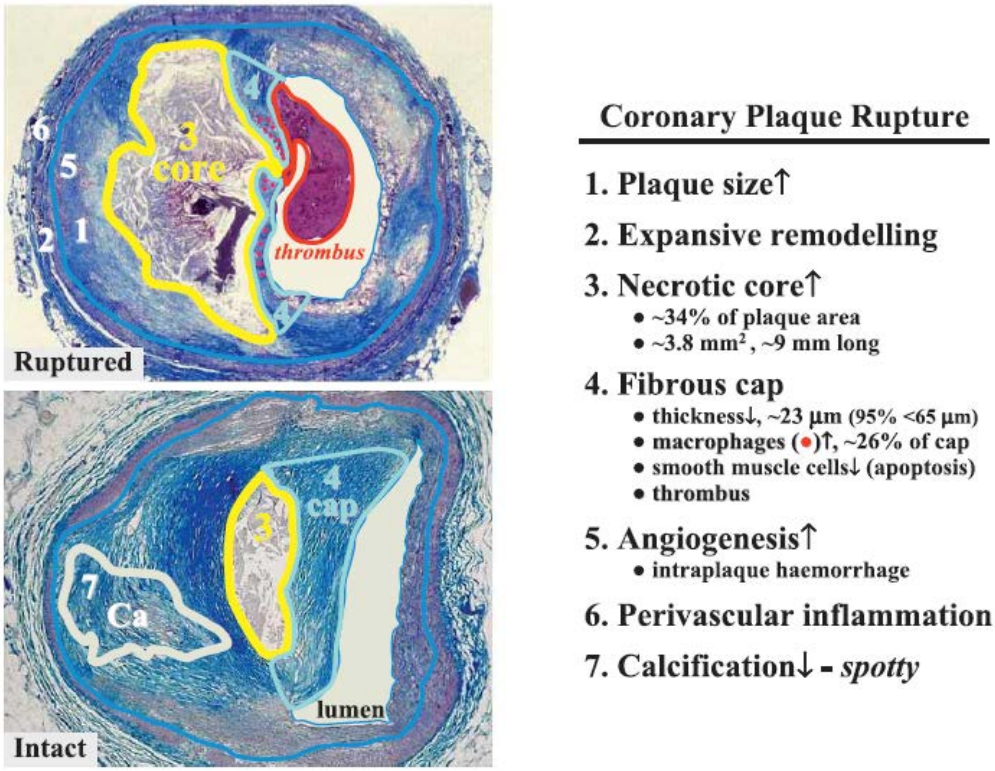


Figure 2.3. Pathological characteristics of both vulnerable and stable plaques. From the European Society of Cardiology (ESC) consensus document 'Stabilization of atherosclerotic plaques'[68]**.** The top cross section demonstrates a ruptured plaque with its characteristic components (details on the right). The bottom section shows a stable atherosclerotic plaque with characteristic thick fibrous cap and a smaller necrotic core.

There is now evidence that 'silent' plaque rupture without the manifestation of clinical events occurs [69, 70]. Thus the presence of vulnerable plaque, as it is currently characterised by morphological imaging methods, may not always lead to a clinical event [59, 71]. Despite this, plaque characterisation and the identification of plaque that is likely to rupture has been shown to predict events in several studies[72, 73]. More studies are needed to first identify the

difference between ruptured culprit plaques responsible for acute events and ruptured non-culprit plaques(RCNP) not responsible for acute events [74] . Molecular imaging techniques, when combined with morphological techniques may improve plaque characterisation to be more clinically robust in predicting which atherosclerotic plaques will lead to overt clinical events[68].

2.3 The role of anti-oxidised LDL antibodies in atherosclerosis.

The reasons for atherosclerotic lesion progression, which may only occur after many years of exposure to classical risk factors, are not well understood. However, research findings over the last few years have increased appreciation of the role of innate and adaptive immunity in atherogenesis. Based on clinical studies on blood and pathological material and on more mechanistic experiments in mice, immunological mediators have been studied and shown to either have a pathological or protective role, and in a complex manner, sometimes both, depending on the surrounding environment[22].

As a chronic inflammatory disease, atherosclerosis involves both the innate and adaptive immune systems[22, 75]. As discussed above, macrophages in particular play an important role in atherosclerosis through uptake and modification of LDL, as well as the formation of foam cells[76 77]. This is countered by the innate humoral immune system (e.g. antibodies, complement and CRP), which removes oxLDL to the reticulo-endothelial system and leads to an adaptive anti-oxLDL response. Moreover, T lymphocytes have been shown to be involved and present within plaque[22].

Immunoglobulin M (IgM) was recently shown by our group[78] to play an inhibitory role, both by inhibiting uptake of oxidised LDL by macrophages, and by helping in the clearance of

LDL through the binding of complement[51, 79]. IgM depletion rapidly accelerates atherosclerosis progression in LDL receptor knockout mice [78]. This is in keeping with previous work that showed ApoE-deficient mice have IgM autoantibodies that can bind to oxidation specific epitopes and inhibit oxLDL uptake into macrophages[80].

Very little is known about the role of IgG antibodies in atherosclerosis[81]. There is now emerging evidence that IgG antibodies can also be protective[36, 82]. This is illustrated, for example, in experiments demonstrating that immunisation with mouse IgG2b mAb against modified LDL can reduce the progression of atherosclerosis in a murine atherosclerotic model[36]. Another study showed that a human-derived anti-oxidised LDL autoantibody, Ik17, blocks uptake of oxidised LDL by macrophages[83]. Furthermore, Ik17 was shown to localise to plaque in animal models[83]. Another group demonstrated that recombinant antibodies to an oxLDL epitope induce rapid regression of atherosclerosis in the *ApoE1* $^{-/-}$, *Ldlr*$^{-/-}$ mice [84]. This can lead to the conclusion that these antibodies play a role in the regulation of the pathogenesis in atherosclerosis.

On the other hand, other experiments have demonstrated marked protection in *Ldlr* $^{-/-}$ mice who also lacked the IgG receptor FcγRIII (CD16)[85]. These mice were shown to have a significantly increased IgG1 and IgG2 titres to OxLDL[85].

The only clinical study to date exploring the possible protective effect of IgG anti-MDA-LDL antibodies as therapeutics was GLACIER (Goal of oxidised LDL and Activated macrophage Inhibition by Exposure to a recombinant antibody)[86], which used a recombinant anti-oxLDL antibody in patients with stable carotid artery or aortic disease. The outcomes were inflammatory read outs including FDG-Positron Emission Tomography (PET). This small trial was reported as negative[87], but is yet to be published.

Thus, the role of these antibodies as either protective or pathological may also be best deduced by studying large cohorts of patients who have had cardiovascular events vs controls. The evidence is discussed below.

2.4 Anti-oxidised LDL Antibodies As Serological Biomarkers in Atherosclerosis

2.4.1 The need for better cardiovascular risk stratification tools

Conventional cardiovascular risk factors and scoring tools such as the Framingham Risk Score are routinely used in clinical practice for predicting adverse cardiovascular events[12]. Despite this, most such events occur in asymptomatic subjects classified as being at low to intermediate risk[57]. Attempts at improving the predictive capacity of risk scoring methods have included the study of novel blood biomarkers[88-90] and coronary artery calcium scoring (CAC) with computed tomography[91], and combinations of these[92]. Nevertheless, other than serum lipids, the need for a cheap and robust non-invasive radiation-free biomarker to improve risk assessment in the asymptomatic population remains largely unmet. Although there has been much interest in the measurement of C-reactive protein (CRP), a recent meta-analysis has concluded that in people without cardiovascular disease, but with an intermediate risk for a cardiovascular event, adding CRP to the risk assessment and treatment could prevent only one additional event over a period of 10 years for every 400-500 people screened[93].

Circulating antibodies against oxidised LDL are readily detected in the general population, with epitope specificities including malondialdehyde (MDA) adducts on the ApoB protein and phosphocholine (PC)[16, 94]. However, despite a relatively large literature, there is relative

paucity of 'hard endpoint' data from randomised controlled trials on the prognostic significance of anti-oxidised LDL antibodies[82].

2.4.2 Summary of the evidence for the use of anti-oxidised LDL antibodies as serological biomarkers of cardiovascular risk

Although several studies have explored the relationship between levels of these antibodies and cardiovascular disease (CVD), there remains a notable knowledge-gap with respect to their pathological significance[95, 96]. Tsimikas et al. prospectively studied the Bruneck study population[97]. They demonstrated that IgG antibodies against copper-oxidised LDL (a heavily oxidised type of LDL that includes the MDA-LDL epitope[14]) were associated with higher risk of CVD; whilst IgM MDA-LDL levels were associated with lower risk. This was also shown in other studies that correlated IgG anti-oxidised LDL antibodies with worse atherosclerosis in peripheral vascular disease (PVD)[81] and possibly unfavourable acute coronary syndrome outcomes[98, 99]. The body of evidence also includes some work that associates IgG anti-MDA-LDL antibodies with protection from coronary artery disease [100]. Another study showed an inverse relationship between IgG anti-MDA-LDL antibodies and PVD only in men[19].

Another paradigm for the role of these antibodies was suggested by the EPIC Norfolk study [101], implicating anti-MDA-LDL IgG and IgM, not as independent predictors of coronary artery disease (CAD) events, but as possible modifiers of the risk associated with other oxidative biomarkers. They found that IgG levels potentiated the risk associated with sPLA(2), whilst IgM reduced the risk associated with Lp(a).

There is a mounting interest in the protective effect of IgG and MDA-LDL antibodies, mainly arising from mechanistic animal work[83, 102], which was encouraging enough to take the work forwards into the GLACIER human vaccination phase 1-IIa study as discussed above[103].

IgM antibodies in general have been shown to be crucial for protection against atherosclerosis in mice[78], and in addition to the Bruneck study and EPIC- Norfolk studies[97], there is some further evidence on the protective effect of IgM anti-oxidised LDL antibodies in humans[82, 104, 105]. In the Women's Ischemia Syndrome Evaluation Study (WISE) [105], there also was a protective effect of lower IgM anti-oxidised LDL antibodies on angiographic coronary disease, but no correlation between IgG antibodies and coronary stenosis.

Thus there remains a need to explore the role of these antibodies in either protecting or conveying risk to populations. Most importantly evidence is still lacking in non-symptomatic populations where these levels may add to the risk stratification protocols that utilise classical risk factors to predict incident cardiovascular events.

2.5 Measuring Circulating OxLDL

There is now growing evidence for the presence of oxidised LDL not just in the atherosclerotic plaque but also in serum and plasma with levels reflecting patient vulnerability in various scenarios[83, 106, 107]. Measuring levels of oxidised LDL is challenging using classical biochemical assays. The role of specific and sensitive antibodies against different types of oxLDL is growing in developing assays for the measurement of oxLDL levels in blood. E06[108] and DLH3[109] both bind PC and 4E6 binds MDA-LDL[110, 111]. Holvoet and his colleagues were the first to clearly demonstrate using the specific murine monoclonal antibody 4E6 in a competition Enzyme-linked immunosorbent assay (ELISA) that patients

with CAD had significantly elevated plasma levels of MDA-LDL[112]. The same group demonstrated that the longitudinal stability of circulating oxLDL, as assessed by multiple measures in people over time, is similar to that of total cholesterol and CRP[113].

Furthermore, in order to align the identification of the vulnerable patient with the presence of vulnerable plaque, another group found MDA-LDL levels as measured by the 4E6 assay were associated with the presence of thin Cap Fibro Atheromas (TCFAs) as determined by Optical Coherence Tomography (OCT) [66].

The largest trial studying the utility of measuring MDA-LDL levels prospectively as a biomarker of CAD was undertaken in 18,140 men and 32,836 women, with follow up for up to 8 years, using non-fatal myocardial infarction (MI) or fatal CAD as endpoints[111]. Amongst both men and women, oxLDL was significantly related to risk of Coronary Heart Disease (CHD) in multivariate analysis before adjustment for any lipid markers. However, when oxLDL, LDL cholesterol, HDL-C, and triglycerides were mutually adjusted, oxLDL was no longer predictive. When oxLDL and apoB were mutually adjusted, only ApoB was predictive of CHD. Thus, this study suggested that circulating oxLDL, measured with antibody 4E6, is not an independent overall predictor of CHD after adjustment of lipid markers and is less predictive in development of CHD than apoB and TC/HDL-C ratio[111].

2.6 Imaging Beyond the Lumen. Plaque Characterisation Using Morphological Imaging Techniques.

Better understanding of plaque vulnerability has emerged from the use of various imaging techniques, such as coronary angiography, Intravascular ultrasound with Virtual Histology analysis (IVUS-VH) [114, 115], OCT[116], and some non-invasive techniques such as Coronary

Artery Computed Tomography (CTCA)[117, 118]. All of these techniques rely mainly on plaque morphology to stratify the risk of plaque rupture. Some of these modalities have entered the clinical world and are being widely used by interventional cardiologists for the assessment of complex CAD and disease progression[114, 119]. The value of the non-invasive techniques such as CTCA, used on its own, without a hybrid functional imaging modality, tends to be in a narrow patient population where calcification truly reflects risk[117]. The more invasive techniques such as IVUS and OCT are seen to be more sensitive for the detection of vulnerable atheroma in humans[119]. Despite this, Thim et al[120], found no correlation between necrotic core size determined by VH-IVUS and real histology in the pig, questioning the ability of VH-IVUS to detect rupture-prone plaques, particularly in the porcine animal model that was used.

More recently, attempts at combining anatomical assessment methods with functional perfusion testing using both invasive and non-invasive modalities have been made, but are yet to be validated[121].

Near-infrared spectroscopy (NIRS) (Figure 2.4) has also been used to intravascularly acquire a 'chemical' signature of lipids within plaque. James Muller *et al*[122] developed a pullback, rotation device, and a dedicated console, comprising a laser light source and a computer that automatically analyses the data. The laser system uses wavelengths of 800 to 2500 nm, converting a diffuse reflectance signal from an object to produce a spectrum. Subsequently, a computer analyses the spectra and produces an algorithm to demonstrate a chemogram that should chemically correspond to lipid content. The initial data suggests that Near-Infrared Spectroscopy (NIRS) derived signals can reflect the 'regression' effect that maybe expected in lipid content of statin treated patients' arteries[123]. Although in its infancy, this technique may be able to reflect the total amount of lipid present in atherosclerotic plaque, but would

not be capable of conveying molecular activity or level of oxidation of the lipid seen in the plaque areas[124, 125].

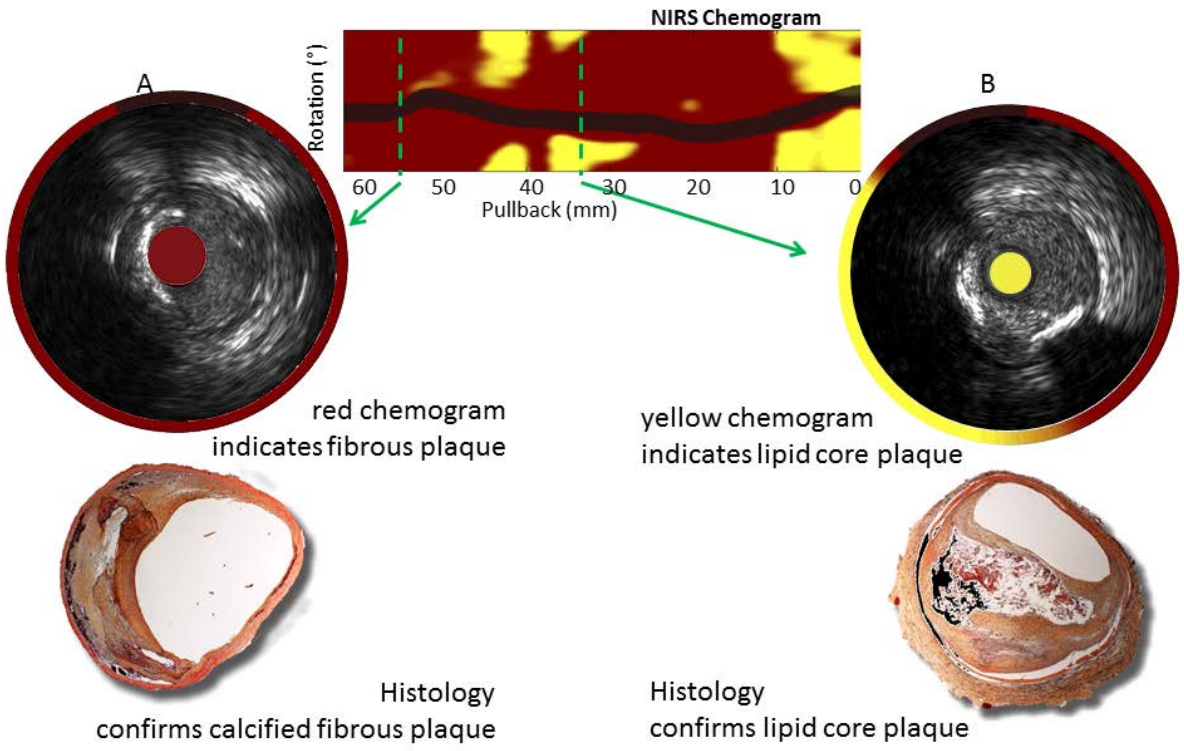


Figure 2.4 Chemograms derived from NIRS, combined with IVUS.

(A) Image on the left demonstrates a fibrous plaque on both IVUS and NIRS (red) with corresponding histology showing the same. The right panel (B), demonstrates a yellow chemogram, representing a lipid core, with corresponding IVUS demonstrating anatomical co-localisation, and corresponding histology is shown below. (Images Courtesy of InfraRedex).

2.7 Molecular Imaging of Atherosclerosis- Visualising the Invisible.

To further stratify plaque in terms of biological activity, efforts in identifying 'biological' targets for imaging plaque activity are underway[126, 127]. Molecular imaging in general has emerged as a collection of novel techniques aimed at "the visualisation, characterisation, and measurement of biological processes at the molecular and cellular levels"[128]. Many molecular targets in imaging of atheroma have been attempted, with various modalities, namely CT, Ultrasound, MRI, and radionuclear Single Photon Emission Computed Tomography (SPECT) and Positron Emission Tomography (PET) scanning. [126]

2.7.1 Requirements for successful molecular imaging of atherosclerosis

Targeting atherosclerosis with molecular probes requires three components: first, the targeting ligand; second, the contrast agent, such as a radionuclear isotope; and thirdly a suitable device to detect the 'contrast agent' such as a PET scanner or an optical scanning console.

2.7.2 Non-optical imaging modalities:

PET offers the advantage of a much superior sensitivity to MRI or ultrasound, offering a suitable modality for molecular imaging of atherosclerosis. The sensitivity of PET can allow for the detection of low concentrations of a specific tracer in the picomolar range[129]. The advantage that PET offers over the few other equally sensitive techniques, such as optical imaging using bioluminescence, is the deep penetrative ability, allowing the technique to be used non-invasively[126, 129]. Furthermore, it is now possible to conduct high resolution coronary artery CT scanning simultaneously with PET scanning, and superimpose the PET images, allowing for both morphological and biological activity data to be available simultaneously[71]. PET also offers the opportunity to perform quantitative analyses, which are

important in translational research and can facilitate the objective analysis of plaque progression/activity in response to therapeutic agents. Having the ability to accurately provide functional quantitative information, such as the density of a specific protein marker, greatly enhances the role of PET as a research technique in comparison to the other non-nuclear based techniques, which provide mainly subjective data[130]. Studies such as IBIS 2, which investigated the effects of the direct lipoprotein-associated phospholipase A2 inhibitor, Darapladib, on human coronary atherosclerotic plaque had to use invasive morphological assessment with IVUS-VH in order to obtain meaningful data[114]. The development of PET/CT as an alternative modality would allow for similar studies to be conducted without the added risk of interventional cardiology modalities[131]. It is also worth noting that the use of interventional techniques does not forgo the use of ionisation radiation. In fact a coronary angiogram with IVUS imaging can expose the patient to more radiation than a CT/PET study[132]. MRI and ultrasound modalities have yet to bridge the sensitivity gap between them and PET in order to compete as prime time molecular imaging techniques with quantification tools[129].

The disadvantages of using PET include the need for ionising radiation, relatively low spatial resolution and, when intended for clinical use, the scarcity of the resources available. The use of very short half-life isotopes such carbon-11 (~20 min), nitrogen-13 (~10 min), oxygen-15 (~2 min), and fluorine-18 (~110 min), to yield high sensitivity imaging data, means that often the presence of an onsite cyclotron to generate the isotopes is needed. More recently rubidium-82 generators have become commercially available. These generators contain strontium-82 which decays by electron capture to positron-emitting rubidium-82. It has been demonstrated that rubidium-82 imaging can be used for the quantitative imaging of

myocardial blood flow [133]. Table 2.1 shows the different imaging modalities and compares their relative sensitivities, spatial and temporal resolutions.

Imaging Modality	Spatial Resolution	Depth of Penetration	Temporal Resolution	Sensitivity (mol/L)	Molecular Probe
PET	1–2 mm	No limit	sec–min	10^{-11}-10^{-12}	ng
SPECT	0.3–1 mm	No limit	min	10^{-10}-10^{-11}	ng
Bioluminescence	3–5 mm	1–2 mm	sec–min	10^{-15}-10^{-17}	ng– μg
Fluorescence	2–3 mm	1 mm	sec-min	10^{-9}-10^{-12}	ng- μg
FMT	1–3 mm	5 cm	min	10^{-6} -10^{-12}	μg
MRI	50–250 μm	No limit	min–hrs	10^{-3}-10^{-5}	μg –mg
X-ray CT	25–150 μm	No limit	min	?	mg
Ultrasound	30–500 μm	mm–cm	sec–min	10^{-6}-10^{-9}	μg –mg

Table 2.1 Comparison of imaging technologies. **Adapted from Sinuses et al.[129]** PET indicates positron emission tomography; SPECT, single photon emission CT; FMT, Fluorescence molecular tomography.

2.7.3 The development of Near-Infrared Optical imaging into 'state of the art' molecular imaging technology

The most commonly used modality for the study of optical molecular imaging in the small animal model has been the IVIS systems from Caliper[134]. However the fluorescence capability of the IVIS technology has yet to be shown effective in imaging diffuse signalling events in deep tissue, which includes the imaging of atherosclerotic plaques in the vicinity of the heart, and this remains an area to which no published data exist using the IVIS system, including the most advanced Spectrum system. Fluorescence Molecular Tomography (FMT)

is a recently developed technology that bridges the gap between sensitivity, penetrance and resolution for small animal imaging. The development of NIRF probes for in vivo molecular imaging has greatly reduced the issue of autofluorescence arising from animal tissue -as light absorption by physiologically abundant molecules (e.g. haemoglobin, oxyhaemoglobin, deoxyhaemoglobin and, to a lesser extent, water) is reduced to a minimum. The newer highly developed FMT imaging systems that allow for sensitive molecular imaging and anatomical co-localisation with CT have revolutionised the ease in which studying molecular targets may be conducted without the use of ionising radiation and offer a near-equivalent to PET.

A clear translational advantage of FMT over other techniques, including PET, is the capacity to integrate well with traditional laboratory techniques. For instance, confocal microscopy and FACS can measure fluorescent molecular agents following in vivo imaging. The multichannel capabilities of optical imaging, which are already widely exploited in multicolour flow cytometry or immunofluorescence histology, are increasingly used in vivo to interrogate several targets simultaneously. This allows investigators to pursue systems approaches not limited to a single biomarker.

A limitation of NIRF for interventional multimodality imaging in humans and large animals is lack of depth [135]. However the development of combined 2D and 3D anatomical and NIRF catheters provide NIRF with huge translational potential for intravascular imaging[136 135 137]. Jaffer et al have demonstrated the first ever intravascular molecular imaging of atherosclerotic plaque *in vivo* by using a novel 2D intravascular NIRF catheter as a tool for high resolution in vivo spatial mapping of arterial inflammation in coronary-sized arteries in a rabbit model[136]. They revealed increased inflammation-regulated cysteine protease activity in atheromata and stent induced arterial injury. Following this advance, a 3D combined NIRF/optical frequency domain imaging (OFDI) catheter was designed (Figure 2.5A and

2.5B) and further replicated elsewhere [137, 138] to allow for the combined three dimensional simultaneous acquisition of morphological data using OCT and molecular data using NIRF tagged agents.

In this thesis we will demonstrate the use of three optical imaging techniques including IVIS Spectrum fused with CT (done at Imperial), FMT fused with CT (done at Imperial) and intravascular NIRF merged with IVUS (done at Harvard).

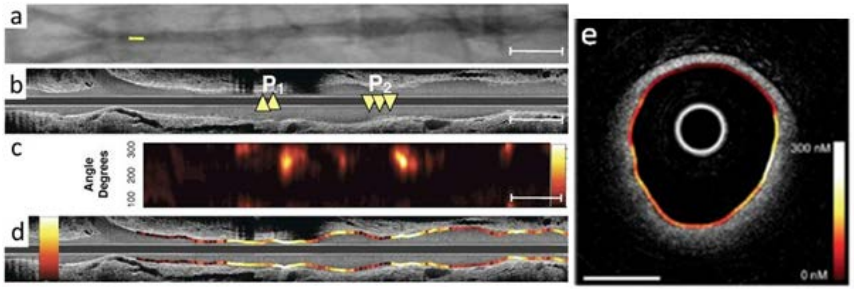


Figure 2.5. Intravascular NIRF molecular imaging. Adapted from Jaffer et al with permission ([139]).Left panel- Standalone intravascular NIRF molecular imaging of inflammatory cathepsin protease activity in atherosclerosis. A rabbit with atheroma was injected with a specialised NIRF cathepsin protease activatable imaging agent, Prosense VM110, 24 h before imaging. (a) Angiography of rabbit aorta, showing radiopaque tip of the imaging catheter in the distal aorta, co-registered with IVUS shown in a longitudinal view (b) with two plaque zones (P1, P2). (c) Aligned pullback image of measured NIRF signal of the catheter along the aorta (vertical axis is rotational 0–360°), demonstrating increased signal in small volume plaques. (d) Fused IVUS and NIRF longitudinal map (yellow/white=strongest NIRF signal, red/black=lowest NIRF signal). (e) Hybrid, fully integrated NIRF/OFDI of atherosclerosis using a single catheter.

2.8 Agent Development for the Molecular Imaging of Atherosclerosis.

2.8.1 Molecular targets and the challenge of translation.

The challenge of any molecular targeting agent is to have adequate sensitivity and specificity and also be readily either metabolised or excreted in order to allow for an imaging compatible target to background ratio (TBR) [139]. There are many preclinical molecular targeting agents that may not be suitable for translation into humans and therefore would only be suitable as research tools in preclinical study models.

Table 2.2 below lists most of the currently available molecular imaging agents that are suitable for human use.

Agent	Modality	Primary Target	Clinically Tested
FDG	PET	Glucose transporter-1, hexokinase	Yes
NaF	PET	Hydroxyapatite	Yes
11C-acetate	PET	Fatty acid synthetase	Yes
[11C]-(R)-PK11195	PET	Benzodiazepine receptor/macrophages	Yes
11C-KR31173	PET	Angiotensin II type I receptor	Yes
18F-EF5	PET	Hypoxic cells	Yes
64Cu-DTPA-ProT	PET	Staphylocoagulase	No
99mTc-annexin V	SPECT	Annexin/macrophages	Yes
99mTc-RIP (radiolabelled RGD imaging peptide)	SPECT	Î±vÎ²3 Integrins	Yes
99mTc-exametazime leukocytes	SPECT	White blood cells	Yes
111In-RP782	SPECT	Matrix metalloproteinases	No
99mTc-RP805	SPECT	Matrix metalloproteinases	No
99mTc-fucoidin	SPECT	P-selectin	No
99mTc-NC100692	SPECT	Î±vÎ²3 Integrins	No
N1177	CT	Macrophages	No
P-selectin microbubbles	Ultrasound	P-selectin	No
Supravist (SHU 555 C)	MRI	Macrophages	Yes
SPIO/USPIO	MRI	Macrophages	Yes
EP-2104R	MRI	Fibrin	Yes
P947	MRI	Matrix metalloproteinases	No
FeCo/graphite nanocrystals	MRI	Macrophages	No
158Gd-ESMA	MRI	Elastin	No
BMS-753951	MRI	Elastin	No
CNA-35	MRI	Collagen	No
Gd-TO	MRI	DNA	No
VS-580H	MRI	Macrophages	No
SPIO-labelled EPC	MRI	Endothelial progenitor cells	No
Human ferritin cages	MRI, NIRF	Macrophages	No
Î±vÎ²3-Targeted nanoparticles	MRI, NIRF	Î±vÎ²3 Integrins	No
18F-CLIO	MRI, NIRF	Macrophages	No
ICG	NIRF	Lipids/macrophages	Yes
ProSense	NIRF	Cysteine proteases	No
MMPsense	NIRF	Matrix metalloproteinases	No
FTP11-Cy7	NIRF	Fibrin	No

Table 2.2. Clinically Targeted Molecular Imaging Agents that may be used in atherosclerosis. Adapted from Jaffer et al [139].

2.8.2 Radionuclear and MRI based Molecular targets

Several radiotracers have been developed to explore plaque vulnerability in particular. ^{99m}Tc-labelled monocyte chemoattractant protein 1 has been used to study intraplaque cell recruitment, which reflects early endothelial dysfunction and atherosclerosis progression [140]. Intraplaque metabolic activity has also been studied by using ^{18}F-radiolabelled Fluorodeoxyglucose (FDG) PET [131]. A proof of concept paper demonstrated that ^{18}FDG micro PET imaging can be used for quantifying aortic wall macrophage content in a rabbit model of atherosclerosis[141]. There is a big question regarding the natural history of ^{18}FDG uptake into atherosclerotic lesions, and whether it is a transient phenomenon[142]. This further underlines the need for a robust specific molecular target with potential translational utility into clinical use.

Adhesion molecules such as E-Selectin, VCAM-1 and ICAM-1 have been used to target atherosclerosis with multimodality imaging techniques.[127] Jamar et al utilised a Fab fragment of an antibody against E-selectin coupled to ^{99m}Tc to image inflammation in rheumatoid arthritis, with good diagnostic sensitivity[143]. Furthermore, the same target was shown to be quantitatively detectable utilising in vivo fluorescence imaging using a small animal model[144]. Hua et al constructed a ^{99m}Tc-labelled peptide targeted at imaging angiogenesis in an ischaemic hindlimb mouse model[145]. The peptide selectively localised to endothelial cells in regions of increased angiogenesis, and could be used for serial tracking of the extent of angiogenesis. More recently, Nahrendorf et al were successful in utilising a radiolabelled peptide (^{18}F-4V) for PET-CT imaging of VCAM-1 expression in a murine model of atheroscloris[146]. They demonstrated co-localisation of ^{18}F- tracer to atheroma using microPET, proven with immunocytochemistry techniques and *en face* lipid staining.

Another target for molecular imaging is the oxidised LDL receptor (LOX-1) which may mediate pathologic effects of oxLDL in atherosclerotic lesions.[147] This was successfully targeted by Li et al, in an ApoE -/- mouse model using multimodality SPECT/CT and magnetic resonance imaging[148]. It was demonstrated by in vitro fluorescence that the LOX-1 probe bound preferentially to the plaque shoulder, a region associated with vulnerable plaque.

A further target using ^{99m}Tc is tissue factor (TF), which is a transmembrane glycoprotein that acts as an essential cofactor to factor VII/VIIa, and which initiates the exogenous blood coagulation cascade leading to thrombin generation and subsequent thrombus formation in vivo. Using a ^{99m}Tc-labelled monoclonal antibody against TF, the Kyoto group showed that myocardial infarction-prone Watanabe heritable hyperlipidemic rabbits had a 6.1 fold increase in tracer uptake within their aortas (mainly in the intima) in comparison to wild type control rabbits [149].

2.8.3 Optical molecular imaging targets

This is a relatively new field and the agents are mostly in preclinical development phases. The attraction of optical agents is that they provide excellent versatility in preclinical imaging, especially when used with the FMT system, which has multiple lasers, allowing for simultaneous monitoring of multiple molecular processes[134]. There are only a few examples where optical imaging has been used to study atherosclerosis[150]. Early studies demonstrated feasibility of detecting MMP activity in atherosclerotic mouse models, albeit not in a quantitative manner [151], More recently Lin et al, using FMT, demonstrated that two commercially available agents that detect cathepsin (ProSense) and alpha(v)beta(3) integrin (CatB FAST) NIRF agents could be used in the longitudinal detection of atherosclerosis[152]. Testing the effects of ezetimibe (a cholesterol lowering agent) in the ApoE mouse model,

they demonstrated a correlation of imaging both signals in vivo with lesion macrophage count [152]. Naherndorf et al have also shown that FMT-CT is a robust and observer-independent tool for noninvasive assessment of inflammatory murine atherosclerosis using different pilot protease activity sensors. [153] The same group has been using metalloprotease reporters to demonstrate the effect of different treatments on plaque inflammation progression [154]. Jaffer's group have also demonstrated the feasibility of optical imaging of atherosclerotic plaque burden using indocyanine green (ICG), a Food and Drug Administration-approved NIRF-emitting compound, both in the rabbit aortic injury model and in pilot human ex vivo studies. They demonstrated that ICG co-localised with plaque macrophages and lipids. ICG does not specifically target a molecular pathway, but is a promising clinical agent that can be easily injected into man[155]. Some more recent attempts to image atherosclerosis with antibodies has included experimenting with an undefined commercially available polyclonal antibody to Cu-oxLDL. This utilised some *in vivo* but mainly *ex vivo* basic non-quantitative 2D NIRF reflectance imaging in the murine *ApoE*$^{-/-}$ model [156]. Despite these efforts, there has been little published to demonstrate the quantitative optical imaging of oxidised LDL in vivo and comparing it to other inflammatory markers, such as MMP activity.

There a few other commercially available agents that may be useful for imaging the different aspects of atherosclerosis (Table 2.3), and may have promise for a multimodality approach to the assessment of vulnerable atherosclerotic plaque

Agent	Agent type	Mechanism	Available Wavelengths and optimal *in vivo* imaging time (post injection)
ProSense	Activatable; fluorescence	Broadly detects cathepsin activity which is upregulated in inflammatory cells such as foam cells. It is taken up in the lysosomes of inflammatory cells associated with atherosclerosis and cleaved by multiple cathepsins, activating fluorescent signal.	680 nm (24-48 hours) 750 nm (FAST) (24 hours) 750 nm (6-24 hours)
Cat B FAST	Activatable; fluorescence	Taken up into the lysosomes of atherosclerosis-associated inflammatory cells and is selectively activated by cathepsin B.	680 nm (36 h) 750 nm (36 h)
Cat K FAST	Activatable; fluorescence	Selectively activated by osteoclast-associated cathepsin K at sites of bone resorption or tissue calcification. This may be used in later stages of atherosclerosis development when calcification occurs.	680 nm (6-24 h)
MMPSense	Activatable; fluorescence	protease activatable fluorescent in vivo imaging agent that is activated by key matrix metalloproteinases (MMPs) including MMP-2, -3, -9 and -13. MMPSense is optically silent in its inactivated state and becomes highly fluorescent following protease-mediated activation.	645 nm (4-24 h) 680 nm (24-36 h) 750 nm (12-24 h)
Annexin-Vivo	Targeted; fluorescence	Targeted probe that labels cells that are undergoing the early stages of apoptosis. It is useful in visualising the progression of atherosclerosis as cellular necrosis occurs increasingly during later stages of the disease.	750 nm (2 h)
IntegriSense	Targeted; fluorescence	Small molecule αvß3 integrin antagonist that contains a NIR fluorophore reporter. This targeted agent detects increased integrin expression associated with neovasculature, tumours, and some inflammatory cells associated with atherosclerosis.	645 nm (48 h) 680 nm (24 h) 750 nm (24 h)
OsteoSense	Targeted; fluorescence	Bisphosphonate imaging agent that enables imaging of bone growth and resorption; can be used to measure bone cancer metastasis.	680 nm (3-24 h) 750 nm (3-24 h) 800 nm (3-24 h)
AngioSPARK	Vascular; fluorescence	Pegylated fluorescent nanoparticles that remain localised in the vasculature for extended periods of time and enable imaging of blood vessels and angiogenesis.	680 nm (0 - 4 hours)

Table 2.3. A collated list of commercially available optical molecular probes that may show promise in the translational space of imaging atherosclerosis. All are supplied by Perkin Elmer (PerkInElmer.com)

2.9 Antibody-based Imaging of Oxidised LDL Targets

The capacity of serum antibodies to bind oxLDL within atherosclerotic lesions can be exploited for in vivo targeting of atherosclerosis. Thus successful atherosclerosis imaging has been reported in preclinical studies using conventional antibodies conjugated with single photon emitting isotopes, or MR-contrast agents [83, 157-159]. It has been demonstrated that is possible to image IgG antibodies to oxidised LDL in murine models[17]. MDA2 is a murine IgG monoclonal that binds MDA modified LDL and other modified LDLs, but not native LDL. It was shown to identify early atherosclerosis in a murine model. IK17 is a human IgG fragment that was shown to bind MDA and copper modified LDL. These antibodies were imaged with MRI and SPECT techniques, but not with PET[17]. Applying this approach to computer tomography–positron emission tomography (CT-PET) imaging offers the opportunity of sensitive detection of oxLDL epitopes in relation to arterial anatomy.

In terms of optical imaging, the antibody targeted efforts to image oxLDL are limited to the one study mentioned above by Lu et al[156],demonstrating non-quantitative mainly ex vivo imaging using a polyclonal antibody that lacks characterisation and is therefore impossible to translate for human use.

An imaging strategy focused on monoclonal antibodies and their derivatives could allow the quantitative evaluation of therapeutic interventions designed to lower the deposition or modification LDL in the arterial wall. Furthermore, the successful targeting of antibodies to atherosclerotic lesions could lead on to the delivery of therapeutic agents, for example in the context of plaque instability. It should be noted that targeting of oxLDL rather than a cell surface antigen has the advantage of avoiding antibody-mediated modulation of cell function, which may down regulate antigen expression and/or stimulate untoward functional effects.

2.10 Use of Recombinant Antibodies to Optimise in Vivo Imaging and Allow for Further Translational Use.

The cloning of immunoglobulin heavy and light chain variable regions (VH and VL respectively) provides the means to manipulate antibody size and effector function. Proteolytic cleavage of the whole antibody releases Fab fragments (50kD) that behave in a similar way to the original antibody. Another example is single chain variable region antibodies (scFv) which consist of VH and VL domains joined by a flexible linker. scFv antibodies are only ~25kD and have greater tissue penetrability and faster blood clearance compared with native IgG (150kD) or IgM (900kD). Provided affinity of the monovalent scFv is sufficient, these qualities provide increased imaging signal to background ratios compared with native antibodies. To increase binding potential, a diabody construct can be made (Figure 2.6), which still is a significantly smaller structure than IgG, but has higher avidity than the scFv. Furthermore, the lack of an Fc domain in scFv antibodies leads to minimal unwanted interactions with complement and Fcγ receptors. Molecular attachment of appropriate tags to recombinant antibodies allows conjugation to single photon emitting or positron-emitting radioisotopes for SPECT and PET imaging respectively. Work done in the field of oncology has demonstrated that the use of recombinant antibodies for imaging is possible. A group from UCLA has successfully utilised an affinity-matured minibody for PET imaging of prostate stem cell antigen-expressing tumours in a murine model[160]. The same group have also used an anti-CD20 diabody for the PET imaging of lymphoma in a murine model.[161]

Changing the size of antibody constructs will have an effect on the clearance dynamics and penetration into tissues, and thus the length of presentation time to the antigen. Furthermore,

there is some evidence that antibody penetrance of atherosclerotic lesions is proportional to their vulnerability. Thus, plaque histology of autopsy lesions from patients revealed that larger particles such as IgM can penetrate into vulnerable plaque[162]. The Histamine-1 receptor was also shown to promote atherosclerosis in a knockout mouse model[163]. The mechanism is increased vascular permeability possibly allowing more LDL into the atherosclerotic lesions. Penetrance into atherosclerotic lesions may also be different for the different construct sizes, possibly allowing us to differentially identify a more permeable plaque from a less permeable plaque.

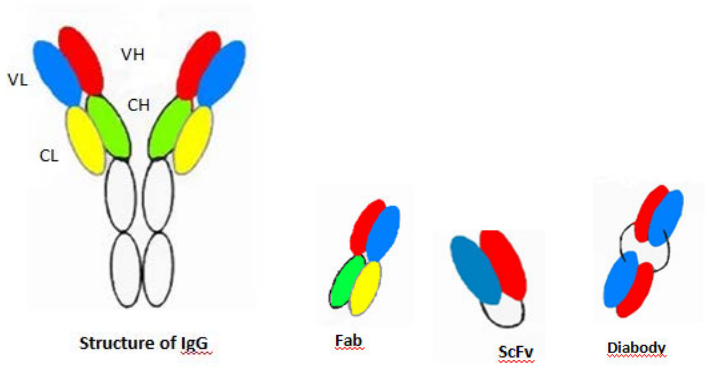


Figure 2.6. Schematic representation of various engineered antibody fragments. Whole IgG antibody (~150KD), Fab fragment (~50KD), ScFv (~25KD), Diabody (50KD)

Therefore using molecular recombinant engineering techniques, it may be possible to express antibodies as chimeric or fully humanised constructs which are poorly immunogenic and suitable for clinical use. These may be varied in size and valency, and may have molecular tags added to allow labelling[160, 161]. Apart from its potential for molecular imaging, antibody targeting may lead on to the delivery of therapeutic agents for the unstable plaque, as demonstrated in oncology studies[164, 165].

2.11 Work Leading Up to the Project and Pilot Data

2.11.1 Introducing LO1 and LO9

Features of many natural IgM anti-oxLDL antibodies have low affinity, polyreactivity and lack of unique antigen specificity. In order to obtain a specific affinity-matured IgG anti-oxLDL antibody for clinical applications, our group generated IgG monoclonal antibodies (mAb) from a relatively old (i.e. one year) atherosclerotic (*Ldlr*$^{-/-}$) mouse. The spleen of this one year old mouse was used to generate hybridomas, without immunisation. A few antibodies were identified, including mAb LO1 and mAb LO9 (referred to as LO1 and LO9 respectively from now on). LO1 which is an IgG3 kappa antibody, reacts well with malondialdehyde-conjugated LDL (MDA-LDL). It does not react with native LDL, and also reacts with copper-oxidised LDL (Cu-oxLDL) (which contains MDA-LDL). LO9, which is an IgG2b antibody, reacts with native LDL adherent on plastic but not with MDA-LDL or Cu-oxLDL. Both these antibodies may be useful probes for imaging atherosclerosis. LO1 was thought to be more suitable for translation as a tool for assessing vulnerable coronary plaque because it was shown in the pilot data to react with heavily modified LDL, possibly reflecting its potential as an identifier of advanced disease with vulnerable plaque. At the start of the thesis work, the binding of LO9 required characterisation.

Furthermore, by screening a phage library expressing single chain variable region antibodies (ScFv), our group selected an anti-idiotype scFv (designated H3) that neutralises LO1 binding to MDA-LDL. This anti-idiotype to LO1 was generated in order to facilitate further work by creating a reliable antigen that can be used for testing LO1 and the various constructs that will be produced. Amino acid substitutions between H3 and an irrelevant control scFv C12 showed that residues in the H3 CDRH2, CDRH3 and CDRL2 are all critical

for LO1 binding, consistent with a conformational epitope on H3 involving both heavy and light chains. Comparison of amino acids in H3 CDRH2 and CDRL2 with apoB, the major LDL protein, showed homologous sequences, suggesting H3 has structural similarities to the mAb LO1 binding site on MDA-LDL (Figure 2.7).

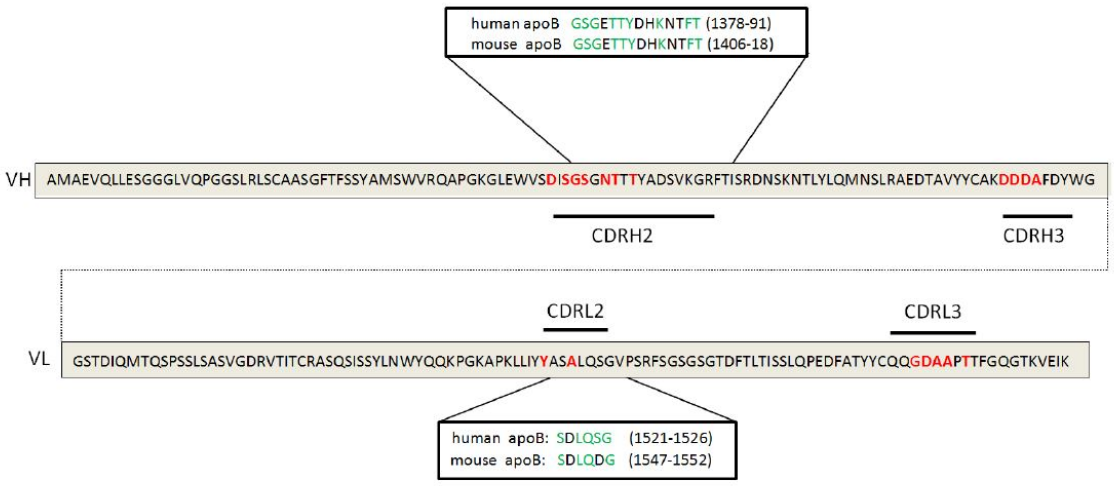


Figure 2.7 Peptide sequence of both the heavy and light chains of H3. Similarities between H3 and ApoB in both mouse and human are highlighted in the boxes. Note the VH also contains a DDD sequence at CDRH3 which may be crucial in providing the positive charge needed for LO1 to interact with the proposed conformational epitope on H3.[166]

We will discuss the detailed characterisation of LO1 and LO9 in this thesis, together with their development into potential imaging agents.

2.12 Aims and Hypotheses

In this thesis we aimed to develop serological assays for the estimation of anti-oxidised LDL antibodies in serum, and to test their utility in a well characterised population as independent serological biomarkers of cardiovascular risk.

We further aimed to develop an antibody-based strategy for the NIRF imaging of atherosclerosis in experimental animal models and further develop partially humanised antibody constructs for the translational development of imaging oxidised LDL in human.

Thus we aimed to test the following hypothesis:

1) Anti-oxidised LDL antibodies, as measured in serum, may be utilised as independent biomarkers for estimating incident cardiovascular events in a well characterised subpopulation of the Anglo-Scandinavian Cardiac Outcomes Trial (ASCOT).

2) LO1, an anti-oxidised LDL antibody, can be characterised as an anti-MDA-LDL antibody in *vitro* and can be used for the *in vivo* NIRF fluorescence imaging of oxidised LDL in experimental atherosclerosis.

3) LO1 can be expressed into a functional chimeric Fab for the translational development of its future use as a molecular targeting agent of atherosclerosis in humans.

4) LO9 can be characterised and further developed into a possible molecular targeting agent in atherosclerosis.

3.0 Methods

3.1 Study Ethics

All human samples including carotid tissue, and blood samples were collected with consent and institutional and national ethical approval. All human studies were subject to the study protocol and conformed to the ethical guidelines of the 1975 Declaration of Helsinki, as reflected in a prior approval by the participating institutions research ethics committees.

All animal studies were ethically reviewed. Mouse studies were undertaken at Imperial and were carried out under the authority of UK Home Office licenses. Rabbit studies were undertaken at Harvard in accordance with US legislation. All animal studies complied with our collaborator GSK Policy "Care, Welfare and Treatment of Animals".

3.2 LDL Modification

3.2.1 Generation of Malondialdehyde-conjugated MDA-LDL

MDA-LDL was prepared as described by Palinski et al through the modification of LDL extracted from human plasma (Merck Millipore, London, UK) [16]. Briefly, LDL was eluted with phosphate buffered saline (PBS) through a PD-10 desalting column (GE healthcare, London, UK) to remove preservative (0.01% EDTA). 0.5M MDA solution was prepared through the acid hydrolysis of MDA-bis-dimethyl acetal and then incubated with LDL, at a ratio of 100µl MDA solution per milligram of apoB, for 3 hours at 37˚C. Following modification, the MDA-LDL conjugate was then eluted with PBS through a PD-10 column and 0.01% EDTA was added to prevent further oxidation. The optical properties of the MDA adduct prevented the measurement of MDA-LDL concentration by spectrophotometry.

Instead, a functional concentration was determined by ELISA of anti-ApoB vs MDA-LDL on solid phase comparing the newly modified MDA-LDL to a standard curve of LDL of a known concentration (calculated by the manufacturers). Thus, ApoB levels were detected with a rabbit polyclonal anti-ApoB antibody (Santa Cruz biotechnology, Santa Cruz, CA). Modification was confirmed by the binding of a monoclonal antibody (LO1) on ELISA.

Successful modification was determined by the relative electrophoretic mobility of the LDL using pre-cast 0.6% agarose, 1.0% barbital buffer gels as per the manufacturer's instructions (Beckman Coulter, Fullerton, Ca) (Figure 3.1)

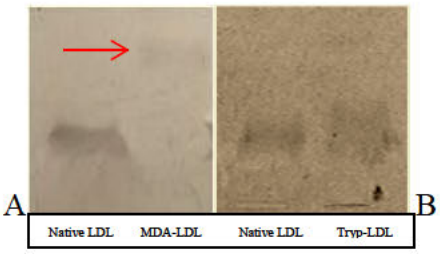


Figure 3.1 Agarose gels of native LDL Vs MDA-LDL and native LDL vs trypsinised LDL. 4.1A demonstrates the higher electrophoretic mobility of MDA-LDL (red arrow) in comparison to native LDL on Agarose. Figure 3.1B demonstrates the evidence for proteolysis of LDL upon trypsinisation, with the left band showing native LDL and right band showing LDL after incubation with trypsin for 2 hours.

3.2.2 Trypsinisation of LDL.

'Light' trypsination was performed by adding 10 µl washed and diluted (60 µl beads in 100 µl of PBS) bovine pancreatic trypsin-conjugated agarose beads (Sigma Aldrich), to 0.5 ml of 342µg/ml LDL. 45µl aliquots were removed at intervals between one minute and overnight, added to 3 µl of 1mg/ml bovine pancreas-derived trypsin inhibitor (Sigma Aldrich) and centrifuged at 9100g for 5 min. Control LDL was processed in the same way but without the

addition of trypsin. The extent of LDL modification was confirmed by electrophoresis as above.

3.2.3 Hypochlorite modification of LDL (Calbiochem, Beeston, UK) was achieved by incubating LDL (1mg protein/ml in PBS) with reagent-grade sodium hypochlorite (1mM, Sigma Aldrich) to a final concentration of 1 mg of LDL/ml of 1 μM hypochlorite solution for 24h.

3.2.4 Autooxidised LDL was created by removing the EDTA preservative and leaving the LDL in a non-air tight Eppendorf tube at $4c^{o}$ for up to two months.

3.3 Human Serology Assay Optimisation

As well as using thawed sera from the ASCOT trial (described below), we also utilised sera from healthy volunteers in the NHLI Vascular Science laboratory to test effects of freeze/ thawing cycles as well as obtaining high reading sera to use for reference.

All ELISA assays for serum antibodies were optimised using 'chequerboard' ELISAs, with a dilution series of both the serum dilution and secondary antibodies. Variation in reaction times was also studied to obtain optimal timings. The ideal concentration to be used in the study assays were selected to be at the steepest part of the standard curve in a selection of normal sera and study sera. The reference sera for each assay were identified from preliminary work as a sample which provided a high titre.

A variety of chequerboard ELISAs varying serum dilutions, secondary antibody dilutions and testing if there are any differences between fresh and thawed plasma were performed.

Assay	Antigen	Optimal dilution of serum	Secondary antibody	Detection antibody
Total IgG	goat anti-human 5µg/mL	1:300K	goat F(ab') 2 anti-human IgG Biotin 10ng/m. (Cambridge Bioscience, Cambridge, UK)	HRP-conjugated streptavidin (R&D Systems, Minneapolis, MN) 1:200
Total IgM	goat anti-human 5µg/mL	1:12K	mouse-anti-human IgM Biotin 33.33ng/m (Cambridge Bioscience, Cambridge, UK)	HRP-conjugated streptavidin (R&D Systems, Minneapolis, MN) 1:200
IgG anti-PC antibodies	PC-BSA Bioresearch technologies (2µg/ ml),	1:300	mouse-anti-human IgG (Cambridge Bioscience, Cambridge, UK) 1:2000	horse radish peroxidase (HRP) conjugated rabbit anti-mouse immunoglobulin (Dako,Cambridgeshire,UK) 1:2000
IgM anti-PC antibodies	PC-BSA Bioresearch technologies (2µg/ ml),	1:300	biotinylated mouse-anti-human IgM (Cambridge Bioscience, Cambridge, UK) 1:2000	HRP-conjugated streptavidin (R&D Systems, Minneapolis, MN)
IgG anti-MDA-LDL	MDA-LDL (10ug/ml)	1:300	mouse-anti-human IgG (Cambridge Bioscience, Cambridge, UK) 1:2000	HRP-conjugated rabbit anti-mouse immunoglobulin (Dako, Cambridgeshire) 1:2000
IgM anti-MDA-LDL	MDA—LDL (10ug/ml)	1:300	biotinylated mouse-anti-human IgM (Cambridge Bioscience, Cambridge, UK) 1:2000	HRP-conjugated streptavidin (R&D Systems, Minneapolis, MN) 1:200
IgG1 anti-MDA-LDL	MDA-LDL (10ug/ml)	1:60	Biotinylated mouse-anti-human IgG1(Cambridge Bioscience, Cambridge, UK) biotinylated mouse-anti-human IgG1antibody of 1:500	HRP-conjugated streptavidin (R&D Systems, Minneapolis, MN) 1:200
IgG2 anti-MDA-LDL	MDA-LDL (10ug/ml)	1:120	Biotinylated mouse-anti-human IgG2 (Cambridge Bioscience, Cambridge, UK) (Southern Biotech)	HRP-conjugated streptavidin (R&D Systems, Minneapolis, MN) 1:200
IgG3 anti-MDA-LDL	MDA-LDL(10ug/ml)	1:120	Biotinylated mouse-anti-human IgG1(Cambridge Bioscience, Cambridge, UK) 1:1000	HRP-conjugated streptavidin (R&D Systems, Minneapolis, MN) 1:200

Table 3.1 ELISA conditions for serology studies as optimised via 'chequerboard' ELISA dilution series and the optimal concentrations of sera as well as secondary and detection antibodies selected to reflect the steepest part of the standard curves.

3.4 The ASCOT Anti-oxLDL Study Methods

3.4.1 Study design and subjects

ASCOT was an independent, investigator-led, multicentre, randomised trial designed to compare two anti-hypertensive treatment strategies for the prevention of CHD events in more than 19,000 hypertensive patients without a clinical history of CHD. Informed consent was obtained from each patient and the study protocol conformed to the ethical guidelines of the 1975 Declaration of Helsinki, as reflected in a prior approval by the participating institutions research ethics committees. Subjects received a beta-blocker with a thiazide diuretic as required or a dihydropyridine calcium channel blocker (CCB) with an angiotensin-converting enzyme inhibitor as required [167]. ASCOT-LLA was a substudy comparing the cardiovascular effects of atorvastatin versus placebo amongst patients who had total cholesterol concentrations of ≤6·5 mmol/L [168, 169]. We identified samples from the Hypertension Associated Cardiovascular Disease (HACVD) substudy of ASCOT, of whom 582 were recruited from the participants recruited at St Mary's Hospital. We identified 200 non-diabetic, white European patients within ASCOT-LLA, half of whom were randomised to atorvastatin 10 mg daily and the other half to placebo. One sample in the placebo group was spoiled, giving an analysis total of 99. A composite endpoint of major adverse cardiovascular events (MACE) was predefined. This included all fatal CHD, symptomatic non-fatal myocardial infarction, coronary revascularization, and fatal and non-fatal stroke occurring in the UK and Ireland during the main ASCOT study period between February 1998 and October 2005. Participants who had had a MACE before the baseline blood sample were excluded. ASCOT was registered as a clinical trial with the European Union Drug Regulating Authorities Clinical Trials (EudraCT 2008-007494-20). The protocol was ratified by central and regional ethics review boards in all relevant countries. Patients included in this

study gave written informed consent to participate in the trial and to storage of samples for biomarker studies. This sub-study was specifically approved by the ASCOT sub study committee as part of ASCOT.

3.4.2 IgG and IgM anti-PC-BSA and MDA-LDL antibody levels

As per Table 3.1, IgG and IgM anti-MDA-LDL and anti-PC-BSA antibody levels were measured by ELISA. PC conjugated to BSA (PC-BSA) was purchased (Biosearch Technologies Novato, CA), whilst MDA-LDL was prepared as described above [94]. The extent of modification was estimated by Agarose gel electropheresis[166]. IgG and IgM antibody binding to solid phase antigens was identified by mouse-anti-human IgG (Cambridge Bioscience, Cambridge, UK) or biotinylated mouse-anti-human IgM (Cambridge Bioscience) followed by HRP-conjugated rabbit anti-mouse immunoglobulin (Dako, Cambridgeshire, UK) or HRP-conjugated streptavidin (R&D Systems, Minneapolis, MN). The plates were read at an optical density of 450nm (OD_{450}), after which the background was subtracted.

All serum sample values were adjusted for inter-assay variability by dividing the OD_{450} values by a standard serum sample used on all plates.

3.4.3 General measurements

All major risk factors were assessed during recruitment, and 10 year CVD Framingham risk score (FRS) calculated [170]. Serum was aliquoted and stored at -70^{o} C prior to analysis. Laboratory tests and carotid intima media thickness (CIMT) were performed as published

(www.ascotstudy.org) [171, 172], with a median interval between baseline and year one measurements of 13 months (range 12-16 months)

3.4.4 Statistical analyses

Power calculation to calculate sample size of this substudy aimed to detect an effect size (mean/standard deviation (SD)) of 0.2 on anti-oxLDL antibody levels, with >80% power at p = 0.05. The estimate of effect size was extrapolated from previous studies [173]. Statistical analysis was performed using Stata/IC (versions 11.2, Stata Corp., College Station, Texas). Continuous variables are reported as mean (standard deviation), or median (interquartile range) for skewed data. Skewed data were log transformed prior to regression analysis. Analysis of bivariate association between variables was performed by Pearson's or Spearman's rank correlation as appropriate. Multivariable regression analysis with forced entry of pre-specified covariates into the model was used to examine relationships between anti-oxLDL antibody levels, CRP and conventional risk factors. After categorizing anti-MDA-LDL IgG levels into tertiles, we performed Kaplan-Meier survival analysis to study the relationship between antibody levels and MACE. Univariate and multivariate hazard ratios (HR) with 95% confidence intervals were also estimated by Cox regression analysis. The validity of the proportional hazard assumption was assessed by examination of Schoenfeld residuals. Further multivariate Cox analysis was performed with classical CVD risk factors or FRS with or without CRP as pre-specified covariates. The predictive power of survival models was compared using Harrell's c statistic calculated by the somersd package in Stata [174]. Net reclassification improvement (NRI) and integrated discrimination improvement by continuous logistical regression analysis[175] was undertaken, so was (IDI) analysis[176].

The statistical data analysis was undertaken in conjunction with Professor Alun Hughes, and independent statistical review was undertaken and study data officially verified by the ASCOT sub-study committee (www.ascotstudy.org) prior to presentation.

3.5 Methods for the Isolation, Characterisation and Development of Monoclonal Antibodies LO1 and LO9.

3.5.1 Culture of LO1 and LO9 hybridomas and generation of antibodies

Selection of the hybridomas and generation of monoclonal antibodies was performed prior to the start of this study. LO1 (IgG3k) and LO9 (IgG2b) mAbs are autoantibodies secreted by hybridomas formed from splenocytes of a 1 year old female LDL receptor knockout mouse, fed on a high fat diet from 6 weeks of age to give a serum cholesterol of 25-30 mmol/l.. Briefly Sp2/0 myeloma cells were fused with murine splenocytes, and culture supernatants were screened by ELISA (bound directly to ELISA plates, 10 µg/ml, and 100µl/well) for the presence of antibodies showing differential binding to native and copper-oxidised (Cu-oxLDL) LDL. Hybridomas shown to have different reactivity were then subcloned twice prior to further characterisation. The isotypes of mAb were determined using a mouse mAb isotyping kit (IsoStrip, Roche Applied Science, Burgess Hill, UK). LO1 was shown to be reactive against Cu-oxLDL but not to native LDL bound to plastic, whilst LO9 was shown to be reactive to plastic bound native LDL and not Cu-oxLDL. Both these antibodies were taken forwards for further characterisation in this study.

For this work, we generated antibodies from frozen hybridoma cells by first expanding the hybridoma colonies in 75cl culture flasks in Dubecco's modified eagle medium (DMEM) and 10% FBS with penicillin/streptomycin and L-Glutamine. Once 2.6 x 10^6 cells were obtained, they were transferred to continuous culture in DMEM and 10% ultralow IgG (Gibco, UK) in

Celline 1000 bioreactor flasks (Integra, Switzerland) in a dedicated incubator. Supernatants were harvested from the cell compartment for antibody collection on a weekly basis, and culture media refreshed with 1/5 dilution of cells.

3.5.2 Enzyme-linked immunosorbent assay (ELISA)

Maxisorb 96-well plates (Nunc, Thermo Fisher Scientific, Waltham, MA) were coated with 50 μl antigen/well at 4°C overnight. Non-adherent material was washed out, and then the plates were blocked with 2% BSA/PBS for 1 hr at room temperature (RT). Appropriately diluted culture supernatant or purified mAb was added and incubated for 1 hr at RT. Plates were then washed, and wells incubated with goat anti-mouse IgG (Southern Biotech, Birmingham, AL) at 1:5000 dilution. After further washing, antibody binding was detected with 3,3',5,5'-tetramethylbenzidine (Sigma), and the reaction was stopped with 0.5M H_2SO_4. The optical density was then measured with a Synergy HT microplate reader (Biotek, USA) at wavelength 450nm. When malondialdehyde modified LDL (MDA-LDL) was used as an antigen, it was modified from native LDL and purified as previously described [166]. When correcting for total levels of ApoB, levels were detected on tested replicates with a rabbit polyclonal anti-ApoB antibody (Santa Cruz biotechnology, Santa Cruz, CA), and ELISA performed with a goat anti-rabbit-HRP secondary antibody. Reaction was developed, stopped as above, and plate read at OD450.

3.5.2.1 Correcting for equal loading of LDL

Equal loading of ELISA plates with native or modified LDL was confirmed in parallel wells using goat polyclonal anti-ApoB (Abcam, Cambridge, UK). Values where possible where expressed as a percentage or a fraction of ApoB.

3.5.2.2 Variation in concentration of salt

Variation in salt concentration was achieved by diluting LO1 in different concentrations of NaCl ranging from 2.15 M to 18mM.

3.5.2.3 Variations in Ph

mAb LO1 was dialysed into 0.1M sodium acetate buffer using Slide-A-Lyzer Dialysis Cassettes (Thermo Scientific, Rockford, IL) and then mixed with 0.1M sodium acetate solutions prepared using combinations of 0.1 M sodium carbonate and 0.05M sodium hydroxide solutions to produce working buffers of pH ranging from 3 to 11.

3.5.2.4 LDL Capture ELISA

100µl/well 10µg/ml rabbit anti-apolipoprotein B (BD Bioscience, San Diego, CA) was used to capture native LDL on half of an ELISA plate. This was left for 24 hours at 4°C, non-adherent material removed by washing as per above, The plate was blocked with 2% BSA for an hour, washed and 100µl/well 10µg/ml native LDL added to the it. This was subsequently left overnight at 20°C. ELISA was then performed as per the above protocol.

3.5.2.5 Native LDL incubation ELISA

An ELISA plate was coated with 10µg/ml native LDL and left overnight at 20°C. A 96 well Costar culture plate (Corning, NY) was blocked for 1 hour with 2% bovine serum albumin in PBS, and non-adherent material removed by plate washer. This plate was chosen because neither LO9 nor LDL readily bound it following blocking with 2% BSA in PBS. 10µg/ml LO9 and IgG2b in PBS were combined with 5µg/ml, 10µg/ml, 20µg/ml or 40µg/ml native LDL in PBS in a 1:1 ratio and left at 20°C for 1 hour, 150µl/well on the pre-blocked non-

adherent plate. This was left for 1 hour at 20°C, following which 100µl/well of the antibody-LDL mixture was transferred to the pre-prepared ELISA plate, and ELISA was performed as per the above protocol.

3.5.2.6 Serum incubation ELISA

This was performed similarly to the native LDL incubation ELISA. In place of native LDL, human serum freshly harvested from non-atherosclerotic donors, diluted 1 in 3, 30, 60, 120, 240 and 480 in PBS was used. This too was left for 1 hour at 20°C, before removal by plate washer. ELISA was subsequently performed as per the above protocol. ELISA was also performed using goat polyclonal anti-ApoB as the detection antibody, in order to confirm that the sample used contained LDL.

3.5.2.7 Preservative incubation ELISA

100µl/well 10µg/ml MDA-LDL (for LO1) and native LDL (for LO9) was added to the plate, and left overnight at 20°C. Following removal of non-adherent material using a plate washer, 100µl/well alcohol preservative (ethanol 100%, isopropanol 100%, methanol 100%) or formalin (1%, 2% or 4%) was added to the wells appropriately. This was left for 1 hour, and an ELISA was performed as above

3.5.2.8 Bone marrow derived macrophages

Briefly, bone marrow was harvested from the femurs and tibias of wild type mice. The bone marrow was spun at 2000 RPM for 10 minutes with the residue resuspended and filtered through 70µm cell filter, yielding a single cell suspension. This was added as a 1:20

suspension in DMEM containing L-Glutamine (L-Glu, 2 mM), fetal calf serum (FCS, 10%), penicillin/streptomycin(P/S) (Penicillin 10,000 μg/ml, Streptomycin 10,000 U/ml). This was supplemented with 15% L929 media, a murine aneuploidy fibrosarcoma cell line, as a source of macrophage-colony stimulating factor. The bone marrow derived cells were cultured for 7 days in an incubator set at 37^{o}C and an environment containing 5% CO_2 to allow maturity from monocytes to macrophages.

3.5.2.9 Zymosan opsonisation

Zymosan (Sigma Aldrich, UK) was suspended at 1% (approx. 20mg/ml) in 0.15M sodium chloride, and left in a boiling water bath for 20 min. It was then centrifuged for 30 min at 4000 RPM, after which the supernatant was discarded and the remaining residue was washed 3 times in PBS. The residue was resuspended in PBS (1mg/ml). Zymosan particles were incubated with fresh mouse serum in a 1:1 ratio for 30 minutes at 37^{o}C. This was then centrifuged for 30 minutes at 4000 RPM. Zymosan was then added to macrophage media to activate the macrophages overnight and the supernatant was then termed Zym MØ.

3.5.2.10 ELISA to test mouse macrophage TNFα production by an FcγR-mediated mechanism

To check the effects of LO9 binding to adherent LDL, we incubated LDL-coated wells (100μg/ml, 100μl overnight) with LO9 or control IgG2b for one hour, and then washed before addition of either mouse bone marrow derived macrophages (BMDM) (2x10^{6}/ well) or mouse BMDMs preincubated with of mAb 2.4G2/ 10ug/ml), The incubation was left overnight at 37c. The supernatant was then tested for TNFα production on ELISA (R&D systems) as per manufacturer's instructions.

3.5.2.11 conditioned medium ELISA

100µl/well 100µg/ml of native LDL was added to an ELISA plate overnight at 20^{o}C. Following washing, the plate was blocked for 1 hour at 20^{o}C. The plate was washed and either conditioned medium from macrophages stimulated with zymosan-activated serum (Zym MØ) or media from unstimulated macrophages (Ctrl MØ) (100µl/well) added and incubated at 20^{o}C for 3 hours. Following further washing, ELISA using LO9 or isotype control as described earlier was performed. Correction for LDL loading was established by probing with rabbit anti-ApoB antibody as described earlier.

3.5.3 Peptide synthesis

Peptides representing sequences of H3 were synthesised by Cambridge Peptides (Cambridge, UK). All peptides were purified by HPLC and quality controlled by mass spectroscopy.

3.5.4 Biotinylation of LO1

LO1 (2mg/ml) was purified using a PD-10 desalting column (GE healthcare, London, UK), Protein concentration was assessed by Nanodrop 1000, Thermo, Wilmington, DE at A280, as per manufacturer's instructions. In order to avoid inactivation of LO1, which is sensitive to the modulation of its lysines, mid-length biotinylation reagent for labelling aldehyde groups (EZ-Link* Biocytin Hydrazide kit, (Thermo Scientific, Rockford, IL) was used. Briefly LO1 was oxidised with sodium meta-periodate, excess periodate was removed by buffer dialysis in a 10K MWCO Slide-a-Lyzer Dialysis Cassette Kit (Thermo Scientific, Rockford, IL). One part 50mM Biocytin Hydrazide solution was added to 9 parts oxidised and buffer exchanged LO1. The reaction was mixed at RT for two hours. The biotinylated sample was separated from non-reacted product via gel filtration. The extent of biotinylation was tested with ELISA.

3.5.5 Biotinylation of LO9

LO9 (2.5mg/ml) was purified using a PD-10 desalting column (GE healthcare, London, UK), and protein concentration assessed by Nanodrop 1000, (Thermo, Wilmington, DE) at A280, as per the manufacturer's instructions. LO9 was biotin conjugated using a Thermo Scientific EZ-link sulfo-NHS-biotin kit. (Thermo Scientific, Rockford). The concentration was further assessed by Nanodrop 1000 atA280 (Thermo, Wilmington, DE) and then extent of biotinylation assessed by ELISA

3.5.6 Production of H3-Biotin (including western blotting to demonstrate biotinylation)

Briefly, the scFv H3 with a myc tag for identification and an Avi tag to allow biotinylation was produced by growing transformed TG1 (T-phage resistant E. Coli) cells in a 2xYT microbial medium (Sigma Y2627) containing ampicillin (100 μg/ml) (Sigma A2804) and glucose (1%, w/v). Growth proceeded with shaking at 37°C until the OD600 was about 0.9. Induction of scFv was with overnight incubation with 1mM IPTG. The sample was then spun down at 4000rpm for 30 minutes at 4^{o}C, after which a protease inhibitor cocktail was added. Sample dialysis was then undertaken in a 12,000 MW cut off dialysis membrane in PBS. The scFv was purified by binding to Protein A beads and eluting with glycine pH 2.5 into a 1M solution of Tris pH 8.8. Further dialysis into Tris 10mM pH 8 solution was then undertaken. Samples were kept at each stage of the process for further testing. The purity and function of the H3 Avi Tag was tested as below.

Briefly, 20 μg of protein were prepared in loading buffer, The sample was separated using SDS-PAGE on a 4-12% Tris SDS-Page in MES buffer at 124V for one hour, and then transferred to a membrane for detection. The membrane was incubated with 5% milk in PBS

with 1% for one hour. Following washing, anti- c-myc (Sigma Aldrich) primary antibody was added to the solution for one hour at RT. Following further washing, the secondary antibody-enzyme conjugate Extravidin Peroxidase (Sigma) was added at 1/200 dilution. ECL plus was then added for one minute, and membrane developed.

Once purity of the Avi-tagged H3 was established, the addition of biotin was undertaken using the Biotin Protein Ligase Kit (GeneCopoeia, Rockville, MD), and product buffer exchanged into PBS using Zeba Desalt Spin Columns (Pierce, Rockfor,IL). Finally, extent of biotinylation and function of the H3 was determined by ELISA.

3.5.7 Purification of LO1 on H3 biotin column

250 µl (solid volume) of Neutravidin agarose resin beads (Thermo Scientific, Rockford, IL), were washed three times in 1.5 ml of PBS. 250µg of biotinylated H3 in 1 ml PBS was mixed with the beads at 4^{o}C for one hour. The beads were then thoroughly washed 5 times with 1 ml of PBS. 1 mg of LO1 in 1 ml PBS was added to the beads following washing, and the mixture was rotated for 1 hour at 4^{o}C. The beads were then loaded into a polystyrene column and washed thoroughly with 10 ml of PBS. LO1 was eluted using 50mM glycine (pH 2.5) in 250 µl elutions into 1M Tris pH 6.9. Ten elution fractions were obtained and buffer exchanged into PBS using Zeba Desalt Spin Columns (Pierce, Rockfor,IL). Protein concentration was measured in each fraction (Nanodrop 1000, Thermo, Wilmington, DE) and that with the highest concentration was then tested with ELISA for function.

An SDS-PAGE gel was loaded with 20µg of the boiled protein and run at 120Vfor 40 minutes. Colloidal blue straining using the Invitrogen Colloidal Blue staining kit was then used to identify the resolved proteins. Both heavy chain and light chain bands were identified and sent for mass spectrometry for analysis of peptide sequences of the purified protein.

3.5.6 Identification of LO1 and LO9 sequence

3.5.6.1 Sequencing of the LO1 VH variable region

The mAb LO1 V_H variable region was amplified from hybridoma mRNA by RT-PCR using a series of degenerate oligonucleotide primers, which had been prepared by Eurofin MWG Operon (Ebersberg, Germany). The sense primer was based upon the leader sequence [177], and used in combination with a universal antisense constant region oligonucleotide[178] to amplify the leader, VDJ and start of the constant region. PCR products were cloned into pCRII (Invitrogen Paisley, UK) and transformed into TOP10 E.coli. Individual colonies were selected and DNA isolated by miniprep (Qiagen) prior to sequence analysis using an ABI 3730 automated DNA analyser. The VH-(D)-JH was analysed by comparison with the International MunoGeneTics information system (IMGT) (http://www.imgt.org) [179]. The veracity of the heavy chain sequence was confirmed by mass spectrometry of tryptic peptides of purified mAb LO1 IgG (as described below).

3.5.6.2 LO1 VL Sequencing and generation of LO1-Fab

Initially we used the same strategy as for sequencing the VH. Due to repeatedly sequencing aberrant light chains expressed by Sp2/0 cells (the fusion partner), the strategy was changed to primer design based on mass spectrometry data. Sense and antisense primers were designed based on mass spectrometry analysis (see below) of purified LO1. PCR products were cloned into pCRII (Invitrogen Paisley, UK)) and transformed into TOP10 E.coli. Individual colonies were selected and DNA isolated by miniprep (Qiagen) prior to sequence analysis using an ABI 3730 automated DNA analyser. The light chain sequence was compared to a combination of variable region, Junction, and constant region combinations from the International MunoGeneTics information system (IMGT) (http://www.imgt.org).

The veracity of the light chain sequence was confirmed by comparison to mass spectrometry of tryptic peptides of purified LO1 (see below).

Mass spectrometry data were analysed using SEQUEST software (University of Washington), which relates collections of tandem mass spectra to peptide sequences that have been generated from databases of protein sequences. Further analysis was undertaken using PEAKS Software (Bioinformatics, Waterloo, Canada). De novo sequencing analysis was undertaken and peptide sequencing matched to the International MunoGeneTics information system® (IMGT) database. DNA sequences of both the VH and VL regions of LO1 were both sequenced as previously described [166].

3.5.6.3 Generation of a chimeric LO1-Fab-Cys construct

As part of the collaboration with GSK, Dr. David Granger molecularly expressed a chimeric Fab construct of LO1 with a cysteine-tagged heavy chain (LO1-Fab-Cys). Constructs consisting of human CH1 and CL regions fused respectively to LO1 VH and VL DNA sequences were each cloned into a mammalian expression vector backbone in frame with a DNA sequence encoding an N-terminal secretory signal peptide. The vectors were transfected into HEK293/6E cells and maintained in suspension to express secreted LO1-Fab-Cys molecules. Supernatants were harvested and clarified after 7 days by centrifugation and passing through a 0.22 μm filter. The samples were then concentrated 10-fold using tangential flow prior to purification. The supernatants were then sent to us at Imperial. Purification was undertaken using an anti-human CH1-IgG purification column (BAC AV, Germany). The purity of LO1-Fab-Cys was confirmed with gel electrophoresis and colloidal blue staining under reducing and non-reducing conditions. Mass spectrometry was used to confirm the mass of the purified LO1-Fab-Cys. Retention of antigen binding function was

confirmed by an ELISA testing the ability of immobilised LO1-Fab-Cys to capture biotinylated anti-LO1 idiotype H3 [1]. Inactivation of LO1-Fab-Cys to obtain a negative control was achieved by blocking critical amines required for antigen binding. To achieve this, LO1-Fab-Cys was labelled with an amine reactive dye (Vivo Tag750) to an equivalent degree of labelling (DOL) as with the malemide reactive dye. Deactivation was tested by ELISA as before.

3.5.6.4 Sequencing of LO9

The sequencing of LO9 was contracted out to an external company (Fusionantibodies/UK). Briefly, hybridoma cells were pelleted, frozen and sent to Fusion Antibodies Ltd. Total RNA was extracted from the pellets using Fusion Antibodies Ltd in-house RNA extraction protocol. cDNA was created from the RNA by reverse-transcription with an oligo(dT) primer. PCR reactions using variable domain primers to amplify both the VH and VL regions of the monoclonal antibody DNA giving the bands shown in figure 3.2.

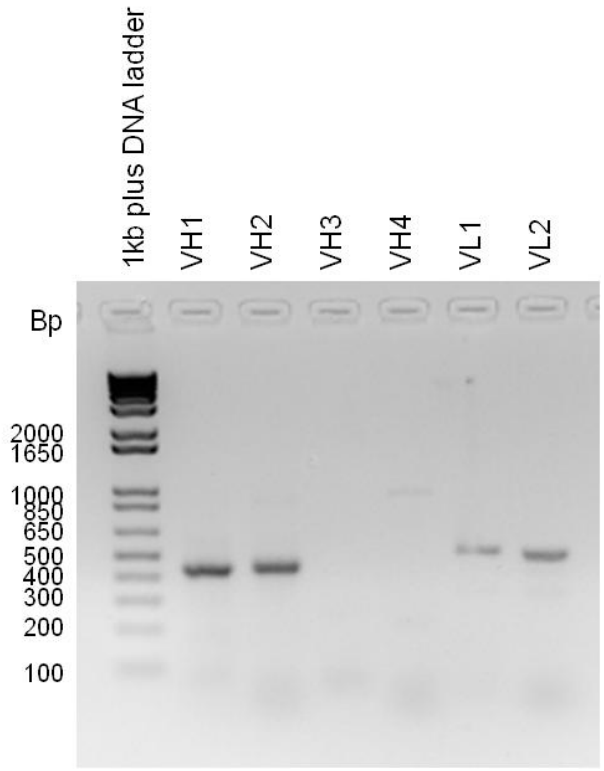


Figure 3.2. LO9- PCR using several combinations of Ig variable domain primers

The VH and VL products were cloned into the Invitrogen sequencing vector pCR2.1, transformed into TOP10 cells and screened by PCR for positive transformants. Selected colonies were picked and analysed by DNA sequencing on an ABI3130xl Genetic Analyser.

The VH and VL sequences were analysed by comparison with the International MunoGeneTics information system® (IMGT) (http://www.imgt.org) [179]. The veracity of the VH and VL sequence provided by Fusion Antibodies Ltd was confirmed internally by cloning and sequencing the variable domains and by mass spectrometry of tryptic peptides of purified mAb LO9.

3.5.7 Fluorescence labelling of LO1, LO9 and LO1-Fab-Cys and isotype controls.

Initial attempts at conjugating LO1 with fluorescein using amine chemistry failed to preserve LO1 functional activity, likely due to the conjugation of crucial lysines in the VH CDR3. Briefly, LO1 was buffer exchanged into PBS with Zeba Desalt Spin Columns (Pierce, Rockfor,IL), and then concentrated using to 2 mg/ml using 100000 NMWL Centricon centrifugal filter devices (Millipore, Watford, UK). Labelling with Alex Fluor 647 was attempted using the SAIVI Alexa Fluor 647 Antibody/ Protein Labelling kit (Invitrogen Paisley, UK). Labelling was attempted at 40% modulation and 70% at RT in 0.1 M sodium bicarbonate buffer for one hour. The resin was first washed thoroughly to remove sodium azide which it contains as a preservative. The reaction mixture was then purified into elutes by filtration through purification resin. Fractions were eluted with PBS buffer, and the different elutes were then tested for both protein and dye content by measuring absorbance at A280 and A650 respectively (Nanodrop 1000, Thermo, Wilmington, DE). The protein concentration in the elutes and the degree of labelling was then established by accounting for both absorbances Formulae below).

We therefore utilised SH groupings to label LO1 with a NIRF agent for imaging. LO1 was buffer exchanged into PBS with Zeba Desalt Spin Columns (Pierce, Rockfor,IL), and then concentrated to 2 mg/ml using 100,000 NMWL Centricon centrifugal filter devices (Millipore, Watford, UK). Following purification, and concentration, the function of LO1 was retested by ELISA, and its integrity confirmed by SDS gel electrophoresis. Labelling with the NIRF fluorochrome Vivo Tag®-S 750-MAL (PerkinElmer, Massachusetts USA) was undertaken with 20 Molar excess of dye to protein, and rotating at 20^{o}C for 2 hr in the dark. Following further purification, and removal of unbound fluorochrome in Zeba Spin

Columns, antibodies were tested for both protein and dye content by measuring absorbance at A280 and A750 respectively (Nanodrop 1000, Thermo, Wilmington, DE). The protein concentration in the eluates and the degree of labelling was then established by accounting for both absorbances, as per formula below. The function of labelled antibodies was then tested by ELISA and immunohistochemistry (IHC) on atherosclerotic murine samples (as below). LO9, and both IgG3 and IgG2b control antibodies' were labelled in a an identical manner.

Formula to calculate the degree of labelling of dye to protein (DOL) :

Pc = Conc. of protein = [abs. at 280 nm – (abs. at dye emission spectrum nm x Correction Factor*)] ÷ Epsilon of protein at 280 nm, where correction factor = 0.05 for a full antibody.

Dc = Conc. of the dye = abs. at emission spectrum (nm) ÷ Epsilon of the dye at same spectrum

Degree of labelling = Dc/Pc

3.5.8 Animal models of experimental atherosclerosis

3.5.8.1 Mouse model of atherosclerosis

All *in vivo* procedures in mice were covered by UK Home Office approval. We used female, *Ldlr* $^{-/-}$ mice (Jackson Laboratories, Bar Harbor, Me) and C57BL/6 wild type control animals. These were all maintained in a specific pathogen-free environment and studied according to institutional guidelines. The *Ldlr* $^{-/-}$ mice were transferred on to a high fat diet at 10 weeks of age. The composition of the diet has been reported previously [5]. Animals were studied and euthanised at different ages as follows: (i) for *in vitro* immunohistochemistry sections of atherosclerotic aortic root were obtained from 22 week old *Ldlr* $^{-/-}$ mice, fed on a low fat diet, and from 12 week old wild type mice as well as animals fed a high fat diet for 30

weeks. For IVIS Sepctrum/CT imaging, *Ldlr* $^{-/-}$ animals were fed a high fat diet for 30 weeks and then imaged. For FMT/CT imaging, animals were studied at either 30 weeks on high fat diet, 30 weeks on high fat followed with 12 weeks on low fat diet, or 42 weeks on high fat diet. For all the imaging studies, the wild type C57BL/6 mice were age-matched and fed a low fat diet.

3.5.8.2 Rabbit model of atherosclerosis

For initial IHC studies, we used female New Zealand White Rabbits fed a diet containing 1% cholesterol from 6 weeks of age for 8 weeks to yield advanced atherosclerotic plaques in the aortic arch that were rich in foamy macrophages. For the intravascular imaging model, we induced plaque rich in inflammatory cells in male New Zealand White Rabbits by balloon injury followed by a high fat diet as previously described.[137]

3.5.9 Immunohistochemistry and confocal microscopy

3.5.9.1 Mouse and human IHC

For mouse studies, aortic root and cusp sections were stored at -80°C before use, as previously described[78] After thawing sections were equilibrated for 5 min in double-distilled water, then for 5 min in PBS, fixed in 100% isopropanol for 15 min, and air dried for 30 min. Sections were subsequently blocked for 1 hr in 10% normal mouse serum (Dako, Glostrup, Denmark). Slides were then dipped in PBS, transferred to fresh PBS for 5 min, and dipped in PBS once again to wash.

Human carotid endarterectomy specimens were freshly collected with consent and institutional and national ethical approval. Specimens were transported and dissected on ice, with a transport time of under 30 min. The tissue was inspected and areas of classical

morphology with fibrous cap, lipid core and shoulder identified and snap-frozen in liquid nitrogen and stored at -80°C. The sections were then cryosectioned at -20^{o} C, embedded in OCT and fixed in isopropanol. Furthermore, well characterised advanced and intermediate lesions from human coronary sections were also studied in a collaborator laboratory(Jason Johnson/ Bristol). As specified in the AtheroExpress protocol[180], histological sections were classified according to overall appearance into: "atheromatous lesions" containing a large lipid core (>40% of plaque area), high macrophage infiltration with low smooth muscle cell and collagen content, "fibrous lesions" with a small (<40%) or absent lipid core, low macrophage content and high smooth muscle cell and collagen content, and "fibrous-atheromatous lesions" as an intermediate between the two other phenotypes.

For assessing the binding of biotinylated LO1 and biotinylated LO9, cryosections were equilibrated in double-distilled water, then PBS, blocked in 10% normal goat serum for 30 min, and then incubated in 10 μg/ml biotinylated LO1, LO9 or biotinylated IgG isotype control at 4°C overnight in a humidified chamber. Antibody was then decanted, and the sections rinsed with PBS. Bound antibody was then detected with Alexa Fluor 633 streptavidin (Molecular Probes, Invitrogen Paisley, UK) at 1:200 for 120 min at 21°C. TOPRO-3 (Molecular Probes, Invitrogen Paisley, UK) was used as a nuclear counterstain for general inspection, and macrophages were detected by 1:100 anti-mouse CD68-AlexaFluor488 (MCA1957, Serotec, Oxford, UK) or 1:50 anti-human CD68-FITC (green) (clone KP-1, F7135, Dako, Ely, UK). Sections were mounted in 80% glycerol /PBS and imaged by confocal microscopy (Zeiss LSM510 Meta) under standard settings. When studying LO1, LO9 or LO1-Fab-Cys directly labelled with VivoTag®-S 750-MAL (designated LO1-750, LO9-750 or LO1-Fab-Cys-750), we optimised the Leica SP5 MP inverted confocal microscope (Facility for Imaging by Light Microscopy (FILM), at Imperial

College London, South Kensington) for NIRF imaging at 750 nm. The 633nm laser power was set to 93% or above. In addition to this, a narrow range had to be selected for the emission level, which ranged between 750 nm and 800 nm, thus eliminating autofluorescence signal. Most images were obtained using a 10x microscope lens with the frame average at around 4, which provided a clear image. *En face* preparations of aortae were prepared by harvesting the aortae, and cutting them longitudinally. They were then thoroughly cleaned, fixed in 2% formalin and mounted *en face* with lumen facing the glass cover slips.. When staining with the directly labelled antibodies, all sections, including *en face* preparations were blocked with 2% Bovine serum albumin, washed. and stained using antibodies and control antibodies at 10µg/ml and incubated for 1 hr at 4°C in a humidified chamber. This was followed by a wash using PBS and finalized by nuclear staining with SYTO-24 (unless stated otherwise at 1:2000) for 10 min. The slides were then washed with PBS and glass cover slips were mounted using Fluoromount G.

3.5.9.2 Ex vivo in situ IHC and en face analysis in the mouse model

Following injection with either LO1-750, LO9-750, LO1-Fab-Cys-750 or isotype controls, termed (designated either IgG3k-750 or IgG2b-750 or deactivated LO1-Fab-Cys-750), animals were euthanised and the aortae collected. All aortae were cut longitudinally, thoroughly cleaned, and mounted using Fluoromount G. Further co-localisation with macrophages was obtained with selected aorta after treatment with 0.5% Triton for one hour, followed by staining with rat anti-mouse macrophages/Monocytes:Alexa Fluor® 647 (Serotec, Oxford, UK). In some animals, localisation of injected antibody in relation to endothelium was studied by injecting 100µl of phycoerythrin (PE)-conjugated anti-CD31 antibody (Biolegend, San Diego, CA) and sacrificing animals 10 min later. To minimize cross-talk between different fluorochromes, each channel was acquired in sequence. To

obtain 3D images of full aortae or regions of interest, images were acquired as above, with Z stacking and tile scanning. Image analysis for all IHC studies was undertaken using Volocity® 3D Image Analysis Software (PerkinElmer, Massachusetts USA).

3.5.9.3 IHC in the rabbit model

The aortic arch was removed and fixed in 4% phosphate buffered formaldehyde and then wax-embedded. Briefly, serial 3 μm paraffin sections were dewaxed and rehydrated. Endogenous peroxidase activity was inhibited by incubation with 3% (v/v) hydrogen peroxide. After blocking sections with 20% (v/v) goat serum in PBS, sections were incubated overnight at 4^{o}C with either 20μg/ml LO1, mouse monoclonal antibody against α-smooth muscle actin (Sigma, UK), or mouse monoclonal antibody against rabbit macrophages (RAM11) (Dako, UK), diluted in 1% (w/v) bovine serum albumin (BSA) in PBS. Cell nuclei were visualised with haematoxylin. A negative control, where the primary antibody was replaced with mouse IgG at the same dilution, was always included.

3.5.9.4 Ex vivo fluorescence microscopy on rabbit aortae

Fluorescence microscopy of plaque and normal vessel sections was performed on adjacent sections from fresh-frozen rabbit aortae as previously described [136]. Images were captured and processed using an epifluorescence microscope (Eclipse 80i, Nikon Instruments, Melville, New York) with filter sets for NIRF (excitation: 673 to 684 nm; dichroic mirror: DM750; emission: 765 to 835 nm) and autofluorescence (excitation: 460 to 500 nm; dichroic mirror: DM505; emission: 510 to 560 nm).

3.6 IVIS Spectrum Fluorescence Imaging and Computed Tomography (IVIS/CT)

Mice were anesthetised with isoflurane using a vaporizer, and 3D fluorescence images were acquired through Fluorescence Imaging Tomography (FLIT; IVIS® Spectrum, Caliper LifeSciences). We used a GFP filter set (excitation wave length, 710nm ± 15 nm; emission wave length, 820 nm± 15 nm) to detect LO1-750. Mice were then transferred anaesthetised in the imaging cassette to the micro-CT imaging suite (Inveon PET-CT, Siemens). CT images were obtained (100μm, 80KVp, 500 μAmp, 120 projections, exposure time 220 ms). Contrast-enhanced high resolution CT localised the aortic root and major arteries in the neck and thorax to guide interpretation. For blood distribution studies, serial tail bleeds at intervals up to 68 hours were performed and samples mixed with equal volumes of heparinised PBS. Blood samples were imaged on a black plate for epifluorescence (ex710, em820) and measured units expressed as total radiant efficiency. Quantification was obtained by non-linear regression curve fit to a known dilution series of the agent. For organ distribution studies, tissues were harvested and imaged in an opaque plate as above.

3.7 Fluorescence Molecular Tomography-Computed Tomography (FMT/CT)

3.7.1 LO1 studies:

FMT was acquired with a FMT 4000 fluorescence tomography imaging system (PerkinElmer, Massachusetts USA) at the appropriate channels. Following agent calibration, all animals were injected with a VivoTag®-S 750-MAL-cojugated antibody, as well as in selected experiments with MMPSense 645 FAST (PerkinElmer, MA) to evaluate matrix

metalloproteinase (MMP) activity or AngioSense 680 (PerkinElmer, MA) to allow for identification of intravascular space in isolation of CT. Animals were imaged 4 hr later. All animals were imaged 4 hours later. In some animals the signals were co-localised with CT images using Siemens Inveon CT scanner (Siemens Healthcare, Erlangen, Germany). An imaging cartridge containing the anesthetised mouse was placed into a custom machined Plexiglas holder that supplies isoflurane during imaging. The CT x-ray source with an exposure time of 200 ms was operated at 80 kVp and 500μA.The CT reconstruction was performed with a cone beam reconstruction algorithm, and the pixel values were scaled to Hounsfield units. Contrast-enhanced high resolution CT localised the aortic root. This anatomical information guided the placement of the region of interest (ROI) in the quantitative activity map concomitantly obtained by the hybrid FMT image. Fusion of both FMT and CT images relied on fiducial markers and used Amide 1.0.4 (Sourceforge.net).

3.7.2 LO9 studies

Studies with LO9-750 and IgG2b-750 were carried out as above. The only adjustment was for the entry of data into the FMT machine with new DOL values for the two antibodies, in order to calculate molar concentrations accurately.

3.8 Two-dimensional NIRF Imaging Device and Catheter

The two-dimensional NIRF imaging device and catheter apparatus for through blood imaging, analogous to IVUS imaging, has been fully described previously[136]. Briefly, the intravascular optical probe is capable of performing an over-the-wire pull back intravascular acquisition using a 750 nm laser light and collects the subsequent NIRF emission. The fibre is rotated and translated using mechanical stages to collect fluorescence and generate a 2D NIRF image. Images were constructed following filtering of electronic noise (MATLAB). [136]

3.8.1 Intravascular NIRF and IVUS imaging

Animals were anesthetized as described previously [136]. A 5-F introducer was inserted into the right carotid artery using fluoroscopic and angiographic guidance. Iodinated contrast was injected and baseline x-ray angiography was recorded using standard cineangiography. An intravascular ultrasound (IVUS) catheter was inserted over a 0.014-inch guide wire and serial pullbacks were performed (Galaxy IVUS System, Boston Scientific/Scimed, Inc., Natick, Massachusetts) from the iliac bifurcation to the renal arteries, with a pullback length of 100 mm. Next, the monorail NIRF catheter was advanced over the guide wire. To cover the entire IVUS-imaged vessel and understand reproducibility of the NIRF signal profiles, the NIRF catheter was advanced into the iliac artery and 3 to 4 contiguous, 110-mm length pullbacks were performed (rotational speed 30 to 100 rev/min, longitudinal pullback rate of 1 mm/sec).). Animals were then euthanised and the iliacs and aortae were resected. The NIRF catheter was gently reintroduced into lumen of the aorta and *ex vivo* NIRF pullbacks were repeated up to 3 times. Corresponding images were aligned using iliac bifurcation and renal arteries as landmarks, and radiopaque catheter markers as fiducials. Areas of plaque and normal vessel were confirmed by IVUS images.

3.9 Fluorescence Reflectance Imaging

Resected vessels underwent multiple wavelength fluorescence reflectance imaging (FRI) (), equipped with an NIR filter set (Carestream Kodak MMPro 4000): bandpass excitation: 716 to 756 nm, bandpass emission: 780 to 820 nm.(Cite Vinegoni Sci Trans Med 2011) Multiple exposure times (0.1 to 60 s) for each wavelength and acquired images were exported as DICOM (Digital Imaging and Communications in Medicine) files for further analysis. Due to vessel shrinkage after resection, the aorta and the iliac vessels were manually elongated to *in*

vivo measured lengths. ROIs were traced manually after visual identification of normal vessel, background, plaque, and injured zones (Osirix version 2.7.5, Pixmeo, Switzerland).

3.10 Statistical analyses

All statistical analysis were undertaken using Prism 5.0. (GraphPad, La Jolla, California). Statistically significant differences between 2 groups were determined using the Mann-Whitney *U* test for unpaired observations, and the Wilcoxon matched-pairs signed-ranks test for paired observations. Amongst multiple groups, significance was assessed via the Kruskal-Wallis test. Variables are reported as mean ± Standard error of the mean (SEM). A p value of <0.05 was considered statistically significant. In the progression/regression study, post-test for linear trend was undertaken and results expressed in R square value with a significant p value of <0.05.

4.0. Serological Assay Optimisation and the Anglo-Scandinavian Cardiac Outcomes Anti-oxLDL Substudy

4.1 Chapter Summary

Antibodies against oxidised LDL (oxLDL) are readily detectable in serum, but their significance for cardiovascular disease remains uncertain. We aimed to optimise assays to measure IgG and IgM anti-MDA-LDL and anti-PC levels as well as IgG1 and IgG3 isotype levels against MDA-LDL.

Following assay optimisation, we aimed to determine if anti-oxLDL antibodies predict incident cardiovascular disease (CVD) in subjects with hypertension and moderately increased CVD risk.

We studied a non-diabetic subgroup (age 63 ± 7 yr; 92% male) of the lipid-lowering arm of the ASCOT. IgG and IgM antibodies against malondialdehyde modified LDL (MDA-LDL) and phosphocholine (PC) were measured by ELISA at baseline and after one year on atorvastatin (10 mg daily; n=100) or placebo (n=99). Antibody levels correlated with subsequent MACE. Event-free survival analysis was performed and data presented as HR [95% CI]). There were 26 MACE over a median follow up of 5 years. Higher levels of IgG anti-MDA-LDL were associated with reduced risk of MACE (log rank test for trend= 0.03; HR=0.33 [0.13,0.85]; p=0.02 in an unadjusted Cox model). This was not attenuated by further adjustment for Framingham Risk Score and baseline CRP; adjusted HR=0.35 [0.13, 0.96]; p=0.04). Antibody levels to MDA-LDL and PC at baseline did not correlate with baseline LDL cholesterol. However, they correlated closely with antibody levels measured at

1 year, despite treatment with atorvastatin and significant reductions in LDL cholesterol and CRP.

High IgG anti-MDA-LDL levels are associated with protection from MACE in this population, independent of classical CVD risk factors and CRP. The independence of IgG anti-MDA-LDL antibody levels from atorvastatin treatment and lowering of LDL strengthens their status as a biomarker. Levels of IgG1 and IgG3 isotype subgroups did not separately account for the protective effect of total IgG and MDA-LDL antibodies, and follow different distribution patterns from one another. In addition, they are weakly correlated with other biomarkers of cardiovascular disease.

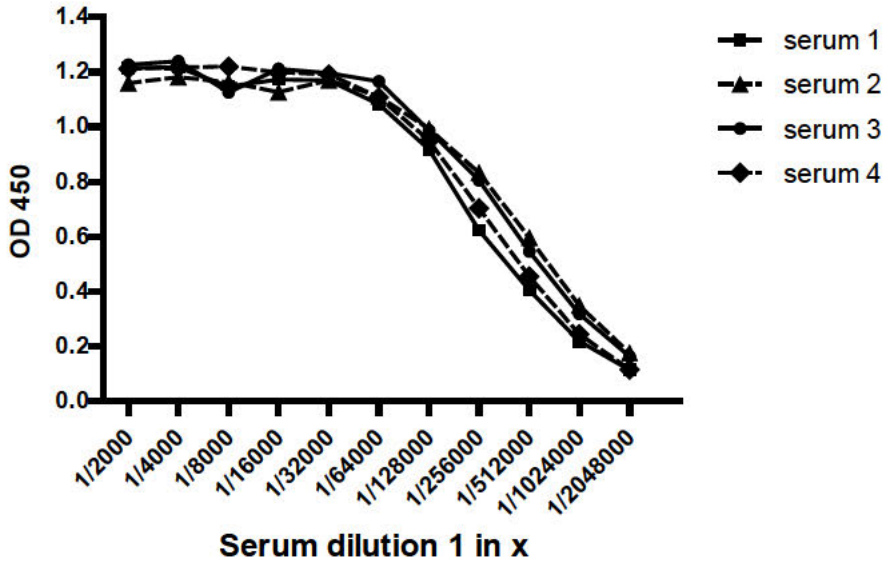
4.2 Assay Optimisation

We aimed to optimise assays for the measurement of IgG, IgM anti-MDA-LDL, and anti-PC-BSA. We also developed assays to measure the IgG1 and IgG3 isotypes against MDA-LDL. Furthermore, in order to ensure that any ability of anti-oxLDL antibodies to predict MACE was not a reflection of the total IgG or IgM levels, we developed further assays for measuring total IgM and IgG levels in serum. All assays were optimised for serum concentration, secondary antibody concentration and timing of the 3,3′,5,5′-Tetramethylbenzidine (TMB) reactions. Examples of the optimisation curves obtained for the different assays are discussed below.

4.2.1 Estimating total IgG and IgM levels by ELISA

Two ELISA based assays were developed to measure total IgG and IgM levels in sera. Representative examples of assay optimisation curves are shown in Figures 3.1A and 3.1B. The result of the optimisation experiments led to selecting the appropriate serum dilutions to use for both assays. The total IgG assay had most sensitivity in detecting small differences when serum was tested at 1:300K dilution and for IgM assay had most sensitivity at 1:12K. The coefficient of variance between the replicates was <5%.,

A



B

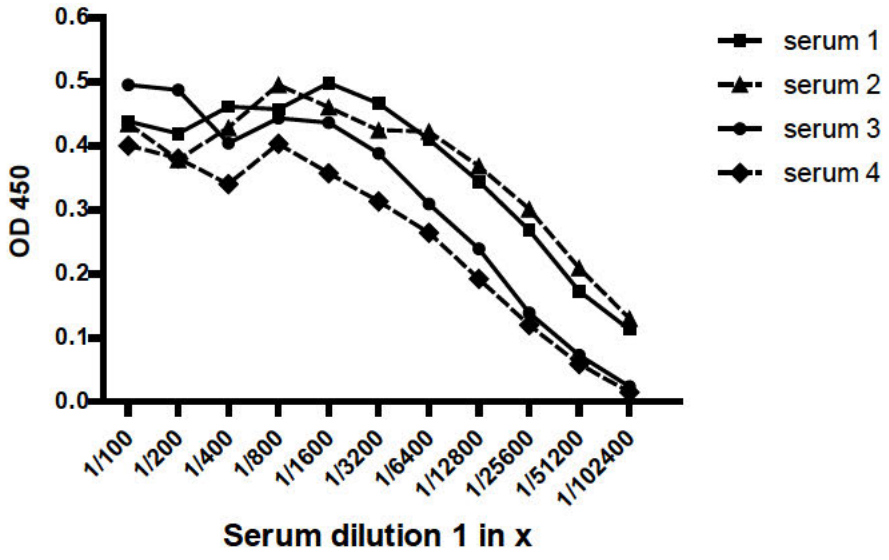
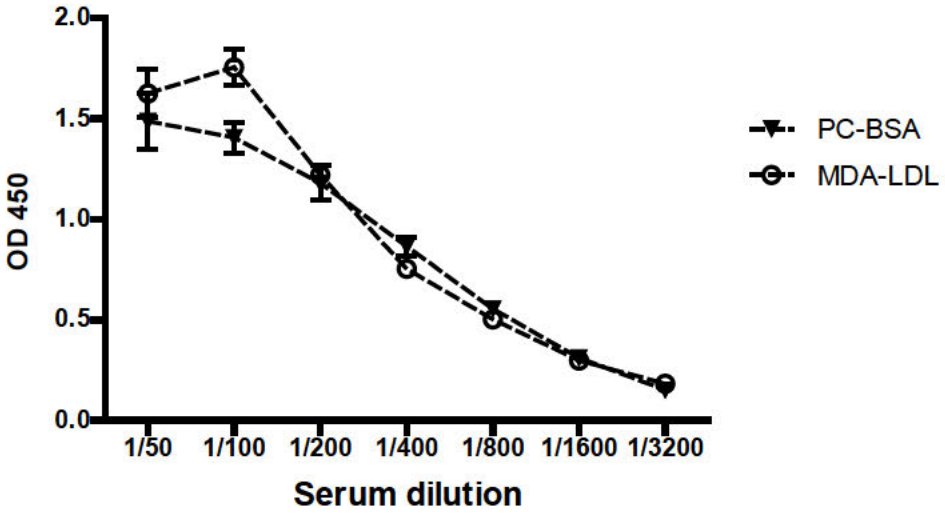


Figure 4.1. ELISA optimisation curves for total IgG and total IgM. estimations of total IgG (A) and total IgM (B) in 4 sera. The X axis represents serum dilution series and the y axis Optical Density at 450nm (OD 450).

4.2.2 Optimisation of an ELISA based assay to estimate anti-MDA-LDL and an anti-PC-BSA IgG and IgM antibody levels in serum

We first tested serum from a single individual at a range of dilutions with different concentrations of secondary antibody. A 1 in 2000 concentration of secondary antibody was chosen as the optimum concentration to be used in future assays as it provides better separation from background signal at lower concentrations of serum. Subsequently, serum from random selected samples from the ASCOT population were studied. Figures 4.2A and B demonstrate sample dilution series chosen as representative optimisation curves performed on a selection of ASCOT sera. The optimum serum dilution, at the steepest part of the curve was chosen to be at a dilution of 1 in 300 for the four assays.

A



B

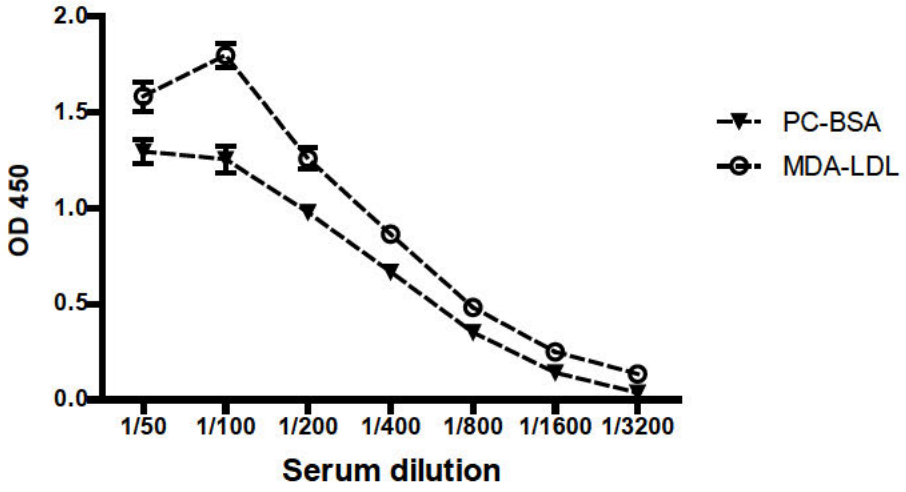


Figure 4.2. Optimisation curves for the IgG and IgM anti-PC-BSA and anti-MDA-LDL antibody assays. Measurement of a representative serum sample in dilution series demonstrating standard curves for the four assays. IgG assays are in (A) and IgM assays are in (B) The optimal concentration of serum to be tested was selected to be 1/300.

4.2.3 Estimation of IgG anti-MDA-LDL isotype levels

We tested serum in dilution series of multiple sera and used secondary antibodies in dilution series as well to discover the optimal concentrations of each needed to detect IgG1, IgG2 and IgG3 antibodies in patient sera. We did not explore IgG4 as previous studies have found extremely low levels of anti-MDA-LDL antibodies of this subclass. We tested both sera of healthy volunteers and also sera that high total IgG anti-MDA-LDL antibody levels from the ASCOT study ('high readers') to optimise the isotype assays. Figure 4.3 shows a dilution series of two sera each tested for the three IgG anti-MDA-LDL isotype levels.

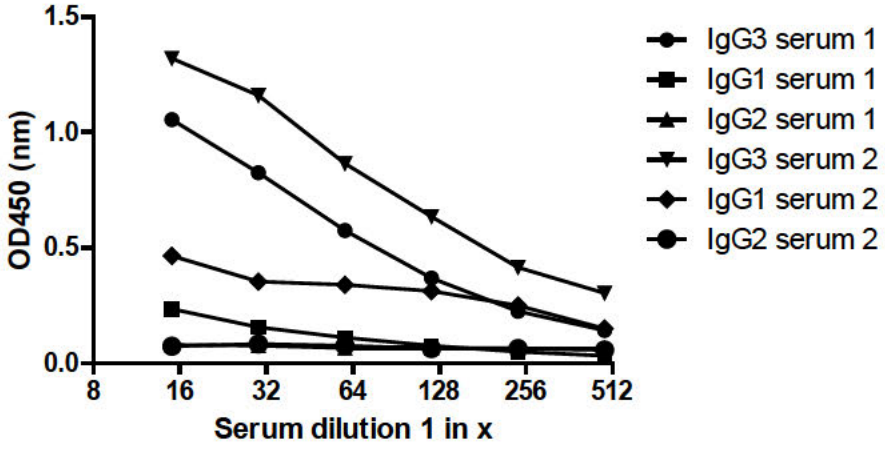


Figure 4.3 Levels of IgG isotypes were determined by ELISA in two healthy volunteers in dilution series. The secondary antibodies were used at a constant 1:1000 dilution.

Anti-IgG3 antibodies were more reactive than either IgG1 or IgG2. An important observation is that the relative OD values measured are affected by the characteristics of the secondary antibodies used in detection. Thus, the levels measured are not in the same magnitude and cannot be expressed as equally measured fractions of total IgG, but levels can be used to compare longitudinal data or inter-patient data within the same assay. This point is demonstrated by anti-MDA-LDL IgG3 levels having a higher OD than total anti-MDA-LDL

IgG levels in some sera. Therefore, the optical density only represents an estimation of the levels of each antibody subclass tested, but not as an absolute value.

4.2.4 IgG3 anti-MDA-LDL antibody assay optimisation

Using the same technique described previously for the anti-MDA IgG assay, a 1:120 dilution of serum and a 1:1000 dilution of biotinylated mouse-anti-human IgG3 antibody were selected as the optimum concentrations for use in our assay. Figure 4.4A shows levels measured in duplicates in 4 different sera randomly selected from the ASCOT population. This was repeated in a range of different sera to demonstrate variability. Interestingly there was little difference in antibody levels or reactivity in frozen serum that was thawed vs. fresh serum as demonstrated in Figure 4.4B

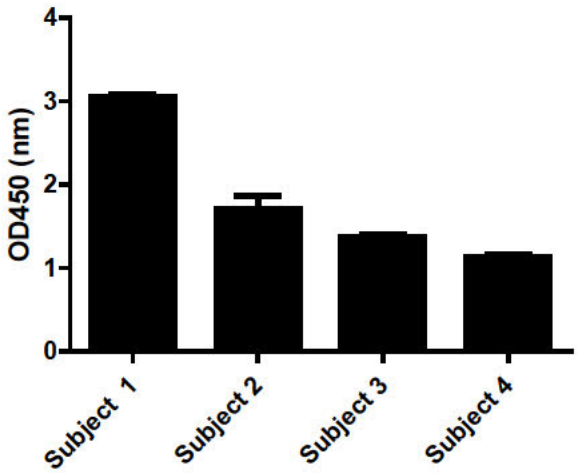


Figure 4.4A Optimisation of the IgG3 anti-MDA-LDL antibody assay. An example of the optimised ELISA detecting anti-MDA-LDL IgG3 antibodies in 4 individual sera from ASCOT - Serum at 1:120 and secondary antibody at 1:300.

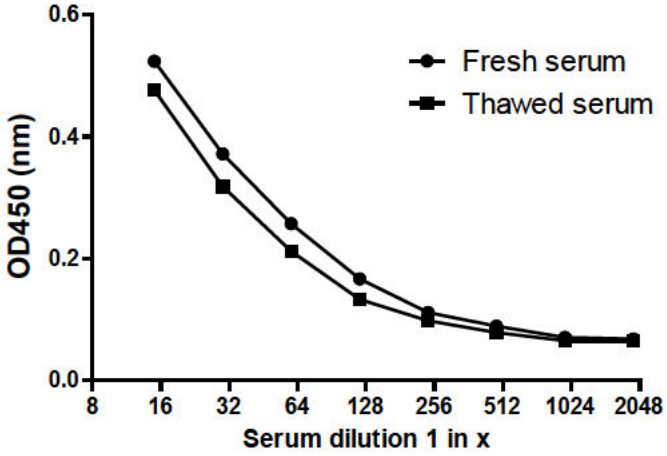


Fig 4.4B ELISA of IgG3 anti-MDA-LDL antibodies in dilution series. The same serum was tested when fresh and when frozen and thawed. There was little difference in antibody levels detected.

4.2.5 IgG1 anti-MDA-LDL antibody assay optimisation

In a similar fashion to the previous assay, the assay was optimised in a series of chequerboard ELISAs with a constant coat of MDA-LDL at 10ug/ml and variable serum concentration as well as secondary antibody concentrations. Dilution series ELISA of both serum concentration and secondary antibody concentration resulted in selecting a 1:60 serum dilution as an optimal concentration to measure with a secondary antibody dilution of 1:500. This is illustrated in Figure 4.5 which demonstrates the dilution series of 4 ASCOT sera reacting against MDA-LDL and probed with biotinylated anti-IgG1 secondary antibody.

When replicating the same for IgG2 we found that the levels of IgG2 are quite low in a variety of samples and therefore decided to estimate IgG3 and IgG1 fractions in the ASCOT

study. An example of the profile of the IgG anti-MDA-LDL antibody subtype levels is illustrated in Figure 4.6.

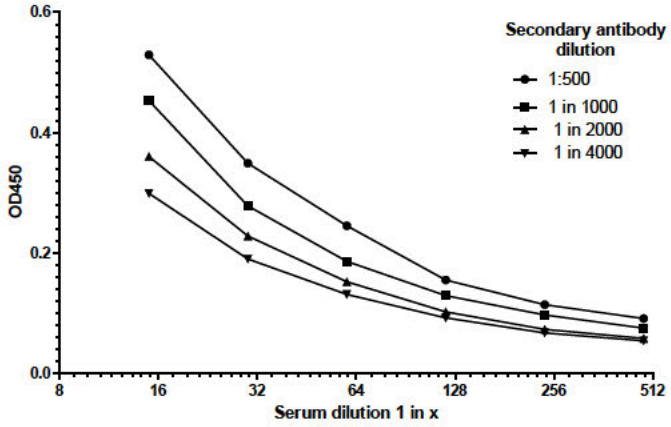


Figure 4.5 Optimisation of the IgG1 anti-MDA-LDL antibody assay. 4 sera from ASCOT are illustrated here, where the serum is measured at a dilution series as well as probed by different concentrations of secondary antibody with a constant antigen level used.

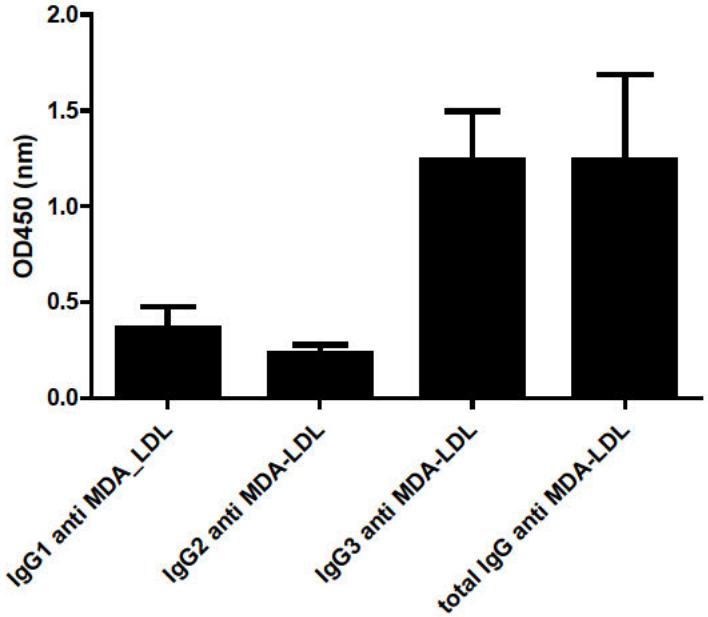


Figure 4.6 A representative analysis of total and isotype levels of IgG anti-MDA-LDL antibody levels in one serum from ASCOT.

4.3 IgG Antibodies Against Anti-malondialdehyde-LDL Predict Freedom from Cardiovascular Events Independently of Traditional Cardiovascular Risk Factors in ASCOT. (The ASCOT Anti-OxLDL Substudy).

An introduction to the ASCOT study and the well characterised population of the ASCOT-HACVD is detailed in the methods section. This study population provided us with a valuable resource to study the correlation between levels of both IgG and IgM anti-oxLDL antibodies in a well characterised, asymptomatic population with a moderate risk of having incident cardiovascular events. We aimed to determine if measuring antibodies to modified or 'oxidised' LDL predicts cardiovascular events in a substudy of the ASCOT population. The value of these added measurements in risk stratifying the study population was explored, with a particular attention given to the stability and independence of antibody levels from other cardiovascular risk factors or treatment.

We first tested the total anti-MDA-LDL and anti-PC LDL antibody levels, as well as total IgG and IgM. We then followed on by testing the predominant isotype levels of the IgG anti-MDA-LDL response.

4.3.1 Assay variability

All assays were optimised to detect antibody levels at the highest sensitivity possible. All the accepted measurements had an intra-plate coefficient of variation (CoV) no greater than 5% and the inter- plate correlation of variation (IPCoV), no greater than 10%. When values fell outside the CoV or a plate fell out of IPCoV, the measurements were repeated by a different

operator. Nevertheless as per the methods section, all values were still corrected to standard to account for any minor inter-plate variation.

4.3.2 IgG anti-MDA-LDL antibodies are a strong predictor of freedom from MACE

There were no differences between the placebo and atorvastatin groups in any of the baseline characteristics (Table 4.1), and participants were representative of the ASCOT-LLA participants as a whole. Overall, there were 26 MACE when the placebo and atorvastatin groups were combined. MACE-free survival analysis showed that higher levels of IgG anti-MDA-LDL were associated with reduced risk (log rank test for trend= 0.03; HR = 0.33 95%CI (0.13, 0.85); p = 0.02 in an unadjusted Cox model). Kaplan-Meier survival estimates confirmed a significant trend for better survival across the higher and middle tertiles of IgG anti-MDA-LDL levels (Figure 4.7). None of the other antibodies measured (IgM anti-MDA-LDL, IgG and IgM anti-PC-BSA) were related to MACE in Kaplan-Meier or unadjusted Cox models. Total IgG had a seemingly strong effect size (HR=0.18 95%CI (0.033,1.0), but a non-significant negative association with events (p-0.052) and IgM had a very weak and non-significant association with events (p=0.85). Therefore the relationship of total IgM and IgG with events is likely to need bigger numbers to explore further.

Table 4.1 Baseline characteristics

Data are mean (SD) or n (%) with the exception of skewed variables[¶] which are median (interquartile range)

Variable	All (n = 199)		Placebo (n = 99)		Atorvastatin (n = 100)	
Male sex, n (%)	184	(92%)	92	(92%)	92	(92%)
Age, years	63.4	(7.6)	63.4	(7.4)	63.5	(7.8)
Body mass index, kg/m^2	28.5	(4.1)	28.6	(4.1)	28.3	(4.1)
Systolic blood pressure, mmHg	159	(16)	159	(16)	159	(16)
Diastolic blood pressure, mmHg	93	(9)	93	(9)	93	(9)
Heart rate, bpm	70	(12)	71	(12)	69	(12)
Total cholesterol, mmol/l	5.6	(0.7)	5.5	(0.7)	5.6	(0.7)
Low density lipoprotein, mmol/l	3.5	(0.7)	3.5	(0.7)	3.4	(0.8)
High density lipoprotein, mmol/l	1.3	(0.4)	1.4	(0.4)	1.3	(0.3)
Triglycerides, mmol/l[¶]	1.6	(1.1, 1.9)	1.5	(1.0, 2.0)	1.6	(1.1, 1.9)
Creatinine, µmol/l	100	(15)	99	(15)	101	(15)
Fasting glucose, mmol/)	5.2	(0.6)	5.2	(0.6)	5.2	(0.6)
CRP, mg/l[¶]	1.98	(1.00, 4.99)	1.68	(0.77, 4.99)	2.56	(1.14, 4.74)
Current smokers, n (%)	44	(22)	21	(21)	23	(23)
IgG anti-MDA-LDL abs at baseline, Standard-Corrected OD$_{450}$	0.70	(0.37)	0.71	(0.40)	0.70	(0.34)
IgM anti-MDA-LDL abs at baseline, Standard- Corrected OD$_{450}$	0.76	(0.71)	0.83	(0.85)	0.69	(0.53)
IgG anti-PC-BSA abs at baseline, Standard-Corrected OD$_{450}$	1.28	(0.68)	1.24	(0.68)	1.32	(0.67)
IgM anti-PC-BSA abs at baseline, Standard- Corrected OD$_{450}$	0.87	(0.45)	0.89	(0.47)	0.85	(0.43)
Total IgG at baseline, Standard-Corrected OD$_{450}$	1.78	(0.27)	1.78	(0.28)	1.77	(0.26)
Total IgM at baseline, Standard-Corrected OD$_{450}$	1.16	(0.32)	1.18	(0.33)	1.14	(0.31)

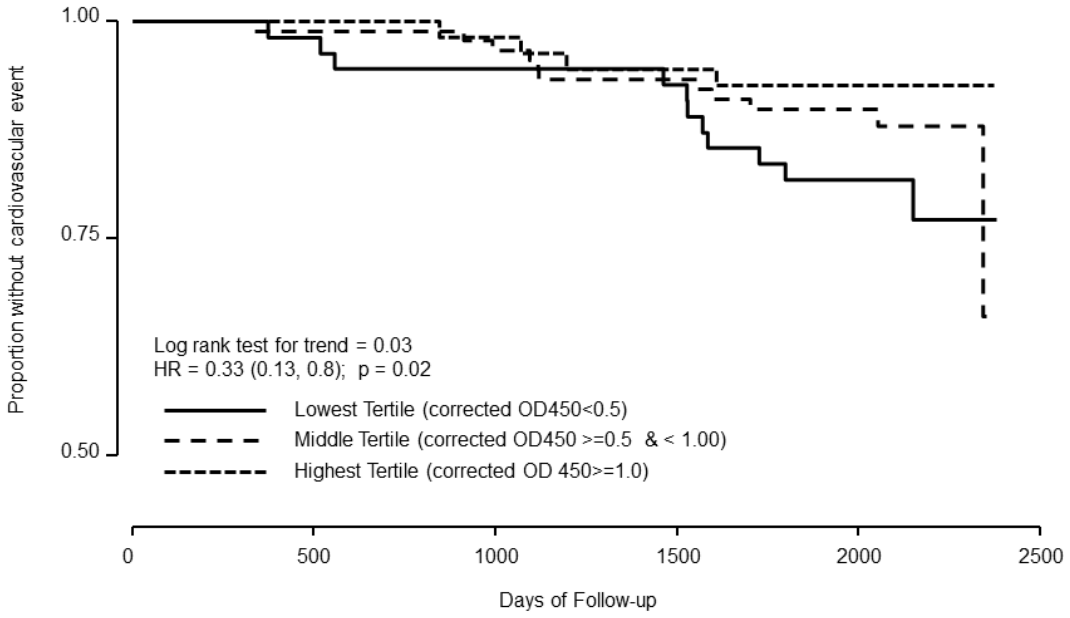


Figure 4.7 Kaplan-Meier survival estimates for population tertiles of IgG anti-MDA-LDL levels

4.3.3 IgG anti-MDA-LDL antibodies are unrelated to FRS, CRP or other classical predictors of cardiovascular risk

As expected, FRS was a strong predictor of MACE (HR 137, 95% CI (8-2397); p=0.001). However, the strong inverse relationship between IgG anti-MDA-LDL levels and MACE was not attenuated by adjustment for FRS in a multivariate analysis model (HR 0.31 95%CI (0.11 to 0.88) (p=0.029)). Inclusion of IgG anti-MDA-LDL antibodies with FRS increased c statistic from 0.67 (0.56, 0.77) to 0.73 (0.64, 0.81) compared with FRS alone and resulted in a continuous NRI[181] of 0.14 (p= 0.07) and IDI of 0.03 (p = 0.02).

Baseline CRP failed to predict MACE (HR 1.05, 95% CI (0.73-1.5); p=0.8 adjusted for age and sex). Moreover, the significant inverse relationship between IgG anti-MDA-LDL levels and MACE withstood inclusion of baseline CRP in addition to FRS in multivariate Cox regression models (adjusted HR = 0.35 95% CI (0.13, 0.96); p=0.04).

In a further multivariate model, where age, sex, statin treatment, treatment for hypertension, left ventricular hypertrophy (LVH), systolic blood pressure (SBP), LDL cholesterol, baseline CRP and smoking were included, IgG anti-MDA-LDL antibodies were associated with a HR of 0.29, (95% CI (0.10 to 0.80);(p= 0.018). In this instance, inclusion of IgG anti-MDA-LDL antibodies increased the c statistic from 0.67 (95% CI (0.56 to 0.78)) to 0.71 (95% CI (0.59 to 0.82)) and gave an NRI = 0.29 (p= 0.02) and IDI = 0.01 (p = 0.06). The association between IgG anti-MDA-LDL antibodies and MACE also remained significant in other multivariate analyses that included total IgG and body mass index (data not shown).

4.3.4 Anti-oxLDL antibodies are unchanged over one year, and are unaffected by atorvastatin treatment despite reduction in LDL and CRP

As shown in Table 3.2, treatment with atorvastatin for a year led to a 1.53 (95% CI (1.42, 1.63)) mmol/litre reduction in LDL ($p<0.001$ by paired t-test) and 0.39 mg/l (geometric mean) reduction in CRP ($p<0.001$). In contrast, baseline levels of both IgG and IgM anti-PC-BSA and MDA-LDL antibodies correlated strongly with one year levels (Tables 4.3A and 4.3B). There was little correlation between IgG anti-BSA-PC and IgG anti-MDA-LDL antibodies, suggesting different underlying mechanistic influences. However, IgM anti-MDA-LDL and IgM anti-PC-BSA showed a strong correlation.

Variable	Placebo (n = 99)		Atorvastatin (n = 100)		Difference (P-A)	95% CI	p
IgG anti-MDA-LDL abs, Standard-Corrected OD450	0.74	(0.46)	0.76	(0.42)	-0.02	(-0.15,0.11)	0.7
IgM anti-MDA-LDL abs, Standard- Corrected OD450	0.85	(0.61)	0.87	(0.83)	-0.02	(-0.23,0.20)	0.9
IgG anti-PC-BSA abs, Standard-Corrected OD450	1.21	(0.59)	1.32	(0.66)	-0.1	(-0.29,0.08)	0.3
IgM anti-PC-BSA abs, Standard- Corrected OD450	0.93	(0.46)	0.92	(0.43)	0.18	(-0.11,0.15)	0.8
Total Cholesterol, mmol/L	5.5	(0.8)	4.0	(0.6)	1.5	(1.3,1.7)	<0.001
Low Density Lipoprotein, mmol/L	3.4	(0.8)	2.1	(0.5)	1.3	(1.1,1.5)	<0.001
High Density Lipoprotein, mmol/L	1.3	(0.4)	1.3	(0.4)	0	(-0.1,0.1)	>0.9
log CRP, mg/l	0.69	(1.08)	0.29	(1.23)	0.39	(0.07,0.7)	0.01

Table 4.2 Antibody, lipid and CRP measures at 1 year.

Data are mean (SD) or mean difference (95% confidence interval).
p values were calculated using a Student's t-test.

Antibody levels were unaffected by statin treatment, despite the significant reduction in LDL cholesterol (Table 4.2). Furthermore, the magnitude of reduction of total LDL cholesterol did not correlate with any change in antibody levels over one year. Thus Spearman's rank correlation coefficient (r) for difference between LDL cholesterol values at baseline and one year *versus* difference in antibody levels at baseline and one year was r=0.04 (p=0.6) for IgG

anti-MDA-LDL, r=0.02 (p=0.8) for IgM anti-MDA-LDL, r=0.08 (p=0.3) for IgG anti-PC-BSA, and r=0.09 (p=0.3) for IgM anti- PC-BSA antibodies.

In addition to the absence of a treatment effect on the antibody levels and their stability over one year, there was a lack of correlation between any of the antibody levels at baseline or one year, and LDL cholesterol at either baseline or one year, as shown in the correlation matrix (Table 4.3c).

There was a weak correlation between baseline IgG anti-MDA-LDL antibodies and baseline CRP (rho=0.16 p=0.03), but as antibody levels remained stable whilst CRP was reduced by statin treatment, there was no correlation between antibody levels and CRP at one year (rho = 0.06; p = 0.4).

We also tested the relationship of antibody levels at one year and CIMT at year 1, but found no significant correlation (data not shown).

Tables 4.3 a-c. Correlation Matrices

Table 4a. Relationships between IgM anti-oxidised LDL antibodies at baseline and one year. Data are Pearson's correlation coefficients (r) and associated p values

Table 4b. Relationships between IgM anti-oxidised LDL antibodies at baseline and one year. Data are Pearson's correlation coefficients (r) and associated p values.

Table 4c. Correlations between LDL at baseline and 1 year and antibodies against oxidised LDL. Data are Pearson's correlation coefficients (r) and p values.

Table 4.3a IgM	MDA-LDL at baseline	MDA-LDL at one year	PC-BSA at baseline
MDA-LDL at one year	0.56 (p<0.001)		
PC-BSA at baseline	0.47 (p<0.001)	0.27 (p<0.001)	
PC-BSA at one year	0.32 (p<0.001)	0.41 (p<0.001)	0.59 (p<0.001)

Table 4.3b IgG	MDA-LDL at baseline	MDA-LDL at one year	PC-BSA at baseline
MDA-LDL at one year	0.53 (p<0.001)		
PC-BSA at baseline	0.19 (p=0.01)	0.15 (p=0.05)	
PC-BSA at one year	0.13 (p=0.1)	0.042 (p=0.6)	0.73 (p<0.001)

Table 4.3c	Baseline LDL		Year 1 LDL	
	r	p	r	p
Baseline anti-MDA-LDL IgG	-0.13	0.10		
Year 1 anti-MDA-LDL IgG			-0.04	0.65
Baseline anti-MDA-LDL IgM	0.03	0.67		
Year 1 anti-MDA-LDL IgM			-0.07	0.37
Baseline anti-PC-BSA IgG	-0.07	0.38		
Year 1 anti-PC-BSA IgG			-0.12	0.12
Baseline anti-PC-BSA IgM	-0.04	0.60		
Year 1 anti-PC-BSA IgM			-0.03	0.72
Baseline Total IgG	-0.08	0.31		
Baseline Total IgM	-0.05	0.54		

4.3.5 IgG1 and IgG3 isotypes are also stable over one year, and are independent entities

Table 4.4 is a correlation matrix demonstrating that both IgG3 and IgG1 anti-MDA-LDL isotype levels positively correlated with total IgG anti-MDA-LDL antibody levels, but not with each other at baseline, indicating that they are independent entities. Total IgG anti-MDA-LDL levels did not correlate with LDL or HDL, but IgG3 anti-MDA-LDL levels were weakly, but positively correlated with HDL (r=0.21,p=0.004). IgG1 anti-MDA-LDL antibody levels correlated with HDL (r=0.178,p= 0.01) and negatively correlated with LDL (r=-0.17,p=0.02). There were no differences in any of the antibody levels in the study group at one year. IgG1 and IgG3 antibody levels were not affected by treatment with statins, despite the marked effect on LDL (p= 0.28 for IgG1 and 0.70 for IgG3). There was an interesting wide-scatter distribution of IgG1 anti-MDA-LDL levels, which appeared to be in a 2-tiered distribution (Figure 4.8).

Table 4.4 Correlation Matrix

Relationships Between isotypes of IgG anti-MDA-LDL antibodies, LDL and HDL at baseline. *Data are Pearson's correlation coefficients (r) and associated p* values.

	Total IgG anti-MDA-LDL antibodies at baseline	IgG3 anti-MDA-LDL antibodies at baseline	IgG1 anti-MDA-LDL antibodies at baseline	LDL	HDL
Total IgG anti-MDA-LDL antibodies at baseline		0.25 (0.0008)	0.27 (0.0002)	-0.12 (0.87)	0.1 (0.14)
IgG3 anti-MDA-LDL antibodies at baseline			0.05 (0.47)	-0.14 (0.055)	0.21 (0.004)
IgG1 anti-MDA-LDL antibodies at baseline				-0.17 (0.02)	0.178 (0.01)

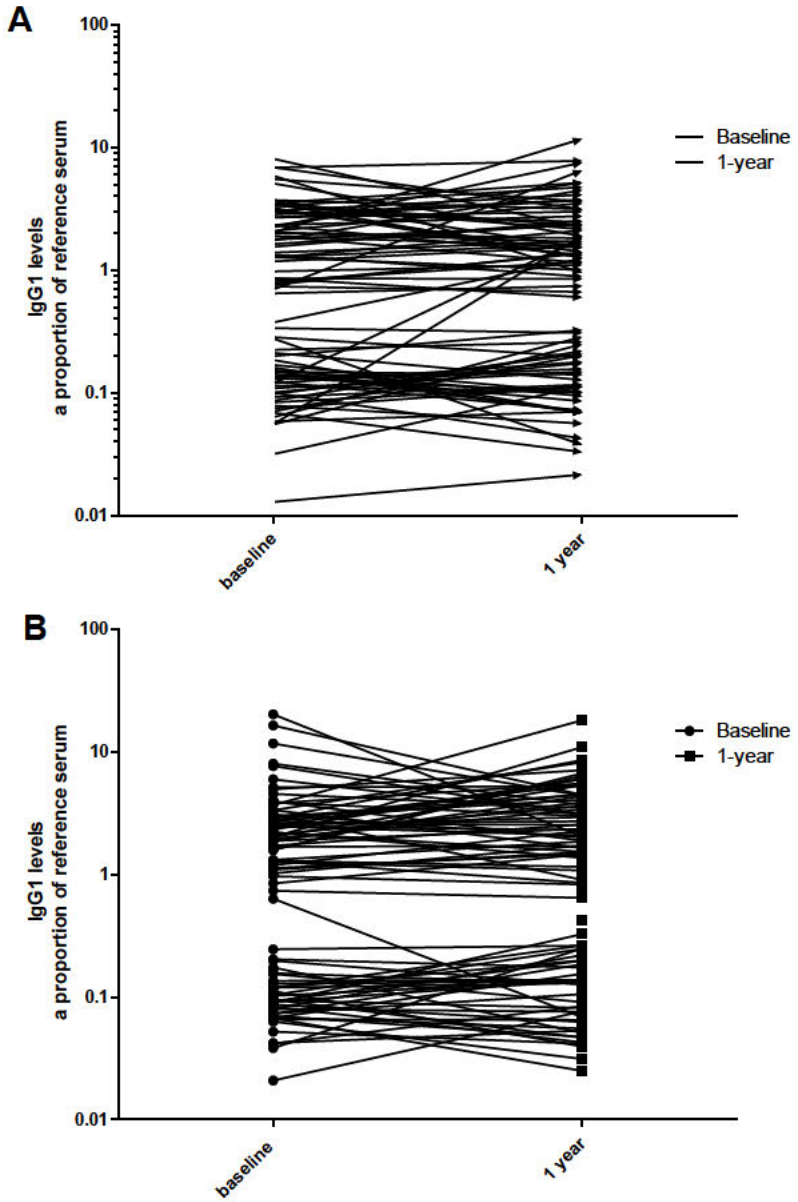


Figure 4.8 Distribution of anti-MDA-LDL IgG1 antibody levels at baseline and 1-year in the (A) Atorvastatin & (B) placebo groups

4.3.6 Total IgG anti-MDA-LDL antibodies but not individual IgG1 or IgG3 isotype levels are strong predictors of protection from MACE

The predictive power of total IgG anti-MDA-LDL antibodies of protection from MACE was not retained when testing individual levels of the two dominant isotypes (HR 0.98 95%CI(0.84 to 1.14) p=0.85 for IgG1, and HR 1.06 95%CI(0.57to1.99) p-0.84 for IgG3). Thus, levels of IgG1 and IgG3 isotype subgroups did not separately account for the protective effect of total IgG and MDA-LDL antibodies, follow different distribution patterns, and are weakly correlated with other biomarkers of cardiovascular disease.

5.0. The Characterisation of LO1, A Monoclonal Autoantibody Against MDA-LDL And Its Development Into A Molecular Imaging NIRF Agent In Experimental Atherosclerosis.

5.1 Chapter Abstract:

In this chapter we describe the characterisation of LO1 against different oxidised forms of LDL, the characterisation of H3 as its anti-idiotype and the sequencing LO1 for the molecular expression into Fab. We further generate a tagged LO1 Fab construct we also label LO1 and utilise it as well as a caged MMP to study oxidised low density lipoprotein (oxLDL) as a NIRF molecular imaging target in mouse and rabbit atherosclerosis models. We further label the Fab construct and demonstrate potential in further imaging studies.

LO1 reacts with malondialdehyde-conjugated LDL (MDA-LDL), it does not bind native LDL or other modifications of LDL. Furthermore, it co-localises to the atherosclerotic necrotic core in both murine aorta and human carotid sections. Both LO1 light and heavy chains were sequenced, and sequences confirmed on published databases. Peptide blocking assays suggested a conformational epitope for LO1 binding to H3. LO1 and an IgG3k control antibody were labelled with a NIRF dye to give LO1-750 and IgG3-750. Targeting to atherosclerosis in mice was compared to an activatable reporter of matrix metalloproteinase activity (MMPSense FAST) by FMT combined with micro-CT. Uptake by rabbit aorta was detected with a custom-built intra-arterial NIRF catheter. We further developed LO1 into a humanised Fab construct with a cysteine tag (LO1-Fab-Cys).

Injection of LO1-750 into high fat (HF) fed *Ldlr*$^{-/-}$ atherosclerotic mice led to specific focal localisation within a region of interest enclosing the aortic arch and its branches when compared to isotype control and wild type animals. *Ex vivo* studies confirmed LO1-750 localisation to sub-endothelium, often in the vicinity of macrophages within atherosclerotic lesions. Both LO1-750 and the MMP reporter quantified statistically significant increases in arterial targeting related to genotype, age, and duration of HF diet; with MMPSense FAST targeting being affected more dramatically by HF diet withdrawal. In the rabbit, LO1-750 localisation was identified in aortic lesions with the intra-arterial catheter. The humanised LO1-Fab-Cys construct was localised in a similar fashion to the parent antibody.

5.2 in Vitro Characterisation on LO1

Previous work in the laboratory undertook the initial screening of LO1. Hybridomas were generated using splenocytes from a one year old female LDL receptor deficient mouse that had not been immunised. Of 950 clones screened, we identified only 10 IgG antibodies with differential reactivity with native versus Cu-oxLDL. From these, we selected LO1 (and LO9 in chapter 6) for further characterisation in this thesis.

5.2.1 LO1 ELISA studies

As shown in Figure 5.1A, LO1 reacts selectively with MDA-LDL, which is a major constituent of Cu-oxLDL, and not with native LDL. In further ELISA studies we found that the LO1 epitope is not revealed by modifying LDL with exposure to trypsin or hypochlorite, or by 'auto-modification' through leaving LDL stored over two months in the absence of EDTA (Figure 5.1B). In order to take LO1 forwards as an imaging agent, we needed to test whether there are factors in human serum capable of blocking LO1 binding. A dilution series of human serum (with a top concentration equivalent to an LDL concentration of 100 μg/ml)

was pre-mixed with LO1 to test whether there are factors in human serum capable of blocking LO1 binding to its antigen. This failed to show evidence that serum inhibits LO1 binding to either the anti-idiotype H3 (described below), or MDA-LDL (Figure 5.1C).

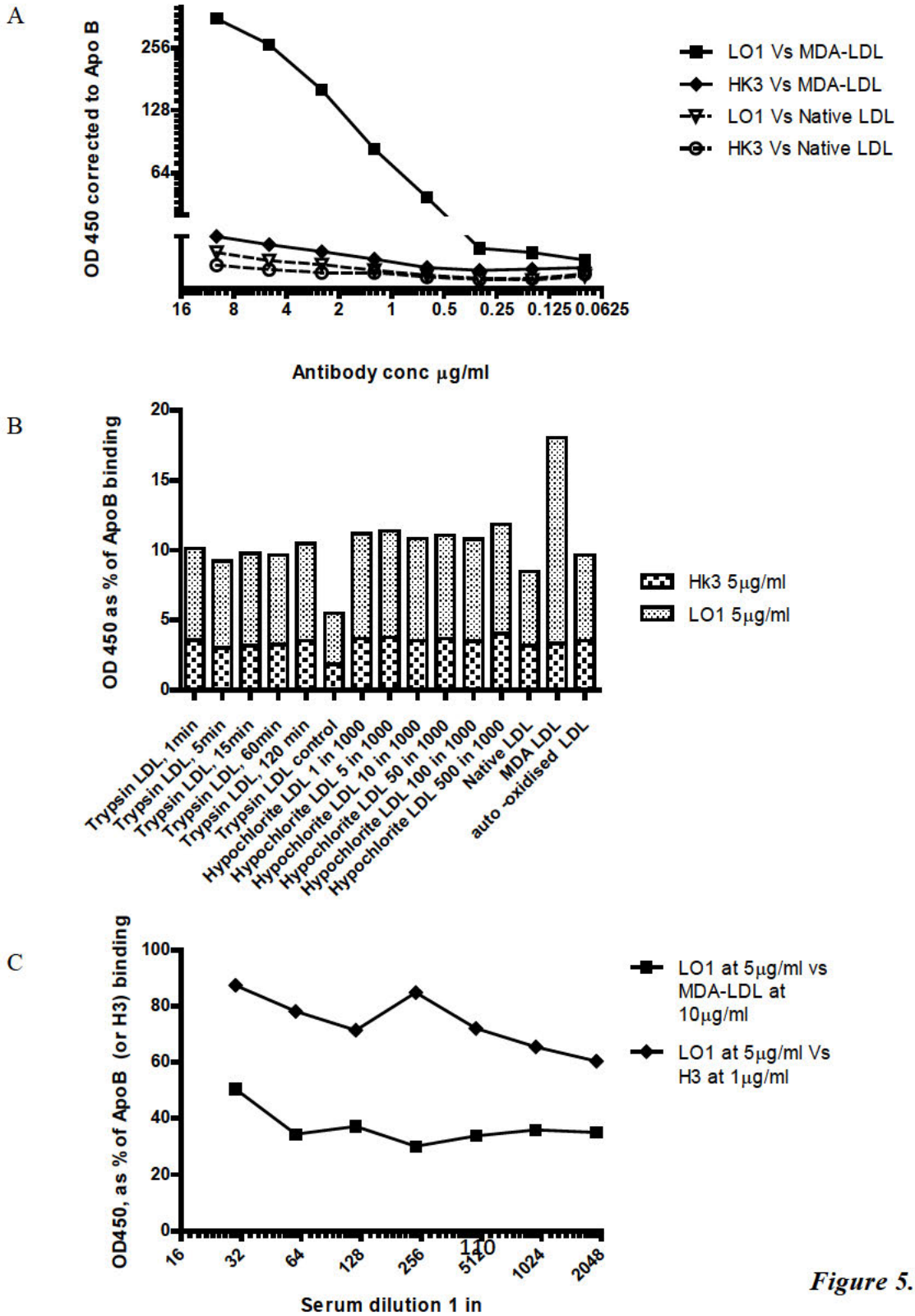


Figure 5.1

Figure 5.1. Initial characterisation of LO1

(A) Reactivity by ELISA of LO1 vs. HK3 (IgG3κ isotype control) against MDA-LDL and native LDL (both at 10μg/ml) in a dilution series with a top concentration of 10μg/ml. (B) LO1 was tested against LDL trypsinised to varying degrees, LDL modified at different hypochlorite concentrations, native LDL, autooxidised LDL, and MDA-LDL. LO1 binds to MDA-LDL but not to the trypsinised, hypochlorite modified or autooxidised LDL. HK3 did not demonstrate significant binding to any of the LDL preparations. (C) Shows the failure of human serum to block the binding of LO1 to both MDA-LDL and H3.

5.2.2 Characterisation of H3

To facilitate the affinity purification of LO1, we isolated H3, an anti-idiotype to LO1, from a single chain antibody phage display library and characterised it in detail.

Figure 5.2A shows LO1 reacting with H3 in a dilution series, but not with a control single chain antibody C12. Figure 5.2B demonstrates that H3, but not C12 blocks the binding of LO1 to MDA-LDL

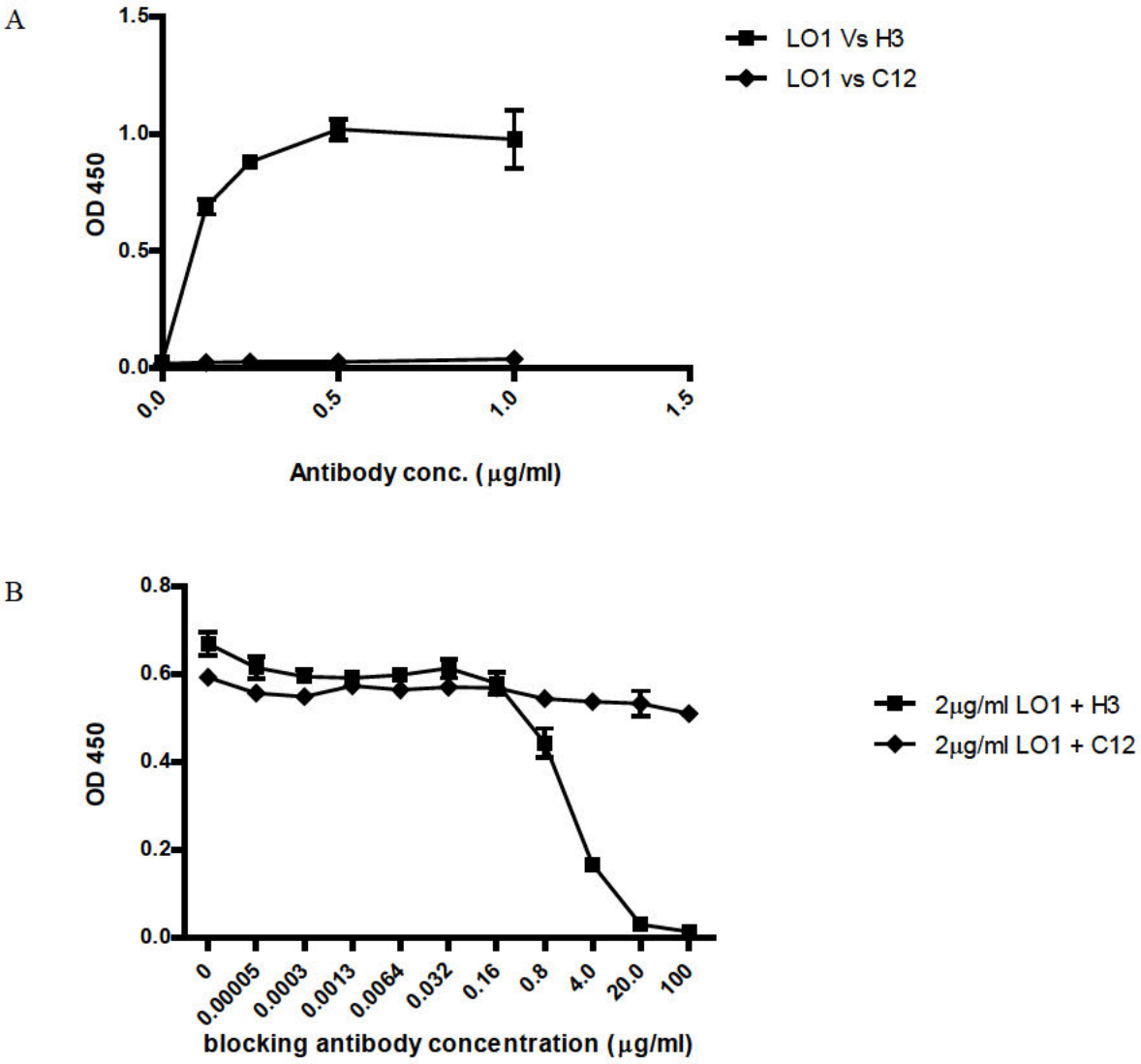


Figure 5.2 LO1 identifies H3 selectively. (A) shows specific binding of LO1 to H3. Microtiter plates were coated with H3 or C12 and then tested for binding of LO1 in a dilution series starting at 10 µg/ml; (B) shows neutralisation of LO1 binding to MDA-LDL by H3. LO1(2 µg/ml) was incubated with plates coated with MDA-LDL (10 µg/ml) in the presence of varying concentrations of H3 or control single chain antibody C12. Data in A and B are from duplicates and are plotted as mean and SEM.

Changing the salt concentration had a very similar effect on binding of LO1 to H3 as to MDA-LDL (Figure 5.3). There was also a similar profile of pH sensitivities with optimal binding at pH 6. Interestingly LO1 binding to H3 had a slightly broader pH range compared to LO1 binding to MDA-LDL.

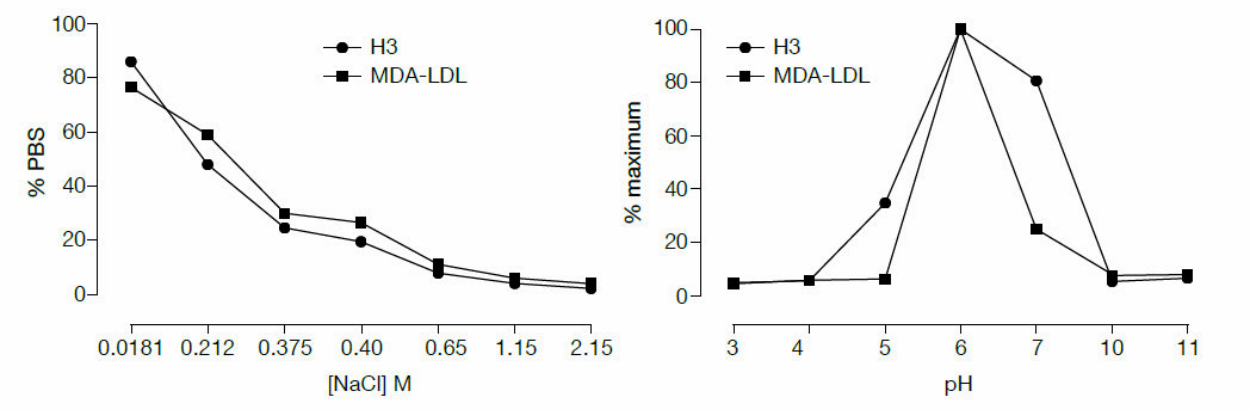


Figure 5.3. LO1 binds H3 and MDA-LDL in similar Ph and salt conditions. The graph on the left demonstrates the similar profiles for LO1 binding to MDA-LDL and H3 under differing Ph conditions. The graph on the right demonstrates similar binding of LO1 to both MDA-LDL and H3 under differing molar concentrations of sodium chloride.

In order to explore the LO1 epitope on H3 further, we designed linear peptides that represent various regions of the H3 structure. These linear peptides were then tested for both specific binding of LO1 (vs HK3) and also ability to block the binding of LO1 to MDA- LDL and H3 separately and in combination.

The peptides below covered the following sections of the H3 structure (Table 3.1) :

Peptide	Sequence	Area Covered
Peptide 1	VSDISGSGNTITYA	CDRH2
Peptide 2	CAKDDDAFDYWG	CDRH3
Peptide 3	YADSVKGRFTIS	CDRH2-FR2 Interface
Peptide 4	NIYYASALQSGVP	CDRL2

Table 5.1. Peptides designed to cover possible binding sites on H3

All peptides failed to bind H3 selectively (data not shown) and failed to block the binding of LO1 to H3 at a dilution series starting with an equivalent molar concentration of H3 that demonstrated block (Figure 5.4). This suggests that the LO1 H3 epitope may be conformational.

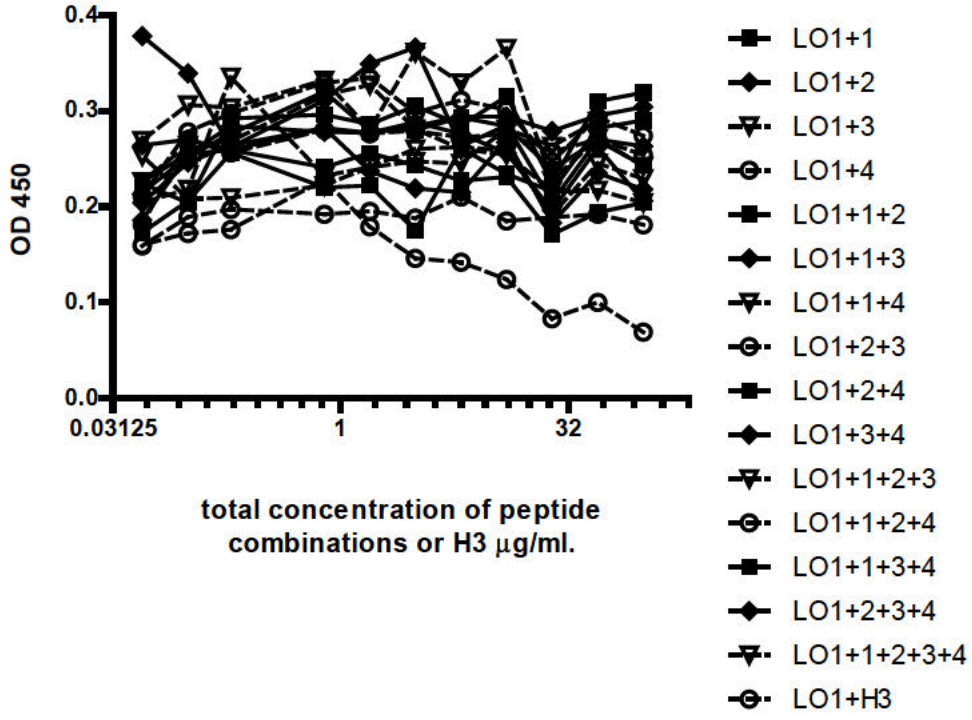


Figure 5.4 Liniear peptides derived from H3 do not block LO1 binding. ELISA at 450 of LO1 (1 µg/ml) vs H3 (0.5 µg/ml) blocked with peptide combinations. Failure of linear peptides 1 to 4 to block the binding of LO1 to H3, either in isolation or in combination. H3 in an equivalent molar concentration blocks the binding at higher concentrations.

5.2.3 Biotinylation of H3

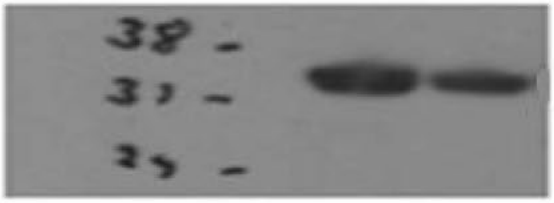
In order to confirm the generation of H3 with an Avi tag, western blotting was performed using anti-c-Myc as a primary antibody. Confirmation of the presence of H3 was obtained by visualising a band at around 32kd (Figure 5.5A). This was equivalent to a band produced by a previously tested batch of H3 with Avi Tag.

ELISA was performed to confirm the preservation of function of H3 following biotinylation. LO1 was coated on the solid phase and both H3 and H3-Biotin were tested in a dilution series.

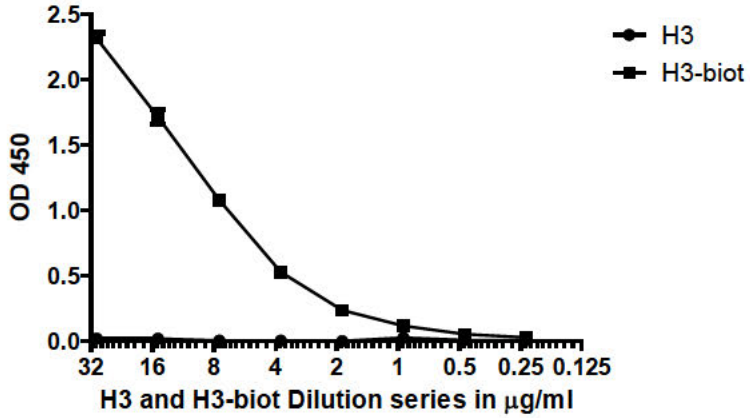
We demonstrated that H3-Biot was functional in binding to LO1, being detectible with streptavidin without a secondary antibody. Non-biotinylated H3 on the other hand was not detected with streptavidin directly (negative control) (Figure 5.5B).

The activity of the biotinylated H3 elutions was also compared to H3 by testing against LO1 and detection with an anti c-Myc secondary. This shows a similar, but slightly attenuated, pattern of binding of H3 to LO1 once H3 is biotinylated (Figure 5.5C).

A



B



C

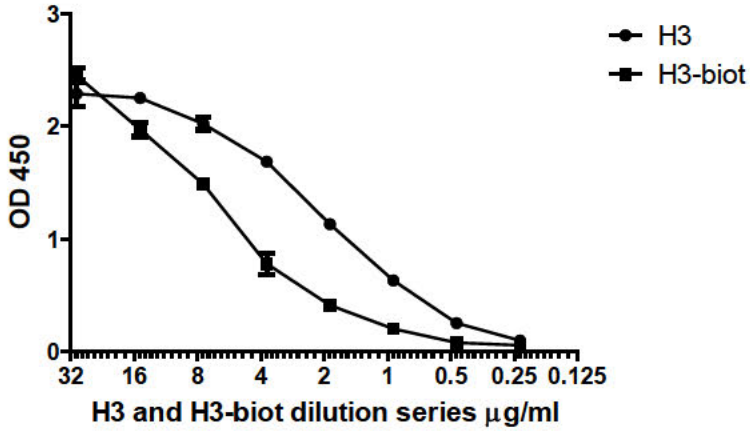


Figure 5.5 Production and biotinylation of H3. (A) Confirmation of the production of H3 (with Avi tag), by western blotting. Anti-c-Myc was used as a primary antibody to detect H3. (B) ELISA of H3 and H3 biotin (dilution series) vs. LO1 at 10µg/ml. Detection was with 1/200 streptavidin followed by TMB. This shows the successful biotinylation and retention of function of H3. (C) ELISA of H3 and H3 Biot in dilution series vs. LO1

detected by ant C-Myc. This shows that both biotinylated and non-biotinylated forms of H3, react with LO1 when on solid phase.

5.2.4 Isolation of purified LO1

The utility of H3 was as a stable, easy to work with, surrogate for MDA-LDL when LO1 needed to be affinity purified. Therefore, LO1 was purified on an H3 biotin affinity column. The purity was demonstrated using a Colloidal blue protein staining kit. Figure 5.6 demonstrates the clear light and heavy chain LO1 bands in comparison to unpurified LO1. The activity of the purified LO1 was tested using ELISA against MDA-LDL and H3 and was shown to be equivalent to the original stock of antibody (data not shown). The purified LO1 was then sent to our mass spectrometry unit for ms/ms tryptic mass spectrometry.

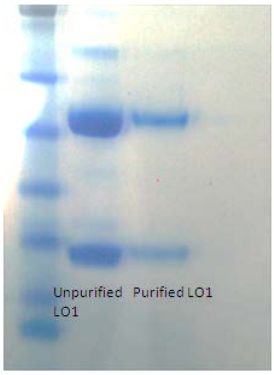


Figure 5.6. Colloidal blue staining shows both heavy and light chains of both purified and unpurified LO1.

5.2.5 LO1 sequencing

The generation of molecularly-engineered derivatives of LO1 which might have improved *in vivo* targeting required us to identify the correct DNA sequences for the LO1 heavy and light chain variable regions. Therefore the DNA sequences were identified, and the veracity of the

sequences was confirmed by mass spectrometry of the tryptic peptides of LO1 that had been affinity purified on an H3 column. Following DNA sequencing, we obtained the amino acid sequences of the variable heavy (VH) and the variable light (VL) regions (Figure 5.7). These were matched by searching the IMGT database and found to correspond to VH1 family (V1-54) and VL family (V6-20) respectively. Both the VH and VL sequences are germ-line, indicative of LO1 being a natural antibody.



Figure 5.7. Amino acid sequences of the LO1 VH and VL. The panel shows the LO1 V_H and V_L sequences and their homology with the germ-line V1-54/JH2 and V6-2-/J2 sequences

5.2.6 LO1 labelling

5.2.6.1 Biotinylation:

Following deactivation of LO1 using amine chemistry, two other techniques were successful in labelling LO1 with biotin. Therefore we used the aldehyde groups and achieved a functional stock of biotinylated LO1 as shown in Figure 5.8

The biotinylation of LO1 was demonstrated by testing 'LO1 Biot' against H3 with unbiotinylated LO1 as positive control and HK3 as negative control. LO1 Biot was detected both by goat anti-mouse Ig, followed by streptavidin, and by streptavidin alone. There was

some loss of signal with streptavidin alone, attributed to the loss of amplification obtained by the usual use of a secondary antibody.

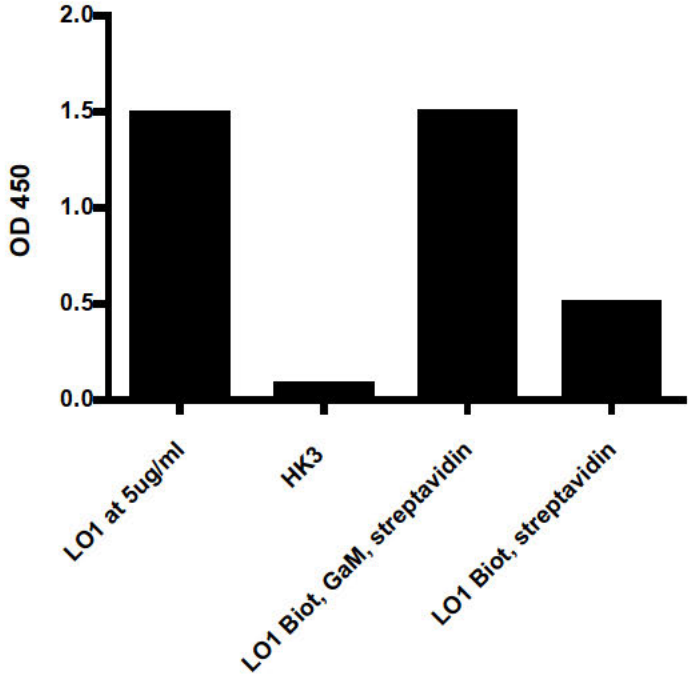


Figure 5.8 Demonstrates the retention of activity of LO1 to H3 following biotinylation.

LO1 and LO1 Biot at 5μg/ml Vs H3 at 1μg/ml with HK3 control. The reduced signal in comparison the LO1 can be explained by the loss of amplification that arises from the utilisation of goat anti-mouse (GaM) as a secondary antibody for the detection of the unbiotinylated LO1.

ELISA to demonstrate equivalent biotinylation of LO1 and control IgG3 showed a relatively higher biotin activity for the control antibody than LO1. This discrepancy in biotinylation would have been corrected for if needed (results not shown).

5.2.6.2 Fluorescence labelling of LO1

Even with modulation of reaction, attempted fluoresceination of LO1 using amine chemistry, with both 40% and 70% modulation of labelling to reduce the amount of label per mole of protein, resulted in the deactivation of the antibody reactivity against both MDA-LDL and H3. The fluoresceination reaction may have affected crucial lysines (e.g. in V_H CDR3) which may be a part of the LO1 interaction with its epitope (Figure 5.9).

The DOL for Alex Fluor 647 vs LO1 was 7.57 Moles dye per moles protein when the reaction was modulated at 40% and 1.54 moles dye per moles protein when the reaction was modulated at 70%.

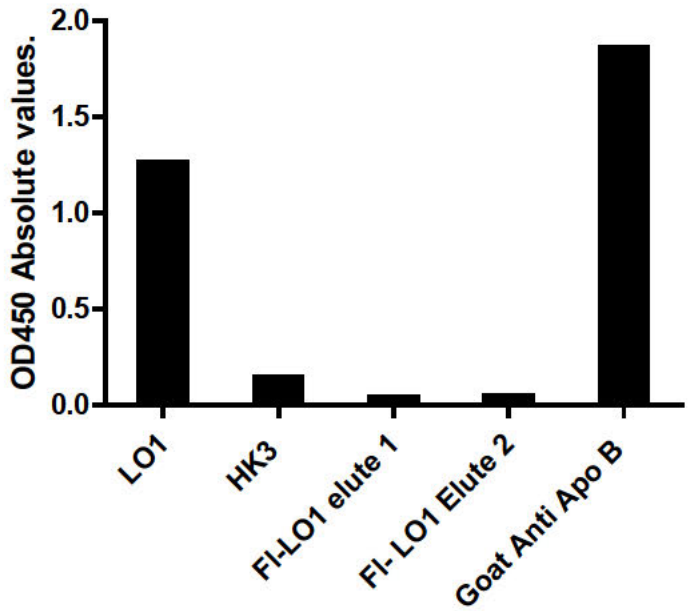


Figure 5.9. Fluoresceinated LO1 (SAIVI Alex Fluor 647) at 70 % modulation vs. MDA and Native LDL at 15 µg/ml as a percentage of ApoB binding. Demonstration of loss of

activity of LO1 vs. MDA-LDL once it is fluoresceinated. FL-LO1 elutes 1 and 2 correspond to two elutes of fluoresceinated LO1 at 70% modulation. The goat anti-ApoB is a positive control for the coating of the ELISA plate with LDL. Similar result was obtained with 40% modulation (not shown)

Therefore we moved to using thiol chemistry and optimised a method where we were able to fluoresceinate LO1 on the SH groups and retain its function as shown below.

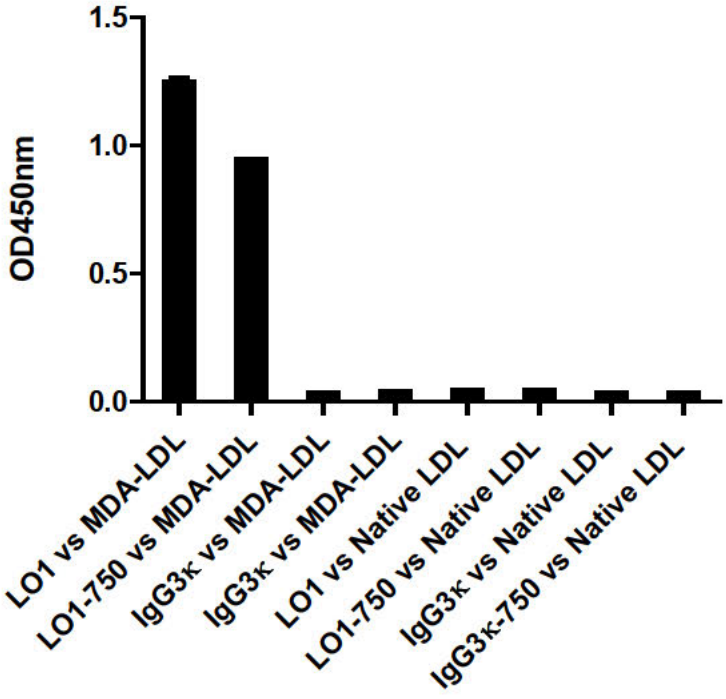


Figure 5.10 ELISA demonstrating the relative retention of function of LO1 when it is labelled with VivoTag MAL 750 (termed LO1-750) in comparison to LO1. Both labelled and unlabelled LO1 did not react with native LDL. The control IgG3κ antibody did not react with either native LDL or MDA-LDL either when unlabelled or labelled.

5.2.7 Binding of LO1 to atherosclerotic lesions in mouse, rabbit and human

In vitro IHC staining with unlabelled LO1 demonstrated that LO1 stained atherosclerotic lesions in the aortic root of *Ldlr*$^{-/-}$ mice but did not bind the aortic root of normocholesterolaemic WT mice, consistent with tissue accumulation of oxidised LDL in *Ldlr*$^{-/-}$ mice[166]. The binding of LO1 was inhibited by either MDA-LDL or the LO1 anti-idiotype H3, demonstrating specificity of LO1 (Figure 5.11). We then tested whether LO1 labelled with VivoTag®-S 750-MAL (LO1-750) binds antigen in the mouse aortic arch using *en face* preparations and confocal microscopy. Figure 5.12A shows that LO1-750 binding was greatest at bifurcations and on the inner curvature of the aorta, sites well known to be susceptible to atherosclerosis[50]. Similarly-conjugated control IgG3 showed no detectable binding to the aortic preparations (Figure 5.12B), demonstrating specificity of the staining obtained with LO1-750. It was notable that LO1-750 binding showed focal accumulation as well as a diffuse distribution, consistent with the known propensity of oxidised LDL to aggregate[182].

We also found by IHC that LO1 binds antigen in atherosclerotic lesions in high fat fed rabbits, staining particularly the macrophage rich areas (Figure 5.13). Unlabelled LO1 (Figure 5.14) and LO1-750 (Figure 5.15) staining of human carotid atherosclerotic plaques showed similar patterns. In Figure 5.15, there was clear co-localisation to macrophages within the necrotic core, but there was also diffuse staining which was not co-localised to macrophages, consistent with free oxidised LDL.

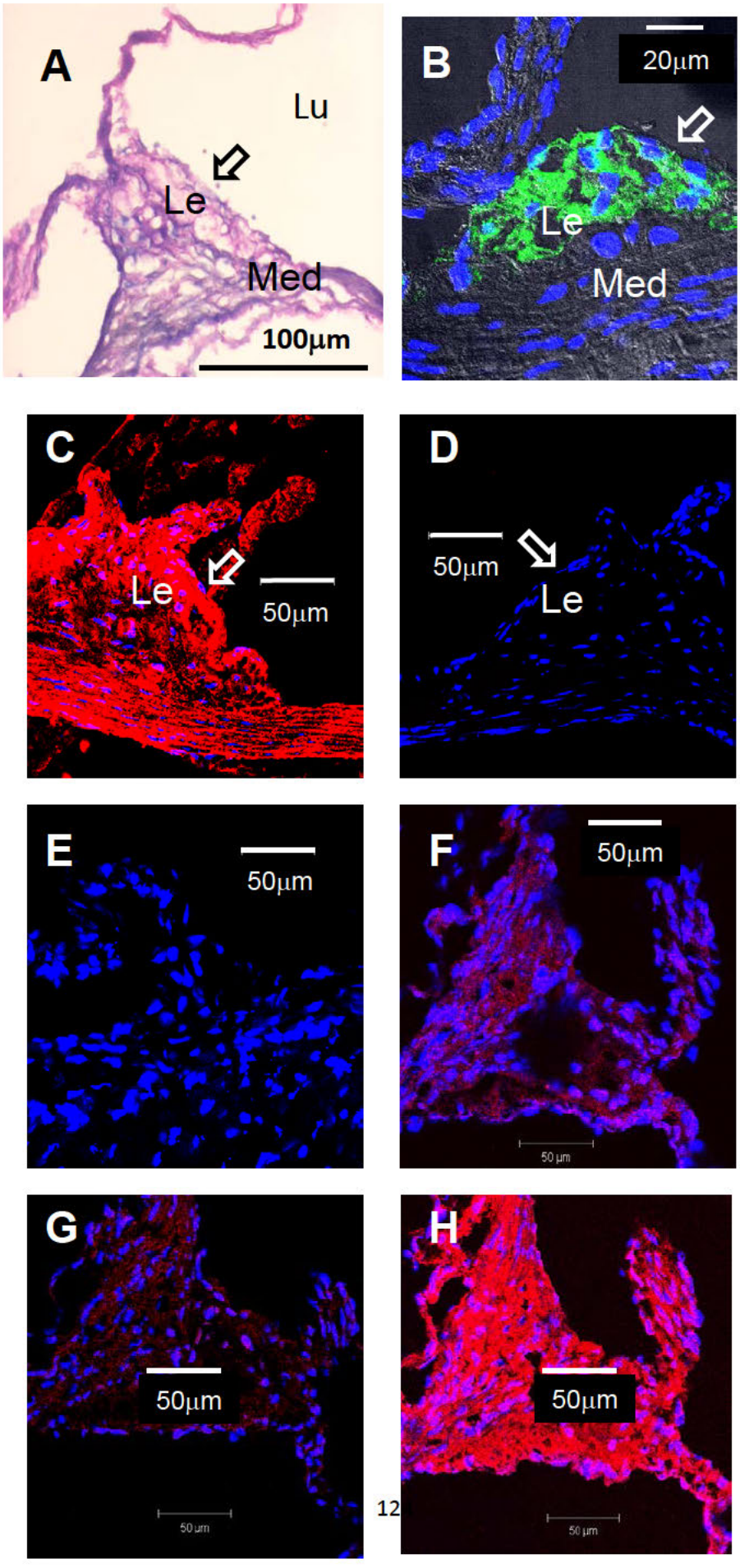

A
Lu
Le
Med
100µm
B
20µm
Le
Med
C
Le
50µm
D
50µm
Le
E
50µm
F
50µm
50 µm
G
50µm
50 µm
H
50µm
50 µm

Figure 5.11

Figure 5.11. Immunocytochemical staining of *Ldlr*$^{-/-}$ mouse aortic root with LO1. (A) shows an aortic valve cusp from a Ldlr$^{-/-}$ mouse stained with Giemsa, a general purpose tissue stain; in **(B)** the region indicated by the arrow is stained with the macrophage-specific marker CD68-AlexaFluor488 (green) and the DNA-binding dye TOPRO (blue), revealing the localised area of macrophage infiltration and the unstained media (Med). Diffuse staining of the whole valve cusp is seen with **(C)** LO1 but not **(D)** control IgG3. In **(E)** no equivalent staining was seen with LO1 applied to the aortic root of a wild type mouse. Pre-incubation of LO1 with **(F)** MDA-LDL or **(G)** H3, but not **(H)** C12 inhibited staining, demonstrating specificity of LO1 binding. Blue = TOPRO counterstain. Red = AlexaFluor 568 fluorescence showing specific binding of LO1.

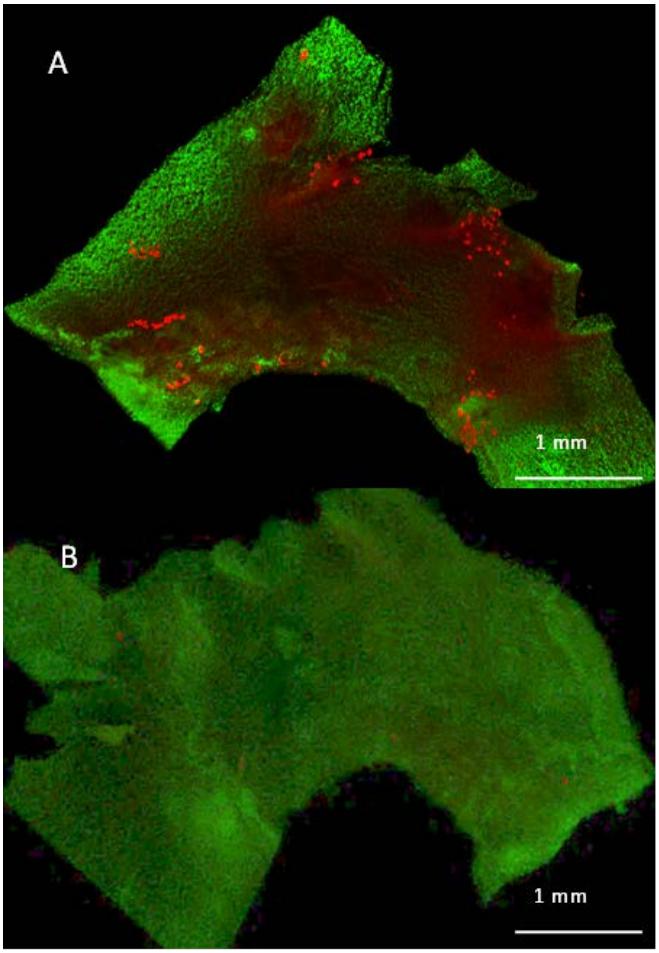


Figure 5.12. Immunofluorescence staining of en face Ldlr$^{-/-}$ mouse aorta, with LO1-750 and isotype control. (**A**) Shows directly labelled LO1 (LO1-750) staining red concentrated at areas that maybe susceptible to atherosclerosis (Green = SYTO-24 nuclear counterstain) There is also diffuse weak staining in the surrounding regions suggesting less concentrated deposits of oxidised LDL; (**B**) Shows isotype control (IgG3k-750) on a litter mate high fat fed *Ldlr*$^{-/-}$ mouse (red) directly labelled in the same manner as LO1 (Green = SYTO-24 nuclear counterstain).

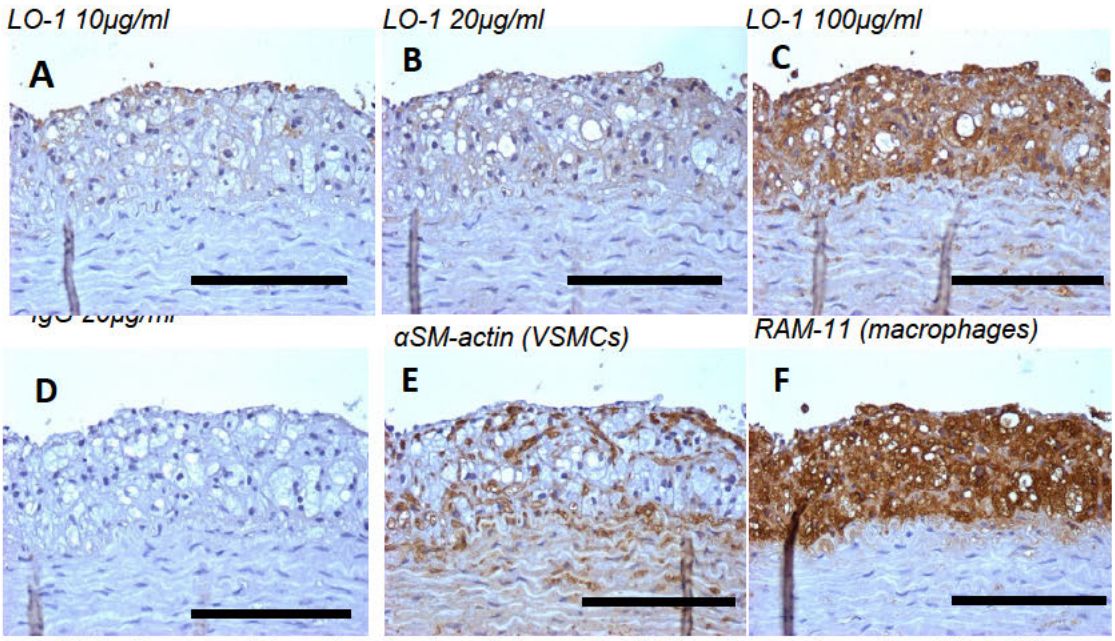


Figure 5.13. Immunohistochemical staining of rabbit atherosclerosis with LO1.

Atherosclerotic sections from the aortic arch of a high fat fed, female New Zealand White Rabbit, were stained for LO1 in a dilution series (**A**-**C**). LO1, but not its isotype control (**D**) localised to macrophage rich (**F**), atherosclerotic area. There was also some staining of free deposits within the plaque and no clear localisation to Vascular Smooth Muscle Cells (**E**). Scale bars represent 100µm. This staining was undertaken by Dr. Jason Johnson (University of Bristol)

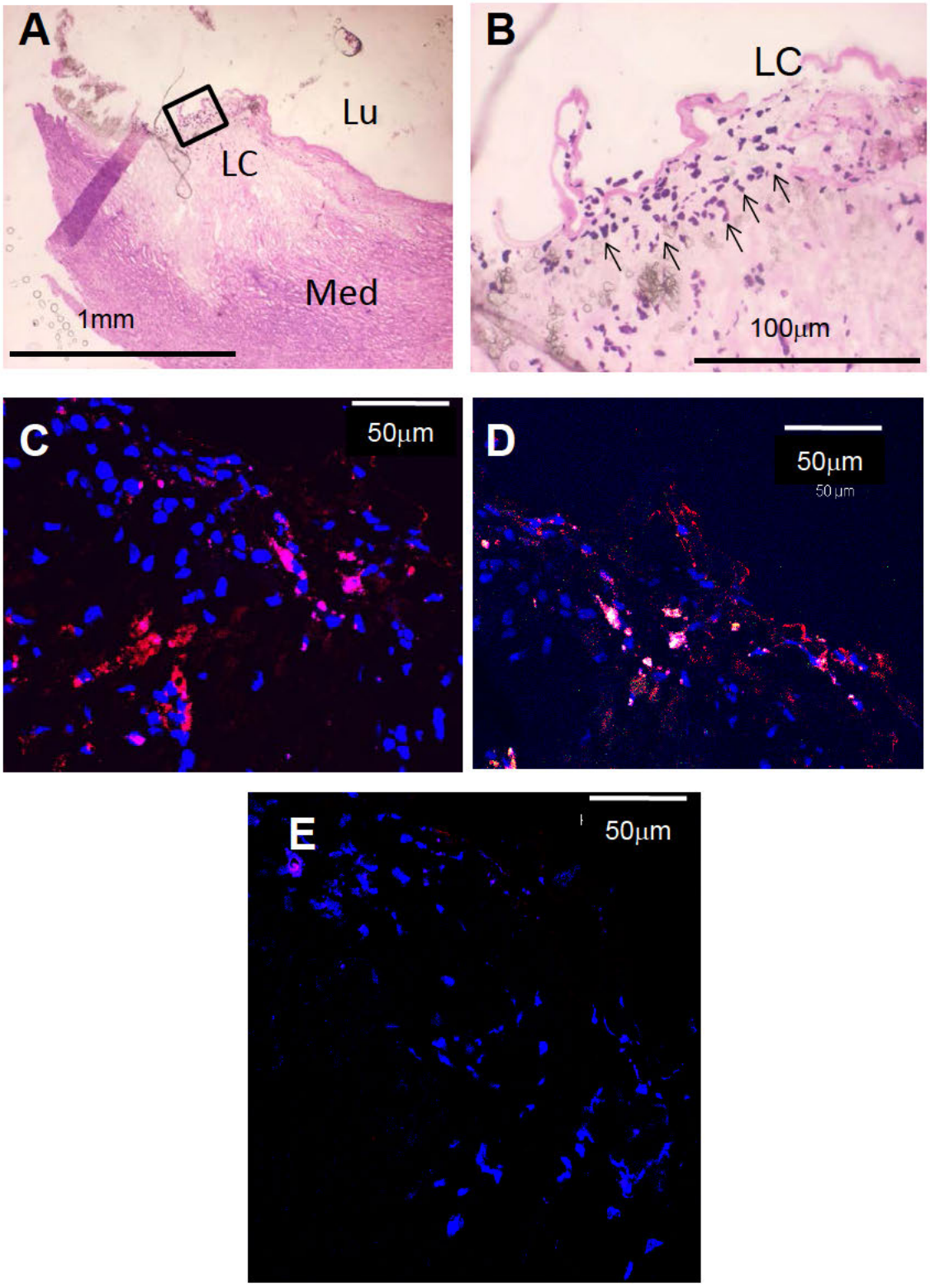


Figure 5.14

Figure 5.14. Immunocytochemical staining of human carotid atherosclerotic plaque with LO1. For orientation **(A)** shows a low power view of a human carotid atherosclerotic plaque stained with Giemsa, with the area within the box magnified in **(B)**. (**C-E**) show confocal imaging of consecutive serial sections in the vicinity of the boxed area in (B): **(C)** single stained with LO1 (red AlexaFluor 568), **(D)** dual-stained by LO1 (red AlexaFluor 568) and CD68-AlexaFluor488 (green) with brilliant yellow-white indicating co-localisation, and **(E)** single stained with control IgG3 with protocol and settings identical to (C). Lu = lumen; LC = lipid core; Med = media. Blue = TOPRO = nuclei (DNA). Fine arrowheads, inflammatory cells at edge of lipid core. Scalebars = distances indicated.

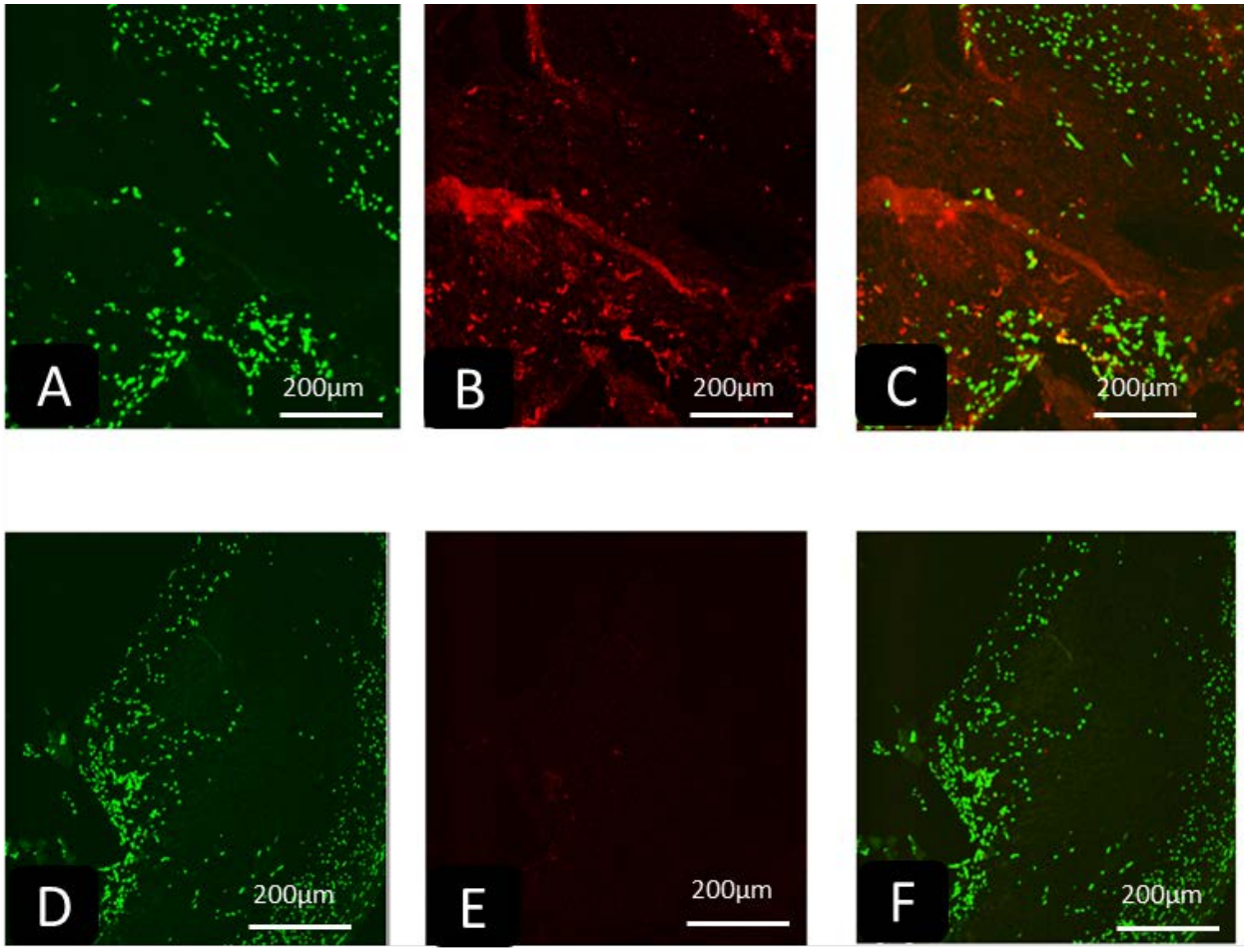


Figure 5.15. Immunofluorescence staining of human carotid atherosclerosis with LO1-750. **(A-F)** show representative consecutive serial sections next to lipid necrotic core of human carotid atherosclerotic plaque stained with (**B**) LO1-750 displaying both a punctate, cellular type staining as well as a more diffuse staining of aggregates within the lipid core; (**E**) is negative staining with control IgG3k-750; (**A**) and (**D**) are nuclear counterstains in green SYTO-24; (**C**) are (**F**) are merged images.

5.3 *In vivo* studies

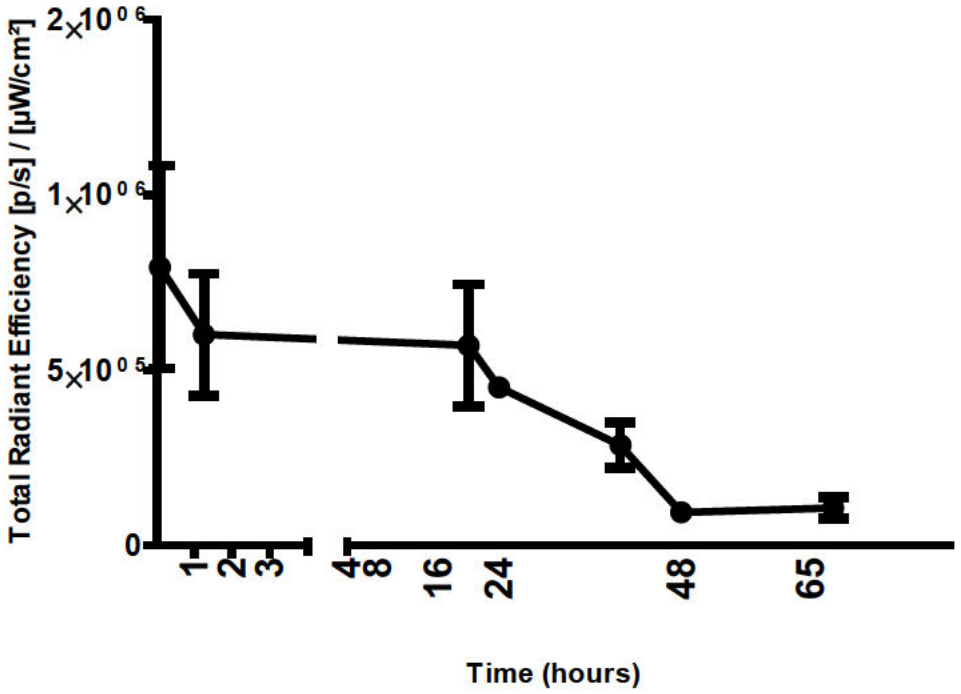
Following *in vitro* characterisation of LO1, we proceeded to in vivo studies. The first imaging experiments were undertaken using the IVIS Spectrum system, then with the FMT 4 laser system for the quantitative studies, and comparison with the MMP reporter, MMP Sense FAST. The rabbit studies were undertaken at Harvard Medical School using a bespoke imaging catheter described in the methods section.

5.3.1 Clearance of LO1-750 after intravenous injection in mice

Following intravenous injection of antibodies, heparinised blood samples from serial tail bleeds were imaged *ex vivo* for epifluorescence using IVIS Spectrum. The blood clearance of LO1-750 demonstrated a phased decay pattern, with no difference between *Ldlr*$^{-/-}$ and WT animals (n=3 mice in each group, at 7 time points tested over 68 hours). There was a rapid immediate phase of clearance lasting minutes, followed by a slower phase with detectable levels of LO1-750 remaining in the circulation over the duration of the experiment, as expected for a 150kd protein (Figure 5.16A). The overall half-life of intravenously injected LO1-750 was estimated as 21 hours.

The overall organ distribution of LO1-750 and IgG3k-750 at 4 hours after injection was broadly equivalent, both in the *Ldlr*$^{-/-}$ mice and WT animals (not shown), with most of the antibodies localising to liver, kidneys and spleen (Figure 5.16B).

A



B

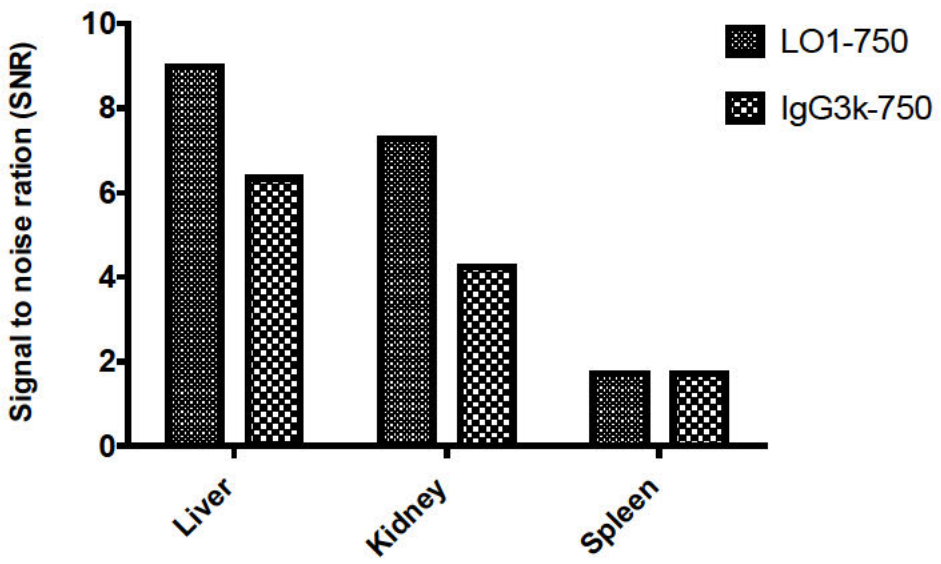


Figure 5.16. Blood clearance and organ distribution of LO1-750 as determined by ex vivo epifluorescence of heparinised serial bleeds and extracted organs **(A)** Shows the clearance from the blood of LO1-750 as determined by serial bleeds of both *Lldr* $^{-/-}$ (n=3) and wild type mice (n=3). There was no difference in clearance between the two groups, and the data points are mean and SEM from the mice combined. The clearance displayed a two phased decay pattern with a

fast and a slow phase. The overall half-life was estimated at 21 hours **(B)** Shows equivalent *ex vivo* organ distribution of both LO1-750 and its isotype control in the *Ldlr*$^{-/-}$ mouse with most of the antibodies localising to liver, kidneys and spleen.

5.3.2 *In vivo* aortic imaging of LO1-750 in the mouse using hybrid IVIS Spectrum/ CT imaging

We performed a pilot imaging study *in vivo* in *Ldlr*$^{-/-}$ mice using IVIS Spectrum/CT. Based on the blood clearance, images were acquired at 4 hr. As shown in Figure 5.17A, LO1-750 localised to focal areas of the ascending thoracic aorta and aortic arch. In contrast, IgG3k-750 showed no such arterial localisation (Figure 5.17B). Interestingly, we found that localisation of LO1-750 corresponded in places to areas of arterial calcification identified by contrast-enhanced high resolution CT (HRCT) (Figure 5.17 C and D). Using *ex vivo* epifluorescence imaging of the extracted aortae, the ratio of uptake at the atherosclerosis-susceptible aortic arch to normal abdominal aorta was higher for LO1-750 compared to IgG3k-750, with a target to background (TBR) ratio of 2 versus 0.9.

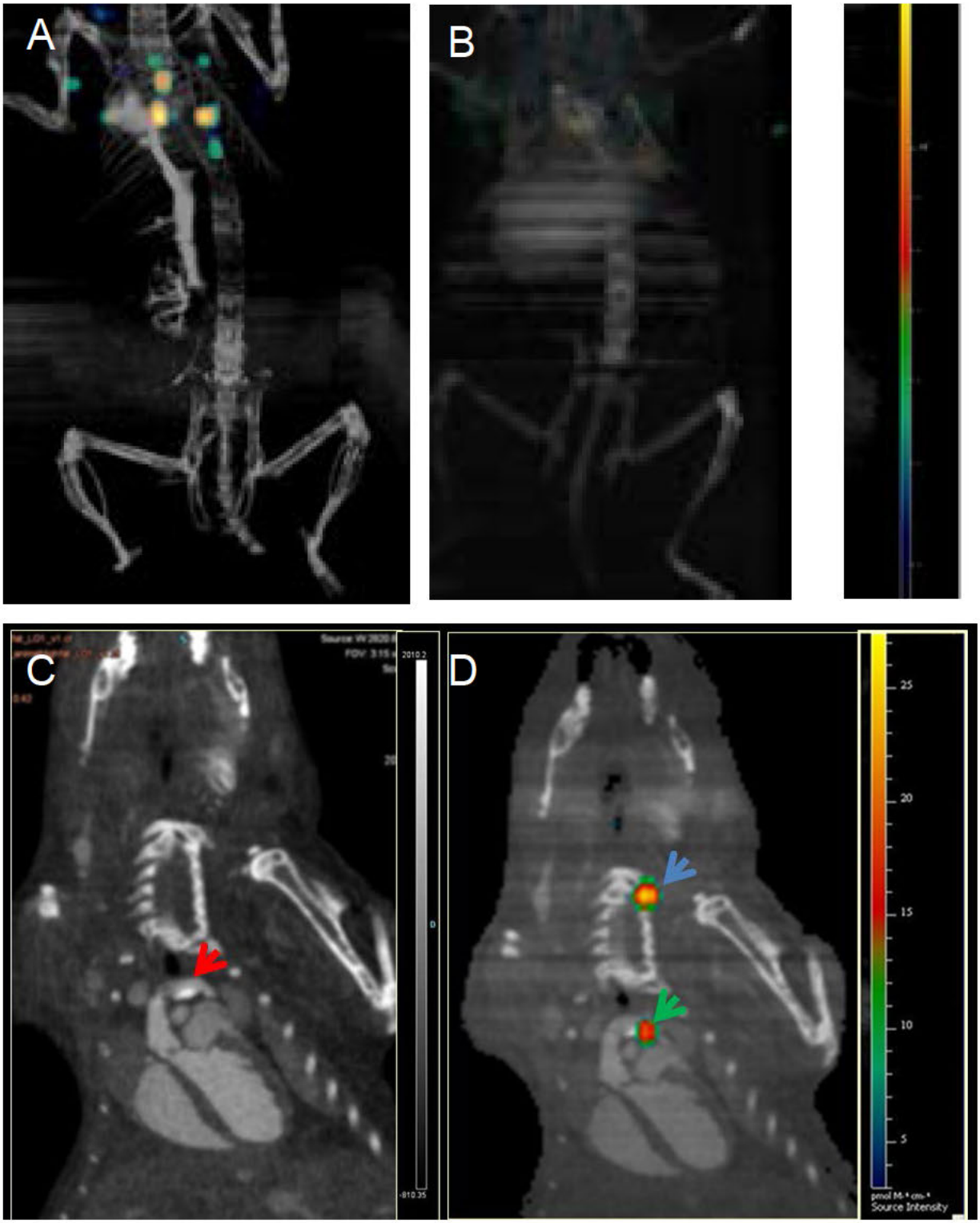


Figure 5.17

Figure 5.17. In vivo aortic imaging of LO1-750 in Ldlr-/- mouse model using hybrid IVIS Spectrum/CT **(A)** LO1-750 localising to the ascending aorta and aortic arch of a one year old *Ldlr* $^{-/-}$ mouse that had been fed with a high fat diet for 42 weeks; **(B)** litter mate control showing very little uptake in the same areas following iv injection of equivalently labelled isotype control antibody (IgG3k-750); **(C)** Demonstrates another example, with calcification in the aortic arch (red arrow) co-localising with LO1-750 signal (green arrow) in **(D)**, as well as a further hotspot (blue arrow), which was demonstrated to be in the left subclavian artery upon cross-sectional imaging.

5.3.3 Quantitative analysis of LO1-750 imaging of mouse atherosclerosis using FMT/CT

We next proceeded to further imaging of LO1-750 localisation using FMT/CT, an imaging modality that allows for three dimensional acquisition and reconstruction of NIF\RF signal and provides absolute uptake quantification. Furthermore, as the FMT has 4 lasers, it is possible to co-inject up to 4 tracers exciting and emitting at different wave lengths. We therefore took the opportunity of using MMPSense 645 FAST (MMPSense) for comparison. MMPSense is a caged fluorescent probe that is activated by a broad range of MMPs including MMP 2, 3, 7, 9, 12, and 13. We compared groups of high fat fed *Ldlr*$^{-/-}$ mice and WT controls, which each received either LO1-750 (50μg) or IgG3k-750 (50μg) intravenously. Each mouse also received 2.4 nmols of MMPSense intravenously. Figure 5.18A demonstrates with 3D FMT/CT reconstruction the localisation of LO1-750 to atherosclerotic areas in the *Ldlr*$^{-/-}$ model, and shows the ROI used for subsequent imaging. As shown as images in Figures 5.18B-E, and quantitatively as a histogram in Figure 10I, the LO1-750 localisation to the aortic arch ROI was specific. Thus, there was a significantly higher level of LO1-750 in the *Ldlr*$^{-/-}$ ROI than in the WT animals (25.3 ± 4.6 pmol vs 1.3 ± 0.9, n=6/group; p = <0.001). The IgG3k-750 antibody had significantly lower levels in both the *Ldlr*$^{-/-}$ mice (0.4 ± 0.3 pmol) and the WT mice (1.2 ± 0.9 pmol) (p<0.001 for both IgG3k-

750 groups in comparison to LO1-750 in the *Ldlr*$^{-/-}$ group). Figures 5.18F and 5.16G show the positive signal seen in the coronal section (Figure 10E), in both the sagittal and transverse planes respectively. We also used the FMT machine to perform selective fluorescence reflective imaging on aortae extracted *post mortem*. Figure 5.18H demonstrates both the LO1 and MMPSense signals seen *ex vivo* in the aortic root and thoracic aorta of a mouse from a *Ldlr*$^{-/-}$ mouse that received LO1-750 (as in Figure 5.18E).

The simultaneously injected MMPSense demonstrated the presence of MMP activity in the ROI, which was equivalent in animals receiving LO1-750 or IgG3k-750. When comparing the MMP signal in the *Ldlr*$^{-/-}$ high fat fed animals vs WT control animals (Figure 10J), the level of MMP activation measured in the ROIs of the *Ldlr*$^{-/-}$ were 37.4 ± 8.9 pmol vs 13± 2.0 pmol in WT mice ($p<0.05$). Comparing MMPSense with L01-750, the latter therefore gave superior positive to negative signal ratio (*Ldlr*$^{-/-}$ to WT) 19.3 vs 2.8 for MMPSense. It was also notable that there was some extravascular MMP activity recorded in some of the animals (for example, limbs and inflamed skin regions) indicating targeting of inflammation more generally.

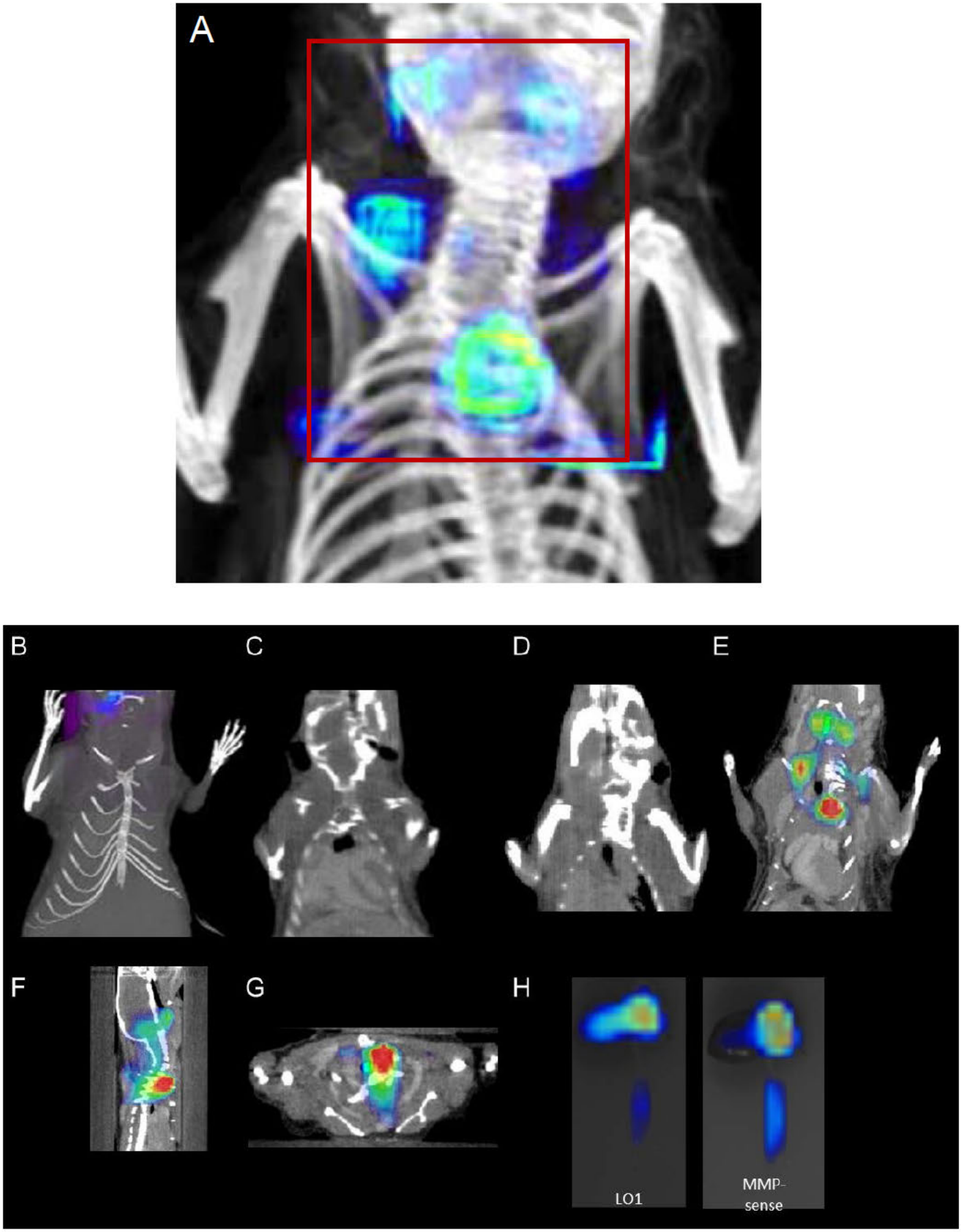
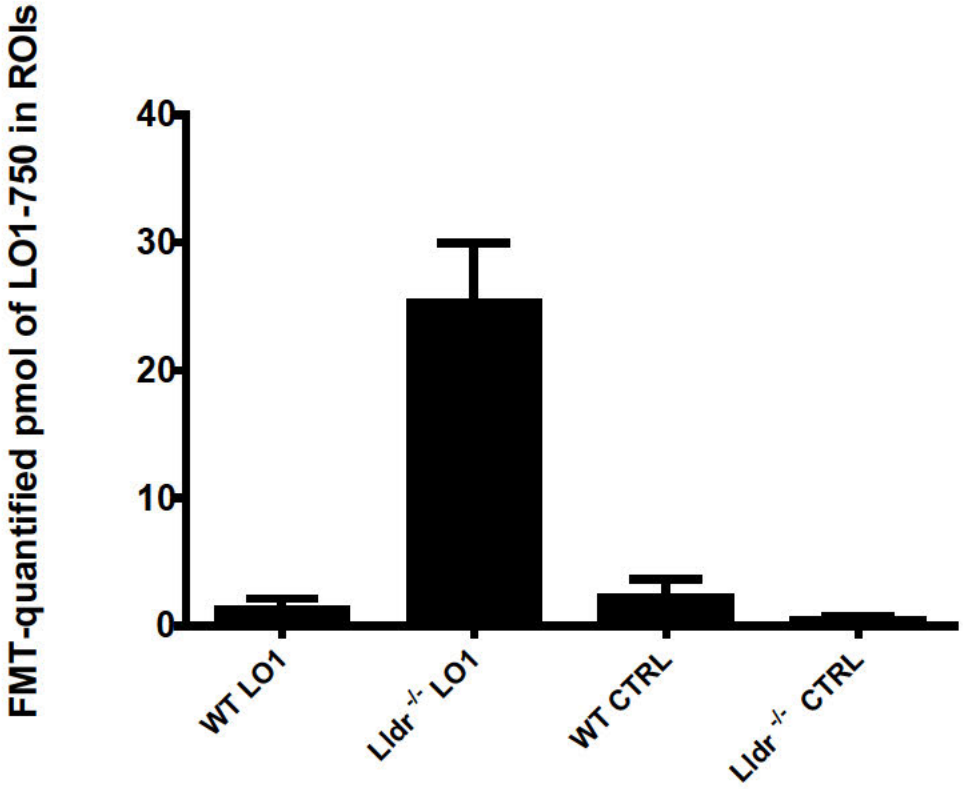


Figure 5.18 A-H

I



J

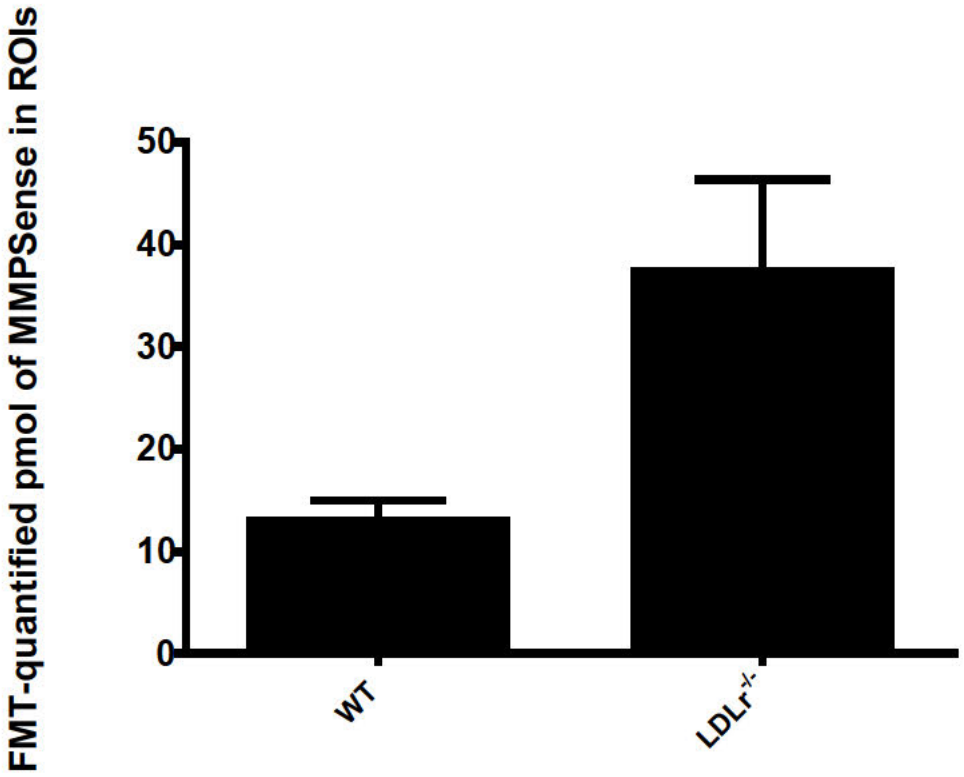


Figure 5.18 I-J

Figure 5.18. FMT/CT imaging and quantification of LO1-750 in the Ldlr-/- mouse model of atherosclerosis. **(A)** 3D FMT/CT reconstruction the localisation of LO1-750 to the aortic arch, both subclavian/brachiocephalic regions and both carotid regions. It also shows the ROI used for subsequent imaging (purple box). Four groups of animals (n=6 in each group) are represented in (**B-D**). Groups (**B**) and (**C**) are age-matched wild type controls (WT) to the *Ldlr*$^{-/-}$ high fat fed mice for 42 weeks in (**D**) and (**E**). (**C**) and (**E**) were injected with LO1-750 (and MMPSense FAST), whilst (**B**) and (**D**) were injected with the equivalently labelled control antibody IgG3k-750 (and MMPSense FAST). Only, the LO1-750 injected, *Ldlr*$^{-/-}$ high fat fed mice in (**E**) displayed a clear signal in the ROI. The signal can be seen in 3 planes (**E-F**), co-localised to CT, and strongest at the aortic arch and related branches. (**H**) is the extracted aorta of another *Ldlr*$^{-/-}$ animal within the same group that shows both a positive LO1-750 and MMPSense signals in the aortic arch and thoracic aorta on FMT epifluorescence imaging. (**I**) demonstrates the quantification of LO1-750 and isotype control in the four groups (**B-D**); there was a significantly higher level of LO1-750 in the *Ldlr*$^{-/-}$ group than in the WT animals. The IgG3k-750 antibody had significantly lower levels in both the *Ldlr*$^{-/-}$ mice the WT mice. (**J**) shows the higher MMPSense signal in the *Ldlr*$^{-/-}$ high fat fed animals vs. WT control animals.

5.3.4 Quantification of LO1-750 localisation distinguishes stages of lesion progression

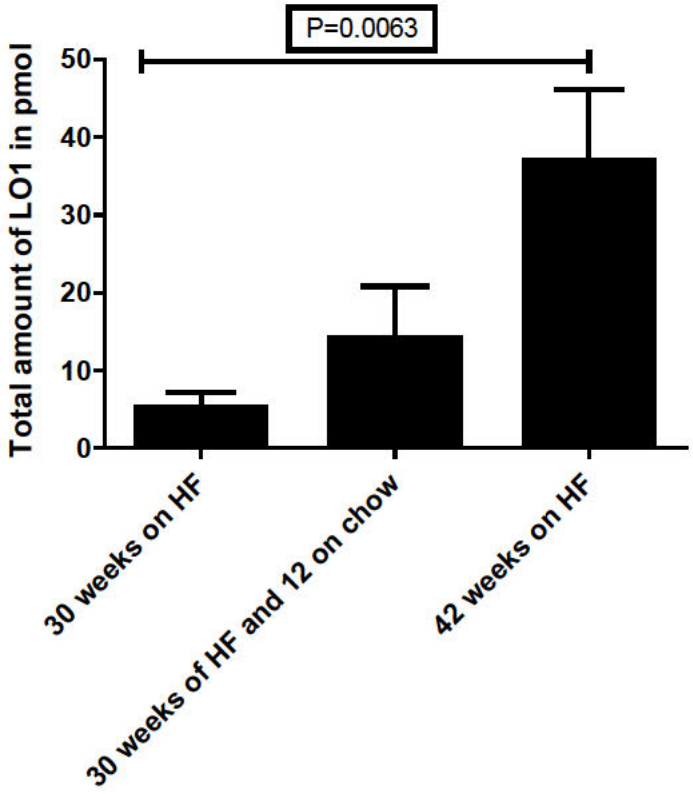
The second FMT study with *Ldlr*$^{-/-}$ mice was designed to determine whether quantification of LO1-750 uptake was sufficiently sensitive to distinguish different stages of disease. For this purpose, mice were given a high fat diet for 30 weeks, starting at 10-12 weeks of age. They were then divided into 3 groups. Group I (baseline) was euthanised at the end of the initial 30 weeks of diet, whereas the other 2 groups were continued for another 12 weeks on either low fat diet (group II) or high fat diet (group III). Mice were imaged with the above protocol, both

with LO1-750 and MMPSense FAST. ROIs were selected and quantification with FMT undertaken as above.

Figure 5.19(A) demonstrates that group III had significantly more LO1-750 uptake at the ROI vs Group I (37.04 ± 9.030 pmol vs. 5.228 ± 1.9 pmol, n=6/group; $p<0.05$). Furthermore, when testing for linear trend between the three groups, LO1-750 demonstrated a positive trend reflecting detection of progression with an R square of 0.42 ($p= 0.004$).

Similarly MMPSense (Figure 5.19B) detected a significant difference between groups III and I with 329.7 ± 134.6 pmol, vs 35.86 ± 15.42 pmol, $p<0.05$. There was, however, less correlation when testing for progression, demonstrating a weaker ability than LO1-750 to correlate the middle group as intermediate (R square of 0.29, $p= 0.02$).

A



B

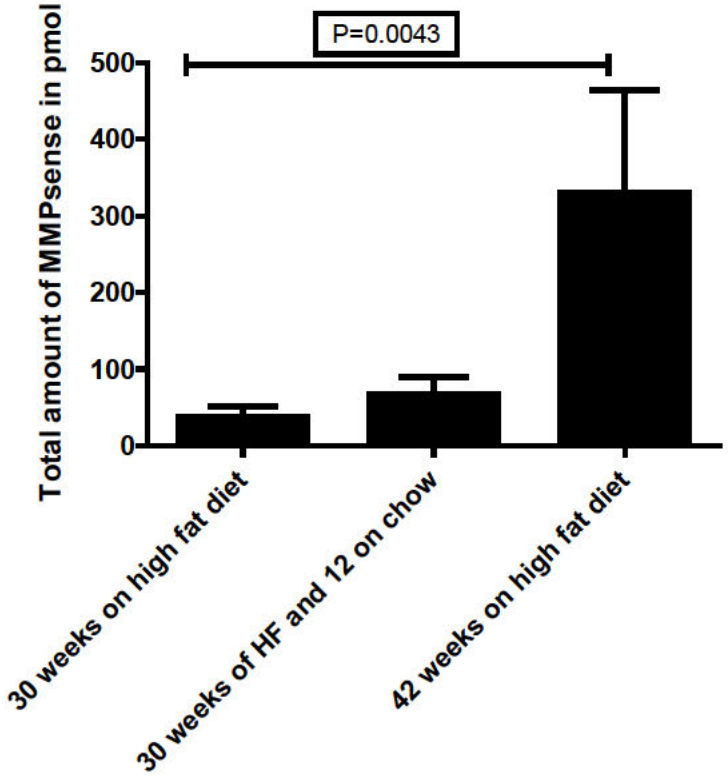


Figure 5.19

Figure 5.19. FMT Quantification of LO1-750 and MMPSense FAST targeting of the aorta and carotids region of interest in 3 stages of atherosclerosis progression. Three groups of *Ldlr*$^{-/-}$ mice (n=6 in each group), mice were given a high fat diet (HF) for 30 weeks vs. 30 weeks on HF followed by 12 weeks of chow vs. 42 weeks on HF. (**A**) demonstrates significantly more LO1-750 uptake in the 42 week HF fed group vs. the 30week HF fed group with a clear linear trend between the three groups (R square 0.42; p= 0.004); (**B**) MMPSense showing a similar difference between the two extreme groups but a weaker linear trend overall (R square 0.29; p=0.02).

5.3.*5 En face* validation of LO1-750 localisation in mouse atherosclerosis using *ex vivo* confocal microscopy

Confocal microscopy was performed *ex vivo* on aortae extracted from animals that had received LO1-750 intravenously 4 hr previously, as for imaging above. Figure 5.20A demonstrates the *en face* appearance of an *Ldlr*$^{-/-}$ aorta, with lesions seen in the inner curvature of the aorta as well as the abdominal aorta. The adjacent panel to the right shows LO1 accumulation (red) as imaged by Z and tile stacking in 750-800 emission channel, co-localising with atherosclerotic lesions. High magnification studies showed partial localisation with macrophages (Figure 5.20B). When studying the signal in 3 dimensions, it became clear that LO1-750 localised beneath endothelium, as identified by co-injected PE-conjugated anti-CD31 (Figure 5.20C), and was both free and bound to macrophages (Figure 5.20D). These confocal *in situ* studies therefore established the ability of LO1-750 to penetrate into lesions, and suggest that its antigen is abundant.

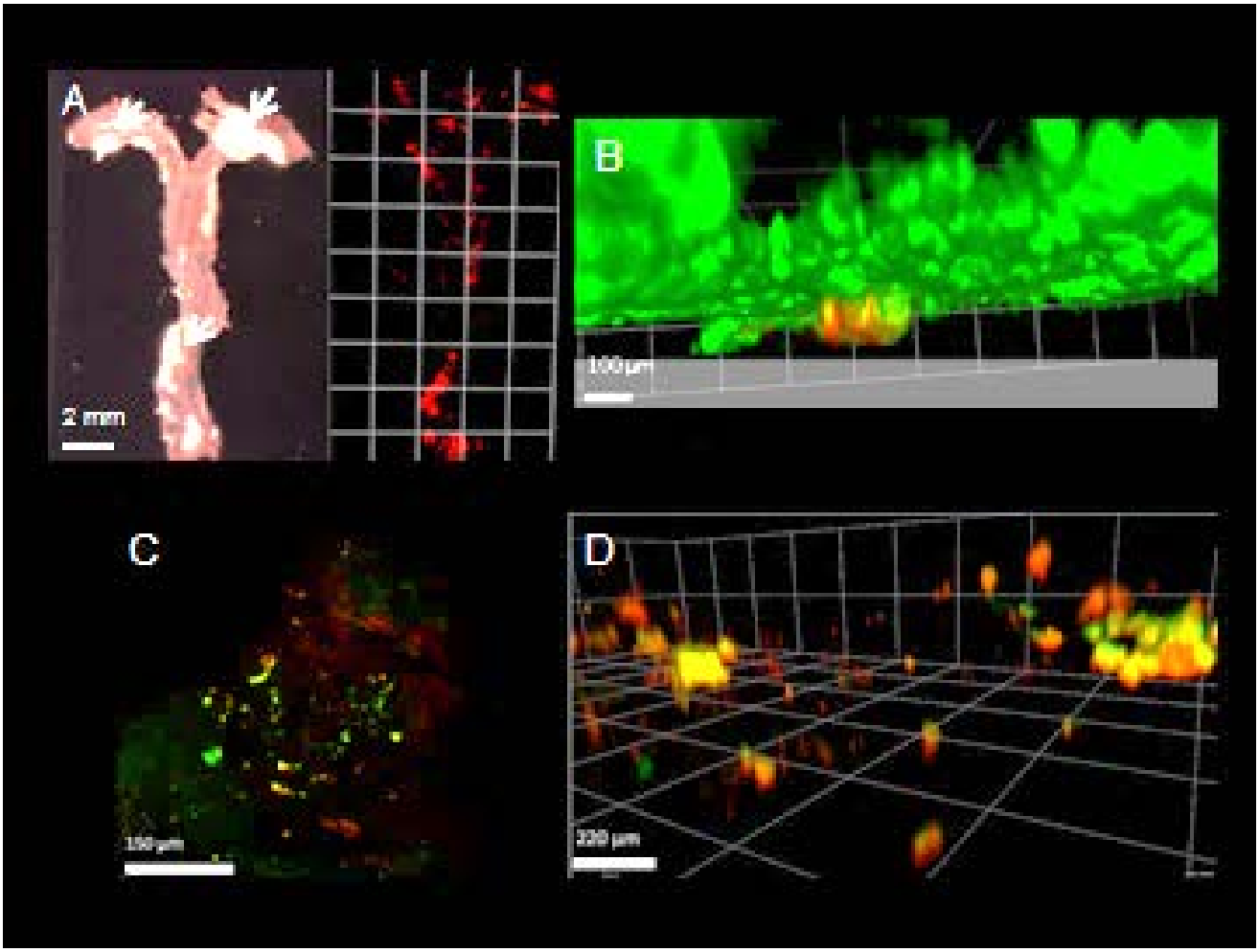
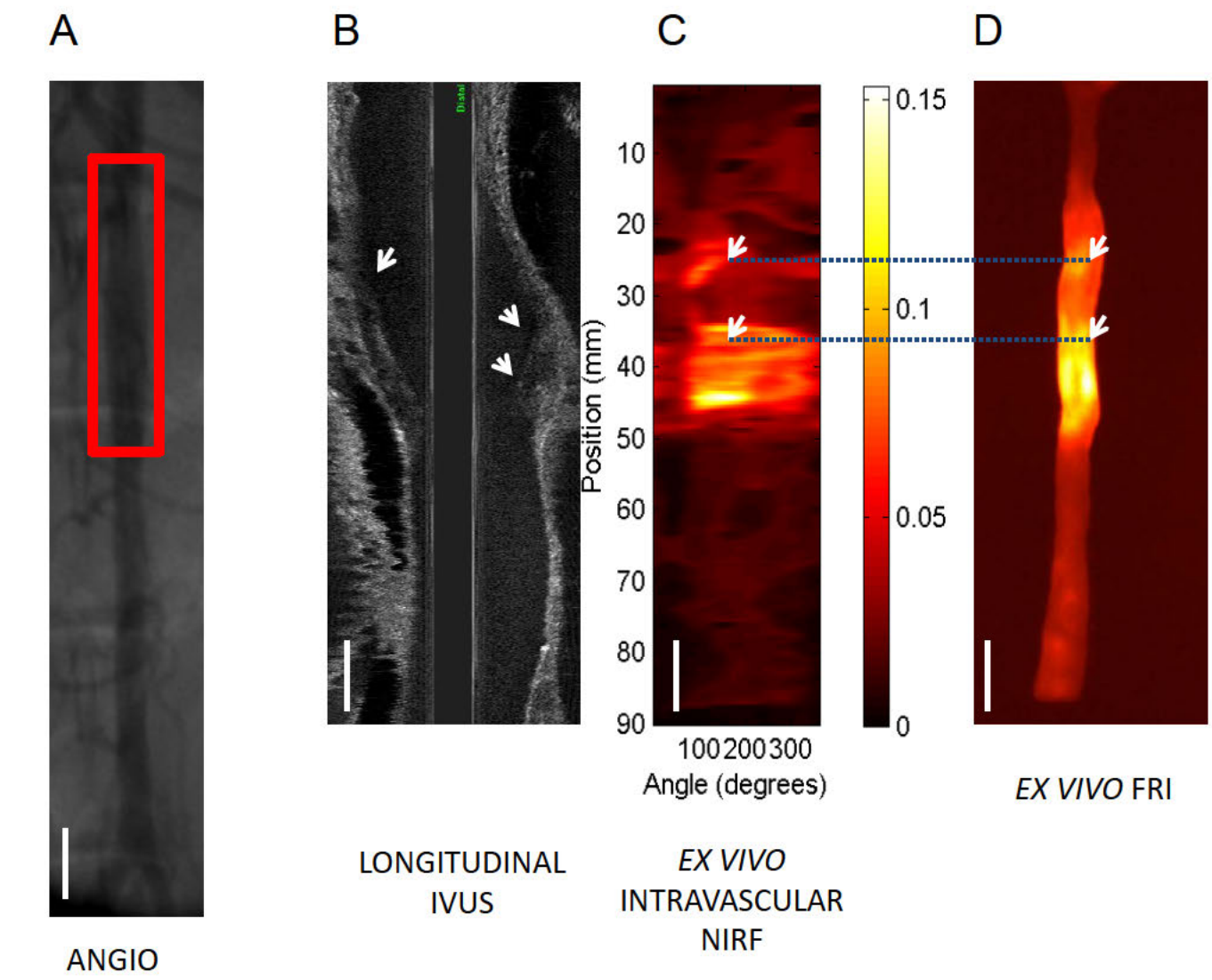


Figure 5.20. En face confocal microscopy of in vivo targeted extracted aorta of the Ldlr-/- high fat fed mouse atherosclerosis model. (**A**) White light image displaying large atherosclerotic lesions (white arrows) in the aortic arch and its bifurcations, as well as the abdominal aorta with corresponding *en face* confocal microscopy showing LO1-750 accumulation (red). **(B)** LO1-750 partially localising to *ex vivo anti-MOMA* stained macrophages (green=macrophages; yellow=merge) (**C**) 3 Dimensional imaging revealing LO1-750 accumulation underneath anti-CD31 in dual targeting with LO1-750 and PE-labelled anti-CD31 antibody. (**D**) 3 Dimensional imaging of the *en face* section of aorta studied in (**B**) demonstrating both localisation to macrophages

(green=macrophage; yellow=merge) and free aggregates within the aortic arch lesional atherosclerotic area.

5.3.6 2D NIRF intravascular imaging of oxidised LDL with LO1-750

NIRF molecular imaging of coronary atherosclerosis in human subjects will likely require high resolution catheter-based approaches [20]. As LO1 binds to rabbit atherosclerotic lesions (figure 5.13), we next explored the ability of LO1-750 to localise to diseased rabbit aorta, a vessel of similar calibre to a human coronary artery. Following *iv* injection of LO1-750, we imaged rabbit aortae with angiography, IVUS and 2D NIRF (n=5). We focused on *ex vivo* intravascular 2D NIRF images of the resected aorta, as the background signal from residual circulating LO1-750 precluded accurate *in vivo* imaging. Figure 5.21A demonstrated the angiographic location of the balloon injury, with atherosclerotic plaque identified by IVUS in Figure 5.21B. We found that the *ex vivo* NIRF signal obtained with the 2D intravascular catheter (Figure 5.21C) was well-matched to that obtained by FRI of the whole aorta (Figure 5.21D). Validation of the deposition of LO1-750 in plaque was performed by *ex vivo* epifluorescence fluorescence microscopy (FM). Figure 5.21E shows a representative cryosection from the larger lesion of the aorta shown in 5.21C and 5.21D, with the distribution of LO1-750 in red and autofluorescence signal from the atherosclerotic lesion in green. This confirmed a similar type of deposition of LO1-750 to that seen in the mouse model, with punctate staining as well as more diffuse staining.


A
B
C
D
0.15
0.1
0.05
0
10
20
30
40
50
60
70
80
90
Position (mm)
100200300
Angle (degrees)
ANGIO
LONGITUDINAL IVUS
EX VIVO INTRAVASCULAR NIRF
EX VIVO FRI

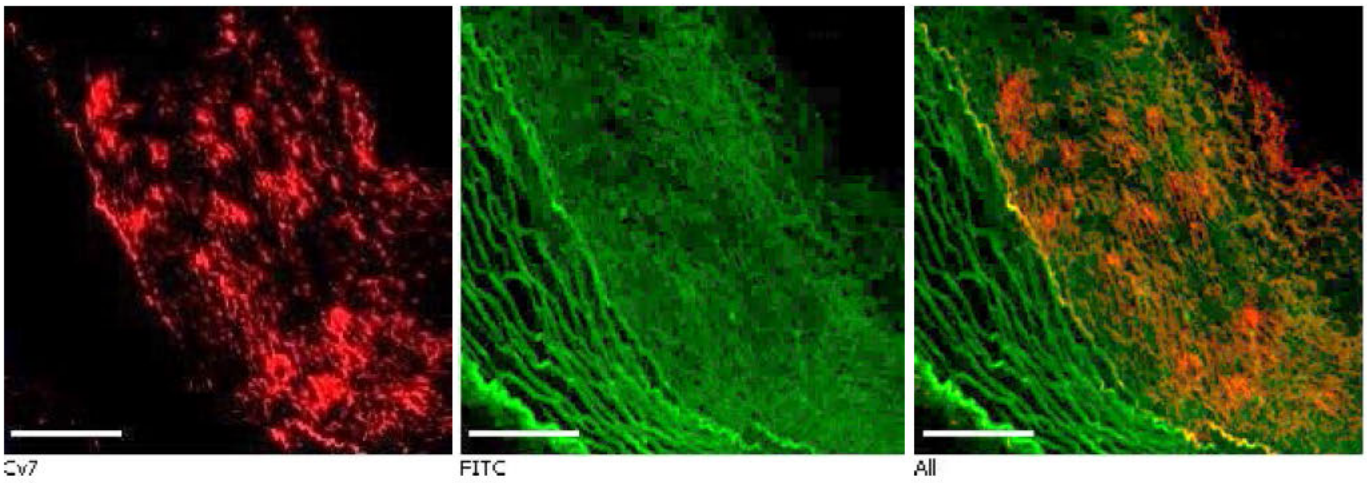

E
Cy7
FITC
All

Figure 5.21

Figure 5.21. NIRF molecular imaging of oxLDL in atherosclerotic balloon-injured rabbit abdominal aortae. LO1-750 (6.6mg/kg in this example) was injected iv into rabbits with aortic atherosclerosis following balloon injury and HF feeding. **(A)** Shows conventional angiography of the rabbit aorta with the red box indicating the balloon-injured area; (**B**) demonstrates the corresponding longitudinal IVUS catheter pullback through the aorta. The white arrows in **(B)** demarcate IVUS evidence of eccentric atherosclerotic plaque; **(C)** shows *ex vivo* two-dimensional (2D) intravascular NIRF imaging of *in vivo* LO1-750 localisation after 21 hr. There are two distinct 'hot-spots' seen on the intravascular 2D NIRF (white arrows in **(C)** and **(D).** The signal-to-noise ratio (SNR) of the 10mm long plaque at the 34 mm to 35mm mark was 86.4 and TBR was 4.8 (yellow/white: higher NIRF signal intensity, red/: lower NIRF signal intensity –arbitrary NIRF units); (**D**) demonstrates corresponding *ex vi*vo FRI (740/790 nm) with augmented NIRF LO1-750 activity in the 2 'hot-spots' seen on intravascular imaging. Corresponding lesions are linked by the dotted blue line; (**E**) demonstrates fluorescence microscopy of a cryosection from the larger lesion of the aorta shown in **(C-D).** The left panel in **(E)** is LO1-750 fluorescence (red) in the NIR channel showing focal and diffuse localisation to constituents of plaque, the middle panel shows the distinctly different atherosclerosis autofluorescence pattern in the FITC channel (green), whilst the right panel is a merged image of both; Scale bars in A-D represent 10mm in A-D and 50 μm in E.

5.4 Generation and Characterisation of LO1-Fab-Cys As a Potential Imaging Agent

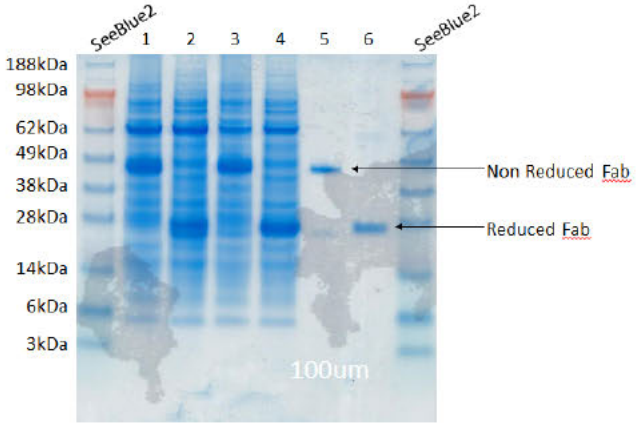
The size, immunogenicity and possible Fc-related effector function of the native LO1 antibody all present possible hurdles to clinical translation. As a step towards the molecular engineering of LO1 constructs for different clinical applications, we used the sequences of the VH and VL regions to express a recombinant 50 kd Fab construct bearing a human CH1 and CL. The terminus of CH1 extends to the THTC of the hinge region to provide a free cysteine for ligand labelling (Figure 5.22A). LO1-Fab was expressed in HEK-293/63 cells (at GSK, Stevenage, by Dr. David Granger), we then obtained the supernatant and purified it over an anti-human CH1 column and demonstrated purity using gel electrophoresis (Figure 5.22B). We then confirmed with mass spectrometry the mass of the molecularly expressed construct to be 118Da greater than the theoretical Fab mass (47627 Da vs 47509 Da) (Figure 5.22C), which is consistent with the cysteinylation of the molecule. Further characterisation by ELISA demonstrated retention of function of LO1-Fab-Cys (Figure 5.22D). We then proceeded to labelling LO1-Fab-Cys with VivoTag®-S 750-MAL, and again confirmed that it retained function *in vitro* (data not shown). We achieved a 3 fold labelling capacity in comparison to LO1 per mg of protein.

Pilot *in vivo* studies in the *Ldlr*$^{-/-}$ vs WT using FMT show similar LO1-Fab-Cys-750 localisation to the atherosclerotic aortic arch area in *Ldlr*$^{-/-}$ mice as LO1-750 (Figure 5.22E). *Ex vivo, confocal* microscopy analysis demonstrated localisation to atherosclerotic murine aorta and co-localisation to-luminal matrix as imaged by autofluorescence is demonstrated in (Figure 5.22F). The appearance of the deposits of LO1-Fab-Cys was similar to that seen with LO1 with both punctate and lesional diffuse staining (Figure 5.22G).

A

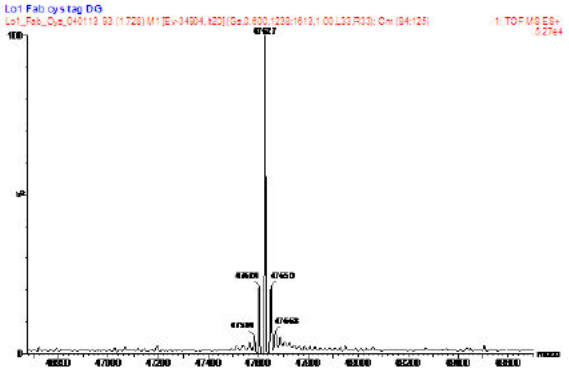
QVQLQQSGAELVRPGTSVKVSCKASGYAFTNYLIEWVKQRPGQGLEWIGVINPGSGGTNYNEKFKGKAT
LTADKSSSTAYMQLSSLTSEDSAVYFCARSF
KWKFDYWGQGTTLTVSSASTKGPSVFPLAPSSKSTSGGTAALGCLVKDYFPEPVTVSWNSGALTSGVHTF
PAVLQSSGLYSLSSVVTVPSSSLGTQTYIC
NVNHKPSNTKVDKKVEPKSCDKTHTC

B



1 – Unpurified LO1 Fab Conc. Non-Red.
2 – Unpurified LO1 Fab Conc. Red.
3 – Unpurified LO1-Cys Fab Conc. Non-Red.
4 – Unpurified LO1-Cys Fab Conc. Red.
5 – Purified LO1-Cys Fab Non-Red.
6 – Purified LO1-Cys Fab Red.

C



D

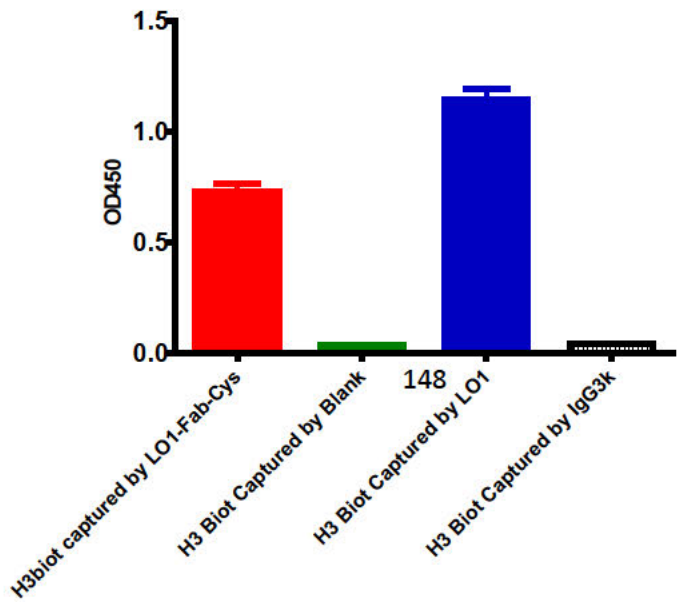


Figure 5.22 A-D

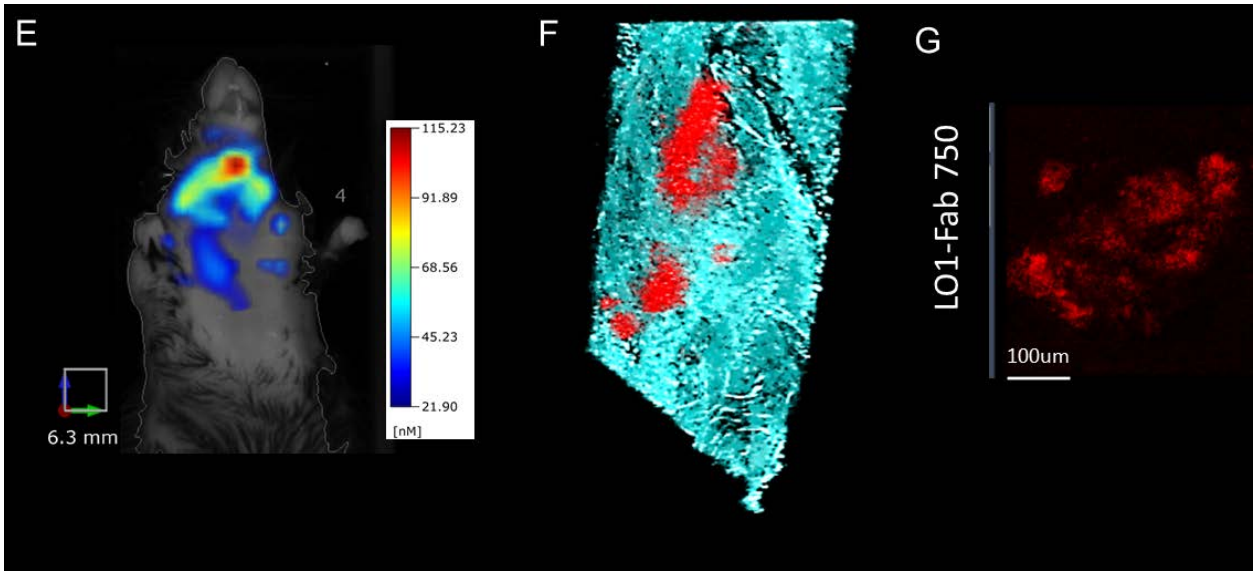


Figure 5.22. LO1-Fab-Cys characterisation. Panel **(A)** demonstrates the heavy chain of molecularly expressed LO1 Chimeric Fab with a cysteine tag. (Blue- LO1VH Black- CH1 Red- Cysteine tag); **(B)** shows the gel electrophoresis of LO1-Cys-Fab affinity purified over an anti- CH1 column, with protein identified by Colloidal Blue staining. Lanes 1-4 are unpurified preparations as indicated in the Figure. Lane 5 is non-reduced purified LO1-Fab-Cys, whilst lane 6 shows the reduced LO1-Fab-Cys; (**C)** demonstrates the mass spectrometry histogram of LO1-Fab-Cys, confirming the mass to be 118Da greater than the theoretical Fab mass (47627 Da vs. 47509 Da), which is consistent with the cysteinylation of the molecule. (**D**) Demonstrates the retention of function in comparison to LO1 by its ability to capture H3. (**E**) An FMT image showing *in vivo* LO1-Fab-Cys-750 localisation to the atherosclerotic aortic arch area in an *Ldlr*$^{-/-}$ mouse The same aorta was harvested *ex vivo*, prepared and imaged *en face* with confocal microscopy in (**F**) with LO1-Fab-Cys-750 (red) in relation to intimal matrix, as identified by autofluorescence (Em 520-590, blue) in the aortic arch. Higher magnification in (**G**) reveals a similar pattern of staining as seen with previous LO1-750 *ex vivo en face* studies.

6.0 Mab LO9, a Novel Immunoglobulin G Autoantibody, Against an Allosteric Epitope on Low Density Lipoprotein (LDL)

6.1 Chapter Abstract:

Introduction IgG autoantibodies, which react with different forms of modified LDL, are found in blood and have been associated with atherosclerosis-related cardiovascular events. However, there is little evidence that they react with allosteric modifications in unmanipulated, 'native' LDL. We set out to characterise LO9 as a novel antibody that reacts against an allosteric epitope on LDL.

Methods/Results We fused splenocytes from an LDL receptor deficient (*Ldlr*$^{-/-}$) atherosclerotic mouse with the Sp2/0 myeloma cell line, and, using ELISA, screened hybridoma culture supernatants for reactivity with solid phase LDL. We selected a monoclonal IgG2b antibody, designated LO9. Sequencing of the LO9 variable heavy (VH) and variable light (V_L) regions revealed numerous somatic mutations in the complementarity determining regions (CDR) of both the V_H and V_L. Together with the IgG2b subclass, these indicate that LO9 is not a natural antibody but has developed from an adaptive immune response. LO9 reacted with unmanipulated LDL adherent to ELISA plates, and showed less reactivity with LDL oxidised by Cu^{++} ions, or malondialdehyde-conjugated LDL (MDA-LDL). LO9 also failed to react with LDL captured onto ELISA plates by immobilised polyclonal anti-apoB rather than by direct adsorption. Furthermore, LO9 binding to adherent LDL was not inhibited by the presence of fluid-phase LDL in excess. The LO9 epitope was

not abolished by organic solvents, suggesting that it is not lipid. Addition of macrophages to LO9 bound to adherent LDL *in vitro* led to significant TNFα release, an effect that was blocked by inhibition of Fcγ receptors (FcγRs), and which was not seen when macrophages were incubated with adherent LDL alone. Expression of the LO9 epitope on adherent LDL was greatly increased by incubation with conditioned medium (CM) from activated macrophages, consistent with the LDL epitope being further revealed by the action of macrophage-derived factors.

Expression of the LO9 epitope in atherosclerosis was confirmed using immunohistochemical staining of human and mouse lesions. Following intravenous injection of LO9 labelled with a near infra-red dye (LO9-750), fluorescence molecular tomography imaging demonstrated specific localisation to a region of interest covering the aortic arch of *Ldlr*$^{-/-}$ mice, but not wild type animals. Confocal microscopy of extracted aortae *en face* confirmed that LO9 localised in atherosclerotic regions beneath endothelium and in the vicinity of macrophages.

Conclusions We believe LO9 is the first example of an autoantibody that reacts with an allosteric epitope on LDL revealed by adhesion to a surface and/or by the action of factors derived from activated macrophages. Binding of LO9-like antibodies to LDL trapped on matrix in the arterial wall could lead to promotion of atherosclerosis via ligation of macrophage FcγRs and release of TNFα and other pro-inflammatory mediators

6.2 Generation and Initial Characterisation of LO9

As with LO1, LO9 was derived from fused splenocytes from a LDL receptor deficient mouse previous to the work undertaken for this thesis[166]. Hybridomas were generated by fusing Sp2/0 myeloma cells with splenocytes from a one year old female LDL receptor deficient

(*Ldlr*$^{-/-}$) mouse that had been fed a high fat diet from the age of 6 weeks, resulting in a serum cholesterol 25-30 mmol/l. LO1 was shown to react with MDA-LDL and not with native LDL, whilst initial screening demonstrated an interesting phenomenon, where an 'auto antibody' from an unimmunised mouse, seemed to react with native LDL adherent to ELISA plastic. This antibody was designated mAb LO9 and was taken forwards for further characterisation in this chapter.

6.2.1 LO9 reacts with native adherent LDL and less with Cu^{-}OxLDL.

Following screening of culture supernatants by ELISA, LO9 was selected as it reacted with unmanipulated "native" LDL and less well with Cu^{++}oxLDL (Figure 6.1A). Also shown in Figure 6.1A is the reactivity of LO1, which reacts with Cu^{++}oxLDL and MDA-LDL; and of pooled *Ldlr*$^{-/-}$ mouse serum, which showed modest binding to native LDL and increased binding to Cu^{++}oxLDL.

Figure 6.1B shows the results of a further ELISA with native LDL and MDA-LDL as the solid phase antigens. This established the specificity of LO9 and LO1 binding in comparison to their respective isotype-matched control immunoglobulins (IgG3κ for LO1 and IgG2b for LO9). Of interest is that LO9 binds native LDL adherent to plastic much better than it binds the heavily oxidised form of LDL, MDA-LDL that has aldehyde adducts on the lysines. We also tested the effects of other modifications to the LDL molecule on LO9 binding.

Figure 6.1C shows that hypochlorite modification does not abolish the binding site of LO9 on LDL. In a similar way, LDL that was left without antioxidants for several months termed 'autooxidised' LDL is bound by LO9 to a similar degree as unmanipulated LDL (Figure 6.1D). Conversely, heavily trypsinising LDL (at room temperature, for an hour, with excess

trypsin) results in fragmentation of the ApoB molecule, which LO9 does not recognise (Figure 6.1D).

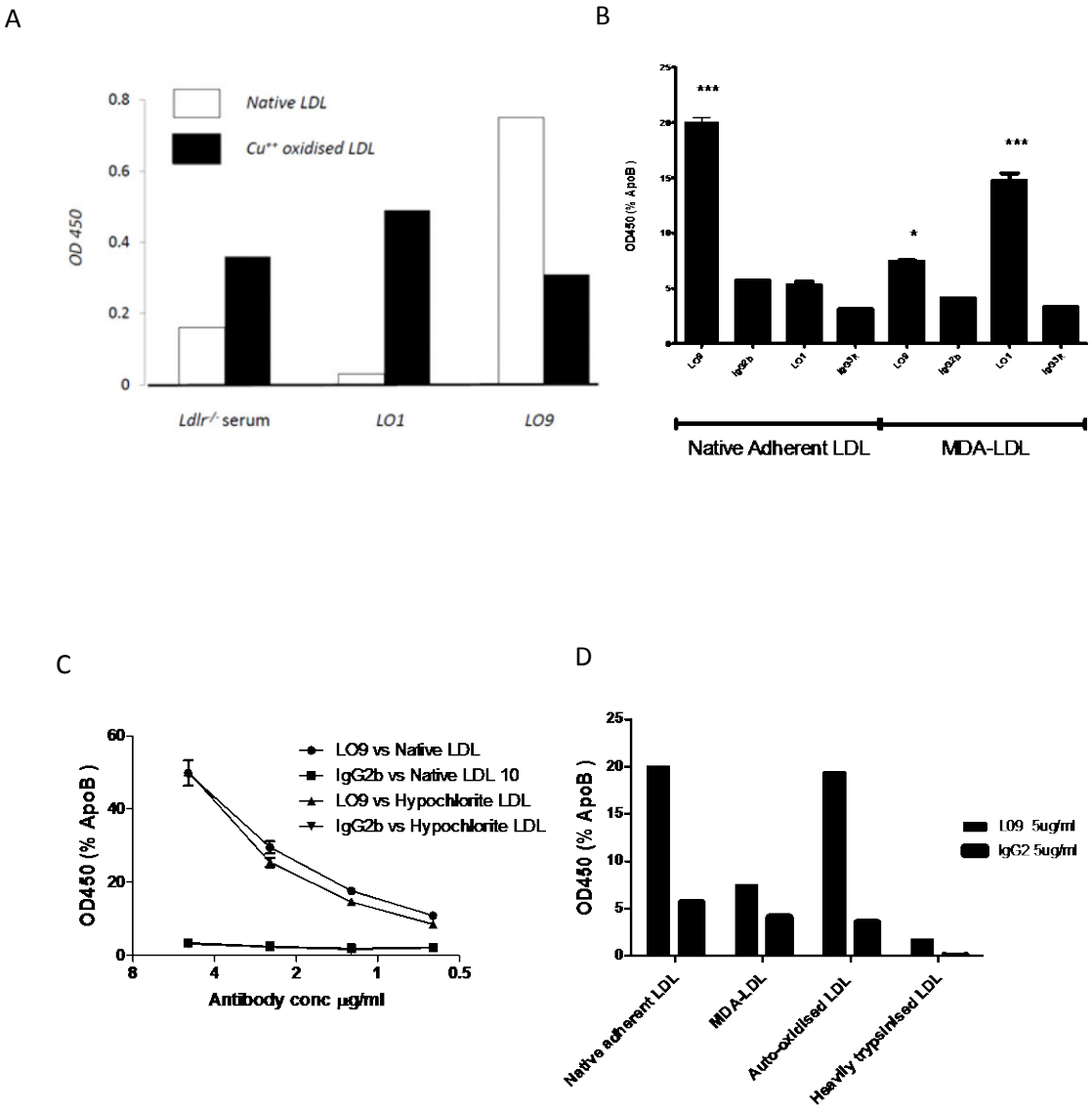


Figure 6.1: LO9 reacts with adherent LDL. Figure 6.1A shows the reactivity by ELISA of IgG antibodies against unmanipulated "native" human LDL and LDL exposed to Cu++ for 16 hr (Cu++oxidised LDL). LO1, which reacts with MDA-LDL, failed to react with native LDL but reacted with Cu++oxidised LDL, whilst the reverse was the case for LO9. Note that pooled lipoprotein receptor deficient (*Ldlr*$^{-/-}$) mouse serum reacted modestly with native LDL and shows enhanced binding to Cu++oxidised LD, consistent with the presence of both LO1-like and LO9-like IgG

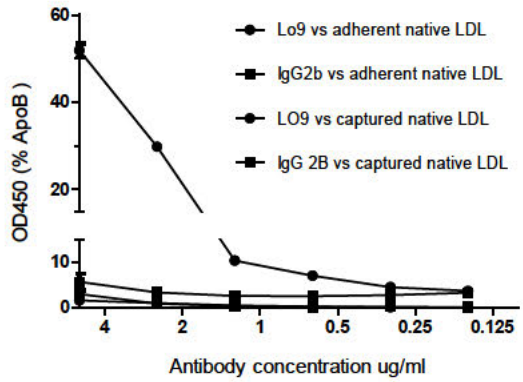
antibodies in the polyclonal repertoire. Figure 6.1B demonstrates the binding of LO9 to adherent native LDL and less so to adherent MDA-LDL, in contrast to LO1 which binds MDA-LDL and not native adherent LDL. Included are the background reactivities of the two isotype control immunoglobulins: IgG2b for LO9 and IgG3κ for LO1. * represents $p<0.05$ and *** represents $p<0.001$ from relevant isotype control. Figure 6.1C demonstrates the LO9 binds native adherent LDL and Hypochlorite modified LDL equally well. The. Figure 6.1D shows that heavily trypsinising LDL loses it the ability to be recognised by LO9, whilst, leaving LDL to autooxidised does not.

6.2.2 LO9 only binds to LDL when adherent, and not when captured. The LO9 and adherent LDL interaction is not blocked by abundant LDL in fluid-phase or by serum.

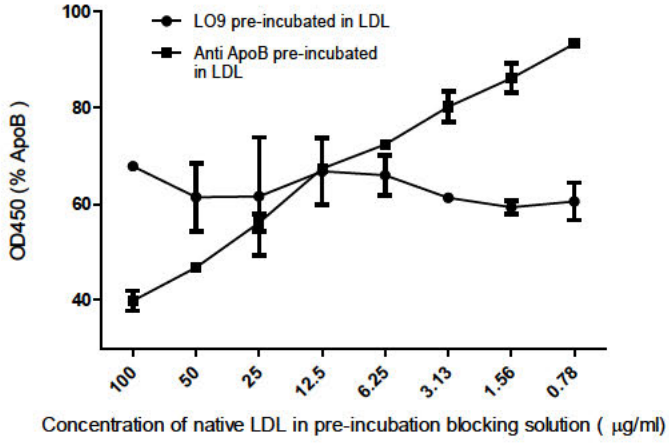
As shown in Figure 6.2A, LO9 specifically binds native LDL that had been adhered directly to the plastic, but does not bind LDL that had been captured on to the assay plate by solid phase rabbit anti-apoB. The isotype control does not bind either adherent or captured LDL. The binding of LDL was corrected to the amount of ApoB using an anti-apoB antibody as a positive control.

Furthermore, we found that the binding of LO9 to adhered LDL was not blocked by inclusion in the assay of fluid-phase LDL at concentrations that clearly prevented the binding of rabbit anti-apoB (Figure 6.2B). Similarly, human serum in dilution series, which contains LDL at a top concentration of 100 μg/ml was able to block anti-apoB but not LO9 binding (Figure 6.2C). Taken together, these observations suggested that the reactivity of LO9 with adherent LDL was dependent on the unmasking of a cryptic epitope by LDL adhesion to plastic. The epitope clearly does not exist in enough abundance either in fluid-phase LDL or serum. This raises the possibility that this may be an epitope that may have a mechanistic effect mediated via antibodies, once LDL is adherent to matrix, for example proteoglycans in the vessel wall.

A



B



C

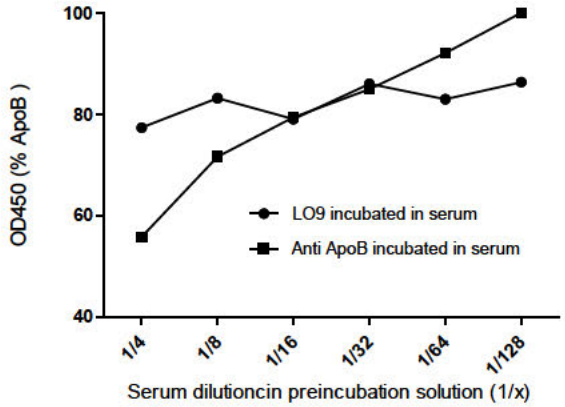


Figure 6.2

Figure 6.2. LO9 binds only adherent LDL and is not blocked by LDL or human serum.

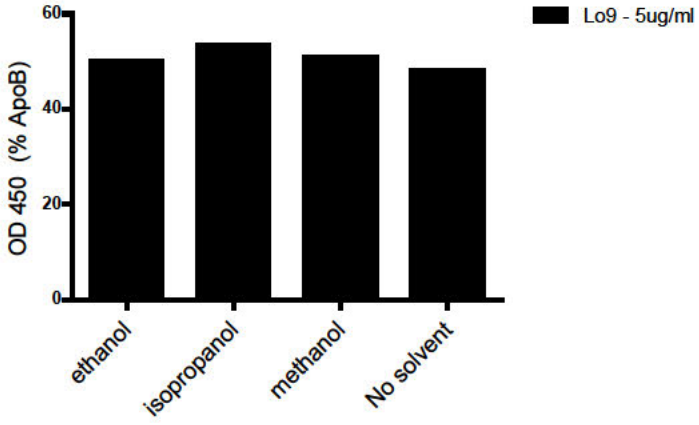
(A) Reactivity of LO9 with adherent LDL but not with LDL captured by anti-apoB. The Figure shows the reactivity by ELISA of LO9 (but not IgG2b isotype control antibody) with LDL adherent onto ELISA plate plastic. In contrast, LO9 did not bind LDL that had been captured by immobilised polyclonal rabbit anti-human apoB. (B) Shows the reactivity by ELISA of LO9 as well as polyclonal rabbit anti-apoB to native LDL adherent onto ELISA plate plastic. Free LDL in the incubation buffer failed to block LO9 reacting with adherent LDL, but blocked the anti-ApoB from interacting with the adherent LDL. Figure 6.2C shows that similarly, mouse serum blocks the binding of anti-Apo B to LDL but does not block the binding of LO9 to native adherent LDL. (C) demonstrates how human serum blocks the interaction of the anti-apoB with adherent native LDL, whilst it fails to do the same to LO9. Thus the LO9 epitope appears to only be revealed upon adherence. To normalise for the quantity of LDL in assay wells, the data are expressed as a percentage of the OD 450 of the test antibody relative to the OD 450 obtained using polyclonal rabbit anti-apoB for detection.

6.2.3 The LO9 epitope is not alcohol sensitive and is partially sensitive to 'on plate' light trypsinisation,

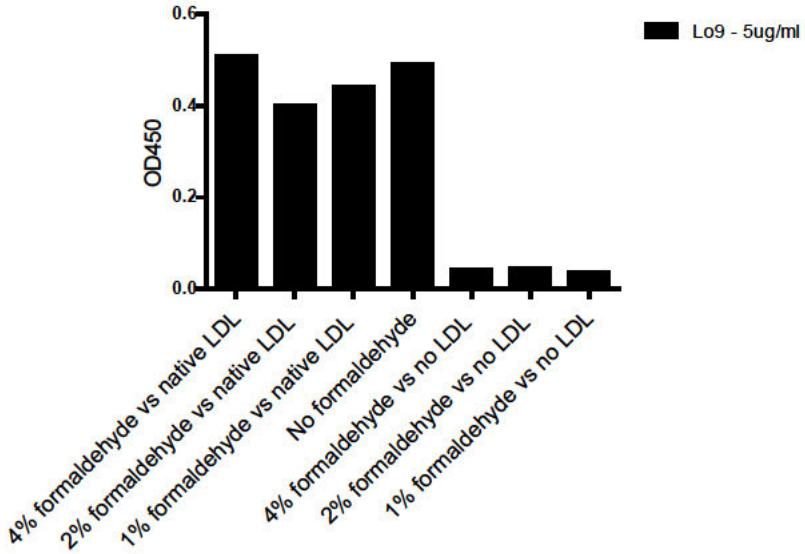
LO9 was tested against native LDL preserved in alcohol preparations at different concentration, and results corrected to ApoB levels (Figure 6.3A). The binding to LO9 to adherent LDL was unchanged despite the incubation of different alcohol preservatives with adherent LDL for an hour prior to testing LO9. This shows both that the LO9 epitope is not lipid dependent, and suggests that it would not be affected if we wish to test LO9 in histological sections that have been preserved in alcohol. The same experiment was conducted using a similar protocol to test LO9 against different concentrations of formalin preserved LDL, and the epitope was also unaffected (Figure 6.3B).

When native LDL is heavily trypsinised, LO9 stops binding it as shown previously (Figure 6.1D). Interestingly, when LDL is lightly trypsinised in fluid-phase and then probed with LO9, the binding remains the same as in native LDL (data not shown). However, once the LDL is adherent and then lightly trypsinised (Figure 6.3C), the LO9 epitope is attenuated after only one minute of light trypsinisation equivalent to that performed in the fluid-phase. This demonstrates that the LO9 epitope is likely to have a protein dependent aspect accessible once the LDL is adherent to plastic.

A



B



C

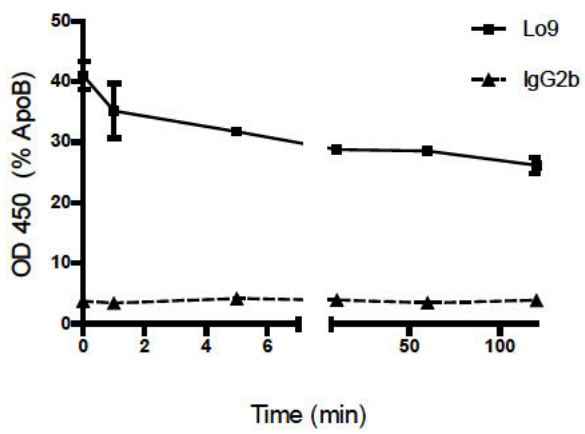


Figure 6.3

Figure 6.3. The LO9 epitope is not alcohol sensitive and can be modulated with on plate light trypsinisation of adherent native LDL. (A) ELISA of LO9 Vs native adherent LDL incubated with different preparations of alcohol for one hour. The LO9 epitope is not alcohol sensitive and therefore is unlikely to be lipid-based. (B) ELISA of LO9 vs native adherent LDL in different concentration of formaldehyde for 3 hours. The experiment was controlled by testing LO9 vs preservatives without LDL. Formaldehyde at a rising concentration does not affect the LO9 epitope on LDL. (C) ELISA of LO9 and IgG2b adherent trypsinised LDL at different time points. This 'light' trypsinisation results in a quick modulation of LO9 interacting with the native LDL. Although this effect is quite small and may not be particularly important.

6.2.4 Cloning and sequencing immunoglobulin genes

We sequenced the variable heavy (VH) and variable light (VL) chain regions of the LO9 cDNA and found that these derive from the germ-line IGHV1-18 and IGKV1-110 sequences. As shown in Figure 6.4, Complement determinant regions of both VH and VL regions have several mutations from the germ-line sequences, indicative of an adaptive immunoglobulin response. Interestingly, the VH has an unusual deletion of 9 amino acids. Both the numerous somatic mutations together with the IgG2b subclass indicate that LO9 is not a natural antibody but more likely has developed from an adaptive immune response.



Figure 6.4. Amino acid sequence of the mAb LO9 VH and VL

Panel A shows the mAb LO9 VH and VL sequences and their similarity to the germ-line IGHV1-18 and IGKV1-110 sequences, as referenced in the IMGT database. LO9 amino acids that differ from germ-line are shown in red. The amino acids shown in green in the VH were found to be deleted in LO9 both by degenerate oligonucleotide sequencing and mass spectrometry. This was confirmed by PCR with oligonucleotides designed to span the deletion from the leader sequence.

Red Box= CDR, Green = deleted in LO9, Purple = different in LO9 but within the CDR, Blue = different in LO9 and in the framework region. Underlined= Confirmed by MS/MS mass spectrometry.

6.3 LO9 Exhibits Pathological Functions in Vitro

6.3.1 LO9 bound to adherent LDL causes mouse macrophages to release TNFα by an FcγR-mediated mechanism

To check the possible pathological effects of LO9 binding to adherent LDL *in vitro*, We performed an experiment undertaken by Dr. Kevin Woollard in immunology, where we incubated LDL-coated wells with LO9 or control IgG2b and then washed before addition of mouse BMDM ($2x10^6$/ well). Supernatants were then collected and assayed for the presence of TNFα. As shown in Figure 6.5, BMDM added to wells containing LO9 bound to adherent LDL released significantly more TNFα than those added to control wells. The control antibody did not have any effect on TNFα levels.

Furthermore, TNFα release was inhibited by inclusion of mAb 2.4G2, which blocks CD16 (FcγRIII) and CD32 (FcγRII). This points towards LO9 having a pathological effect on macrophage function which is mediated via the Fcγ receptor pathway.

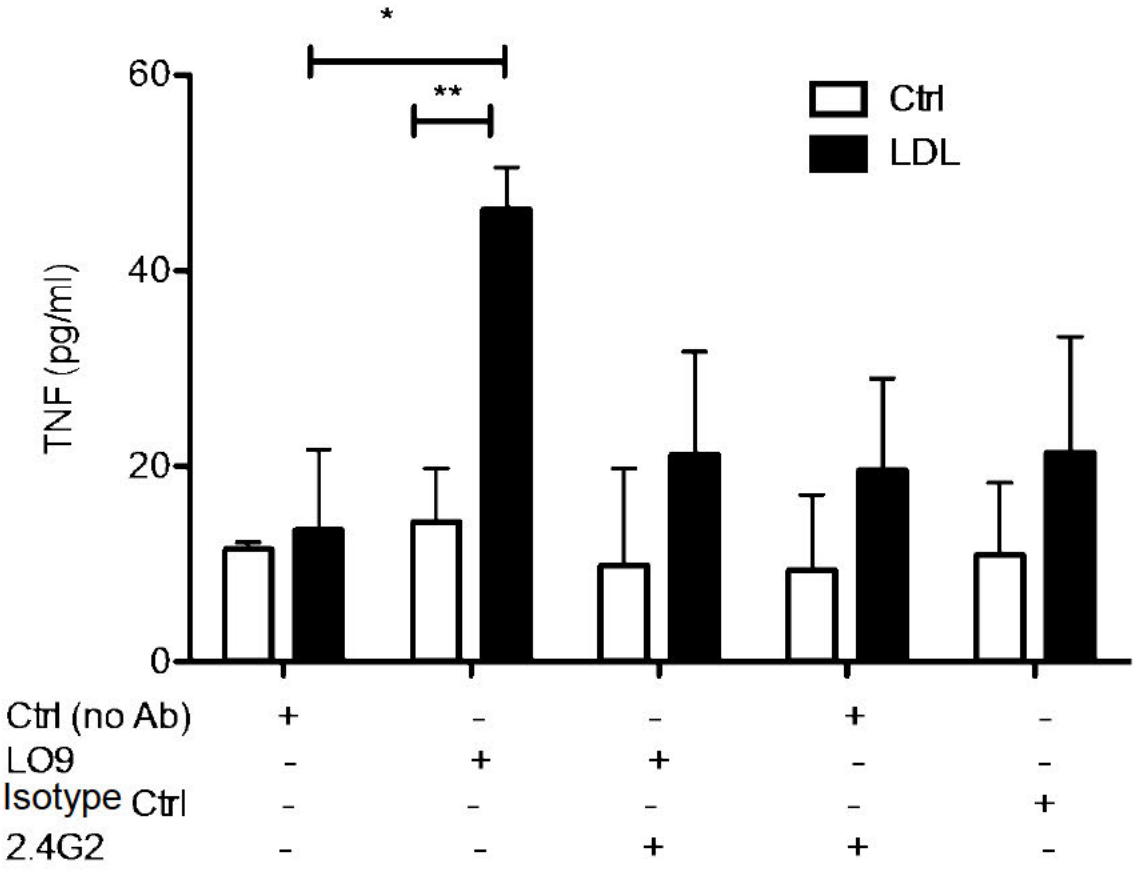


Figure 6.5: LO9 bound to adherent LDL causes mouse macrophages to release TNFα by an FcγR-mediated mechanism

Mouse bone marrow derived macrophages $2x10^6$ were added to wells containing adherent LDL (10µg/ml) or to control wells without LDL, and incubated overnight at 37°C, after which the supernatant was collected and analysed for TNFα by ELISA. The Figure show the stimulatory effect of preincubating adherent LDL with LO9 compared with IgG2b isotype control (IC) antibody (both 10µg/ml), as well as the inhibitory action of blocking FcγR with 2.4G2 (CD32/16 blocking antibody; 10µg/ml). Data are Mean ± SD of three experiments. * and ** represents $P<0.05$ and $P<0.01$ respectively as analysed by one-way ANOVA Tukey post-hoc test.

6.3.2 The LO9 epitope is further revealed by activated macrophage conditioned medium

We reasoned that not all LDL particles may express the LO9 epitope upon adherence, and that more may do so in response to factor(s) secreted by macrophages. To address this possibility, we incubated LDL with the conditioned medium of macrophages stimulated by zymosan-activated serum (ZCM). As shown in Figure 6.6, this procedure led to a substantial increase in reactivity of LO9 with adherent LDL, whereas the control CM (CCM) of unstimulated macrophages had no effect.

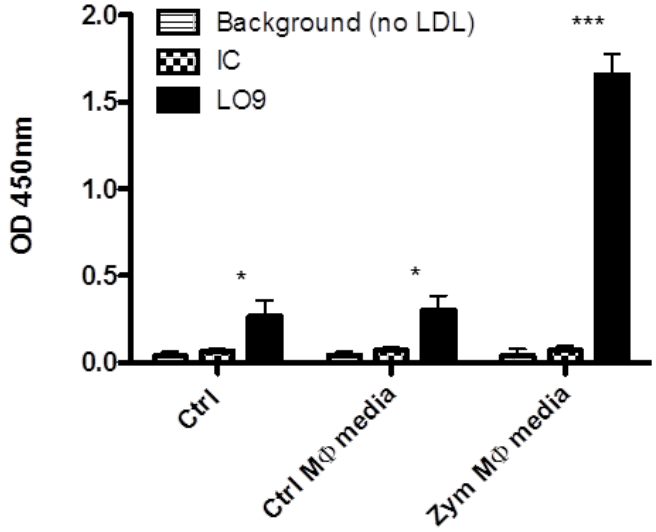


Figure 6.6: Treatment of adherent LDL with CM from activated macrophages leads to enhanced LO9 epitope expression.

LDL (10µg/ml) was adsorbed to ELISA plate plastic and then incubated for 3 hr at 37^{o}C with CM from macrophages stimulated with zymosan-activated serum (Zym MØ) or from unstimulated macrophages (Ctrl MØ). Other wells were not exposed to macrophage CM. The Figure shows binding of LO9 and IgG2b isotype control antibody in comparison to background. Data are Mean ± SD of three experiments. *, ** and *** represents $P<0.05$, $P<0.01$ and $P<0.001$ respectively (indicated or in comparison to IC) as analysed by one-way ANOVA Tukey post-hoc test.

6.4 Biotinylation and Fluorescence Labelling of LO9

LO9 was biotinylated using amine chemistry as per the methods section. We demonstrated the partial preservation of function of biotinylated LO9 by performing an ELISA with native LDL in adherent phase detected by both biotinylated and non-biotinylated LO9 and as shown in Figure 6.7. This allowed us to proceed to immunohistochemical studies. We labelled LO9 with a NIRF agent in a similar way to LO1 using thiol chemistry. LO9 was labelled with a fluorophore (VT-MAL 750) directly and tested for function (Figure 6.7). The DOL was also calculated as per the methods section in order for us to use equal amount of protein when testing LO9 vs its isotype control.

The reduced function of both biotinylated and labelled LO9 in comparison to unlabelled LO9 can be partly accounted for by the change in molecular weight (as all three preparations were tested at 10μ/ml).

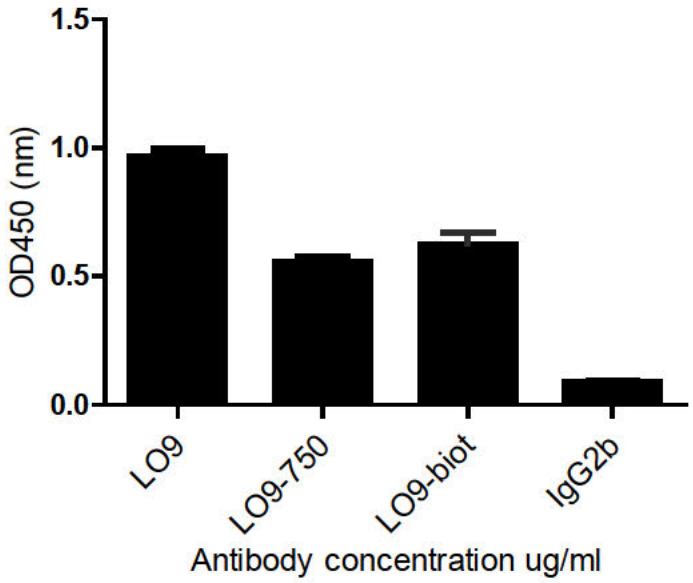


Figure 6.7 Function of LO9 against native adherent LDL when unlabelled, biotinylated and labelled with VT-MAL 750.

There was a small loss of function per mg of preparation when all three preparations were tested against adherent native LDL. The preparations, however remained capable of recognising adherent LDL in comparison to isotype control

6.5 Detection of LO9-reactive Material in Atherosclerosis

6.5.1 Immunohistochemistry in mouse aortic root and cusp and human carotid and coronary lesions.

We next addressed whether the LO9 epitope could be detected in atherosclerotic tissues. Sections of the atherosclerotic aortic root of an *Ldlr*$^{-/-}$ mouse showed specific LO9 staining with biotinylated LO9 followed by Alex Fluor 633-conjugated streptavidin, with foci of high

signal (Figure 6.8A). The isotype control had a negative signal. We also tested LO9 and IgG2b control antibodies on wild type animals and both were negative (data not shown).

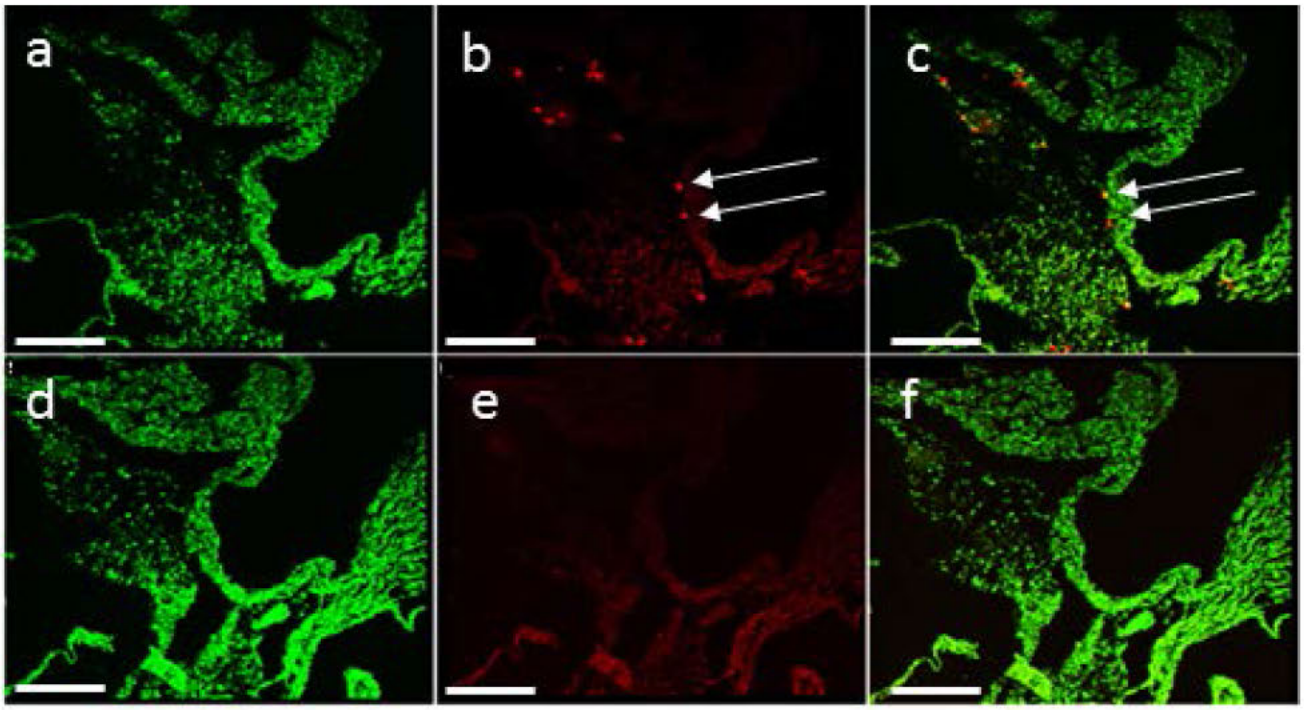
Similarly, LO9 reacted with deposits in atherosclerotic human carotid endarterectomy tissue, High magnification studies showed areas of positive staining both adjacent to macrophages but more commonly in free aggregates within the necrotic core and lesion borders (Figure 6.8B).

We then aimed to study well characterised human atherosclerotic lesions from the AtheroExpress Study[180]. This experiment was undertaken by our collaborator Dr. Jason Johnson at Bristol University. We selected both a an advanced lesion with a large lipid core and thin cap, classically characterised as a TCFA, as well as an intermediate 'stable' lesion with a thick fibrous cap and a smaller lipid core (<40% of lesional area). We performed

comparative staining with LO1 and co-localising to anti-CD-68 (Figure 6.8C), it was clear that LO9 localises partially to macrophages but also stains free LDL deposits. LO9 gave scanty staining in intermediate plaque in comparison to LO1, but the staining was specific and in some places granular, suggesting possible staining of LDL aggregates. In advanced plaque there was more staining with both LO1 and LO9 but the LO9 signal was less prevalent and less associated with the macrophage staining than LO1 as well as less concentrated in the lesional cap.

Thus LO1 is much more abundant in lipid core than LO9. LO1 may well be a good surrogate for elements of plaque vulnerability as it stains TCFA as well as highly lipid laden lipid core. LO9 seems to be less affected by plaque progression and may be staining a dynamically changing entity as the LDL adheres, and then gets oxidised by local factors, LO9 staining may be diminished and LO1 staining enhanced.

A



B

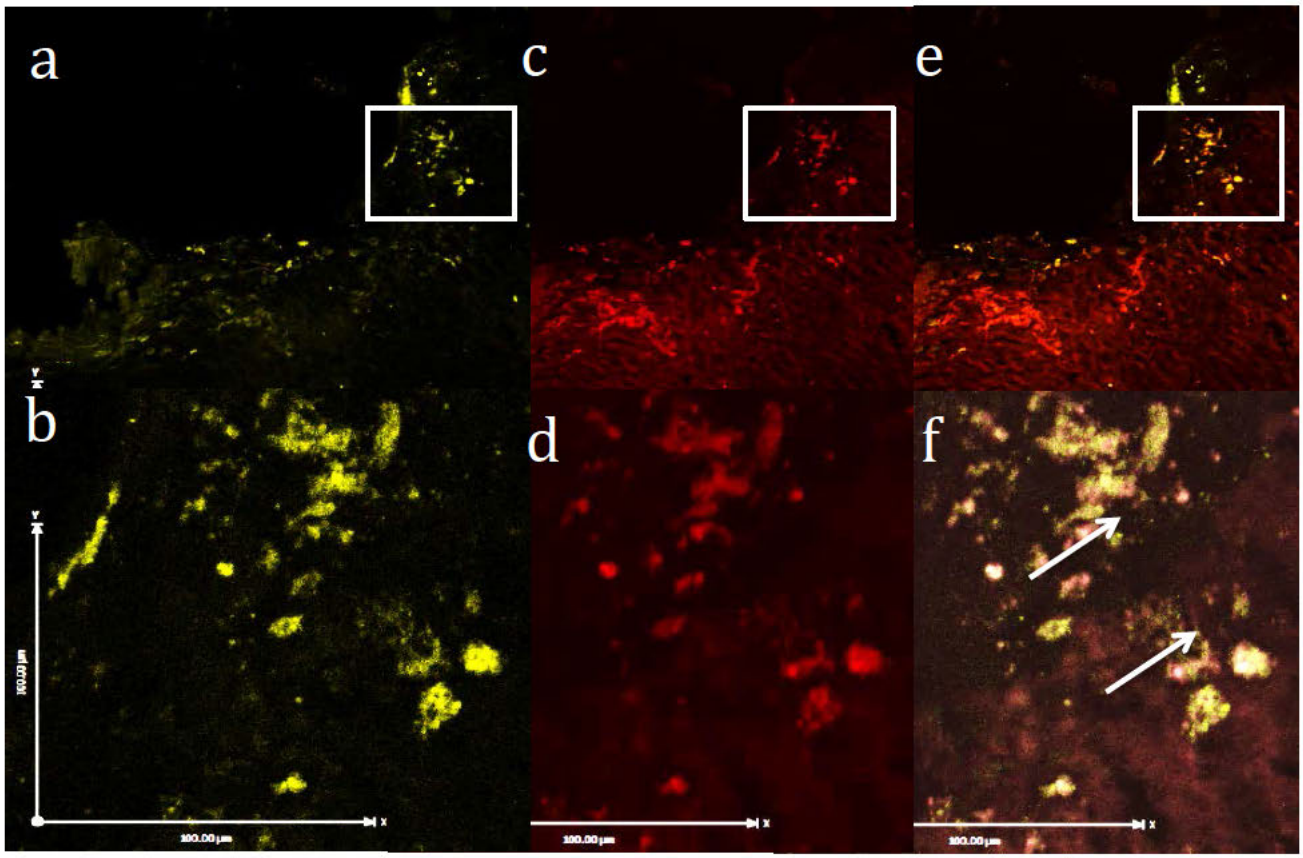


Figure 6.8 A-B

C

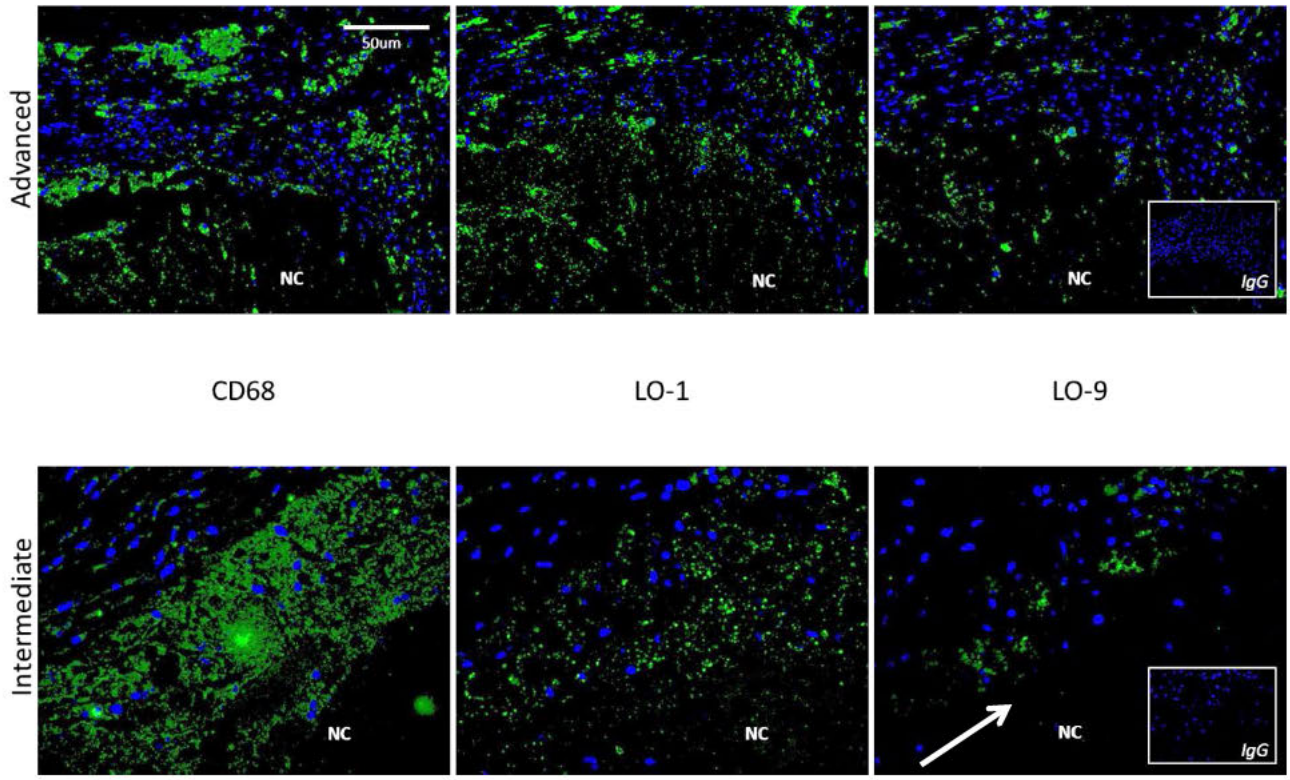


Figure 6.8. Detection of antigen recognised by LO9 in atherosclerosis.

(A) Serial sections of the aortic root of a 36 week old *Ldlr*$^{-/-}$ mouse were stained with **(a,d)** Syto 24 nuclear stain (green), **(b)** biotinylated LO9 (red) or **(e)** biotinylated control IgG2b followed by Alex Fluor 633-conjugated streptavidin. **(c,f)** shows merged images. Arrows show examples of the punctate staining with LO9 within lesional areas. Scale bar = 250μm; **(B)** serial sections of human carotid endarterectomy tissue were stained for CD68 **(a,b)** and LO9 **(c,d)**. Overlays shown in (**e**) and **(f)**. **(b), (d)** and **(f)** represent zoomed images of ROI from (**a**), **(c)** and (**e**) respectively. Arrows show co-localisation of CD68 and LO9 signal. **(C)** Serial sections of human intermediate (bottom panel) and advanced (top panel) carotid lesions from the AtheroExpress study, stained with anti-CD68 (macrophages), LO1 and LO9. Staining with non-specific IgG was negative and is shown in the insets. Blue is TOPRO nuclear stain.

6.5.2 LO9 injected intravenously localises to atherosclerosis. The in vivo detection of LO9-750 with FTM-CT

Using LO9 conjugated with the near infra-red Fluorophore VT-MAL 750 (termed LO9-750), we were able to demonstrate localisation of LO9 to areas of atherosclerosis in the *Ldlr*$^{-/-}$ model.

As shown in Figure 6.9A, whole body fluorescence molecular tomography combined with micro-CT of mice injected with LO9-750 gave clear focal signal in the aortic arch, ascending aorta and its branches, whereas no signal was obtained with control IgG2b conjugated with VivoTag-S 750-MAL (designated IgG2b-750). WT animals injected with both LO9-750 or IgG2b-750 also had little signal. The 3D reconstruction of the LO9 signal in a mouse imaged with both FMT and CT and images fused demonstrate the localisation in this instance (panel 6.9B) to the aortic arch and right subclavian. The sagittal view in 6.9C demonstrates the signal at the level of the aortic arch anterior to the spine at T3-T5. The localisation of the signal was confirmed by ex vivo analysis and will be discussed in the next section.

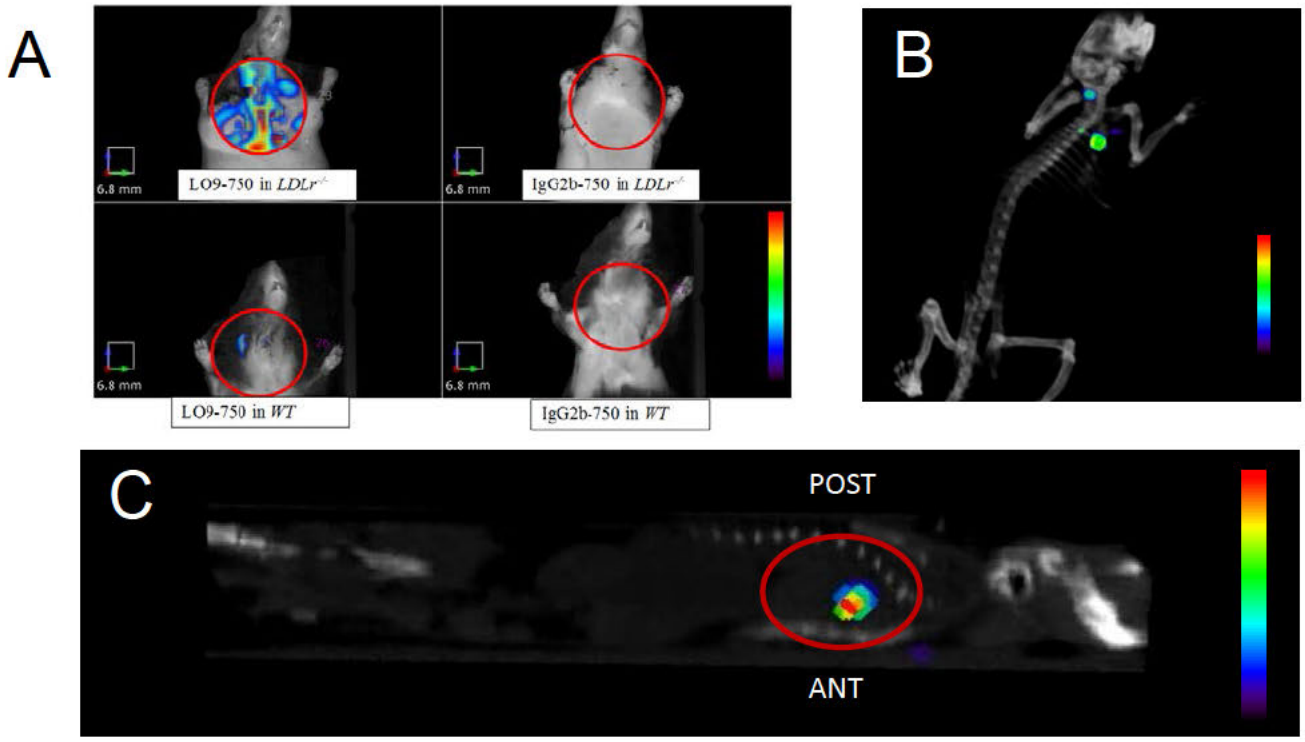


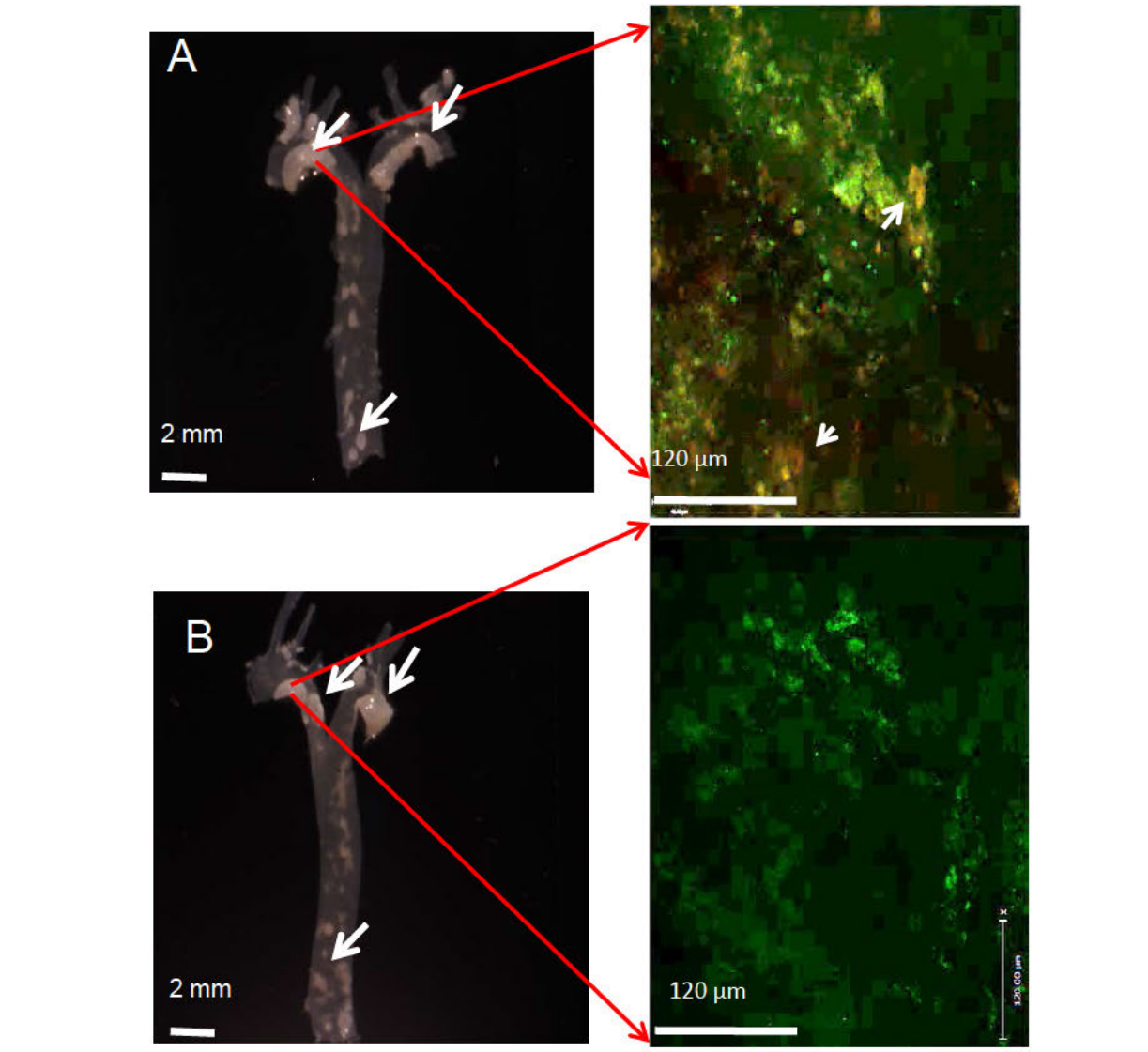
Figure 6.9. FMT and FMT/CT imaging with LO9-750 and isotype control antibody in Ldlr$^{-/-}$ and WT animals.

Figure **6.9A** demonstrates that LO9-750 and not the isotype control accumulates in the thoracic aorta and its branches within the tested ROI of the *Ldlr*$^{-/-}$ mouse model (top panel) and not in the WT controls (bottom panel). **6.9B** and **6.9C** are 3D FMT-CT reconstructions of an *Ldlr*$^{-/-}$ animal injected with LO9-750 and imaged 4 hours later. **(B)** demonstrates the 3D localisation in the aortic arch and right subclavian and **(C)** demonstrates the sagittal plane of signal in the aortic arch. The scale indicates signal intensity (black- low, blue intermediate, red- high). All signals are represented on a uniform scale adjusted to μmol/ml of protein detected.

6.5.3 ex vivo characterisation of the localisation of injected LO9-750 in murine atherosclerosis.

Ex vivo analysis of tissues from mice injected with LO9-750 and IgG2b-750 confirmed the localisation of LO9 to areas of atherosclerosis (Figure 6.10). There was more staining of free aggregates at lesional areas than adjacent to macrophages (6.10A). The staining was more intense at lesion edges. Interestingly the staining was scantier than LO1, but quite specific. The isotype control was negative, but the MOMA antibody stained positive in the lesional areas of the same animal (6.10B). When injecting animals with a PE-conjugated an anti-CD-31 antibody and co-localising with previously injected LO9-750, it is apparent on 3D microscopy that LO9 localises to the sub-endothelial space (6.10 C). The isotype control was negative and did not localise to aortic lesional areas (6.10D). Wild type animals injected with LO9-750 did not exhibit any positive signals in the aortae either when co-localising to macrophages (not shown), or to sub-endothelium (6.10E). Wild type animals injected with the IgG2b-750 isotype control also had a negative signal and yet showed a clear endothelial layer with the PE-conjugated anti-CD31.

The distribution pattern of LO9 suggests an epitope that is present in the sub-endothelial layer of lesional areas, with scanty partial co-localisation to macrophages in the advanced atherosclerosis animal model. Although the *in vitro* human lesional staining was similar to that of the mouse, *in vivo* targeting experiments in human are clearly not feasible with a full mouse antibody. The localisation maybe different as it would be difficult to account for lesion permeability, blood and organ distribution as well as *in vivo* specificity.


A
2 mm
120 µm
B
2 mm
120 µm

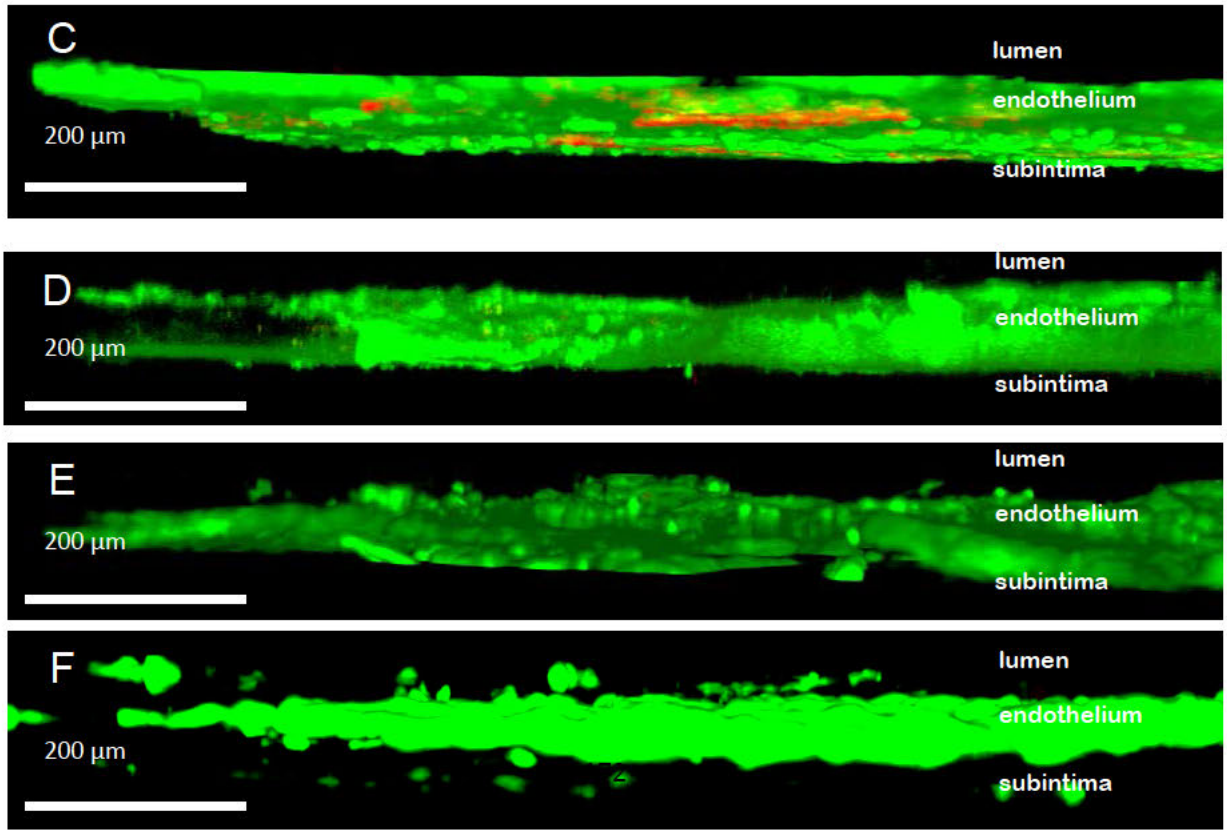

C
200 µm
lumen
endothelium
subintima
D
200 µm
lumen
endothelium
subintima
E
200 µm
lumen
endothelium
subintima
F
200 µm
lumen
endothelium
subintima

Figure 6.10

Figure 6.10. Localisation of in vivo injected LO9-750 in the Ldlr-/- aorta. **(A,B)**

Ldlr$^{-/-}$ mice received LO9-750 (50 µg) or IgG2b-750 (50 µg) by *iv* injection, 4 hr. after which the aorta was removed for staining with MOMA macrophage stain and *ex vivo* confocal microscopy analysis. White light image displaying atherosclerotic lesions (arrows) in the aortic arch as well as the abdominal aorta, with corresponding *en face* confocal microscopy showing LO9-750 (**A**-right panel) or IgG2b (**B**-right panel) in red in relation to MOMA stained macrophages (green= macrophages; yellow=merged); **(C-F)** Localisation of LO9 beneath aortic endothelium in *Ldlr*$^{-/-}$ following intravenous (iv) injection. **(C,D)** *Ldlr*$^{-/-}$ mice that had been fed a high fat diet for 30 weeks or **(E,F)** wild type mice received tail vein injections of **(C,E)** VT-MAL-750 conjugated LO9 or **(D, F)** isotype control IgG2b four hours prior to killing. All mice also received a tail vein injection of PE-conjugated anti-CD31 (green) 10 min before sacrifice. Tissues were analysed *ex vivo* by Z stacking and tile scanning confocal microscopy. The image is of the aortic lesser curve and shows localisation of LO9 beneath endothelium of the *Ldlr*$^{-/-}$ in **C,** with **D,E and F** displaying negative signals.

7.0 Discussion

From identifying the vulnerable patient to the targeting and identification of the vulnerable plaque- The identification and utilisation of autoantibodies against oxidised LDL

7.1 A Brief Summary of the Findings

In this thesis we have shown the utility of serological assays measuring anti-oxidised LDL antibodies as predictors of survival in the well-characterised ASCOT-HACVD population. One assay, measuring IgG anti-MDA-LDL antibody levels, was strikingly robust at predicting protection from cardiovascular risk, even when correcting for classical risk factors and other inflammatory predictors of risk such as CRP.

The model of homeostatic natural autoantibodies[9, 100] against OSE[103] contributing to protection against cardiovascular events led us to consider that similar mAbs isolated from mice may be able to target MDA-LDL in vivo. This was facilitated by the fact that our laboratory had moved towards isolating autoantibodies against oxidised LDL from mice. Previous work performed in the laboratory had selected LO1, an IgG3 autoantibody reacting against copper-oxidised LDL and MDA-LDL[166]. The same work had also identified LO9, an IgG2b antibody reacting with native LDL. This has provided us with a unique opportunity to study the characterisation of these antibodies in detail, as previous attempts to isolate IgG autoantibody clones to oxidised LDL have been largely unsuccessful[183].

Furthermore, targeting of vulnerable plaque with molecular imaging techniques is recognised as a priority in both field of invasive and non-invasive cardiovascular imaging[68]. Thus the opportunity to develop antibodies against oxidised LDL as imaging agents was explored and taken towards translation.

We selected NIRF imaging as it has the greatest translation potential, with excellent spatial resolution when using intravascular techniques transitionally. Therefore, we strived to gain access to cutting edge near infrared optical imaging techniques that do not rely on radiation to identify atherosclerotic plaque. This culminated in us choosing to image the *Ldlr*$^{-/-}$ mouse model with whole body IVIS Spectrum, FMT imaging, and the balloon- injured rabbit model with the novel intravascular NIRF catheter.

LO1 was shown to identify MDA-LDL in vitro and was taken forwards for detailed characterisation. It was sequenced and expressed as a chimeric partially humanised Fab construct. The whole antibody was shown to target advanced atherosclerotic plaques. Its comparison to MMP sense demonstrated that both these agents in concert might be valuable in identifying both the oxidised LDL content in plaque as well as more dynamic plaque inflammatory activity. This may become useful clinically when trying to characterise both plaque progression and acute inflammation in the vulnerable patient.

When we first screened for anti-oxidised LDL antibodies, LO9 was an incidental finding. It is a novel antibody that reacts with LDL once adherent, but not when in solution. Exploring the characterisation of this antibody led us to conclude that it may have a role in early atherosclerosis by triggering the cycle of FcγR medicated activation of macrophages. Furthermore, we have begun to explore the value of LO9 in targeting of atherosclerotic plaques; studies have shown some promise, but further work is needed.

We will discuss below our results in detail, reaching a conclusion and a proposed direction for the future development of these tools, towards the panacea of targeting vulnerable plaque in patients, as well as identifying the vulnerable patient.

7.2 The Development and Utility of Anti-oxidised LDL Antibodies as Biomarkers for Cardiovascular Risk

7.2.1 Choice and Optimisation of assays detecting antibodies against oxidised LDL

Natural antibodies represent a major component of the innate immune system, and are predominantly comprised of the IgM subclass[184]. These antibodies mainly arise from B1 type lymphocytes. Their antigen binding sites have not undergone somatic mutation, and thus have a limited repertoire of binding specificities to diverse antigens. They act usually as a first line defence against infections and work as housekeepers in clearing endogenous debris.

OSEs are major targets of natural antibodies and many OSEs contribute to the development of atherosclerosis[103]. The two epitopes that we selected to study antibody levels against were MDA-LDL and PC. Both have been shown to be particularly important in the pathogenesis of atherosclerosis[1, 26, 158, 182, 185].

7.2.2 Assay development

In vitro synthesised MDA-LDL[97 94] has been used as an antigen in ELISA studies since it was developed by Palinski *et al.* in the early 1990's. We utilised his well-validated technique to create *in vitro* MDA-LDL[94] that has been shown in the past to be very similar to biological MDA-LDL found in human atherosclerotic lesions [14, 65, 67]. MDA-LDL levels in blood have

also been shown to reflect both plaque vulnerability and association with MACE in population studies[65, 67, 186].

PC as an antigen[187] has been shown to be expressed in oxidised LDL, as well as in cell apoptosis, microbes, and neo-epitopes in autoimmune disease. PC-BSA as an *in vitro* antigen has also been well validated for use in ELISA studies[188], and has been used to estimate levels of anti-PC antibodies[188].

We optimised the assays with these well-validated antigens to measure total IgG and IgM, as well as IgG and IgM anti-MDA-LDL, and anti-PC antibodies (Section 4.2). We ensured that the assays were sensitive, with a low background optical density (4.2.1-3). Serial experiments with chequerboard ELISA studies were used to ensure that we were utilising the correct concentration of antigen, serum, and secondary antibodies to measure small variations in the specific serum antibody levels. We also demonstrated a valid standard curve for each assay used, using healthy sera, as well as sera from our study population.

Although assays using MDA-LDL and PC-BSA as antigens have been well validated and extensively studied[189-191], methodology and study populations have varied widely. This has possibly given rise to the conflicting evidence of anti-oxidised LDL antibodies either conveying risk or protection from cardiovascular events.

In particular, the use of anti-PC antibodies as biomarkers to predict cardiovascular risk has several potential issues. The PC epitope is expressed on several pathogens including *Streptococcus pneumoniae*, and previous infection may result in higher serum levels [192]. This may be of interest when studying the relationship between previous infection and susceptibility to atherosclerosis. However, it also muddies the field when studying antibodies in populations where previous infection data is lacking. Furthermore, the response to PC is

susceptible to the phenomenon of 'repertoire shift' as the immune response progresses[193, 194]. This means that some of the anti-PC antibodies may become more specific to their selected antigens and lose affinity to the general PC hapten as more maturation occurs[194]. Therefore, the immunologically crude assay of measuring anti-PC-BSA antibodies may not identify the entire anti-PC repertoire, and thus may lead to inaccurate estimation of total levels.

Different assays have been used to measure anti-MDA-LDL antibodies in the past [97, 106, 189, 195-197]. We selected the most commonly used and extensively validated type of assay, where MDA-LDL is used as a solid phase antigen and levels of anti-MDA-LDL antibodies are measured by adding serum to adherent MDA-LDL and then probing for antibody subtypes with anti-human antibodies. This approach maybe a limitation of the assay as soluble immune complexes[7] may be missed, as well as the added detection of reactivity to other 'autooxidised' LDL epitopes, that may form on MDA-LDL plating onto the ELISA plate.

We also used a similar technique to optimise sensitive assays to distinguish between the different isotypes of IgG reacting with MDA-LDL (sections 4.2.4 and 4.2.5).

We will discuss the relevance of antibody levels against these antigens in the context of cardiovascular risk prediction as part of the ASCOT anti-oxLDL substudy.

7.2.3 IgG anti-MDA-LDL antibodies are independent markers of protection from incident cardiovascular events in the Anglo-Scandinavian Cardiac Outcomes anti-oxLDL substudy

ASCOT offered a valuable opportunity to study the ability of biomarkers to predict cardiovascular events in a normocholesterolaemic hypertensive population. The major finding of this study was that IgG anti-MDA-LDL antibodies robustly and independently

predicted protection. The results are presented in section 4.3. Using the Kaplan-Meier survival estimate model, patients in the upper tertile of these antibody levels had more than 6-fold protection from MACE in comparison to those in the lowest tertile. IgG anti-MDA-LDL antibodies were independent of all other risk factors measured, including FRS, CRP, treatment with statins, LDL cholesterol and CIMT. Notably, the predictive value of IgG anti-MDA-LDL antibodies was not reduced by correction for systolic or diastolic blood pressure, or by anti-hypertension treatment, suggesting a more general relevance than that reflected by ASCOT which applied only to a hypertensive population.

The ASCOT group have previously demonstrated the added benefit and long-term positive effects of statin treatment in ASCOT[168, 198]. The lack of effect of statin treatment on IgG MDA-LDL antibodies is notable. A recent study exploring the prediction of cardiovascular events in statin treated, stable coronary patients, using lipid and non-lipid biomarkers, showed that the concentrations of ~18 biomarkers (including CRP, NT-proBNP, MMP-9, sVCAM-1, sICAM-1, Lp-PLA2, insulin, cystitis C and others) were reduced by atorvastatin independent of dose (10 or 80 mg)[199]. Importantly, these biomarkers ceased to be predictive of cardiovascular risk after the 8-week run-in period, or after one-year treatment with either dose of atorvastatin, implying that their usefulness in risk prediction in patients who are already on statin treatment is limited.

7.2.4 Anti-oxidised LDL antibodies are stable despite one-year treatment with atorvastatin.

We present the data showing the stability of all measured anti-oxLDL antibodies over one year in section 4.3.4. The stability of IgG anti-MDA-LDL antibody levels, despite atorvastatin and reduction in LDL cholesterol, may be advantageous in providing a measure of cardiovascular risk, uninfluenced by lipid-lowering treatment already initiated. Thus, the c statistic for FRS was augmented when IgG anti-MDA-LDL antibody levels were included in the model, even when studying the subjects with at least two other risk factors. This suggests that patients on the 'borderline' for treatment may be usefully further stratified on the basis of IgG anti-MDA-LDL antibody levels to lower or higher risk brackets, thus guiding further management decisions.

The failure of atorvastatin to influence antibody levels over a year is in line with more short-term previously published data[200], but discrepant to the MIRACL study, which found that atorvastatin (80 mg daily) led to a significant increase of IgG anti-MDA-LDL antibodies in an acute coronary syndrome population[195]. Explanations for this include the hypothesis that differences in the atorvastatin dose and antibody levels are also being influenced by the stress of ACS[99].

7.2.5 Proposed mechanisms by which anti-oxidised LDL antibodies maybe protective against cardiovascular events

We know very little about how and why anti-MDA-LDL and anti-PC antibody levels vary in the general population. They may obviously be driven by environmental challenges (e.g. infections, diet), but could also have a hereditary basis or be subject to epigenetic

programming secondary to early life events. Certainly, many IgM anti-PC and IgM anti-MDA-LDL antibodies are germ-line and IgG anti-PC antibodies can readily be detected in infants[191]. Furthermore, a recent study has detected a heritable contribution to levels of both IgG and IgM anti-MDA-LDL[201]. This is a potentially fertile area for further research.

Although this type of study cannot demonstrate mechanistic causality, the data are consistent with a functional, biological role for IgG anti-MDA-LDL antibodies in protection from cardiovascular disease. Such a role is supported by preclinical experiments showing that IgG anti-MDA-MDL antibodies reduce atherosclerosis in mice[84, 202]. The most obvious explanation is by the 'neutralisation effect' or blocking of oxLDL uptake by macrophages, thereby reducing the formation of foam cells and subsequent macrophage cell death[83, 102]. However, the experiments used a Fab fragment and this may not be an accurate representation of the *in vivo* function of native autoantibodies not derived by immunisation.

Complement activation is discussed in the introduction and may have a 'double-edged sword' role in atherosclerosis. Therefore despite IgG potentially having the capability to activate complement, this activation may not always be pathological[51]. It is well established that activating the terminal complement pathway is pathogenic in atherosclerosis[51]. We previously demonstrated that amplification of complement activation by the alternative pathway in response to lipopolysaccharide or high fat diet plays a pro-atherogenic role[53]. But we also demonstrated that C1q deficiency causes larger atherosclerotic lesions in the *Ldl*$^{-/-}$ mouse model[5]. Thus, there is likely a homeostatic role for C1q in the disposal of dying cells. The importance of effective apoptotic cell removal is paramount in keeping atherosclerosis under control, and therefore there may be a protective role played by the IgG anti-MDA-LDL antibodies in stimulating this complement pathway.

The ligation of FcγRs is another characteristic demonstrated by IgG antibodies (specifically of the IgG1 and 3 subtypes). Animals that lack the Fc receptors FcγRI and FcγRIIIA have reduced lesion formation; in contrast, those lacking the inhibitory receptor FcγRIIb develop more severe disease[85]. Therefore the ligation of FcγRs depending on subtype may also be either protective or pathogenic.

Furthermore the context in which the antibodies interact with the antigen could have functional consequences. As shown by JJ Boyle in our group, both IgM and IgG interaction with antigen in solid phase induces a pro-inflammatory phenotype of macrophages, whereas, in fluid-phase IgM prevents oxLDL uptake and foam cell formation[162].

7.2.6 Not all anti-oxidised LDL antibodies correlated with protection from cardiovascular disease, despite a general positive correlation amongst them.

The lack of significance of the other markers we measured (IgM anti-MDA, IgG and IgM anti-PC-BSA) in the prediction of protection from cardiovascular events may be related to the sample size and the effect size of these antibody levels. It was clear that all antibody levels correlated with each other, and with total IgG and IgM. It may be possible that when studying a larger cohort with more events, any of these biomarkers may become significant in predicting protection from cardiovascular events, with a similar biological explanation as was given for IgG anti-MDA-LDL antibodies.

7.2.6 Dissecting the IgG response to MDA-LDL

As we demonstrated that IgG anti-MDA-LDL antibodies were of most interest and had the largest statistical effect in predicting protection from cardiovascular events, we then aimed to

dissect the autoantibody profile to examine the relationship of IgG isotypes against MDA-LDL in the same population. It may be that some IgG anti-MDA-LDL antibodies are not correlated with protection, as they may ligate FcγR and activate complement beyond its haemostatic capacity to pathological effect. Therefore, dissecting the immune response to MDA-LDL was of interest.

Previous work had recognised that IgG1 and IgG3 isotypes were the predominant isotypes seen in reactivity to copper-oxidised LDL in humans[203]. We found a similar pattern with the isotypes against MDA-LDL in a random sample of the patient population and therefore measured these levels in the 200 patients.

As presented in section 4.3.6, we found no association between anti-MDA-LDL IgG3 or IgG1 levels and cardiovascular events. However, IgG3 levels were positively correlated with HDL and IgG1 levels positively correlated with HDL and negatively correlated with LDL. Both levels were unaffected by treatment with statins for one year. Therefore the suggestion is that the two most predominant isotypes of autoantibodies to MDA-LDL in this patient population correlated with markers that provided protection from cardiovascular disease. There was certainly no signal that these isotypes correlated with any negative risk factors.

The interaction of IgG subtype levels with HDL, and inverse relationship of IgG1 subtype with LDL, may reflect a possible correlation with components of the metabolic syndrome. It is well recognised that the metabolic syndrome is a pro-inflammatory state[204], and levels of circulating oxLDL are correlated with the metabolic syndrome[205]. HDL is also associated with an 'anti-inflammatory' profile[206] and this may be reflected in the positive correlation of IgG anti-MDA-LDL levels.

There was also an interesting distribution of the IgG1 antibodies seen. The bimodal distribution with most patients either in the highest or lowest tertiles may reflect a genetically coded distribution, or a previous exposure to a specific antigen such as a childhood infection. This warrants further study and may provide an insight on the possible 'auto-immunisation' of individuals that will in future life convey protection.

7.3 the Generation, Characterisation and Development of LO1 and Its Molecularly Expressed Chimeric Fab Construct for the Targeted Imaging of Oxidised LDL *in Vivo*

7.3.1 In vitro characterisation of LO1

As shown in section 5.2, we demonstrated the LO1 selectively binds MDA-LDL in preference to native LDL. In order to characterise the LO1 epitope further, we tested LO1 against other modifications of LDL. Trypsinised LDL and hypochlorite oxidised LDL, as well as autooxidised LDL, do not react with LO1, suggesting that the reaction of LO1 to Cu-oxLDL (the assay in which it was first selected), may be due to the reactivity with MDA-LDL. The crude Cu-oxLDL that was initially used for the selection of LO1 contains not only the above-mentioned modifications of LDL, but also others such as 4-hydroxynoneal, which we did not study. We also demonstrated that MDA-conjugated albumin does not bind LO1 (previous work, not shown), indicating that the LDL carrier is as important in the binding of LO1 to MDA-LDL as the MDA hapten. Another possibility is that LDL changes structurally during the MDA binding, to reveal a cryptic epitope within the LDL molecule.

The selection and development of H3 as a single chain anti-idiotype has provided useful insights into the epitope targeted by LO1[166]. It has also enabled us to have a stable antigen

surrogate for the affinity purification of LO1. In order to demonstrate the common epitope between H3 and MDA-LDL, blocking ELISAs were performed. H3 blocked the binding of LO1 to MDA-LDL. Further similarities between LO1 binding to MDA-LDL and to H3 were shown by demonstrating similar binding profiles in a range of pH and salt concentrations. Furthermore, the robust specific reactivity of LO1 against H3, and the ability of H3 to block the interaction of LO1 with MDA-LDL effectively, was utilised later on when studying the *in vitro* interaction of LO1 on atherosclerotic sections, which was blocked by the addition of H3. This supported the conclusion that LO1 binds specifically to MDA-LDL within plaque sections.

Further ELISA studies of a series of peptides derived from the H3 structure failed to bind LO1 or block the binding of LO1 to MDA-LDL either in isolation or in combination. This increases the possibility that the LO1 epitope is conformational, dependant on architectural interaction.

It has been shown previously that MDA-LDL can be detected in plasma[111, 113]. We therefore conducted ELISA studies which showed that the binding of LO1 to MDA-LDL on the solid phase was not inhibited by plasma or by fluid-phase LDL at high physiological level, supporting the potential use of the antibody for imaging.

Alcohol fails to eliminate the epitope from MDA-LDL, which would suggest that it is protein dependant rather than lipid dependant. Formaldehyde did not destroy the epitope on ELISA, and therefore using it as a preservative in IHC studies would have not prevent detection of the LO1 antigen.

The work we undertook in the sequencing of LO1 utilised classical immunological techniques combining both DNA sequencing and the isolation of purified LO1 on an H3

column followed by mass spectrometry, de Novo sequencing and matching to germ-line IGMT database. As shown in section 5.2.5, we identified the heavy chain as described above, and found a close match from the light chain. The few amino acid differences in the CDR regions between our sequenced light chain and the IgK V6-20 VL may reflect somatic hypermutation and affinity maturation of the LO1 antibody. It is possible that the LO1 VH CDR3, which has an arginine and two lysines, all positively charged, plays a vital role in the binding of LO1 to H3 (CDRH3 of H3 contains a stretch of six amino acids with four aspartates (DDDAFD)- all negatively charged), and to MDA-LDL.

7.3.2 LO1 identifies atherosclerotic lesions *in vitro*

As presented in section 5.2.7, immunohistochemical studies in both LDL-/- vs. wild type with isotype control show that LO1 binds to antigen accumulated in the atherosclerotic plaque in the aortic root of the *Ldlr*$^{-/-}$ mice, and with clinical pathological carotid tissue LO1 binds to vulnerable plaque with an advanced lipid necrotic core and thin fibrous cap. In this area, it is thought that macrophages further modify mildly modified LDL, and are killed by their load of heavily modified LDL. The selectivity of LO1 staining for this zone of the plaque is consistent with current ideas about plaque LDL handling. Most of the extracellular LO1 staining (i.e., not obviously around nuclei) was also cell-shaped, reflecting either that the nucleus was out of section (in the z-plane) or reflecting release from dead cells. Corroborating this interpretation was the co-localisation of LO1 specific staining (not found in the isotype control) in the AlexaFluor 568 (red emission) channel with classical oxidised LDL-associated autofluorescence in the green emission channel (not shown).

The similar LO1 staining of mouse and human plaques, with punctate localisation to macrophages, and also to extracellular aggregates within the necrotic core, was in contrast to

that in the rabbit model. LO1 staining was seen particularly in macrophage rich areas, rather than vascular smooth muscle cells[58, 207].

We believe the extracellular staining seen in both the mouse and human sections is particularly relevant pathophysiologically, as it is indicative of failure of macrophage debris clearance and suggests lesional activity. Furthermore, extracellular antigen is potentially available to molecular targeting by antibodies.

7.4.4 LO1 specifically targets experimental atherosclerosis *in vivo* in the *Ldlr*$^{-/-}$ mouse model

Modalities that identify vulnerable plaque by characterising morphology are still limited in their ability to determine plaque vulnerability and predict cardiovascular events[119]. New diagnostic modalities are evolving that focus on the identification of biological factors responsible for the development and rupture of vulnerable plaque[208]. The wide variety of factors contributing to plaque vulnerability poses both an opportunity and a challenge for the emerging technologies aimed to be translational tools to help in pre-emptive intervention[59, 209]. The need for such technology is becoming more urgent with the rapid emergence of newer low-risk intravascular therapeutic options, such as drug eluting bio-absorbable stents[210]. It may soon become possible that pre-emptive interventional treatment of individual high-risk plaques is clinically relevant[211].

As shown in section 5.3, using labelled LO1, we aimed to develop an antibody targeted NIRF-based imaging modality for the identification of OxLDL. The developmental trajectory for such a modality requires antibody generation, characterisation and engineering to go hand in hand with advances in imaging technologies[139]. NIRF imaging offers the opportunity to

move forwards from optical basic science techniques and small animal imaging into more clinically relevant developments, such as that of the newer catheter-based NIRF imaging modalities[136, 137].

The pilot work undertaken with IVIS Spectrum imaging allowed us to study organ distribution and blood half-life of LO1-750 following intravenous injection. The organ distribution of LO1-750 and its isotype control showed trafficking to the liver in preference to the spleen or kidney. This is in line with other large NIRF labelled molecules that are not readily filtered in the kidneys[212]. The half-life was consistent with a two-phase decay, likely due to the rapid initial distribution of the antibody into extracellular space, followed by a slow background decay that is in line with other IgG antibodies.

Using IVIS/CT we were also able to observe the localisation of LO1 to plaque areas in the *Ldlr*$^{-/-}$ atherosclerosis model. LO1-750 localised to plaque areas on fused IVIS/CT images in the *Ldlr* $^{-/-}$ animals and not wild type controls, with the isotype control being negative in both. Furthermore, it was clear that the signal was concentrated in areas of advanced plaque with calcification (as identified on high resolution contrast-enhanced CT) in the aortic arch areas and bifurcations. This pattern of uptake is consistent with the distribution of lesions in this mouse model. The localisation of LO1-750 at the lesional areas was confirmed *ex vivo* with fluorescence reflectance imaging (not shown).

The IVIS/CT data was encouraging enough for us to take the work further into a modality that allows precise quantification, namely FMT fused with CT (FMT/CT). We aimed to determine the *in vivo* targeting of atherosclerotic plaque in the advanced atherosclerosis *Ldlr*$^{-/-}$ model vs. wild type controls, whilst comparing the localisation with that of an alternative probe[213]. MMPSense FAST is a targeting agent that is activated by several MMPs and was

chosen as it has shown promise in other disease models[214]. It has been shown *in vitro* to be activated by entities in vulnerable plaque[215], but as far as we are aware, has not previously been studied in detail as an imaging agent in preclinical atherosclerosis models.

Having initially determined using contrast-enhanced FMT/CT that LO1 localises to the aortic arch and branches, we selected a standard ROI over the thorax for further quantification studies. These showed focal localisation of LO1-750 in the *Ldlr*$^{-/-}$ but not the wild type mice, with the isotype control being negative in both. MMPSense FAST also showed statistically significantly higher activity at the ROIs in the *Ldlr*$^{-/-}$ group vs. wild type animals. However, MMPSense FAST demonstrated a higher background in the wild type animals when compared to LO1-750.

7.4.6 LO1 tracks the effects of high fat and aging *in vivo.*

The ability of LO1-750 to distinguish between degrees of atherosclerosis was further tested in a progression study in the *Ldlr*$^{-/-}$ model. As shown in section 5.3.4, LO1-750 clearly distinguished between a group fed a high fat diet for 42 weeks, and a group fed for just 30 weeks. We also studied a middle group that was fed for 30 weeks with a high fat diet, and low fat diet for 12 further weeks, and found a correlation trend (R square 0.42, $p<0.05$) between all groups. MMPSense was also able to distinguish between the two extremes of the experiment but had a lower correlation for trend, indicating that the middle group was not as clearly distinguished as with LO1.

7.4.7 Could LO1-750 and MMPSense have a complementary role in the identification of vulnerable atherosclerotic plaque?

The differential identification of the middle group by LO1, suggests that it tracks the accumulation of the antigen it identifies in plaque- namely MDA-LDL. MMPSense however, tracks MMP activity, and stopping the pro-inflammatory stimulus of fat diet, 'turned off' the progression of the MMP signal in the intermediate group. This may offer a valuable translational opportunity to use both agents simultaneously to distinguish between plaque progression in terms of oxLDL content and plaque inflammation in terms of MMP activity. For example, it may be that a certain plaque may still continue to slowly build up deposits of oxidised LDL, despite adequate treatment, but may be less susceptible to rupture in comparison to an equally oxLDL filled plaque that is also actively displaying strong MMP activity. The value of this combination imaging may not become apparent until studied in either models that can actually display plaque rupture (non-existent to date) or in high-risk human studies in the peri-ACS syndrome situation.

7.4.8 *ex vivo* validation of LO1-750 targeting in atherosclerotic plaque.

We validated the LO1 *in vivo* imaging with *ex vivo* fluorescence reflectance imaging, and *en face* confocal microscopy on whole aortae with Z stacking and tile scanning. As shown in section 5.3.5, this demonstrated the localisation of the probe to visible atherosclerotic plaque within the heavily diseased aortic arch and its bifurcations, as well as a weaker signal in plaque within the abdominal aorta. Furthermore we established the localisation of the injected antibody to sub-endothelium by co-injecting PE-conjugated anti-CD31. Three-dimensional imaging, showed partial localisation of LO1-750 to macrophages.

7.4.9 Proof of concept intravascular imaging of LO1 targeting OxLDL in the atherosclerotic, balloon-injured rabbit model

As a proof of concept that NIRF imaging with LO1 is applicable to a catheter-based approach, we undertook pilot studies using the 2D NIRF system combined with IVUS, that has been used to image balloon injury and stent induced inflammation in the high fat fed rabbit model[135-137]. The imaging of LO1-750 with 2D NIRF in the live animal identified localisation to the atherosclerotic balloon injury site, but was suboptimal and did not reflect the whole area identified on *ex vivo* fluorescence reflectance imaging. This was likely due to a high LO1-750 background signal remaining in blood, despite imaging being undertaken 21 hours post injection. Interestingly, as demonstrated in section 5.3.6, using *ex vivo* intravascular 2D NIRF imaging, with the aorta flushed empty of blood and perfused with saline, we did robustly demonstrate that intravenously injected LO1-750 can be detected in the disease area as identified on IVUS. This was confirmed by matching whole aorta fluorescence reflectance imaging *ex vivo* with the lesional areas identified by LO1 intravascularly. It should be noted that we also demonstrated that the LO1-750 signal was different to that seen with autofluorescence in the FITC channel. Furthermore, *ex vivo* fluorescence microscopy studies of freshly frozen sections showed a pattern of staining in the rabbit atherosclerosis model similar to that seen in LO1-750 injected mice, with lesion specific punctate and diffuse staining.

7.4.10 The generation and expression of LO1-Fab and LO1-Fab-Cys

Although LO1 showed great promise in targeting oxidised LDL within plaque in two different experimental models and *in vitro* in human, there are obvious problems in using a native mouse IgG clinically. These include the relatively slow blood clearance,

immunogenicity and Fc-related effector function. By creating recombinant molecular constructs of an antibody, it is possible to minimize immunogenicity and remove the Fc region. Furthermore, the size and valency can be varied to increase tissue penetration and avidity and obtain faster blood clearance. With this in mind we have successfully sequenced and cloned the LO1 heavy and light chain variable regions, allowing us to molecularly express the antibody as demonstrated in section 5.4. As a start, we created a cysteine-tagged human chimeric Fab construct and shown its function to resemble that of LO1 *in vitro*. Moreover, our initial pilot data *in vivo* show that LO1-Fab-Cys targets atherosclerotic plaque in a similar manner to its parent antibody. Further work will focus on the detailed characterisation of the Fab construct and exploring further molecular expressed constructs such as diabodies.[165]

What is of functional interest is the retention of function of the Fab structure suggesting that the interaction of LO1 with its antigen is not dependant on the FcγR ligation ability of the full antibody. Clearly, both valency and conformation are also important factors to consider and the Fab did not have a significantly reduced functional interaction with MDA-LDL or H3. A Fab structure may or may not be able to retain function due to valency and conformational factors, but the initial data from the Fab are encouraging enough to allow us to pursue this as a future direction of work.

In addition to its intended use as an imaging agent, LO1-Fab-Cys or other LO1 derivatives may have further potential. Recent advances in targeted delivery of statins using HDL as a carrier have been demonstrated to be viable in mouse atherosclerosis[153]. Along these lines, it may be possible to design drug-eluting nanoparticles tagged with an anti-OxLDL antibody for specific therapeutic targeting to plaque.

7.5 LO9, an IgG Monoclonal Autoantibody Reacting with a Cryptic Allosteric Epitope on Low Density Lipoprotein

7.5.1 LDL deposition within the sub-endothelial space may represent an initial event in atherosclerosis, presenting adherent LDL an antigen to the innate immune system

As an initial event in atherosclerosis, LDL becomes trapped in the arterial wall possibly through binding to anionic proteoglycans in the sub-endothelial space[216]. The importance of LDL adhesion to matrix proteoglycans causing structural alterations, and converting it from a non-antigenic to an antigenic entity has received some attention[217], but never in the context of interaction with an IgG antibody such as LO9. It has traditionally been postulated that the deposition of LDL in the sub-endothelial layer acts as a precursor to the involvement of macrophages, when some of the LDL is taken up by the macrophages and deposited within a necrotic core[29, 42].

Finding an 'autoantibody' that is specific to adherent LDL would therefore present an opportunity to aim to target atherosclerosis, as well as study the functional importance of such antibodies.

7.5.1 LO9 is unique as an IgG autoantibody specific to adherent LDL, and not to captured LDL or LDL in solution

LO9 was identified when initially screening for anti-oxidised LDL antibodies. It is an IgG2b isotype autoantibody, having been isolated by earlier work in our group through screening against plate-adherent LDL. The presence of an autoantibody against truly 'native' LDL is

highly unlikely to be biologically useful, and so characterising the LO9 epitope became of interest.

We demonstrated that LO9 reacts against adherent LDL, rather than with native LDL in suspension or captured onto plastic by anti-apoB antibody. Furthermore, LO9 reacts less well with heavily modified LDL. It has an epitope that is lipid independent, and once the epitope is revealed by adhesion to plastic, it can be modified with trypsinisation. We demonstrated that LDL in serum does not significantly block the binding of LO9 to adherent LDL, suggesting that this autoantibody is not raised against the majority of LDL in plasma, which otherwise would be difficult to justify in terms of normal biology.

Although autoantibodies, similar to LO1, are well described that react with chemically modified forms of LDL, these are mainly germ-line antibodies that react with oxidation specific epitopes on LDL, such as phosphocholine and malonedialdehyde[9,218], The only other example in the literature of an antibody reacting with adherent LDL is that of an IgM[9], which showed modest binding to native LDL adherent to the surface of ELISA plates, and similarly to LO9, this could not be blocked by the same preparation of LDL in solution.

Therefore LO9 is unique in being an IgG autoantibody that reacts with 'non-manipulated' LDL on adherence, and may harbour both a functional role *in situ* as well as potential utility in translational applications.

7.5.2 LO9 sequence suggests that it is an adaptive rather than a germ-line antibody

Sequencing of the variable heavy (VH) and variable light (VL) regions revealed numerous somatic mutations in the CDR of both the VH and VL, consistent with it being significantly mutated away from its natural antibody origin.

There was also an unusual deletion of a series of 9 amino acids from the germ-line sequence in the VH. This re-enforces the hypothesis that LO9 is a result of an adaptive immune response.

Together with the IgG2b subclass, these indicate that LO9 is not a natural antibody but has developed from an adaptive immune response, but nevertheless, an autoantibody as it was isolated from an unimmunised animal.

7.5.2 LO9 is likely to have pathological functions when reacting with solid phase antigen, and its epitope is further revealed by macrophage activation.

The concept of an antibody to minimally modified LDL having a biological activity was explored by Grosso et al[36]. They showed that passive transfer of an IgG2b monoclonal antibody reactive against electronegative LDL (a form of minimally modified LDL present in plasma in increased concentration in atherosclerotic mice) reduced development of disease. There has been little work in exploring the role of a spontaneously occurring autoantibody to minimally modified LDL. However, LO9 is different in the fact that it only binds adherent antigen. This makes it is unlikely to have a haemostatic role and further increases the chance of ligating FcγR and activating complement when trapped on a solid phase antigen.

A clear precedent exists for an autoantibody against an allosteric conformational epitope being pathogenic. Thus antibodies have been discovered that react with β_2GP1, and that may play a pathogenic role in anti-phospholipid syndrome[219].

We found that the addition of macrophages to LO9 bound to adherent LDL *in vitro* led to significant TNFα release, an effect that was blocked by inhibition of FcγRs. Furthermore, expression of the LO9 epitope on adherent LDL was greatly increased by incubation with CM from activated macrophages, consistent with the LDL epitope being further revealed by macrophage-derived factors.

Put together, this suggests a mechanism by which LO9 acts as a link in a vicious circle of LDL turning into an antigenic entity upon adherence, causing macrophage activation and the further modification of LDL and thus progression of atherosclerosis as depicted in the hypothetical model represented in Figure 7.1.

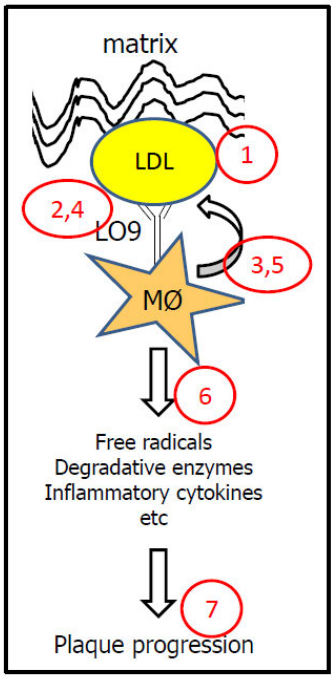


Figure 7.1: Hypothetical model of how LO9 and similar antibodies may accelerate atherosclerosis

1. LDL particles are trapped by tissue proteoglycans leading to LO9 epitope expression.
2. LO9 binds LDL and activates macrophages (MØ) via FcγR ligation.
3. Activated macrophages secrete products that enhance LO9 epitope expression.
4. Further LO9 binding to FcγR leads to increased macrophage activation.
5. Activated macrophages digest extracellular LDL leading to LDL aggregation, oxidation and free fatty acid release.
6. Activated macrophages release pro-inflammatory mediators.
7. The outcome is plaque progression.

7.5.3 LO9 can be labelled, and utilised to identify atherosclerosis *in vitro* and *in vivo*

Expression of the LO9 epitope in atherosclerosis was confirmed by immunohistochemical staining of human and mouse lesions and using *en face* whole aorta imaging with LO9 conjugated with a near-infrared fluorescent dye.

The pattern of staining seen with LO9 on murine atherosclerosis was in keeping with partial co-localisation to macrophages, but also scanty staining of free deposits that maybe adherent LDL that is yet to attract macrophages.

The human staining of LO9 in comparison to LO1 was interesting in that the staining was less prevalent, but was also more prevalent on the peripheral regions of the atherosclerotic lesions. There was more staining in advanced rather than intermediate lesions but certainly less than LO1.

The *in vivo* pilot studies performed with LO9-750 with FMT/CT, demonstrated localisation to atherosclerotic areas in the aortic root and branches of the aorta. What is of interest is that the *ex vivo* studies confirmed the signal was sub-endothelial by localisation to a layer underneath a PECAM targeted endothelial layer. Also the pattern was similar to what was seen with the *in vitro* staining, both scantier than what was seen with LO1 and with partial localisation to macrophages.

The utility of LO9 as an imaging agent may be explored in the future. The pattern of staining in the murine tissue suggests possible use as a detector of a different form of oxLDL than that which LO1 identifies, or even to localise areas which may be susceptible to aneurysm formation in the future.

This approach may provide deep insight into progression of atherosclerosis and the graded modification of LDL from minimally modified, as recognised by LO9 to heavily modified and deposited in necrotic core, as identified by LO1. One long-term aim is to utilise both these antibodies simultaneously in longitudinal progression studies. Effects of drugs such as statins on both modifications of LDL could be studied together, forming an insight into the effect of modulating agents.

7.6 Conclusion and Further Work

The main outcome of this thesis is the demonstration of the role of autoantibodies against oxidised LDL as serological and imaging biomarkers in atherosclerosis.

From the serological studies, we concluded that high IgG anti-MDA-LDL antibody levels are strongly associated with significant protection from cardiovascular events in hypertensive patients selected based on traditional risk factors. This association is independent of classical

risk factors and CRP. Furthermore, levels are stable despite one year of atorvastatin and lowered LDL, suggesting the characteristics of a robust biomarker that may be useful for stratification. Further studies exploring the prognostic significance of these antibodies are warranted.

We also concluded that LO1 specifically identifies MDA-LDL and atherosclerosis in experimental atherosclerosis. It can be used in identifying progression of atherosclerotic lesions and in concert with other imaging biomarkers may provide a useful insight into the biology of atherosclerotic plaque. LO1-Fab-Cys is a functional partially humanised Fab fragment that may pave the way towards the translational development of LO1 as an imaging tool in the intravascular NIRF identification of oxidised LDL in human atherosclerotic plaque.

We also introduced LO9, a novel autoantibody that reacts with an allosteric epitope on LDL revealed by adhesion to a surface and/or by the action of factors derived from activated macrophages. Binding of LO9-like antibodies to LDL trapped on matrix in the arterial wall could lead to promotion of atherosclerosis via ligation of macrophage FcγRs and release of TNFα and other pro-inflammatory mediators. We also demonstrated that LO9 can target atherosclerotic lesions in vivo, and may have utility, in concert with LO1 and others markers of inflammation in determining the biological activity of atherosclerotic plaque.

We plan to perform the following, and have already established appropriate research collaborations to allow us to undertake the work:

1) Develop LO1 and LO9 into fully humanised ScFv constructs for the NIRF intravascular imaging to LDL in atherosclerosis

2) Study the utility of anti-oxidised LDL antibodies as predictors of risk as well as establish a genomic link in a Case Control and genome-wide association study (GWAS) of IgG anti-oxidised low density lipoprotein (oxLDL) autoantibodies in >500 and their controls (1000) in ASCOT.

8.0 References

1. Libby P. Inflammation in atherosclerosis. *Nature*. 2002;420:868-874

2. Prassl R, Laggner P. Molecular structure of low density lipoprotein: Current status and future challenges. *Eur Biophys J*. 2009;38:145-158

3. Pease RJ, Harrison GB, Scott J. Cotranslocational insertion of apolipoprotein b into the inner leaflet of the endoplasmic reticulum. *Nature*. 1991;353:448-450

4. Ridker PM. LDL cholesterol: Controversies and future therapeutic directions. *Lancet*. 2014;384:607-617

5. Bhatia VK, Yun S, Leung V, Grimsditch DC, Benson GM, Botto MB, Boyle JJ, Haskard DO. Complement c1q reduces early atherosclerosis in low-density lipoprotein receptor-deficient mice. *Am J Pathol*. 2007;170:416-426

6. Davis BT, Wang XJ, Rohret JA, Struzynski JT, Merricks EP, Bellinger DA, Rohret FA, Nichols TC, Rogers CS. Targeted disruption of ldlr causes hypercholesterolemia and atherosclerosis in yucatan miniature pigs. *PLoS One*. 2014;9:e93457

7. Tsimikas S, Willerson JT, Ridker PM. C-reactive protein and other emerging blood biomarkers to optimize risk stratification of vulnerable patients. *J Am Coll Cardiol*. 2006;47:C19-31

8. Rizzo M, Kotur-Stevuljevic J, Berneis K, Spinas G, Rini GB, Jelic-Ivanovic Z, Spasojevic-Kalimanovska V, Vekic J. Atherogenic dyslipidemia and oxidative stress: A new look. *Transl Res*. 2009;153:217-223

9. Chou MY, Fogelstrand L, Hartvigsen K, Hansen LF, Woelkers D, Shaw PX, Choi J, Perkmann T, Backhed F, Miller YI, Horkko S, Corr M, Witztum JL, Binder CJ. Oxidation-specific epitopes are dominant targets of innate natural antibodies in mice and humans. *J Clin Invest*. 2009;119:1335-1349

10. Yang CY, Gu ZW, Weng SA, Kim TW, Chen SH, Pownall HJ, Sharp PM, Liu SW, Li WH, Gotto AM. Structure of apolipoprotein b-100 of human low density lipoproteins. *Arteriosclerosis, Thrombosis, and Vascular Biology*. 1989;9:96-108

11. Velican C, Velican D. Progression of coronary atherosclerosis from adolescents to mature adults. *Atherosclerosis*. 1983;47:131-144

12. D'Agostino RB, Sr., Vasan RS, Pencina MJ, Wolf PA, Cobain M, Massaro JM, Kannel WB. General cardiovascular risk profile for use in primary care: The Framingham Heart Study. *Circulation*. 2008;117:743-753

13. Paananen K, Saarinen J, Annila A, Kovanen PT. Proteolysis and fusion of low density lipoprotein particles strengthen their binding to human aortic proteoglycans. *J Biol Chem*. 1995;270:12257-12262

14. Rosenfeld ME, Palinski W, Yla-Herttuala S, Butler S, Witztum JL. Distribution of oxidation specific lipid-protein adducts and apolipoprotein b in atherosclerotic lesions of varying severity from WHHL rabbits. *Arteriosclerosis*. 1990;10:336-349

15. Kita T, Kume N, Minami M, Hayashida K, Murayama T, Sano H, Moriwaki H, Kataoka H, Nishi E, Horiuchi H, Arai H, Yokode M. Role of oxidized LDL in atherosclerosis. *Annals of the New York Academy of Sciences*. 2001;947:199-206

16. Palinski W, Rosenfeld ME, Yla-Herttuala S, Gurtner GC, Socher SS, Butler SW, Parthasarathy S, Carew TE, Steinberg D, Witztum JL. Low density lipoprotein undergoes oxidative modification in vivo. *Proc Natl Acad Sci U S A*. 1989;86:1372-1376

17. Briley-Saebo KC, Cho YS, Tsimikas S. Imaging of oxidation-specific epitopes in atherosclerosis and macrophage-rich vulnerable plaques. *Curr Cardiovasc Imaging Rep*. 2011;4:4-16

18. Haberland ME, Fong D, Cheng L. Malondialdehyde-altered protein occurs in atheroma of watanabe heritable hyperlipidemic rabbits. *Science*. 1988;241:215-218

19. Bertoia ML, Pai JK, Lee JH, Taleb A, Joosten MM, Mittleman MA, Yang X, Witztum JL, Rimm EB, Tsimikas S, Mukamal KJ. Oxidation-specific biomarkers and risk of peripheral artery disease. *J Am Coll Cardiol*. 2013

20. Steinberg D. The LDL modification hypothesis of atherogenesis: An update. *J Lipid Res*. 2009;50 Suppl:S376-381

21. Packard CJ. Lipoprotein-associated phospholipase a2 as a biomarker of coronary heart disease and a therapeutic target. *Curr Opin Cardiol*. 2009;24:358-363

22. Hansson GK, Libby P. The immune response in atherosclerosis: A double-edged sword. *Nat Rev Immunol*. 2006;6:508-519

23. Binder CJ, Shaw PX, Chang M, Boullier A, Hartvigsen K, Horkko S, Miller YI, Woelkers DA, Corr M, Witztum JL. The role of natural antibodies in atherogenesis. *J Lipid Res*. 2005;46:1353-1363

24. Brown MS, Goldstein JL. Lipoprotein metabolism in the macrophage: Implications for cholesterol deposition in atherosclerosis. *Annu Rev Biochem*. 1983;52:223-261

25. Steinberg D. Low density lipoprotein oxidation and its pathobiological significance. *J Biol Chem*. 1997;272:20963-20966

26. Weismann D, Binder CJ. The innate immune response to products of phospholipid peroxidation. *Biochim Biophys Acta*. 2012;1818:2465-2475

27. Binder CJ, Horkko S, Dewan A, Chang M, Kieu EP, Goodyear CS, Shaw PX, Palinski W, Witztum JL, Silverman GJ. Pneumococcal vaccination decreases atherosclerotic lesion formation: Molecular mimicry between streptococcus pneumoniae and oxidized LDL. *Nat Med*. 2003;9:736-743

28. Torzewski M, Suriyaphol P, Paprotka K, Spath L, Ochsenhirt V, Schmitt A, Han SR, Husmann M, Gerl VB, Bhakdi S, Lackner KJ. Enzymatic modification of low-density lipoprotein in the arterial wall: A new role for plasmin and matrix metalloproteinases in atherogenesis. *Arterioscler Thromb Vasc Biol*. 2004;24:2130-2136

29. Bhakdi S, Dorweiler B, Kirchmann R, Torzewski J, Weise E, Tranum-Jensen J, Walev I, Wieland E. On the pathogenesis of atherosclerosis: Enzymatic transformation of human low density lipoprotein to an atherogenic moiety. *J Exp Med*. 1995;182:1959-1971

30. Torzewski M, Klouche M, Hock J, Messner M, Dorweiler B, Torzewski J, Gabbert HE, Bhakdi S. Immunohistochemical demonstration of enzymatically modified human LDL and its colocalization with the terminal complement complex in the early atherosclerotic lesion. *Arterioscler Thromb Vasc Biol*. 1998;18:369-378

31. Barros MR, Bertolami MC, Abdalla DS, Ferreira WP. Identification of mildly oxidized low-density lipoprotein (electronegative LDL) and its auto-antibodies IgG in children and adolescents hypercholesterolemic offsprings. *Atherosclerosis*. 2006;184:103-107

32. Yoshida H, Quehenberger O, Kondratenko N, Green S, Steinberg D. Minimally oxidized low-density lipoprotein increases expression of scavenger receptor a, cd36, and macrosialin in resident mouse peritoneal macrophages. *Arterioscler Thromb Vasc Biol*. 1998;18:794-802

33. Avogaro P, Bon GB, Cazzolato G. Presence of a modified low density lipoprotein in humans. *Arteriosclerosis*. 1988;8:79-87

34. Estruch M, Sanchez-Quesada JL, Ordonez Llanos J, Benitez S. Electronegative LDL: A circulating modified LDL with a role in inflammation. *Mediators Inflamm*. 2013;2013:181324

35. Chu CS, Wang YC, Lu LS, Walton B, Yilmaz HR, Huang RY, Sawamura T, Dixon RA, Lai WT, Chen CH, Lu J. Electronegative low-density lipoprotein increases c-reactive protein expression in vascular endothelial cells through the LOX-1 receptor. *PLoS One*. 2013;8:e70533

36. Grosso DM, Ferderbar S, Wanschel AC, Krieger MH, Higushi ML, Abdalla DS. Antibodies against electronegative LDL inhibit atherosclerosis in Ldlr-/- mice. *Braz J Med Biol Res*. 2008;41:1086-1092

37. Greaves DR, Gordon S. The macrophage scavenger receptor at 30 years of age: Current knowledge and future challenges. *J Lipid Res*. 2009;50:11

38. Takahashi K, Takeya M, Sakashita N. Multifunctional roles of macrophages in the development and progression of atherosclerosis in humans and experimental animals. *Med Electron Microsc*. 2002;35:179-203

39. Bobryshev YV. Monocyte recruitment and foam cell formation in atherosclerosis. *Micron*. 2006;37:208-222

40. Wu R, de Faire U, Lemne C, Witztum JL, Frostegard J. Autoantibodies to oxLDL are decreased in individuals with borderline hypertension. *Hypertension*. 1999;33:53-59

41. Bui QT, Prempeh M, Wilensky RL. Atherosclerotic plaque development. *Int J Biochem Cell Biol*. 2009;41:2109-2113

42. Moore KJ, Tabas I. Macrophages in the pathogenesis of atherosclerosis. *Cell*. 2011;145:341-355

43. Kuchibhotla S, Vanegas D, Kennedy DJ, Guy E, Nimako G, Morton RE, Febbraio M. Absence of cd36 protects against atherosclerosis in apoe knock-out mice with no additional protection provided by absence of scavenger receptor a i/ii. *Cardiovasc Res*. 2008;78:185-196

44. Manning-Tobin JJ, Moore KJ, Seimon TA, Bell SA, Sharuk M, Alvarez-Leite JI, de Winther MP, Tabas I, Freeman MW. Loss of sr-a and cd36 activity reduces atherosclerotic lesion complexity without abrogating foam cell formation in hyperlipidemic mice. *Arterioscler Thromb Vasc Biol*. 2009;29:19-26

45. Buton X, Mamdouh Z, Ghosh R, Du H, Kuriakose G, Beatini N, Grabowski GA, Maxfield FR, Tabas I. Unique cellular events occurring during the initial interaction of macrophages with matrix-retained or methylated aggregated low density lipoprotein (LDL). Prolonged cell-surface contact during which LDL-cholesteryl ester hydrolysis exceeds LDL protein degradation. *J Biol Chem*. 1999;274:32112-32121

46. Zhang WY, Gaynor PM, Kruth HS. Aggregated low density lipoprotein induces and enters surface-connected compartments of human monocyte-macrophages. Uptake occurs independently of the low density lipoprotein receptor. *J Biol Chem*. 1997;272:31700-31706

47. Coppola G, Caro C. Arterial geometry, flow pattern, wall shear and mass transport: Potential physiological significance. *J R Soc Interface*. 2009;6:519-528

48. Cecchi E, Giglioli C, Valente S, Lazzeri C, Gensini GF, Abbate R, Mannini L. Role of hemodynamic shear stress in cardiovascular disease. *Atherosclerosis*. 2011;214:249-256

49. Warboys CM, de Luca A, Amini N, Luong L, Duckles H, Hsiao S, White A, Biswas S, Khamis R, Chong CK, Cheung WM, Sherwin SJ, Bennett MR, Gil J, Mason JC, Haskard DO, Evans PC. Disturbed flow promotes endothelial senescence via a p53-dependent pathway. *Arterioscler Thromb Vasc Biol*. 2014;34:985-995

50. Frueh J, Maimari N, Homma T, Bovens SM, Pedrigi RM, Towhidi L, Krams R. Systems biology of the functional and dysfunctional endothelium. *Cardiovasc Res*. 2013;99:334-341

51. Haskard DO, Boyle JJ, Mason JC. The role of complement in atherosclerosis. *Curr Opin Lipidol*. 2008;19:478-482

52. Buono C, Come CE, Witztum JL, Maguire GF, Connelly PW, Carroll M, Lichtman AH. Influence of C3 deficiency on atherosclerosis. *Circulation*. 2002;105:3025-3031

53. Malik TH, Cortini A, Carassiti D, Boyle JJ, Haskard DO, Botto M. The alternative pathway is critical for pathogenic complement activation in endotoxin- and diet-induced atherosclerosis in low-density lipoprotein receptor-deficient mice. *Circulation*. 2010;122:1948-1956

54. Rohwedder I, Montanez E, Beckmann K, Bengtsson E, Duner P, Nilsson J, Soehnlein O, Fassler R. Plasma fibronectin deficiency impedes atherosclerosis progression and fibrous cap formation. *EMBO Mol Med*. 2012;4:564-576

55. Winn WB, Schmiedl UP, Reichenbach DD, Beach KW, Nghiem H, Dimas C, Daniel E, Maravilla KR, Yuan C. Detection and characterization of atherosclerotic fibrous caps with T2-weighted MR. *AJNR Am J Neuroradiol*. 1998;19:129-134

56. Rudijanto A. The role of vascular smooth muscle cells on the pathogenesis of atherosclerosis. *Acta Med Indones*. 2007;39:86-93

57. Lloyd-Jones D, Adams RJ, Brown TM, Carnethon M, Dai S, De Simone G, Ferguson TB, Ford E, Furie K, Gillespie C, Go A, Greenlund K, Haase N, Hailpern S, Ho PM, Howard V, Kissela B, Kittner S, Lackland D, Lisabeth L, Marelli A, McDermott MM, Meigs J, Mozaffarian D, Mussolino M, Nichol G, Roger VL, Rosamond W, Sacco R, Sorlie P, Stafford R, Thom T, Wasserthiel-Smoller S, Wong ND, Wylie-Rosett J. Executive summary: Heart disease and stroke statistics--2010 update: A report from the American Heart Association. *Circulation*. 2010;121:948-954

58. Kullo IJ, Edwards WD, Schwartz RS. Vulnerable plaque: Pathobiology and clinical implications. *Ann Intern Med*. 1998;129:1050-1060

59. Liang M, Puri A, Devlin G. The vulnerable plaque: The real villain in acute coronary syndromes. *Open cardiovasc med j*. Netherlands; 2011:123-129.

60. Shah PK, Falk E, Badimon JJ, Fernandez-Ortiz A, Mailhac A, Villareal-Levy G, Fallon JT, Regnstrom J, Fuster V. Human monocyte-derived macrophages induce collagen breakdown in fibrous caps of atherosclerotic plaques. Potential role of matrix-degrading metalloproteinases and implications for plaque rupture. *Circulation*. 1995;92:1565-1569

61. Quillard T, Araujo HA, Franck G, Tesmenitsky Y, Libby P. Matrix metalloproteinase-13 predominates over matrix metalloproteinase-8 as the functional interstitial collagenase in mouse atheromata. *Arterioscler Thromb Vasc Biol*. 2014

62. Moreno PR, Bernardi VH, Lopez-Cuellar J, Murcia AM, Palacios IF, Gold HK, Mehran R, Sharma SK, Nemerson Y, Fuster V, Fallon JT. Macrophages, smooth muscle cells, and tissue factor in unstable angina. Implications for cell-mediated thrombogenicity in acute coronary syndromes. *Circulation*. 1996;94:3090-3097

63. Toschi V, Gallo R, Lettino M, Fallon JT, Gertz SD, Fernandez-Ortiz A, Chesebro JH, Badimon L, Nemerson Y, Fuster V, Badimon JJ. Tissue factor modulates the thrombogenicity of human atherosclerotic plaques. *Circulation*. 1997;95:594-599

64. Bhattacharjee G, Ahamed J, Pedersen B, El-Sheikh A, Mackman N, Ruf W, Liu C, Edgington TS. Regulation of tissue factor--mediated initiation of the coagulation cascade by cell surface grp78. *Arterioscler Thromb Vasc Biol*. 2005;25:1737-1743

65. Tajika K, Okamatsu K, Takano M, Inami S, Yamamoto M, Murakami D, Kobayashi N, Ohba T, Hata N, Seino Y, Mizuno K. Malondialdehyde-modified low-density lipoprotein is a useful marker to identify patients with vulnerable plaque. *Circ J*. 2012;76:2211-2217

66. Matsuo Y, Kubo T, Okumoto Y, Ishibashi K, Komukai K, Tanimoto T, Ino Y, Kitabata H, Hirata K, Imanishi T, Akagi H, Akasaka T. Circulating Malondialdehyde-modified low-density lipoprotein levels are associated with the presence of thin-cap fibroatheromas determined by optical coherence tomography in coronary artery disease. *Eur Heart J Cardiovasc Imaging*. 2013;14:43-50

67. Sigala F, Kotsinas A, Savari P, Filis K, Markantonis S, Iliodromitis EK, Gorgoulis VG, Andreadou I. Oxidized LDL in human carotid plaques is related to symptomatic carotid disease and lesion instability. *J Vasc Surg*. 2010;52:704-713

68. Yla-Herttuala S, Bentzon JF, Daemen M, Falk E, Garcia-Garcia HM, Herrmann J, Hoefer I, Jukema JW, Krams R, Kwak BR, Marx N, Naruszewicz M, Newby A, Pasterkamp G, Serruys PW, Waltenberger J, Weber C, Tokgozoglu L. Stabilisation of atherosclerotic plaques. Position paper of the european society of cardiology (ESC) working group on atherosclerosis and vascular biology. *Thromb Haemost*. 2011;106:1-19

69. Hiro T, Fujii T, Yoshitake S, Kawabata T, Yasumoto K, Matsuzaki M. Longitudinal visualization of spontaneous coronary plaque rupture by 3d intravascular ultrasound. *Circulation*. 2000;101:E114-115

70. Bauters C. Silent coronary plaque rupture. *Arch Cardiovasc Dis*. 2008;101:79-80

71. J R. Molecular imaging: Getting closer to the vulnerable plaque? 2010

72. Kim SH, Hong MK, Park DW, Lee SW, Kim YH, Lee CW, Kim JJ, Park SW, Park SJ. Impact of plaque characteristics analyzed by intravascular ultrasound on long-term clinical outcomes. *Am j cardiol*. United States; 2009:1221-1226.

73. Wykrzykowska JJ, Mintz GS, Garcia-Garcia HM, Maehara A, Fahy M, Xu K, Inguez A, Fajadet J, Lansky A, Templin B, Zhang Z, de Bruyne B, Weisz G, Serruys PW, Stone GW. Longitudinal distribution of plaque burden and necrotic core-rich plaques in nonculprit lesions of patients presenting with acute coronary syndromes. *JACC Cardiovasc Imaging*. 2012;5:S10-18

74. Tian J, Ren X, Vergallo R, Xing L, Yu H, Jia H, Soeda T, McNulty I, Hu S, Lee H, Yu B, Jang IK. Distinct morphological features of ruptured culprit plaque for acute coronary events compared to those with silent rupture and thin-cap fibroatheroma: A combined optical coherence tomography and intravascular ultrasound study. *J Am Coll Cardiol*. 2014;63:2209-2216

75. Boyle JJ, Harrington HA, Piper E, Elderfield K, Stark J, Landis RC, Haskard DO. Coronary intraplaque hemorrhage evokes a novel atheroprotective macrophage phenotype. *Am j pathol*. United States; 2009:1097-1108.

76. Hartvigsen K, Chou MY, Hansen LF, Shaw PX, Tsimikas S, Binder CJ, Witztum JL. The role of innate immunity in atherogenesis. *J Lipid Res*. 2009;50 Suppl:S388-393

77. Seimon T, Tabas I. Mechanisms and consequences of macrophage apoptosis in atherosclerosis. *J lipid res*. United States; 2009:S382-387.

78. Lewis MJ, Malik TH, Ehrenstein MR, Boyle JJ, Botto M, Haskard DO. Immunoglobulin M is required for protection against atherosclerosis in low-density lipoprotein receptor–deficient mice. *Circulation*. 2009;120:417-426

79. Binder CJ, Silverman GJ. Natural antibodies and the autoimmunity of atherosclerosis. *Springer Semin Immunopathol*. 2005;26:385-404

80. Horkko S, Bird DA, Miller E, Itabe H, Leitinger N, Subbanagounder G, Berliner JA, Friedman P, Dennis EA, Curtiss LK, Palinski W, Witztum JL. Monoclonal autoantibodies specific for oxidized phospholipids or oxidized phospholipid-protein adducts inhibit macrophage uptake of oxidized low-density lipoproteins. *J Clin Invest*. 1999;103:117-128

81. Monaco C, Crea F, Niccoli G, Summaria F, Cianflone D, Bordone R, Bellomo G, Maseri A. Autoantibodies against oxidized low density lipoproteins in patients with stable angina, unstable angina or peripheral vascular disease; pathophysiological implications. *Eur Heart J*. 2001;22:1572-1577

82. Nilsson J, Nordin Fredrikson G, Schiopu A, Shah PK, Jansson B, Carlsson R. Oxidized LDL antibodies in treatment and risk assessment of atherosclerosis and associated cardiovascular disease. *Curr Pharm Des*. 2007;13:1021-1030

83. Shaw PX, Horkko S, Tsimikas S, Chang MK, Palinski W, Silverman GJ, Chen PP, Witztum JL. Human-derived anti-oxidized LDL autoantibody blocks uptake of oxidized LDL by macrophages and localizes to atherosclerotic lesions in vivo. *Arterioscler Thromb Vasc Biol*. 2001;21:1333-1339

84. Schiopu A, Frendeus B, Jansson B, Soderberg I, Ljungcrantz I, Araya Z, Shah PK, Carlsson R, Nilsson J, Fredrikson GN. Recombinant antibodies to an oxidized low-density lipoprotein epitope induce rapid regression of atherosclerosis in Apobec-1(-/-)/low-density lipoprotein receptor(-/-) mice. *J Am Coll Cardiol*. 2007;50:2313-2318

85. Kelly JA, Griffin ME, Fava RA, Wood SG, Bessette KA, Miller ER, Huber SA, Binder CJ, Witztum JL, Morganelli PM. Inhibition of arterial lesion progression in CD16-deficient mice: Evidence for altered immunity and the role of IL-10. *Cardiovasc Res*. 2010;85:224-231

86. A study to evaluate the safety, tolerability, and activity of intravenous mldl1278a in patients on standard-of-care therapy for stable atherosclerotic cardiovascular disease (GLACIER) - no study results posted - clinicaltrials.Gov. 2012

87. Bioinvent international: Announcement of topline results from the glacier study. https://www.bio.org. 2012

88. Persson M, Engström G, Björkbacka H, Hedblad B. Soluble urokinase plasminogen activator receptor in plasma is associated with incidence of CVD. Results from the malmö diet and cancer study. *Atherosclerosis*. 2012;220:502-505

89. Packard CJ, O'Reilly DS, Caslake MJ, McMahon AD, Ford I, Cooney J, Macphee CH, Suckling KE, Krishna M, Wilkinson FE, Rumley A, Lowe GD. Lipoprotein-associated phospholipase A2 as an independent predictor of coronary heart disease. West of Scotland coronary prevention study group. *N Engl J Med*. 2000;343:1148-1155

90. Ishigaki Y, Oka Y, Katagiri H. Circulating oxidized LDL: A biomarker and a pathogenic factor. *Curr Opin Lipidol*. 2009;20:363-369

91. Rozanski A, Gransar H, Shaw LJ, Kim J, Miranda-Peats L, Wong ND, Rana JS, Orakzai R, Hayes SW, Friedman JD, Thomson LE, Polk D, Min J, Budoff MJ, Berman DS. Impact of coronary artery calcium scanning on coronary risk factors and downstream testing the eisner (early identification of subclinical atherosclerosis by noninvasive imaging research) prospective randomized trial. *J Am Coll Cardiol*. 2011;57:1622-1632

92. Mohlenkamp S, Lehmann N, Moebus S, Schmermund A, Dragano N, Stang A, Siegrist J, Mann K, Jockel KH, Erbel R. Quantification of coronary atherosclerosis and inflammation to predict coronary events and all-cause mortality. *J Am Coll Cardiol*. 2011;57:1455-1464

93. Kaptoge S, Di Angelantonio E, Pennells L, Wood AM, White IR, Gao P, Walker M, Thompson A, Sarwar N, Caslake M, Butterworth AS, Amouyel P, Assmann G, Bakker SJ, Barr EL, Barrett-Connor E, Benjamin EJ, Bjorkelund C, Brenner H, Brunner E, Clarke R, Cooper JA, Cremer P, Cushman M, Dagenais GR, D'Agostino RB, Sr., Dankner R, Davey-Smith G, Deeg D, Dekker JM, Engstrom G, Folsom AR, Fowkes FG, Gallacher J, Gaziano JM, Giampaoli S, Gillum RF, Hofman A, Howard BV, Ingelsson E, Iso H, Jorgensen T, Kiechl S, Kitamura A, Kiyohara Y, Koenig W, Kromhout D, Kuller LH, Lawlor DA, Meade TW, Nissinen A, Nordestgaard BG, Onat A, Panagiotakos DB, Psaty BM, Rodriguez B, Rosengren A, Salomaa V, Kauhanen J, Salonen JT, Shaffer JA, Shea S, Ford I, Stehouwer CD, Strandberg TE, Tipping RW, Tosetto A, Wassertheil-Smoller S, Wennberg P, Westendorp RG, Whincup PH, Wilhelmsen L, Woodward M, Lowe GD, Wareham NJ, Khaw KT, Sattar N, Packard CJ, Gudnason V, Ridker PM, Pepys MB, Thompson SG, Danesh J. C-reactive protein, fibrinogen, and cardiovascular disease prediction. *N Engl J Med*. 2012;367:1310-1320

94. Palinski W, Yla-Herttuala S, Rosenfeld ME, Butler SW, Socher SA, Parthasarathy S, Curtiss LK, Witztum JL. Antisera and monoclonal antibodies specific for epitopes generated during oxidative modification of low density lipoprotein. *Arteriosclerosis*. 1990;10:325-335

95. Tsimikas S, Miller YI. Oxidative modification of lipoproteins: Mechanisms, role in inflammation and. *Curr Pharm Des*. 2011;17:27-37

96. Gounopoulos P, Merki E, Hansen LF, Choi SH, Tsimikas S. Antibodies to oxidized low density lipoprotein: Epidemiological studies and potential clinical applications in cardiovascular disease. *Minerva Cardioangiol*. 2007;55:821-837

97. Tsimikas S, Willeit P, Willeit J, Santer P, Mayr M, Xu Q, Mayr A, Witztum JL, Kiechl S. Oxidation-specific biomarkers, prospective 15-year cardiovascular and stroke outcomes, and net reclassification of cardiovascular events. *J Am Coll Cardiol*. 2012;60:2218-2229

98. Laczik R, Szodoray P, Veres K, Szomjak E, Csipo I, Sipka S, Jr., Shoenfeld Y, Szekanecz Z, Soltesz P. Assessment of IgG antibodies to oxidized LDL in patients with acute coronary syndrome. *Lupus*. 2011;20:730-735

99. Tsimikas S, Bergmark C, Beyer RW, Patel R, Pattison J, Miller E, Juliano J, Witztum JL. Temporal increases in plasma markers of oxidized low-density lipoprotein strongly reflect the presence of acute coronary syndromes. *J Am Coll Cardiol*. 2003;41:360-370

100. Che J, Li G, Wang W, Li Q, Liu H, Chen K, Liu T. Serum autoantibodies against human oxidized low-density lipoproteins are inversely associated with severity of coronary stenotic lesions calculated by Gensini score. *Cardiol J*. 2011;18:364-370

101. Ravandi A, Boekholdt SM, Mallat Z, Talmud PJ, Kastelein JJ, Wareham NJ, Miller ER, Benessiano J, Tedgui A, Witztum JL, Khaw KT, Tsimikas S. Relationship of IgG and IgM autoantibodies and immune complexes to oxidized LDL with markers of oxidation and inflammation and cardiovascular events: Results from the EPIC-Norfolk study. *J Lipid Res*. 2011;52:1829-1836

102. Tsimikas S, Miyanohara A, Hartvigsen K, Merki E, Shaw PX, Chou MY, Pattison J, Torzewski M, Sollors J, Friedmann T, Lai NC, Hammond HK, Getz GS, Reardon CA, Li AC, Banka CL, Witztum JL. Human oxidation-specific antibodies reduce foam cell formation and atherosclerosis progression. *J Am Coll Cardiol*. 2011;58:1715-1727

103. Leibundgut G, Witztum JL, Tsimikas S. Oxidation-specific epitopes and immunological responses: Translational biotheranostic implications for atherosclerosis. *Curr Opin Pharmacol*. 2013

104. Garrido-Sanchez L, Chinchurreta P, Garcia-Fuentes E, Mora M, Tinahones FJ. A higher level of IgM anti-oxidized LDL antibodies is associated with a lower severity of coronary atherosclerosis in patients on statins. *Int J Cardiol*. 2010;145:263-264

105. Chen Q, Reis SE, Kammerer C, Craig W, McNamara DM, Holubkov R, Sharaf BL, Sopko G, Pauly DF, Merz CN, Kamboh MI. Association of anti-oxidized LDL and candidate genes with severity of coronary stenosis in the women's ischemia syndrome evaluation study. *J Lipid Res*. 2011;52:801-807

106. Tsimikas S, Lau HK, Han KR, Shortal B, Miller ER, Segev A, Curtiss LK, Witztum JL, Strauss BH. Percutaneous coronary intervention results in acute increases in oxidized phospholipids and lipoprotein(a): Short-term and long-term immunologic responses to oxidized low-density lipoprotein. *Circulation*. 2004;109:3164-3170

107. Fefer P, Tsimikas S, Segev A, Sparkes J, Otsuma F, Kolodgie F, Virmani R, Juliano J, Charron T, Strauss BH. The role of oxidized phospholipids, lipoprotein (a) and biomarkers of oxidized lipoproteins in chronically occluded coronary arteries in sudden cardiac death and following successful percutaneous revascularization. *Cardiovasc Revasc Med*. 2012;13:11-19

108. Holvoet P, Mertens A, Verhamme P, Bogaerts K, Beyens G, Verhaeghe R, Collen D, Muls E, Van de Werf F. Circulating oxidized LDL is a useful marker for identifying patients with coronary artery disease. *Arterioscler Thromb Vasc Biol*. 2001;21:844-848

109. Toshima S, Hasegawa A, Kurabayashi M, Itabe H, Takano T, Sugano J, Shimamura K, Kimura J, Michishita I, Suzuki T, Nagai R. Circulating oxidized low density lipoprotein levels. A biochemical risk marker for coronary heart disease. *Arterioscler Thromb Vasc Biol*. 2000;20:2243-2247

110. Fraley AE, Tsimikas S. Clinical applications of circulating oxidized low-density lipoprotein biomarkers in cardiovascular disease. *Curr Opin Lipidol*. 2006;17:502-509

111. Wu T, Willett WC, Rifai N, Shai I, Manson JE, Rimm EB. Is plasma oxidized low-density lipoprotein, measured with the widely used antibody 4E6, an independent predictor of coronary heart disease among u.S. Men and women? *J Am Coll Cardiol*. 2006;48:973-979

112. Holvoet P, Vanhaecke J, Janssens S, Van de Werf F, Collen D. Oxidized LDL and malondialdehyde-modified LDL in patients with acute coronary syndromes and stable coronary artery disease. *Circulation*. 1998;98:1487-1494

113. Holvoet P, Macy E, Landeloos M, Jones D, Jenny NS, Van de Werf F, Tracy RP. Analytical performance and diagnostic accuracy of immunometric assays for the measurement of circulating oxidized LDL. *Clin Chem*. 2006;52:760-764

114. Garcia-Garcia HM, Klauss V, Gonzalo N, Garg S, Onuma Y, Hamm CW, Wijns W, Shannon J, Serruys PW. Relationship between cardiovascular risk factors and biomarkers with necrotic core and atheroma size: A serial intravascular ultrasound radiofrequency data analysis. *Int J Cardiovasc Imaging*. 2011

115. Serruys PW, Garcia-Garcia HM, Buszman P, Erne P, Verheye S, Aschermann M, Duckers H, Bleie O, Dudek D, Botker HE, von Birgelen C, D'Amico D, Hutchinson T, Zambanini A, Mastik F, van Es GA, van der Steen AF, Vince DG, Ganz P, Hamm CW, Wijns W, Zalewski A. Effects of the direct lipoprotein-associated phospholipase A(2) inhibitor Darapladib on human coronary atherosclerotic plaque. *Circulation*. 2008;118:1172-1182

116. Lindsay AC, Viceconte N, Di Mario C. Optical Coherence Tomography: Has its time come? *Heart*. 2011;97:1361-1362

117. Berman DS, Shaw LJ, Hachamovitch R, Friedman JD, Polk DM, Hayes SW, Thomson LE, Germano G, Wong ND, Kang X, Rozanski A. Comparative use of radionuclide stress testing, coronary artery calcium scanning, and noninvasive coronary angiography for diagnostic and prognostic cardiac assessment. *Semin Nucl Med*. 2007;37:2-16

118. Greenland P, Bonow RO, Brundage BH, Budoff MJ, Eisenberg MJ, Grundy SM, Lauer MS, Post WS, Raggi P, Redberg RF, Rodgers GP, Shaw LJ, Taylor AJ, Weintraub WS. Accf/aha 2007 clinical expert consensus document on coronary artery calcium scoring by computed tomography in global cardiovascular risk assessment and in evaluation of patients with chest pain: A report of the American College of Cardiology Foundation clinical expert consensus task force (accf/aha writing committee to update the 2000 expert consensus document on electron beam computed tomography) developed in collaboration with the society of atherosclerosis imaging and prevention and the society of cardiovascular computed tomography. *J Am Coll Cardiol*. 2007;49:378-402

119. Diletti R, Garcia-Garcia HM, Gomez-Lara J, Brugaletta S, Wykrzykowska JJ, van Ditzhuijzen N, van Geuns RJ, Regar E, Ambrosio G, Serruys PW. Assessment of coronary atherosclerosis progression and regression at bifurcations using combined IVUS and OCT. *JACC Cardiovasc Imaging*. 2011;4:774-780

120. Thim T, Hagensen MK, Wallace-Bradley D, Granada JF, Kaluza GL, Drouet L, Paaske WP, Botker HE, Falk E. Unreliable assessment of necrotic core by virtual histology intravascular ultrasound in porcine coronary artery disease. *Circ cardiovasc imaging*. United States; 2010:384-391.

121. Hetterich H, Redel T, Lauritsch G, Rohkohl C, Rieber J. New X-ray imaging modalities and their integration with intravascular imaging and interventions. *Int J Cardiovasc Imaging*. 2010;26:797-808

122. Garg S, Serruys PW, van der Ent M, Schultz C, Mastik F, van Soest G, van der Steen AF, Wilder MA, Muller JE, Regar E. First use in patients of a combined near infra-red spectroscopy and intra-vascular ultrasound catheter to identify composition and structure of coronary plaque. *EuroIntervention*. 2010;5:755-756

123. Kini AS, Baber U, Kovacic JC, Limaye A, Ali ZA, Sweeny J, Maehara A, Mehran R, Dangas G, Mintz GS, Fuster V, Narula J, Sharma SK, Moreno PR. Changes in plaque lipid content after short-term intensive versus standard statin therapy: The YELLOW trial (reduction in yellow plaque by aggressive lipid-lowering therapy). *J Am Coll Cardiol*. 2013;62:21-29

124. Brugaletta S, Garcia-Garcia HM, Serruys PW, de Boer S, Ligthart J, Gomez-Lara J, Witberg K, Diletti R, Wykrzykowska J, van Geuns RJ, Schultz C, Regar E, Duckers HJ, van Mieghem N, de Jaegere P, Madden SP, Muller JE, van der Steen AF, van der Giessen WJ, Boersma E. NIRS and IVUS for characterization of atherosclerosis in patients undergoing coronary angiography. *JACC Cardiovasc Imaging*. 2011;4:647-655

125. Madder RD, Goldstein JA, Madden SP, Puri R, Wolski K, Hendricks M, Sum ST, Kini A, Sharma S, Rizik D, Brilakis ES, Shunk KA, Petersen J, Weisz G, Virmani R, Nicholls SJ, Maehara A, Mintz GS, Stone GW, Muller JE. Detection by near-infrared spectroscopy of large lipid core plaques at culprit sites in patients with acute st-segment elevation myocardial infarction. *JACC Cardiovasc Interv*. 2013;6:838-846

126. Fayad ZA. Cardiovascular molecular imaging. *Arterioscler Thromb Vasc Biol*. 2009;29:981-982

127. Gibbons RJ, Araoz PA, Williamson EE. The year in cardiac imaging. *J Am Coll Cardiol*. United States; 2011:1721-1734.

128. Mankoff DA. A definition of molecular imaging. *J Nucl Med*. 2007;48:18N, 21N

129. Sinusas AJ, Bengel F, Nahrendorf M, Epstein FH, Wu JC, Villanueva FS, Fayad ZA, Gropler RJ. Multimodality cardiovascular molecular imaging, part i. *Circ cardiovasc imaging*. United States; 2008:244-256.

130. Curillova Z, Yaman BF, Dorbala S, Kwong RY, Sitek A, El Fakhri G, Anagnostopoulos C, Di Carli MF. Quantitative relationship between coronary calcium content and coronary flow reserve as assessed by integrated PET/CT imaging. *Eur J Nucl Med Mol Imaging*. 2009

131. Davies JR, Izquierdo-Garcia D, Rudd JH, Figg N, Richards HK, Bird JL, Aigbirhio FI, Davenport AP, Weissberg PL, Fryer TD, Warburton EA. FDG-PET can distinguish inflamed from non-inflamed plaque in an animal model of atherosclerosis. *Int J Cardiovasc Imaging*. 2009

132. Einstein AJ, Moser KW, Thompson RC, Cerqueira MD, Henzlova MJ. Radiation dose to patients from cardiac diagnostic imaging. *Circulation*. 2007;116:1290-1305

133. Yoshinaga K, Katoh C, Manabe O, Klein R, Naya M, Sakakibara M, Yamada S, Dekemp RA, Tsutsui H, Tamaki N. Incremental diagnostic value of regional myocardial blood flow

quantification over relative perfusion imaging with generator-produced Rubidium-82 PET. *Circ j*. 2011.

134. Cool SK, Breyne K, Meyer E, De Smedt SC, Sanders NN. Comparison of in vivo optical systems for bioluminescence and fluorescence imaging. *J Fluoresc*. 2013;23:909-920

135. Calfon MA, Rosenthal A, Mallas G, Mauskapf A, Nudelman RN, Ntziachristos V, Jaffer FA. *In vivo* near infrared fluorescence (NIRF) intravascular molecular imaging of inflammatory plaque, a multimodal approach to imaging of atherosclerosis. *J Vis Exp*. 2011

136. Jaffer FA, Calfon MA, Rosenthal A, Mallas G, Razansky RN, Mauskapf A, Weissleder R, Libby P, Ntziachristos V. Two-dimensional intravascular near-infrared fluorescence molecular imaging of inflammation in atherosclerosis and stent-induced vascular injury. *J Am Coll Cardiol*. 2011;57:2516-2526

137. Yoo H, Kim JW, Shishkov M, Namati E, Morse T, Shubochkin R, McCarthy JR, Ntziachristos V, Bouma BE, Jaffer FA, Tearney GJ. Intra-arterial catheter for simultaneous microstructural and molecular imaging in vivo. *Nat Med*. 2011;17:1680-1684

138. Lee S, Lee MW, Cho HS, Song JW, Nam HS, Oh DJ, Park K, Oh WY, Yoo H, Kim JW. Fully integrated high-speed intravascular optical coherence tomography/near-infrared fluorescence structural/molecular imaging in vivo using a clinically available near-infrared fluorescence-emitting indocyanine green to detect inflamed lipid-rich atheromata in coronary-sized vessels. *Circ Cardiovasc Interv*. 2014

139. Osborn EA, Jaffer FA. The advancing clinical impact of molecular imaging in CVD *JACC Cardiovasc Imaging*. 2013;6:1327-1341

140. Hartung D, Petrov A, Haider N, Fujimoto S, Blankenberg F, Fujimoto A, Virmani R, Kolodgie FD, Strauss HW, Narula J. Radiolabeled monocyte chemotactic protein 1 for the detection of inflammation in experimental atherosclerosis. *J Nucl Med*. 2007;48:1816-1821

141. Hyafil F, Cornily JC, Rudd JH, Machac J, Feldman LJ, Fayad ZA. Quantification of inflammation within rabbit atherosclerotic plaques using the macrophage-specific CT contrast agent n1177: A comparison with 18f-FDG PET/CT and histology. *J Nucl Med*. 2009;50:959-965

142. Menezes LJ, Kayani I, Ben-Haim S, Hutton B, Ell PJ, Groves AM. What is the natural history of 18f-FDG uptake in arterial atheroma on PET/CT? Implications for imaging the vulnerable plaque. *Atherosclerosis*. Ireland: 2010 Elsevier Ireland Ltd; 2010:136-140.

143. Jamar F, Houssiau FA, Devogelaer JP, Chapman PT, Haskard DO, Beaujean V, Beckers C, Manicourt DH, Peters AM. Scintigraphy using a Technetium 99m-labelled anti-e-selectin fab fragment in rheumatoid arthritis. *Rheumatology (Oxford)*. 2002;41:53-61

144. Gompels LL, Madden L, Lim NH, Inglis JJ, McConnell E, Vincent TL, Haskard DO, Paleolog EM. In vivo fluorescence imaging of E-Selectin: Quantitative detection of endothelial activation in a mouse model of arthritis. *Arthritis Rheum*. 2011;63:107-117

145. Hua J, Dobrucki LW, Sadeghi MM, Zhang J, Bourke BN, Cavaliere P, Song J, Chow C, Jahanshad N, van Royen N, Buschmann I, Madri JA, Mendizabal M, Sinusas AJ. Noninvasive

imaging of angiogenesis with a 99mtc-labeled peptide targeted at alphavbeta3 integrin after murine hindlimb ischemia. *Circulation*. 2005;111:3255-3260

146. Nahrendorf M, Keliher E, Panizzi P, Zhang H, Hembrador S, Figueiredo JL, Aikawa E, Kelly K, Libby P, Weissleder R. 18f-4v for PET-CT imaging of VCAM-1 expression in atherosclerosis. *JACC Cardiovasc Imaging*. 2009;2:1213-1222

147. Ishino S, Mukai T, Kuge Y, Kume N, Ogawa M, Takai N, Kamihashi J, Shiomi M, Minami M, Kita T, Saji H. Targeting of lectinlike oxidized low-density lipoprotein receptor 1 (LOX-1) with 99mtc-labeled anti-LOX-1 antibody: Potential agent for imaging of vulnerable plaque. *J nucl med*. United States; 2008:1677-1685.

148. Li D, Patel AR, Klibanov AL, Kramer CM, Ruiz M, Kang BY, Mehta JL, Beller GA, Glover DK, Meyer CH. Molecular imaging of atherosclerotic plaques targeted to oxidized LDL receptor LOX-1 by SPECT/CT and magnetic resonance. *Circ cardiovasc imaging*. United States; 2010:464-472.

149. Temma T, Ogawa Y, Kuge Y, Ishino S, Takai N, Nishigori K, Shiomi M, Ono M, Saji H. Tissue factor detection for selectively discriminating unstable plaques in an atherosclerotic rabbit model. *J nucl med*. United States; 2010:1979-1986.

150. Subramanian S, Jaffer FA, Tawakol A. Optical molecular imaging in atherosclerosis. *J Nucl Cardiol*. 2010;17:135-144

151. Deguchi JO, Aikawa M, Tung CH, Aikawa E, Kim DE, Ntziachristos V, Weissleder R, Libby P. Inflammation in atherosclerosis: Visualizing matrix metalloproteinase action in macrophages in vivo. *Circulation*. 2006;114:55-62

152. Lin SA, Patel M, Suresch D, Connolly B, Bao B, Groves K, Rajopadhye M, Peterson JD, Klimas M, Sur C, Bednar B. Quantitative longitudinal imaging of vascular inflammation and treatment by ezetimibe in apoe mice by FMT using new optical imaging biomarkers of cathepsin activity and alpha(v)beta(3) integrin. *Int J Mol Imaging*. 2012;2012:189254

153. Duivenvoorden R, Tang J, Cormode DP, Mieszawska AJ, Izquierdo-Garcia D, Ozcan C, Otten MJ, Zaidi N, Lobatto ME, van Rijs SM, Priem B, Kuan EL, Martel C, Hewing B, Sager H, Nahrendorf M, Randolph GJ, Stroes ES, Fuster V, Fisher EA, Fayad ZA, Mulder WJ. A statin-loaded reconstituted high-density lipoprotein nanoparticle inhibits atherosclerotic plaque inflammation. *Nat Commun*. 2014;5:3065

154. Nahrendorf M, Waterman P, Thurber G, Groves K, Rajopadhye M, Panizzi P, Marinelli B, Aikawa E, Pittet MJ, Swirski FK, Weissleder R. Hybrid in vivo FMT-CT imaging of protease activity in atherosclerosis with customized nanosensors. *Arterioscler Thromb Vasc Biol*. 2009;29:1444-1451

155. Vinegoni C, Botnaru I, Aikawa E, Calfon MA, Iwamoto Y, Folco EJ, Ntziachristos V, Weissleder R, Libby P, Jaffer FA. Indocyanine Green enables near-infrared fluorescence imaging of lipid-rich, inflamed atherosclerotic plaques. *Sci Transl Med*. 2011;3:84ra45

156. Lu T, Wen S, Cui Y, Ju SH, Li KC, Teng GJ. Near-infrared fluorescence imaging of murine atherosclerosis using an oxidized low density lipoprotein-targeted fluorochrome. *Int J Cardiovasc Imaging*. 2014;30:221-231

157. Tsimikas S, Shortal BP, Witztum JL, Palinski W. In vivo uptake of radiolabeled MDA2, an oxidation-specific monoclonal antibody, provides an accurate measure of atherosclerotic lesions rich in oxidized LDL and is highly sensitive to their regression. *Arterioscler Thromb Vasc Biol*. 2000;20:689-697

158. Torzewski M, Shaw PX, Han KR, Shortal B, Lackner KJ, Witztum JL, Palinski W, Tsimikas S. Reduced in vivo aortic uptake of radiolabeled oxidation-specific antibodies reflects changes in plaque composition consistent with plaque stabilization. *Arterioscler thromb vasc biol*. United States; 2004:2307-2312.

159. Briley-Saebo KC, Shaw PX, Mulder WJ, Choi SH, Vucic E, Aguinaldo JG, Witztum JL, Fuster V, Tsimikas S, Fayad ZA. Targeted molecular probes for imaging atherosclerotic lesions with magnetic resonance using antibodies that recognize oxidation-specific epitopes. *Circulation*. United States; 2008:3206-3215.

160. Lepin EJ, Leyton JV, Zhou Y, Olafsen T, Salazar FB, McCabe KE, Hahm S, Marks JD, Reiter RE, Wu AM. An affinity matured minibody for PET imaging of prostate stem cell antigen (PSCA)-expressing tumors. *Eur J Nucl Med Mol Imaging*. 2010;37:1529-1538

161. Olafsen T, Sirk SJ, Betting DJ, Kenanova VE, Bauer KB, Ladno W, Raubitschek AA, Timmerman JM, Wu AM. Immunopet imaging of B-cell lymphoma using 124i-anti-cd20 ScFv dimers (Diabodies). *Protein eng des sel*. England; 2010:243-249.

162. Boyle JJ, Christou I, Iqbal MB, Nguyen AT, Leung VW, Evans PC, Liu Y, Johns M, Kirkham P, Haskard DO. Solid-phase immunoglobulins IgG and IgM activate macrophages with solid-phase IgM acting via a novel scavenger receptor a pathway. *Am J Pathol*. 2012;181:347-361

163. Rozenberg I, Sluka SH, Rohrer L, Hofmann J, Becher B, Akhmedov A, Soliz J, Mocharla P, Boren J, Johansen P, Steffel J, Watanabe T, Luscher TF, Tanner FC. Histamine H1 receptor promotes atherosclerotic lesion formation by increasing vascular permeability for low-density lipoproteins. *Arterioscler thromb vasc biol*. United States; 2010:923-930.

164. Tortorella S, Karagiannis TC. The significance of transferrin receptors in oncology: The development of functional nano-based drug delivery systems. *Curr Drug Deliv*. 2014

165. Girgis MD, Federman N, Rochefort MM, McCabe KE, Wu AM, Nagy JO, Denny C, Tomlinson JS. An engineered anti-ca19-9 cys-diabody for positron emission tomography imaging of pancreatic cancer and targeting of polymerized liposomal nanoparticles. *J Surg Res*. 2013;185:45-55

166. Chang SH, Johns M, Boyle JJ, McConnell E, Kirkham PA, Bicknell C, Zahoor-ul-Hassan Dogar M, Edwards RJ, Gale-Grant O, Khamis R, Ramkhelawon KV, Haskard DO. Model IgG monoclonal autoantibody-anti-idiotype pair for dissecting the humoral immune response to oxidized low density lipoprotein. *Hybridoma*. 2012;31:87-98

167. Sever P, Dahlof B, Poulter N, Wedel H, Beevers G, Caulfield M, Collins R, Kjeldsen S, Kristinsson A, McInnes G, Mehlsen J, Nieminem M, O'Brien E, Ostergren J. Potential synergy between lipid-lowering and blood-pressure-lowering in the Anglo-Scandinavian Cardiac Outcomes Trial. *Eur Heart J*. 2006;27:2982-2988

168. Sever PS, Dahlöf B, Poulter NR, Wedel H, Beevers G, Caulfield M, Collins R, Kjeldsen SE, Kristinsson A, McInnes GT, Mehlsen J, Nieminen M, O'Brien E, Ostergren J, investigators A. Prevention of coronary and stroke events with atorvastatin in hypertensive patients who have average or lower-than-average cholesterol concentrations, in the Anglo-Scandinavian Cardiac Outcomes Trial--lipid lowering arm (ASCOT-LLA): A multicentre randomised controlled trial. *Lancet*. 2003;361:1149-1158

169. Dahlof B, Sever PS, Poulter NR, Wedel H, Beevers DG, Caulfield M, Collins R, Kjeldsen SE, Kristinsson A, McInnes GT, Mehlsen J, Nieminen M, O'Brien E, Ostergren J. Prevention of cardiovascular events with an antihypertensive regimen of amlodipine adding perindopril as required versus atenolol adding bendroflumethiazide as required, in the Anglo-Scandinavian Cardiac Outcomes Trial-blood pressure lowering arm (ASCOT-BPLA): A multicentre randomised controlled trial. *Lancet*. 2005;366:895-906

170. Sever PS, Dahlof B, Poulter NR, Wedel H, Beevers G, Caulfield M, Collins R, Kjeldsen SE, McInnes GT, Mehlsen J, Nieminen M, O'Brien E, Ostergren J. Rationale, design, methods and baseline demography of participants of the Anglo-Scandinavian Cardiac Outcomes Trial. ASCOT investigators. *J Hypertens*. 2001;19:1139-1147

171. Sever PS, Poulter NR, Chang CL, Hingorani A, Thom SA, Hughes AD, Welsh P, Sattar N. Evaluation of C-reactive protein prior to and on-treatment as a predictor of benefit from atorvastatin: Observations from the Anglo-Scandinavian Cardiac Outcomes Trial. *Eur Heart J*. 2012;33:486-494

172. Tapp RJ, Sharp A, Stanton AV, O'Brien E, Chaturvedi N, Poulter NR, Sever PS, Thom SA, Hughes AD, Mayet J. Differential effects of antihypertensive treatment on left ventricular diastolic function: An ASCOT(Anglo-Scandinavian Cardiac Outcomes Trial) substudy. *J Am Coll Cardiol*. 2010;55:1875-1881

173. Tsimikas S, Witztum JL, Miller ER, Sasiela WJ, Szarek M, Olsson AG, Schwartz GG. High-dose atorvastatin reduces total plasma levels of oxidized phospholipids and immune complexes present on apolipoprotein b-100 in patients with acute coronary syndromes in the MIRACL trial. *Circulation*. 2004;110:1406-1412

174. Newson RB. Comparing the predictive powers of survival models using Harrell's c or Somers' d. *Stata Journal*. 2010;10:339-358

175. Pencina MJ, Steyerberg EW, D'Agostino RB. Extensions of net reclassification improvement calculations to measure usefulness of new biomarkers. *Stat Med*. 2011;30:11-21

176. Pencina MJ, D'Agostino RB, Sr., D'Agostino RB, Jr., Vasan RS. Evaluating the added predictive ability of a new marker: From area under the ROC curve to reclassification and beyond. *Stat Med*. 2008;27:157-172; discussion 207-112

177. Jones ST, Bendig MM. Rapid PCR-cloning of full-length mouse immunoglobulin variable regions. *Biotechnology (N Y)*. 1991;9:88-89

178. Kettleborough CA, Saldanha J, Ansell KH, Bendig MM. Optimization of primers for cloning libraries of mouse immunoglobulin genes using the polymerase chain reaction. *Eur J Immunol*. 1993;23:206-211

179. Lefranc MP, Giudicelli V, Ginestoux C, Jabado-Michaloud J, Folch G, Bellahcene F, Wu Y, Gemrot E, Brochet X, Lane J, Regnier L, Ehrenmann F, Lefranc G, Duroux P. Imgt, the international immunogenetics information system. *Nucleic Acids Res*. 2009;37:D1006-1012

180. Verhoeven BA, Velema E, Schoneveld AH, de Vries JPP, de Bruin P, Seldenrijk CA, de Kleijn DP, Busser E, Van der Graaf Y, Mol F. Athero-express: Differential atherosclerotic plaque expression of mRNA and protein in relation to cardiovascular events and patient characteristics. Rationale and design. *European journal of epidemiology*. 2004;19:1127-1133

181. Peters SA, Ruijter HM, Bots ML, Moons KG. Improvements in risk stratification for the occurrence of cardiovascular disease by imaging subclinical atherosclerosis: A systematic review. *Heart*. 2011

182. Hoff HF, O'Neil J. Lesion-derived low density lipoprotein and oxidized low density lipoprotein share a lability for aggregation, leading to enhanced macrophage degradation. *Arterioscler Thromb*. 1991;11:1209-1222

183. Palinski W, Horkko S, Miller E, Steinbrecher UP, Powell HC, Curtiss LK, Witztum JL. Cloning of monoclonal autoantibodies to epitopes of oxidized lipoproteins from apolipoprotein E-deficient mice. Demonstration of epitopes of oxidized low density lipoprotein in human plasma. *J Clin Invest*. 1996;98:800-814

184. Tsiantoulas D, Diehl CJ, Witztum JL, Binder CJ. B cells and humoral immunity in atherosclerosis. *Circ Res*. 2014;114:1743-1756

185. Horkko S, Binder CJ, Shaw PX, Chang MK, Silverman G, Palinski W, Witztum JL. Immunological responses to oxidized LDL. *Free Radic Biol Med*. 2000;28:1771-1779

186. Lopes-Virella MF, Hunt KJ, Baker NL, Virella G, Moritz T. The levels of MDA-LDL in circulating immune complexes predict myocardial infarction in the VADT study. *Atherosclerosis*. 2012;224:526-531

187. Freire de Carvalho J, Sherer Y, Shoenfeld Y. The fine-tuning of anti-oxidized low-density lipoprotein antibodies in cardiovascular disease and thrombosis. *Thromb Haemost*. 2007;98:1157-1159

188. Caidahl K, Hartford M, Karlsson T, Herlitz J, Pettersson K, de Faire U, Frostegard J. IgM - Phosphorylcholine autoantibodies and outcome in acute coronary syndromes. *Int j cardiol*. 2012. Published by Elsevier Ireland Ltd.; 2012.

189. Maiolino G, Pedon L, Cesari M, Frigo AC, Barisa M, Rossitto G, Seccia TM, Zanchetta M, Rossi GP. Antibodies to Malondialdehyde oxidized low-density lipoproteins predict long term cardiovascular mortality in high risk patients. *Int J Cardiol*. 2013;168:484-489

190. Wu R, Shen G, Morris R, Patnaik M, Peter JB. Elevated autoantibodies against oxidized palmitoyl arachidonoyl phosphocholine in patients with hypertension and myocardial infarction. *Journal of Autoimmunity*. 2005;24:353-360

191. Freijd A, Jonsson A, Rynnel-Dagoo B. Age-dependent IgG subclass distribution of phosphocholine antibodies in humans. *APMIS*. 1988;96:901-905

192. Harris SL, Park MK, Nahm MH, Diamond B. Peptide mimic of phosphorylcholine, a dominant epitope found on Streptococcus Pneumoniae. *Infect Immun*. 2000;68:5778-5784

193. Wiens GD, Brown M, Rittenberg MB. Repertoire shift in the humoral response to Phosphocholine-keyhole limpet hemocyanin: VH somatic mutation in germinal center B cells impairs T15 IG function. *J Immunol*. 2003;170:5095-5102

194. Brown M, Schumacher MA, Wiens GD, Brennan RG, Rittenberg MB. The structural basis of repertoire shift in an immune response to phosphocholine. *J Exp Med*. 2000;191:2101-2112

195. Fraley AE, Schwartz GG, Olsson AG, Kinlay S, Szarek M, Rifai N, Libby P, Ganz P, Witztum JL, Tsimikas S. Relationship of oxidized phospholipids and biomarkers of oxidized low-density lipoprotein with cardiovascular risk factors, inflammatory biomarkers, and effect of statin therapy in patients with acute coronary syndromes: Results from the MIRACL (myocardial ischemia reduction with aggressive cholesterol lowering) trial. *Journal of the American College of Cardiology*. 2009;53:2186-2196

196. van de Vijver LP, Steyger R, van Poppel G, Boer JM, Kruijssen DA, Seidell JC, Princen HM. Autoantibodies against MDA-LDL in subjects with severe and minor atherosclerosis and healthy population controls. *Atherosclerosis*. 1996;122:245-253

197. Slot MC, Theunissen R, van Paassen P, Damoiseaux J, Cohen Tervaert JW. Anti-oxidized low-density lipoprotein antibodies in myeloperoxidase-positive vasculitis patients preferentially recognize hypochlorite-modified low density lipoproteins. *Clin Exp Immunol*. 2007;149:257-264

198. Sever PS, Chang CL, Gupta AK, Whitehouse A, Poulter NR. The Anglo-Scandinavian Cardiac Outcomes Trial: 11-year mortality follow-up of the lipid-lowering arm in the U.K. *Eur Heart J*. 2011;32:2525-2532

199. Arsenault BJ, Barter P, DeMicco DA, Bao W, Preston GM, LaRosa JC, Grundy SM, Deedwania P, Greten H, Wenger NK, Shepherd J, Waters DD, Kastelein JJ. Prediction of cardiovascular events in statin-treated stable coronary patients by lipid and nonlipid biomarkers. *J Am Coll Cardiol*. 2011;57:63-69

200. Ky B, Burke A, Tsimikas S, Wolfe ML, Tadesse MG, Szapary PO, Witztum JL, FitzGerald GA, Rader DJ. The influence of Pravastatin and atorvastatin on markers of oxidative stress in hypercholesterolemic humans. *J Am Coll Cardiol.* 2008;51:1653-1662

201. Paavola T, Kangas-Kontio T, Salonurmi T, Kuusisto S, Huusko T, Savolainen MJ, Kakko S. Plasma levels of antibodies against oxidized LDL are inherited but not associated with HDL cholesterol level in families with early coronary heart disease. *Atherosclerosis*. 2012;224:123-128

202. Schiopu A, Bengtsson J, Soderberg I, Janciauskiene S, Lindgren S, Ares MP, Shah PK, Carlsson R, Nilsson J, Fredrikson GN. Recombinant human antibodies against aldehyde-modified Apolipoprotein B-100 peptide sequences inhibit atherosclerosis. *Circulation*. 2004;110:2047-2052

203. Virella G, Koskinen S, Krings G, Onorato JM, Thorpe SR, Lopes-Virella M. Immunochemical characterization of purified human oxidized low-density lipoprotein antibodies. *Clin Immunol*. 2000;95:135-144

204. Fernandez-Berges D, Consuegra-Sanchez L, Penafiel J, Cabrera de Leon A, Vila J, Felix-Redondo FJ, Segura-Fragoso A, Lapetra J, Guembe MJ, Vega T, Fito M, Elosua R, Diaz O, Marrugat J. Metabolic and inflammatory profiles of biomarkers in obesity, metabolic syndrome, and diabetes in a Mediterranean population. Darios inflammatory study. *Rev Esp Cardiol (Engl Ed)*. 2014;67:624-631

205. Ueba T, Nomura S, Nishikawa T, Kajiwara M, Yamashita K. Circulating oxidized LDL, measured with FOH1a/DLH3 antibody, is associated with metabolic syndrome and the coronary heart disease risk score in healthy japanese. *Atherosclerosis*. Ireland; 2009:243-248.

206. Davidson MH, Ballantyne CM, Jacobson TA, Bittner VA, Braun LT, Brown AS, Brown WV, Cromwell WC, Goldberg RB, McKenney JM, Remaley AT, Sniderman AD, Toth PP, Tsimikas S, Ziajka PE, Maki KC, Dicklin MR. Clinical utility of inflammatory markers and advanced lipoprotein testing: Advice from an expert panel of lipid specialists. *J Clin Lipidol*. 2011;5:338-367

207. den Dekker WK, Tempel D, Bot I, Biessen EA, Joosten LA, Netea MG, van der Meer JW, Cheng C, Duckers HJ. Mast cells induce vascular smooth muscle cell apoptosis via a toll-like receptor 4 activation pathway. *Arterioscler Thromb Vasc Biol*. 2012;32:1960-1969

208. Chatzizisis YS, Coskun AU, Jonas M, Edelman ER, Feldman CL, Stone PH. Role of endothelial shear stress in the natural history of coronary atherosclerosis and vascular remodeling: Molecular, cellular, and vascular behavior. *J Am Coll Cardiol*. 2007;49:2379-2393

209. Jaffer FA, Libby P, Weissleder R. Optical and multimodality molecular imaging: Insights into atherosclerosis. *Arterioscler Thromb Vasc Biol*. 2009;29:1017-1024

210. Serruys PW, Onuma Y, Dudek D, Smits PC, Koolen J, Chevalier B, de Bruyne B, Thuesen L, McClean D, van Geuns RJ, Windecker S, Whitbourn R, Meredith I, Dorange C, Veldhof S, Hebert KM, Sudhir K, Garcia-Garcia HM, Ormiston JA. Evaluation of the second generation of a bioresorbable everolimus-eluting vascular scaffold for the treatment of de novo coronary artery stenosis: 12-month clinical and imaging outcomes. *J Am Coll Cardiol*. 2011;58:1578-1588

211. Stone PH, Coskun AU, Yeghiazarians Y, Kinlay S, Popma JJ, Kuntz RE, Feldman CL. Prediction of sites of coronary atherosclerosis progression: In vivo profiling of endothelial shear stress, lumen, and outer vessel wall characteristics to predict vascular behavior. *Curr Opin Cardiol*. 2003;18:458-470

212. Dietzel F, Boettger MK, Dahlke K, Holzer J, Lehmann F, Gajda M, Brauer R, Schaible HG, Kaiser WA, Hilger I. Assessment of rat antigen-induced arthritis and its suppression during glucocorticoid therapy by use of hemicyanine dye probes with different molecular weight in near-infrared fluorescence optical imaging. *Invest Radiol*. 2013;48:729-737

213. Quillard T, Libby P. Molecular imaging of atherosclerosis for improving diagnostic and therapeutic development. *Circ Res*. 2012;111:231-244

214. Waschkau B, Faust A, Schafers M, Bremer C. Performance of a new fluorescence-labeled MMP inhibitor to image tumor MMP activity in vivo in comparison to an MMP-activatable probe. *Contrast Media Mol Imaging*. 2013;8:1-11

215. Razansky D, Harlaar NJ, Hillebrands JL, Taruttis A, Herzog E, Zeebregts CJ, van Dam GM, Ntziachristos V. Multispectral optoacoustic tomography of matrix metalloproteinase activity in vulnerable human carotid plaques. *Mol Imaging Biol*. 2012;14:277-285

216. Flood C, Gustafsson M, Richardson PE, Harvey SC, Segrest JP, Boren J. Identification of the proteoglycan binding site in Apolipoprotein B48. *J Biol Chem*. 2002;277:32228-32233

217. Camejo G, Hurt-Camejo E, Wiklund O, Bondjers G. Association of Apo B lipoproteins with arterial proteoglycans: Pathological significance and molecular basis. *Atherosclerosis*. 1998;139:205-222

218. Shaw PX, Horkko S, Chang MK, Curtiss LK, Palinski W, Silverman GJ, Witztum JL. Natural antibodies with the T15 idiotype may act in atherosclerosis, apoptotic clearance, and protective immunity. *J Clin Invest*. 2000;105:1731-1740

219. Agar C, van Os GM, Morgelin M, Sprenger RR, Marquart JA, Urbanus RT, Derksen RH, Meijers JC, de Groot PG. Beta2-Glycoprotein i can exist in 2 conformations: Implications for our understanding of the antiphospholipid syndrome. *Blood*. 2010;116:1336-1343